Session 2:

Remote sensing based monitoring of land degradation and desertification

Monitoring of land degradation and desertification dynamics using coarse-scale satellite data

C.J. Tucker[a], A. Anyamba[a] and P. Gonzales[b]

[a] Code 614.0, NASA/Goddard Space Flight Center, Greenbelt, Maryland 20771 USA
[b] The Nature Conservancy, 4245 North Fairfax Drive, Arlington, VA 22203-1606 USA

ABSTRACT

The analyses of coarse-resolution remote sensing data at scales of 250 m to 4 km provides an excellent tool for studying arid and semi-arid areas, their primary productivity, and effects of climate upon vegetation in these dry zones. Starting in 1981 with the launch of NOAA-7, 4-km data from the advanced very high resolution radiometer have been available from several satellites in the NOAA-series of polar orbiting meteorological satellites for almost 25 years. These 4-km data have been complimented by 1-km data from the same instruments in regional areas, where they were received and maintained. SeaWiFS 4-km data have been available globally since late 1997 and SPOT Vegetation data have been available globally since May 1998. Data from the MODIS instruments have been available globally at 500 m since 2000 and 2002 from the Terra and Aqua platforms, respectively, and have been available regionally in many areas at 250 m. The uses and limitations of these data will be discussed and a new dry season application of these data from highly-calibrated instruments like SeaWiFS will also be presented. In addition, an example of the use of ~1 m satellite and aerial photography data for counting trees and bushes will be presented as a compliment to course-resolution satellite data.

1 INTRODUCTION

A consistent, continuous, and long record of remote sensing data is crucial for desertification studies. Arid and semi-arid areas, where most desertification is thought to occur, have highly variable climatic conditions, and thus data from only a few years are not informative. However, coarse-resolution data over several years and at frequent intervals within each year are necessary to gain a representation of climatic variation in these locales. Simultaneously, ~ 1 m high spatial resolution data are very important for counting trees and bushes, as this information is also extremely important in desertification studies. This paper deals primarily with coarse-resolution time series data but will also touch upon hyper-spatial resolution data for counting trees and bushes. We restrict our paper to the south side of the Sahara Desert but acknowledge there are many other areas of our planet where climatic and/or human degradation influences are of topical concern.

Although significant improvements have been made with new, global, land vegetation-sensing instruments (table 1), the existing July 1981 to the present 4-km archive of data from the advanced very high resolution radiometer (AVHRR) instrument is an invaluable and irreplaceable archive of historical land surface information. This archive of global 4-km AVHRR data results from five different AVHRR instruments on five different NOAA polar-orbiting meteorological satellites [1, 2]. The 1981-2005 record of AVHRR data has been processed in a consistent and quantitatively comparable manner [3] with the new generation of sensors to bring the global land surface satellite climate data record an additional ~20 years to compliment the 5+ years of data presently in hand from the improved sensors listed in table 1.

New improved coarse-resolution global land surface satellite data are available from SeaWiFS (October 1997 – present), SPOT-4's Vegetation Sensor (May 1998 – present), and NASA's moderate resolution imaging spectrometers (MODIS) on the Terra and Aqua platforms (January 2000 – present and December 2002 - present, respectively) (table 1).

2 STUDY AREA

To illustrate the use of monitoring land degradation and desertification dynamics using coarse-scale satellite data, we will use the southern boundary of the Sahara and the adjacent semi-arid transition zone known as the "Sahel". "Sahel", a word apparently meaning "shoreline" in Arabic [4], is a climatic and vegetation transition zone between the hyper arid Sahara and the more humid savannas to the south. From the Sahara to the south there is an unusual north-south precipitation gradient of ~1 mm yr^{-1} km^{-1}, extending for over 6,000 km from the Atlantic Ocean to the Red Sea. Associated with this unusual precipitation gradient is an almost imperceptible gradient of vegetation, as

Table 1. Global coarse-resolution satellite spectral vegetation index data sets.

Instrument	Dates of Coverage	Spatial Resolution (nadir)	Spectral Bands	Global Data Volume (gb/day)	References, comments
NOAA AVHRR					[1, 2]
NOAA-7	07/1981-02/1985	4-km	5	0.6	
NOAA-9	02/1985-09/1988	4-km	5	0.6	
NOAA-11	09/1988-9/1994	4-km	5	0.6	
NOAA-9-d	9/1994-01/1995	4-km	5	0.6	Descending node 09:00 data
NOAA-14	01/1995-11/2000	4-km	5/6	0.6	
NOAA-16	11/2000-12/2003	4-km	5/6	0.6	
NOAA-17	5/2002-now	4-km	5/6	0.6	
NOAA-18	7/2005-now	4-km	5/6	0.6	
SeaWiFS	9/1997-present	4-km	8	0.4	[5]
SPOT-4 Vegetation	05/1998-present	1-km	4	5	[6]
MODIS	01/2000-present	250-1000 m	32	70	[7]

one moves up or down the gradient, from the Sahara to tropical forests and back [4, 8, 9]. We use the following generalized definitions after Le Houreou (1980) [4] and others:

Sahara Desert:	<100 mm/yr
Saharan-Sahelian Transition:	100-200 mm/yr
Sahel Zone:	200-400 mm/yr
Sahelian-Sudanian Transition:	400-600 mm/yr
Sudan Zone:	600-800 mm/yr

Since the 1970s international interest has frequently focused on the south side of the Sahara Desert, upon the Sahel Zone, the semi-arid grassland or steppe area immediately to the south of the Sahara. A prevalent suggestion in the 1970s and 1980s was the continuous expansion of the Sahara Desert to the south into the semi-arid Sahelian Zone, via the process of “desertification” or “desert creep”. Desertification has been defined as the process by which more productive arid and semi-arid lands become less productive or more "desert like" (reviewed in [10, 11]). This can result from many causes, but generally is associated with over-use by man that then results in reinforcing climatic tendencies toward dryer climates.

The occurrence of a period of successive wet years (1950 to 1960), followed by a period of successive dry years (1969 to 1997), has also contributed to the controversy in the location of the southern Sahara boundary [12]**.** Lamprey [13] estimated the southern Saharan boundary had shifted southward in western Sudan 90 to 100 km between 1958 (a wet year) and 1975 (a dry year). Hellden [14], working in the same western Sudan area, found no evidence to support a southern Saharan expansion from 1958 to the early 1980s. Disagreement on the location of the southern Saharan boundary is not new--it has occurred since the early part of the 20th century [15, 16, 17, 18].

We expand upon previous work [19] and extend to 2004 a satellite-derived vegetation index to map inter-annual changes in vegetative cover and, by inference, rainfall, along the Saharan-Sahelian boundary from the Atlantic Ocean to the Red Sea. Our use of satellite data for mapping annual variations through corresponding changes in the density of green vegetation cover is based on precipitation being the principal determinant of primary production below ~800 mm/yr in the Sahel and Sudan Zones of Africa [20, 21, 22, 23].

3 REMOTE SENSING INDICES

We will discuss the use of 3 very different remote sensing indices for studying arid and semi-arid lands: surface reflectance data from the dry season, after the work of Charney et al. [25]; spectral vegetation indices to define arid boundaries by their less arid adjacent semi-arid zones (after [19]); and Ikonos and Quickbird hyper spatial ~ 1 m data to count trees and bushes to infer aridity and climatic effects in arid and semi-arid areas as these are expressed in tree and bush cover.

3.1 Dry Season Surface Reflectance

Charney et al. [25] proposed a "feedback" situation, where degradation of arid and semi-arid lands resulted in a reduced vegetation cover and a higher surface reflectance or albedo. The higher the reflectance, the lower the amount of absorbed energy, the lower the temperature of the surface, a lower degree of convection, and less rainfall, thus "locking in" drier conditions.

Although the existence of this positive feedback remains to be seen, the tool of using satellite data to infer land degradation by the means of albedo or surface reflectance variations can be a useful tool in arid and semi-arid land research and desertification studies.

We have been investigating the use of SeaWiFS land data for a variety of applications, including studying arid and semi-arid land degradation. One of the features of SeaWiFS data is a high degree of calibration accuracy through time because this is extremely important for ocean primary productivity studies. To achieve a high degree of sensor calibration, the SeaWiFS platform "flips" and images the lunar disk every full moon. Lunar imaging combined with constraint monitoring of the SeaWiFS instrument's dark current enables a very high degree of calibration accuracy (figure 1).

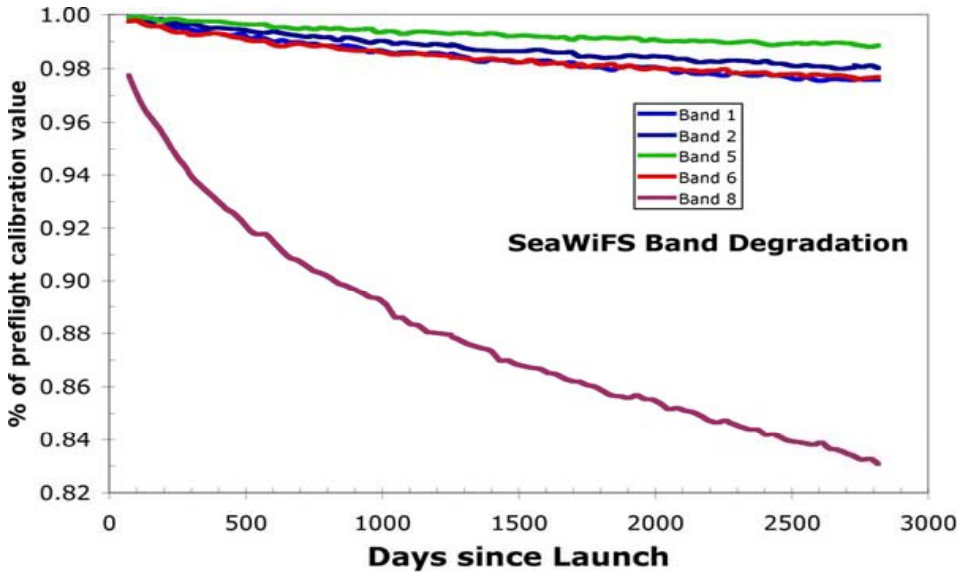

Figure 1. Degradation of SeaWiFS' bands 1 (440-460 nm), 2 (480-495 nm), 5 (550-570 nm), 6 (660-680 nm), and 8 (820-860 nm) from the launch of SeaWiFS in September 1997. The *ex post facto* calibration of SeaWiFS corrects each channel or band so that a given surface reflectance is quantitatively comparable through time.

The high degree of calibration accuracy of the SeaWiFS instrument results in data that can be used to monitor the albedo of arid and semi-arid lands through time. An example of this is figure 2 that shows the subsequent dry season reflects the strength of the previous rainy season in the Sahel Zone of Africa. That is, following a wetter rainy season, the dry season surface reflectance is lower than the dry season following a poor rainy season, because there is more dormant or dead vegetation obscuring the highly reflective soil background (figure 2). This is a new and promising remote sensing approach for studying arid and semi-arid lands and their degradation. It is very highly dependent upon *ex post facto* sensor calibration and explicit atmospheric correction.

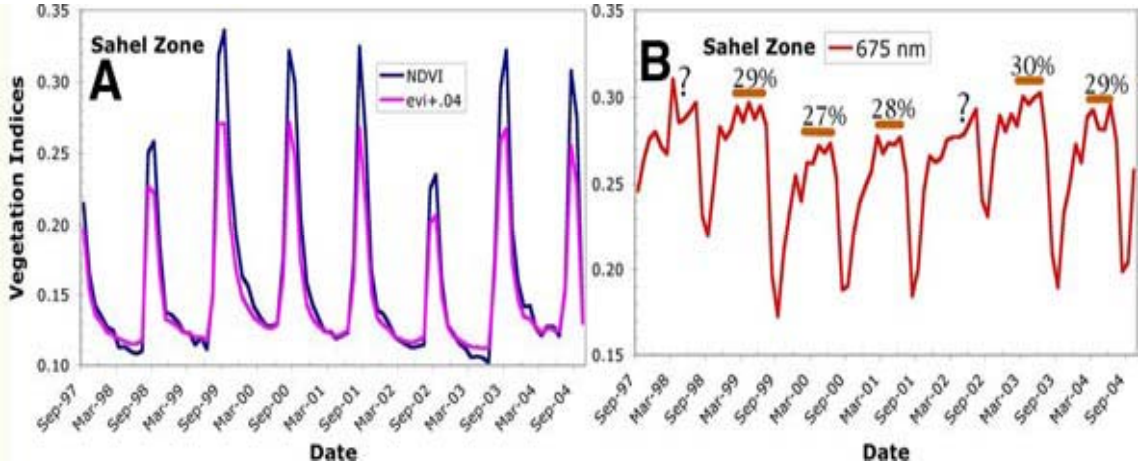

Figure 2. SeaWiFS data from the Sahelian Zone. (A) SeaWiFS NDVI and EVI from September 1997 to December 2004. Note the extremely high correlation between these two vegetation indices (r=0.99) and (B) SeaWiFS red surface reflectance data showing how the dry season red reflectance is lower following a good rainy season and higher following a poor rainy season in the Sahel Zone. The lower the red surface reflectance in September the more rain has fallen during the growing season, the more green vegetation is present, and the more red absorption and photosynthesis results.

3.2 Spectral Vegetation Indices

Spectral vegetation indices are usually composed of red and near infrared radiances or reflectances [26], sometimes with additional channels included [27]. They are highly correlated with the photosynthetically-active biomass, chlorophyll abundance, and energy absorption [28].

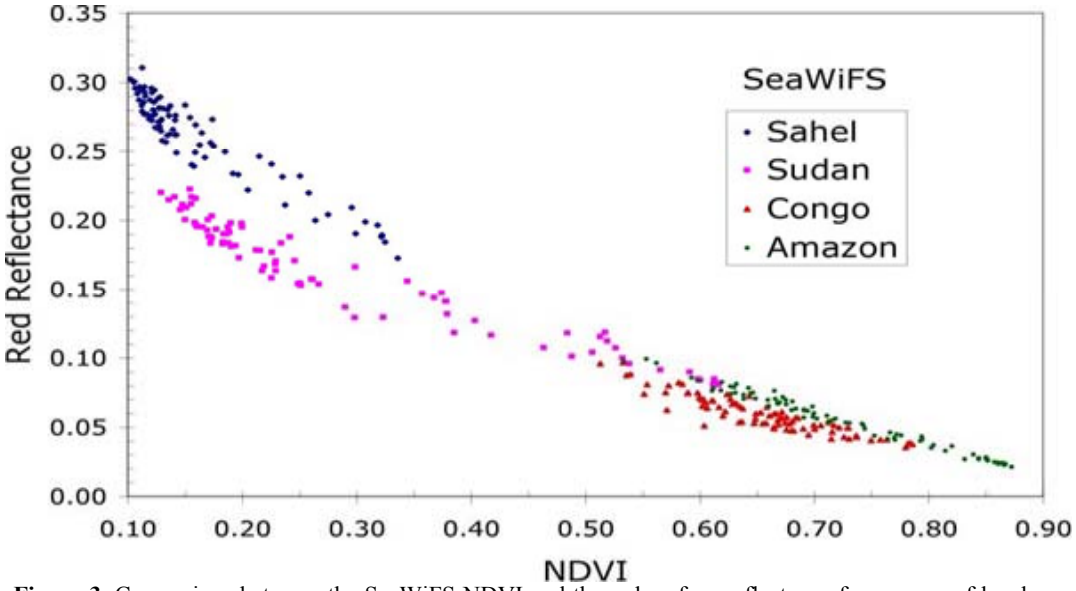

Figure 3. Comparison between the SeaWiFS NDVI and the red surface reflectance for a range of locales, from the Sahel Zone to tropical forests. The down-welling red radiation is absorbed by chlorophyll within green leaves. The greater the density of green leaves the greater the absorption of red radiation and the higher the NDVI. The NDVI is a non-destructive measure of the energy absorbed by chlorophyll.

The use of spectral vegetation indices derived from AVHRR satellite data followed the launch of NOAA-6 in June 1979 and NOAA-7 in July 1981. Since then, the normalized difference vegetation index (NDVI) has become the most used product derived from NOAA AVHRR data [29], largely from the use of NDVI data sets formed via maximum value compositing [30]. Composite NDVI data minimize cloud and atmospheric contamination without corrections to the channel 1 and channel 2 radiance data in question. While spectral vegetation indices are the most

widely used of any of the products derived from the AVHRR instruments, this was never anticipated by the designers of the AVHRR instruments who had no idea what a vegetation index was.

Examples of the use of AVHRR data for studying arid and semi-arid lands are Tucker and Nicholson [19], Rasmussen [31, 32], Eklundh and Olsson [33], Hermann et al. [34], Anyamba and Tucker [35], and Olsson et al. [36], among others.

We have taken the NDVI data described in Tucker et al. [3], formed the July to October average by year, and correlated these satellite data to Nicholson's [12] ground-collected precipitation data (figure 4). We selected the 200 mm/yr precipitation amount as an arbitrary boundary between desert (<200 mm/yr) and non-dessert (>200 mm/yr). We used the regression equation between precipitation and NDVI to convert our spatially explicit NDVI data into estimated precipitation, applied this to our NDVI data from Africa, and restrict our analysis to the equivalent of the 0 to 400 mm/yr precipitation zone (figure 5).

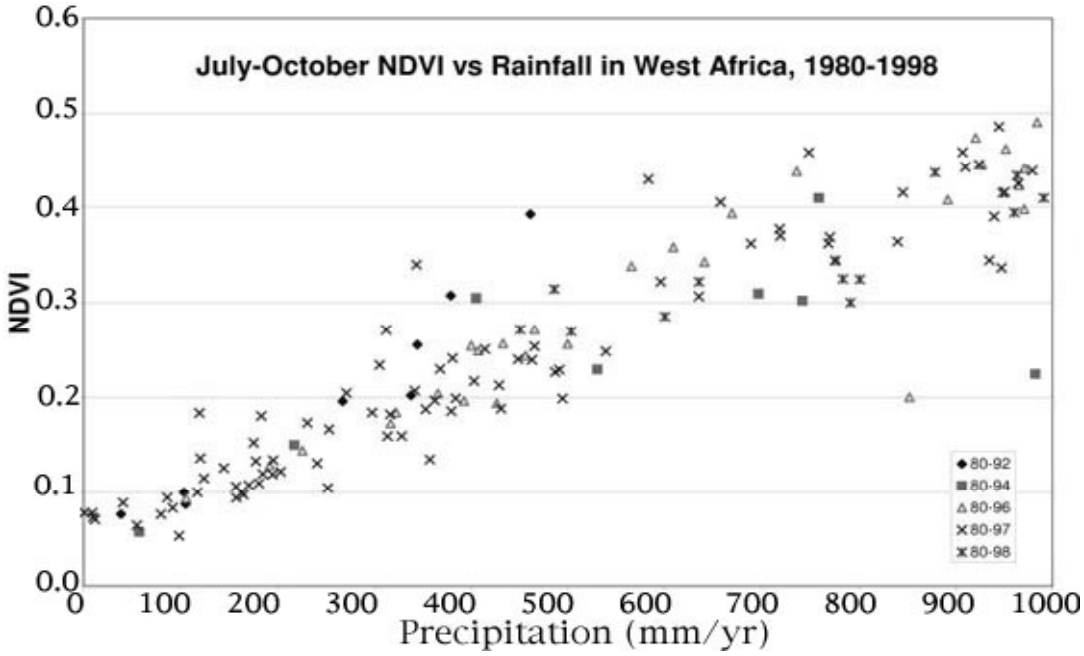

Figure 4. The relationship between the July-October NDVI and seasonal rainfall in West Africa from 1980 to 1998. July to October was selected to bracket the rainy season in the Sahelian Zone. Note the linear relationship from 100 to ~800 mm/yr precipitation.

We next determine the latitude of the change from <200 to > 200 mm/yr estimated precipitation at every 0.5 degree of longitude by year. When this is accomplished, it is an easy matter to produce a figure like figure 6 which shows the variation in the estimated 200 mm/yr isoline by year for the Sahel Zone. Figure 6 shows a high degree of variability in the year-to-year location of the estimated 200 mm/yr precipitation boundary on the south side of the Sahara Desert. However, when satellite data are available for 40 years, comparisons can be made over decades to determine if climate shifts have occurred as they are manifested in resulting vegetation distributions.

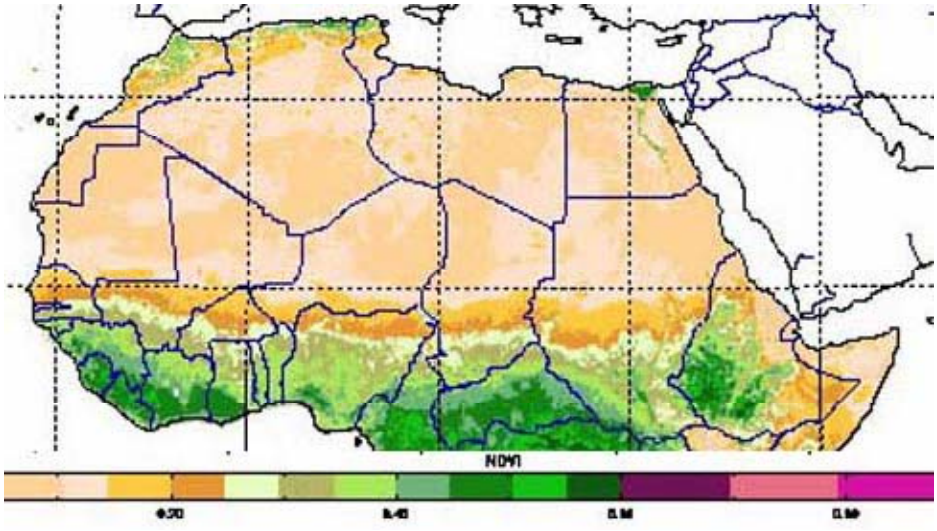

Figure 5. The average NDVI from July 1981 to July 2004 formed by averaging bimonthly composites derived from AVHRR data. Note the isolines of NDVI that are roughly parallel to lines of equal latitude.

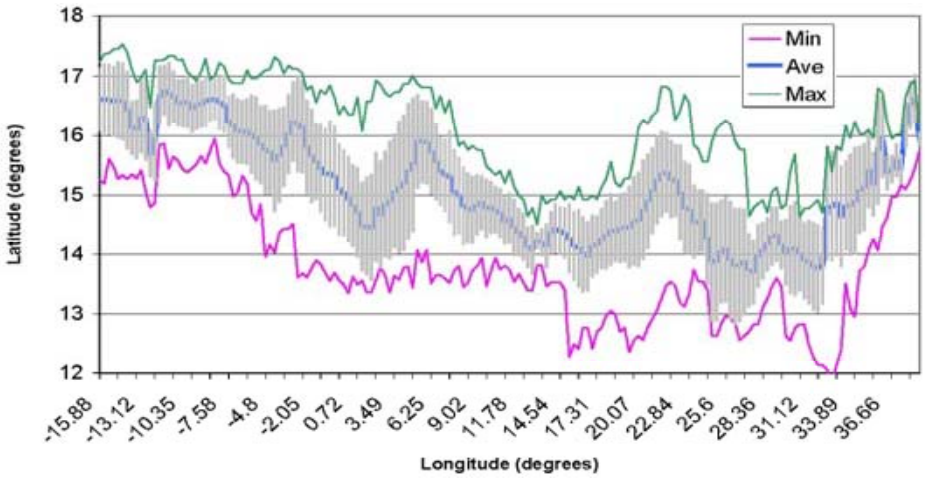

Figure 6. We have used the NDVI-precipitation relationship in figure 4, converted NDVI into estimated precipitation, and determined the location of the 200 mm/yr estimated precipitation isoline by year. This figure is based upon the data in figure 5 and was derived from ~30,000 orbits of AVHRR data over 24 years. One standard deviation is plotted ± to the 1981 to 2004 mean value as are the minima and maxima.

3.3 Hyper-Spatial Data to Count Trees and Bushes

One of the problems with using coarse-resolution satellite data is you have no clue what is happening on the ground. It is possible, for example, that herbaceous vegetation would show one trend while the tree and bush density might show the opposite. Consequently it is extremely important to study aerial photography and/or 1 m satellite data like Ikonos and Quickbird.

As a test of the use of 1-m Ikonos data from the Sahelian Zone, we acquired three 10 x10 km Ikonos scenes in the dry season from northern Senegal and southern Mauritania. The Ikonos data were compared to digitized aerial photography from 1954 and 1989. Specific areas were selected to count trees and bushes among these three dates and determine the tree and bush density variations over these 50 years (figure 7).

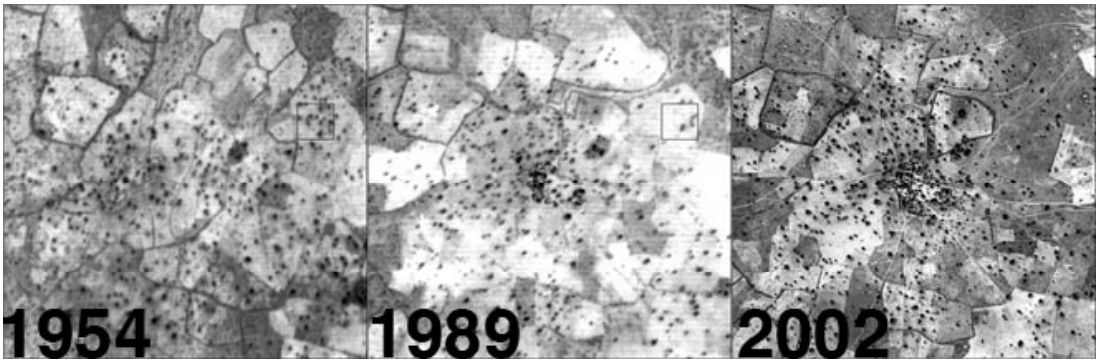

Figure 7. A comparison among aerial photographs taken in 1954 and 1989 and a 1-m Ikonos image from 2002 in Northern Senegal. The spatial resolution of the aerial photographs is approximately the same as the Ikonos spatial resolution. Each image is ~ 800 m x 800 m and the dark spots are individual trees and bushes. Note how individual trees and bushes can be counted and compared among years.

The combination of coarse-resolution time series data using highly-calibrated reflectance data from SeaWiFS and MERIS, time series NDVI data from the AVHRR, SPOT Vegetation, and MODIS, and 1 m aerial photography and Ikonos/Quickbird data together offer new tools for studying desertification and land degradation.

REFERENCES

[1] CRACKNELL, A.P., 1997: The Advanced Very High Resolution Radiometer, Taylor and Francis, London, 534 p.

[2] KIDWELL, K.B., 1997: Polar Orbiter Data Users' Guide (TIROS-n, NOAA-6, NOAA-7, NOAA-8, NOAA-9, NOAA-10, NOAA-11, NOAA-12, and NOAA-14), National Oceanic and Atmospheric Administration, Washington, D. C.

[3] TUCKER, C.J., PINZON, J.E., BROWN, M.E., SLAYBACK, D.A., PAK, E.W., MAHONEY, R., VERMOTE, E.F., AND EL SALEOUS, N., 2005: An Extended AVHRR 8-km NDVI data set compatible with MODIS and SPOT Vegetation NDVI data. *Int. J. Remote Sens.* (in press).

[4] LE HOUEROU, H.N., 1980: The rangelands of the Sahel. *J. Range Manage., 33*, pp. 41-46.

[5] HOOKER, S.B., ESAIAS, W.E., FELDMAN, G.C., GREGG, W.W., AND MCCLAIN, C.R., 1992: An overview of SeaWiFS and Ocean Color, NASA Tech. Memo. 104566, vol. 1, 24p.

[6] SAINT, G., 1995: Spot-4 vegetation system--association with high-resolution data for multi-scale studies. *Advances in Space Research, 17*, pp. 107-110.

[7] JUSTICE, C.O., ET AL., 1998: The Moderate Resolution Imaging Spectroradiometer (MODIS): Land remote sensing for global change research. *IEEE Transactions on Geoscience and Remote Sensing, 36*, pp. 1228-1249.

[8] BREMEN, H. AND DE WIT, C.T. 1983. Rangeland productivity and exploitation in the Sahel. *Science, 221*, pp. 1341-1347.

[9] MONOD, T., 1986: The Sahel zone north of the equator. In: Evenari, M., Noy-Meir, I. and Goodall, D.W. (eds.): Ecosystems of the World, Hot Deserts and Arid Shrublands. Elsevier, New York, pp. 203-243.

[10] HELLDEN, U., 1988: Desertification monitoring: Is the desert encroaching? *Desertification Control Bulletin 17*, pp. 8-12.

[11] HELLDEN, U., 1991: Desertification--time for an assessment*? Ambio, 20*, pp. 372-383.

[12] NICHOLSON, S.E., TUCKER, C.J. AND BA, M.B., 1998: Desertification, drought and surface vegetation, an example from the West African Sahel. *Bulletin of the American Meteorological Society, 79*, pp.815-829.

[13] LAMPREY, H.F. 1988: Report on the desert encroachment reconnaissance in northern Sudan, 21 October to 10 November 1975. UNESCO/UNEP, Paris/Nairobi, 16 p.; republished in *Desertification Control Bulletin 17*, pp. 1-7.

[14] HELLDEN, U., 1984: Drought impact monitoring. Lunds Universitets Naturgeografiska Institution. Rapporter och Notiser 61, Lund, Sweden, 61 p.

[15] BOVILL, E., 1921: The encroachment of the Sahara on the Sudan. *Journal of the Royal African Society, 20*, pp. 175-185.

[16] CANA, F.R., 1915: The Sahara in 1915. *Geographical Journal, 46*, pp. 333-357.

[17] CLOUDSLEY-THOMPSON, J.L., 1974: The expanding Sahara. *Environmental Conservation, 1*, pp. 5-13.

[18] ECKHOLM, E. AND BROWN, L.R., 1977: Spreading Deserts, the Hand of Man. Worldwatch Paper 13 (Worldwatch Institution, Washington, D.C.), 40 p.

[19] TUCKER, C.J. AND NICHOLSON, S.E., 1999: Variations in the size of the Sahara Desert from 1980 to 1997. *Ambio, 28*, pp. 587-591.
[20] LAUENROTH, W.K., 1979: Grassland primary production, North American grasslands in perspective. In: French, N. (ed.): Perspectives in Grassland Ecology. Springer-Verlag, New York, pp. 3-24.
[21] RUTHERFORD, M.C., 1980: Annual plant production-precipitation relations in arid and semi-arid regions. *So. African J. Science, 76*, pp. 53-56.
[22] SEELY, M.K., 1978. Grassland productivity, the desert end of the curve. *So. African J. Science, 74*, pp. 295-297.
[23] LE HOUEROU, H.N. AND HOSTE, C.H., 1977: Rangeland production and annual rainfall relations in the Mediterranean Basin and in the African Sahelo-Sudanian Zone. *J. Range Manage., 30*, pp. 181-189.
[24] White, F., 1983: The Vegetation of Africa, UNESCO, Paris.
[25] CHARNEY J., STONE, G., AND QUIRK, W.J., 1975: Drought in the Sahara, a biophysical feedback mechanism. *Science, 187*, pp. 434-435.
[26] TUCKER, C.J., 1979: Red and photographic infrared linear combinations for monitoring vegetation. *Remote Sens. Environ., 8*, pp. 127-150.
[27] HUETE, A.R., LIU, H.Q., BATCHILY, K. AND VAN LEEUWAN, W.J.D., 1997: A comparison of vegetation indices over a global set of TM images for EOS-MODIS. *Remote Sens. Environ., 59*, pp. 440-451.
[28] MYNENI, R.B., HALL, F.G., SELLERS, P.J. AND MARSHAK, A.L., 1995: The interpretation of spectral vegetation indexes. *IEEE Transactions on Geoscience and Remote Sens., 33*, pp. 481-486.
[29] CRACKNELL, A.P., 2001: The exciting and totally unanticipated success of the AVHRR in applications for which it was never intended. *Advances in Space Research, 28*, pp. 233-240.
[30] HOLBEN, B.N., 1986: Characteristics of maximum-value composite images from temporal AVHRR data. *Int. J. Remote Sens., 7*, pp. 1417-1434.
[31] RASMUSSEN, M.S., 1998a: Developing simple, operational, consistent NDVI-vegetation models by applying environmental and climatic information: Part I. Assessment of net primary production. *Int. J. Remote Sens., 19*, pp. 97-117.
[32] RASMUSSEN, M.S., 1998b: Developing simple, operational, consistent NDVI-vegetation models by applying environmental and climatic information. Part II: Crop yield assessment. *Int. J. Remote Sens., 19*, pp. 119-139.
[33] ECKLAND, L. AND OLSSON, L., 2003: Vegetation trends for the African Sahel 1982-1999. *Geophysical Research Letters, 30*, pp. 1430-1434.
[34] HERMANN, S.M., ANYAMBA, A. AND TUCKER, C.J., 2005: Recent trends in vegetation dynamics in the African Sahel and their relationship to climate. *Global Environmental Change* (in press).
[35] ANYAMBA, A. AND TUCKER, C.J., 2005: Analysis of Sahelian vegetation dynamics using NOAA-AVHRR NDVI data from 1981 to 2003. *J. Arid Environments* (in press).
[36] OLSSON, L., EKLUNDH, L. AND ARDOE, J. 2005. A recent greening of the Sahel—trends, patterns, and potential causes. *J. Arid Environments* (in press).

Assessing land degradation and improvement using NASA GIMMS, Shaanxi, China

Z.G. Bai[a], D.L. Dent[a], H. Bartholomeus[b] and M.E. Schaepman[b]

[a] ISRIC – World Soil Information, PO Box 353, 6700 AJ Wageningen, The Netherlands, Email: Zhanguo.Bai@wur.nl

[b] Centre for Geo-Information, Wageningen University & Research Centre, The Netherlands

ABSTRACT

Spatial patterns and temporal trends of green biomass straddling the Mu Us Desert and the Loess Plateau, North China, are analyzed using 22 years of bi-monthly NOAA-AVHRR NDVI data. Annual, growing season (May-October) and non-growing season (November-April) NDVI indicators and net primary productivity (NPP) were derived for each pixel and their trends were analysed by linear regression. Over the area as a whole, biomass increased; signs of declining biomass are few despite an overall decrease in rainfall. Correlations of the NDVI indicators and NPP with annual rainfall are low to moderate, but higher with monthly rainfall. Rain-use efficiency increased at Yulin, in the north of the area, and decreased at Dingbian in the south where biomass decreased. The results throw light upon several recent researches on land reclamation and improvement in the region. The indices developed here can be used as an input to early warning systems for land degradation.

Keywords: Land degradation, NDVI, Net primary productivity, Rain-use efficiency, Early-warning system, North China

1 INTRODUCTION

Land degradation is believed to be a severe and widespread problem [1, 2] but there is no authoritative, global measure. The only harmonized assessment, the *Global Assessment of Human-induced Soil Degradation* [3], is a map of perceptions - the kinds and degree of degradation, not a measure of degradation - and is now out-of-date; land degradation and perceptions have moved on. A quantitative global assessment of land degradation and improvement (GLADA) is under way within the FAO/UNEP *Land Degradation in Drylands* program to identify: 1) the status and trends of land degradation; 2) *hotspots* suffering severe degradation and 3) and their counterpoint – areas where degradation has been arrested or reversed. This pilot tests a methodology for assessing land degradation and improvement using time-series NDVI data and ancillary information, specifically: i) procedures for handling the dataset, and ii) analysis of the NDVI deviations and trends.

Biomass is an integrated measure of biological productivity; its deviance from the norm may be taken as a measure of land degradation or improvement. Global satellite data, in particular the normalized difference vegetation index (NDVI) or greenness index, enable measurement of changes in green biomass from the field scale (1:10 000) where it can be validated by observation to the degree of generalization required for national or international policy development (1:1 million to 1:5 million). Local and regional norms may be calculated by stratifying the land area according to climate, soils and terrain, and land cover; deviance may then be calculated locally and regionally. NDVI has a strong linear relationship with the fraction of photo-synthetically active radiation absorbed by the plant [4, 5] and above-ground net primary productivity [6], so it has been used in studies of land degradation at local and regional scales [7, 8, 9, 10].

2 METHODOLOGY

2.1 Study Area

Yulin Prefecture, Shaanxi Province, North China, latitude 36˚ 57’ – 39˚ 34’ N and longitude 107˚ 28’ - 111˚ 15’ E, encompasses twelve counties – in all, 42 986 km2 with some 3.4 million inhabitants (Fig.1). It is a transitional zone between the sandy Mu Us Desert, in the north-west, and the high, gullied Loess Plateau in the middle-south. Elevation increases from the southeast to the northwest; mean elevation is 1000m above sea level, rising to 1907m on Mount Baiyun. Climate ranges from arid in the northwest to sub-humid in the southeast: spring is dry and windy; summer short and hot with a rainfall maximum; autumn brings short rains; followed by a long, dry and cold winter. Mean maximum temperature is 32 ºC, mean minimum -6 ºC. At Yulin, mean annual rainfall is 396mm,

ranging from 159-695mm (1934-2003); at Dingbian, mean annual rainfall is 293mm, ranging from 145 mm to 587mm (1954-1996). Rain falls mostly in July and August, with great variation year to year. Soils are Kastanozems and Arenosols [11] under natural vegetation grading from forest steppe through steppe to desert. It is an agro-pastoral region in which rampant land degradation has been reported [12, 13].

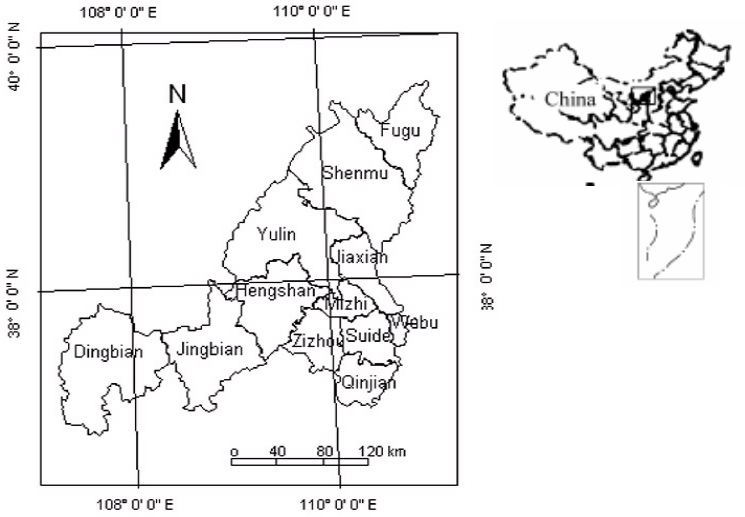

Figure 1. Location.

2.2 Datasets

The Global Inventory Modelling and Mapping Studies (GIMMS) dataset was collected between 1981 and 2002 by advanced very high resolution radiometer (AVHRR) on National Oceanic and Atmospheric Administration (NOAA) satellites. It comprises two-weekly NDVI images of 8km spatial resolution, corrected for calibration, view geometry, volcanic aerosols, and other effects unrelated to vegetation change [14]. Daily rainfall and temperature data are from Yulin and Dingbian. Monthly net primary productivity (NPP) data (1981-1998) derived from the Carbon Exchange between Vegetation, Soil, and Atmosphere (CEVSA) model [15] were provided by Tao et al. (personal communication). Data for land degradation status for six counties (Dingbian, Jingbian, Hengshan, Yulin, Shenmu, and Fugu) were provided by Liu et al. [12].

2.3 Approaches

NDVI data were extracted and geo-referenced using ERDAS IMAGINE and ArcGIS. Algorithms were developed to calculate indicators of land degradation, namely: NDVI minimum, maximum, maximum-minimum, mean, sum, and coefficient of variation (CoV). Annual, growing season (May-October) and non-growing season (November-April) indicators were derived for each pixel; their temporal trends were determined by linear regression and mapped to depict spatial changes. A negative regression coefficient indicates a decline of green biomass and positive, an increase – except for CoV which indicates trends in variability. Relationships were established between NDVI and rainfall, NPP, and rain-use efficiency (RUE).

3 RESULTS AND DISCUSSION

3.1 NDVI indicators

Table 1 summarizes the values of the NDVI indicators. Temporal trends for each pixel, determined by the slope of the linear regression equation, were classed as *no change* (slope <0.0001 and >-0.0001), *increase* (positive slope ≥0.0001), and *decrease* (negative slope ≤-0.0001).

Minimum NDVI: the lowest value in any one year (annual), which is almost invariably at the end of winter, any growing season, or any non-growing season. Over the 22-year period, annual values tended to increase for 67% of the area, decreased for 23%, while 10% remained unchanged; for the non-growing season the picture is predictably the same as the annual pattern. For the growing season, 90% increased, 6% was unchanged and only 4% decreased. These differences might be attributed to land use change: conversion of barren land to grassland increases minimum

biomass in the growing season, whereas change from grassland to arable decreases minimum green biomass in the non-growing period.

Table 1. Statistics of NDVI indicators.

NDVI indicators	Range (minimum, maximum, mean)			No change no. (%)	Increase no. (%)	Decrease no. (%)
Annual						
Minimum	0.006	0.105	0.08	80 (10)	537 (67)	182 (23)
Maximum	0.006	0.663	0.445	1 (0.1)	798(99.9)	0
Max-min	0.000273	0.324	0.189	25 (3)	769 (96)	5 (1)
Mean	0.006	0.263	0.192	41 (5)	726 (91)	32 (4)
Sum	3.1	138	100.6	1 (0.1)	778(96.9)	20 (3)
CoV	0.00074	0.472	0.307	24 (3)	738 (92)	37 (5)
Growing season						
Minimum	0.006	0.15	0.115	45 (6)	720 (90)	34 (4)
Maximum	0.006	0.663	0.445	57 (7)	738 (92)	4 (1)
Max-min	0.003	0.591	0.375	35 (4)	720 (90)	44 (6)
Mean	0.006	0.338	0.241	41 (5)	746 (93)	12 (2)
Sum	1.6	89	63.5	1 (0.1)	746(92.9)	52 (7)
CoV	0.00037	0.316	0.196	44 (6)	454 (57)	301 (38)
Non-growing season						
Minimum	0.006	0.176	0.119	77 (10)	579 (73)	143 (17)
Maximum	0.006	0.247	0.17	48 (6)	714 (89)	37 (5)
Max-min	0.003	0.108	0.049	0	799(100)	0
Mean	0.006	0.201	0.142	70 (9)	636 (80)	93 (11)
Sum	1.6	53.1	37.2	24 (3)	661 (83)	114 (14)
CoV	0.001	0.181	0.102	42 (5)	681 (85)	76 (10)

Maximum NDVI: the maximum green biomass. The patterns of the monthly maximum NDVI over the period, personal experience and communication with local experts suggest that peak biomass occurs between late July and early September, mostly in August. The large spatial variations reflect the diverse landscape and climate, but the 22-year trends of annual and growing-season values are nearly all positive: annual and growing-season maximum NDVI increased for 93% of the area while 7% remained unchanged. For the non-growing period, it increased for 89% of the area, remained unchanged for 6%, while 5% decreased.

Maximum-minimum NDVI: the difference between maximum and minimum NDVI. It reflects biomass production. Both annual and growing-season max-min NDVI increased over more than 90% of the area, 3-4% remained unchanged, while less than 5% decreased.

Mean NDVI: The spatial patterns of annual and growing-season mean NDVI mean are the same, so are the slope coefficients of their linear regression equations - showing an increase for more than 91% of the area with 5% remaining unchanged and 4% decreasing. For non-growing season, however, there was a negative trend for 11% of the area, 9% remaining unchanged and 80% increasing.

Sum or integrated NDVI: the sum of fortnightly NDVI values for the year and for the growing season most nearly integrates biomass and biomass production, respectively. The spatial distribution of the annual and growing-season sum NDVI are similar; likewise, the slope coefficients of their linear regression equations. Rather more pixels with negative slopes occurred for the growing season (52) than for the annual sum (12 pixels). The pattern of

sum NDVI is very similar to the max-min and mean NDVI: for the annually integrated NDVI, 97% of the total pixels increased; 93% increased for the growing season.

Coefficient of variation (CoV): can be used to compare the amount of variation in different sets of sample data. CoV images were generated by computing, for each pixel, the standard deviation (STD) of the set of individual NDVI values and dividing this by the mean (M) of these values (CoV = STD/M). This represents the dispersion of NDVI values relative to the mean value over time, which can be: 1) positively increasing, 2) positively decreasing, 3) negatively decreasing, 4) negatively increasing, or 5) constant. A positive change in the value of a pixel-level CoV over time relates to increased dispersion of values, not increases NDVI; similarly, a negative CoV means decreasing dispersion of NDVI around mean values, not decreasing NDVI. As an indication of variability, CoV may be combined with other biomass parameters, such as maximum-minimum NDVI, to detect land degradation or improvement (table 2).

Table 2. Combination of NDVI and CoV for detection of biomass variation.

Max-min NDVI	NDVI CoV	Interpretation
+	+	Increased biomass but unstable
-	+	Decreased biomass but unstable
+	-	Increased biomass, stable
-	-	Decreased biomass, stable

The spatial patterns of growing-season NDVI CoV are similar to the annual NDVI pattern but their temporal trends are quite different: for the growing period, 301 pixels display decreasing dispersion and 454 increasing dispersion; for the annual values, 37 show decreasing dispersion and 738 increasing dispersion. Although 301 pixels show a negative trend in the growing season NDVI CoV, only 5 of these showed a decreasing trend in the mean NDVI while 296 showed an increasing positive trend. These values emphasize that a negative trend of CoV does not mean biomass decrease, and *vice versa*, although some authors have made this connection [e.g. 16]. Rather, the trends in NDVI CoV may reflect land cover change.

Interpretation of NDVI indicators: If land use remains stable, changes in NDVI reflect the trend of green biomass production that may be attributed to land quality and the success of management in dealing with variable weather, pests and disease. Overall, green biomass increased over the 22-year period. This can hardly be explained by changes in rainfall:

1. Correlations between NDVI indicators and annual rainfall are weak at Yulin and only moderate at Dingbian (table 3) and the trend of rainfall is downwards whereas the trend of NDVI is upwards;

Table 3. Correlation coefficients between annual rainfall and NDVI indicators.

Sites	Rainfall *v* mean NDVI	Rainfall *v* max NDVI	Rainfall *v* min NDVI	Rainfall *v* sum NDVI	Rainfall *v* NDVI CoV
Yulin*	0.049	0.053	0.366	0.049	0.325
Dingbian**	0.644	0.549	0.417	0.504	0.608

* n=22, P<0.01; ** n=16, P<0.05

2. Conversion of barren land to grassland, grassland to cropland, or agricultural land to built-up land could bring about decrease in NDVI in the non-growing season and increase in growing season (cropland, forest, grassland and built-up land have increased by 3%, 5%, 4% and 18% respectively; barren land has decreased by 22% [13]);
3. Changes in grassland and arable management, such as increased application of fertilizer and manure, should increase biomass production. In the context of decreasing rainfall, this may be equated with land improvement.

The spatial distribution of the negative trends in mean, max-min and sum NDVI occurred mainly in the northeast and southwest parts of the area; it may be significant that there has been a large increase in the exploitation of coal in the northeast and oil in the south-west.

3.2 Relationships of NDVI with rainfall and temperature

Fig. 2 compares trends in annual rainfall with NDVI: over the 22-year period, rainfall has been decreasing and yet the area as a whole shows increasing green biomass (Fig. 3).

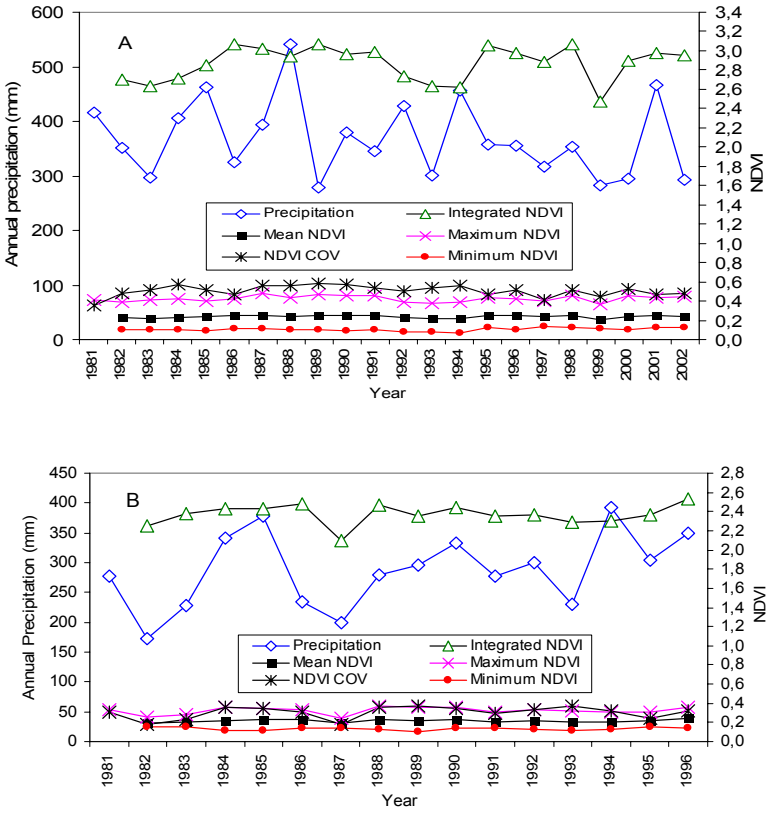

Figure 2. Annual rainfall and NDVI at Yulin (A) and Dingbian (B) from 1981 to 1996/2002.

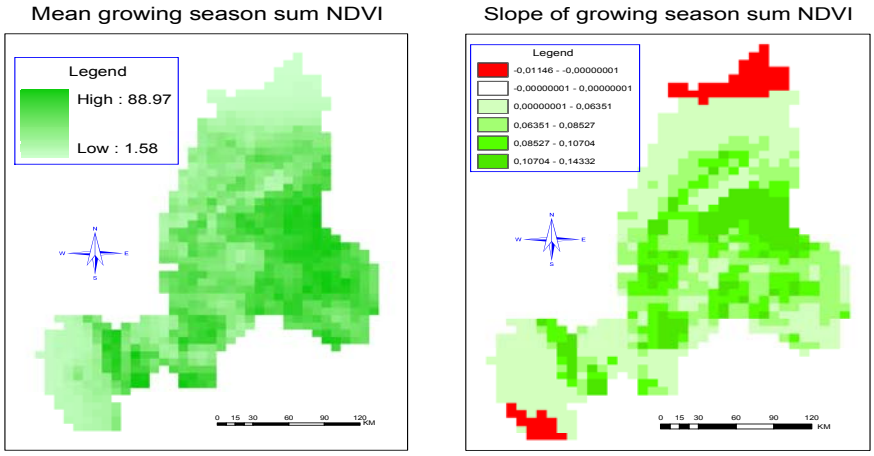

Figure 3. Map trend of sum NDVI for the study area.

NDVI is strongly correlated with monthly rainfall and temperature. Most rain falls during the summer growing period so plant growth responds to increasing warmth and moisture in spring and summer (table 4).

Table 4. Correlation coefficients of NDVI with monthly rainfall and temperature.

	Rainfall - NDVI	**Temperature - NDVI**
Yulin*	0.607	0.719
Dingbian**	0.618	no data

3.3 Relationships between rainfall and NPP

NPP is the net flux of carbon from the atmosphere into a unit area of vegetation per unit time [17]; it is a driver of life and, so, a good measure of land degradation and improvement [18]. Half-monthly values of NDVI were summed to monthly NDVI for the same locations as the data from Tao et al. (personal communication) to explore the relationship between NPP and NDVI. Linear regression between monthly NPP and NDVI was derived as:

$$NPPm\ [g\ C\ m\text{-}2\ month\text{-}1] = 41.691 * \Sigma NDVIm + 33.192 \quad (1)$$

where NPPm is monthly NPP and ΣNDVIm the sum of first and second half-monthly NDVI ($n = 1768$, $r = 0.283$, $P<0.001$).

Growing-season and yearly sums of NPP and NDVI were integrated:

$$NPPMay\text{-}Oct\ [g\ C\ m\text{-}2\ May\text{-}Oct\text{-}1] = 13.776 * \Sigma NDVIMay\text{-}Oct + 281.54 \quad (2)$$

where NPPMay-Oct is the summation of NPP May-October, ΣNDVIMay-Oct is integrated NDVI May-October ($n = 303$, $r = 0.18$, $P<0.001$) and

$$NPPa\ [g\ C\ m\text{-}2\ yr\text{-}1] = 0.0349 * \Sigma NDVI + 294.85 \quad (3)$$

where NPPa is the annual sum of NPP; ΣNDVI annual NDVI ($n = 303$, $r = 0.18$, $P<0.001$).

Table 5 compares monthly rainfall, NPP and NDVI data for Yulin and Dingbian. Agreement between NPP and NDVI is weak for annual time intervals but strong at monthly intervals; NPP seems to be in step with monthly rainfall with no significant time lag. The trend in NPP over time, in the area as a whole, increased.

Table 5. Correlations of NPP with NDVI and rainfall at Yulin and Dingbian*.

Parameters	Time intervals	Yulin	Dingbian
NPP-NDVI	Yearly	NPP=4.070NDVI+300 r=0.09, n=18	NPP=44.362NDVI+87 r=0.381, n=16
	May-October	NPP=3.536NDVI+284 r=0.066, n=18	NPP=32.752NDVI+155 r=0.315, n=16
	Monthly	NPP=28.621NDVI+32 r=0.253, n=104	NPP=49.644NDVI+20 r=0.273, n=94
NPP-Rainfall	Yearly	NPP=0.833Rain+9 r=0.66, n=18	NPP=0.323Rain+165 r=0.44, n=16
	May-October	NPP=0.742Rain+53 r=0.73, n=18	NPP=0.312Rain+158 r=0.46, n=16
	Monthly	NPP=0.320Rain+33 r=0.51, n=104	NPP=0.301Rain+27 r=0.50, n=94
	Monthly (1 month lag of NPP)	NPP=0.0756Rain+46 r=0.038, n=103	NPP=0.053Rain+37 r=0.087, n=93

* $P<0.001$

3.4 RAIN-USE EFFICIENCY

A reduction in NDVI or NPP does not necessarily mean land degradation; green biomass also fluctuates between and within years according to variation in rainfall, phenology, and changes in land use – which may or may not be related to the land degradation. Rain-use efficiency (RUE) – the ratio of NPP to precipitation – seeks to overcome this problem by combining information on biomass and rainfall [19, 20]. Although RUE is systematically lower in ecosystems subject to drought stress, it is also lower in degraded drylands than in equivalent non-degraded areas [21], so negative deviations from the conservative value of RUE may still be a useful index of land degradation.

Temporal trends in RUE (computed as the ratio between NPP and rainfall, RUENPP, and as the ratio between NDVI and rainfall, RUENDVI) increased at Yulin and decreased at Dingbian (Fig. 4). This suggests land improvement at Yulin and degradation at Dingbian. The correlation between RUENPP and RUENDVI is significant, with correlation coefficients of 0.33 at Yulin (n=18, P<0.01) and 0,74 at Dingbian (n=16, P<0.01), respectively so they can be used interchangeably.

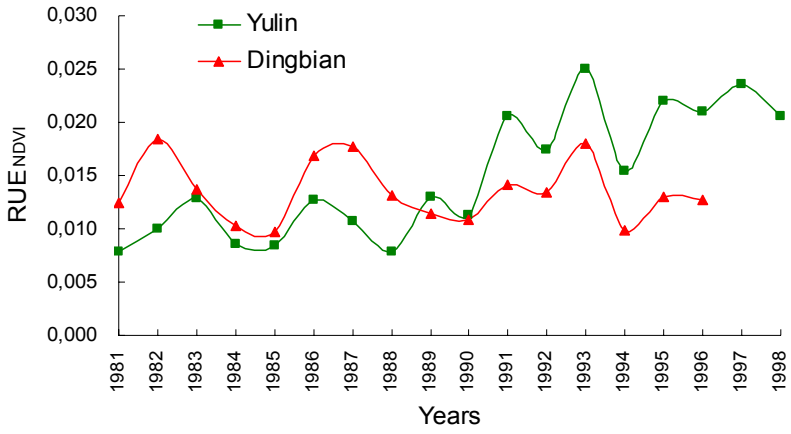

Figure 4. Rain-use efficiency at Yulin and Dingbian.

4 CONCLUSIONS

All NDVI indicators have biological meaning. Their temporal trends can be indicated by linear regression. NDVI CoV may be combined with other indicators to detect land degradation or improvement. Rain-use efficiency is a sensitive indicator that can be derived from NDVI and rainfall.

Most areas show increase in all key indices. The contrast between Yulin, where all indicators increased, and Dingbian, where all indicators decreased, is significant. Yulin is a flagship of China's land rehabilitation program; counter-measures against soil erosion include increasing vegetation cover through aerial seeding, direct planting, sand dune stabilization, and fencing and shelterbelt systems for farmland and pasture [22]. In contrast, Dingbian is blighted by the oil industry.

The indices developed here can be used as an input in an early warning system of land degradation based on NDVI data from satellites – once they are validated by field measurements.

ACKNOWLEDGEMENTS

We thank CJ Tucker, JE Pinzon and ME Brown for access to the GIMMS dataset; YS Liu, MC Runnström, B Tao and ZF Li for their valuable data; ISRIC colleagues J Hunting for assistance in ArcGIS and VWP van Engelen, GWJ van Lynden, JH Kauffman, AE Hartemink and S Mantel for discussion. ZG Bai was supported by the Fellowship Program of the Netherlands Ministry of Agriculture Nature Management and Fisheries.

REFERENCES

[1] UNCED, 1992: Managing fragile ecosystems: Combating desertification and drought. Agenda 21, Chapter 12: United Nations Conference on Environment and Development.
[2] UNEP, 2002: Global environmental outlook 3, UN Environment Programme, Nairobi/Earthscan, London.
[3] OLDEMAN, L.R., HAKKELING, R.T.A. AND SOMBROEK, W.G., 1991: World map of the status of human-induced soil degradation: an explanatory note, ISRIC, Wageningen, and UNEP, Nairobi.
[4] SELLERS, P., RANDALL, D.A., BETTS, A.H., HALL, F.G., BERRY, J.A., COLLATZ, G.J., DENNING, A.S., MOONEY, H.A., NOBRE, C.A., SATO, N., FIELD, C.B. AND HENDERSON-SELLERS, A., 1997: Modeling the exchanges of energy, water and carbon between continents and the atmosphere. *Science, 275*, pp. 502-509.
[5] PUREVDOJ, T., TATEISHI, R., ISHIYAMA, T. AND HONDA, Y., 1998: Relationships between percentage vegetation cover and vegetation indices. *International Journal of Remote Sensing, 19*, pp. 3519-3535.
[6] PARUELO, J.M., EPSTEIN, H.E., LAUENROTH, W.K. AND BURKE, I.C., 1997: ANPP estimates from NDVI for the central grassland region of the United States. *Ecology, 78*, pp. 953-958.
[7] HOLM, A.M., CRIDLAND, S.W. AND RODERICK, M.L., 2003: The use of time-integrated NOAA NDVI data and rainfall to assess landscape degradation in the arid shrubland of Western Australia. *Remote Sensing of Environment, 85*, pp. 145-158.
[8] SYMEONAKIS, E. AND DRAKE, N., 2004: Monitoring desertification and land degradation over sub-Saharan Africa. *International Journal of Remote Sensing, 25*, pp. 573-592.
[9] WESSELS, K.J., PRINCE, S.D., FROST, P.E. AND VAN ZYL, D., 2004: Assessing the effects of human-induced land degradation in the former homelands of northern South Africa with a 1 km AVHRR NDVI time-series. *Remote Sensing of Environment, 91*, pp. 47-67.
[10] TUCKER, C.J., DREGNE, H.E. AND NEWCOMB, W.W., 1991: Expansion and contraction of the Sahara Desert from 1980-1990. *Science, 253*, pp. 299-301.
[11] WRB, 2005: World reference base for soil resources, revised draft. ISRIC – World Soil Information, Wageningen.
[12] LIU, Y.S., GAO, J. AND YANG, Y.F., 2003: A holistic approach towards assessment of severity of land degradation along the Great Wall in northern Shaanxi Province, China. *Environmental Monitoring and Assessment, 82*, pp. 187-202.
[13] LI, Z., LI, X, WANG, Y., MA, A. AND WANG, J., 2004: Land-use change analysis in Yulin prefecture, northwestern China using remote sensing and GIS. *International Journal of Remote Sensing, 25*, pp. 5691-5703.
[14] TUCKER, C.J., PINZON, J.E. AND BROWN, M.E., 2004: Global Inventory Modeling and Mapping Studies (GIMMS) Satellite Drift Corrected and NOAA-16 incorporated Normalized Difference Vegetation Index (NDVI), Monthly 1981 The University of Maryland.
[15] CAO, M.K. AND WOODWARD, F.I., 1998: Dynamic responses of terrestrial ecosystem carbon cycling to global climate change. *Nature, 393*, pp. 249-252.
[16] WEISS, E., MARSH, S.E. AND PFIRMAN, E.S., 2001: Application of NOAA-AVHRR NDVI time-series data to assess changes in Saudi Arabia's rangelands. *International Journal of Remote Sensing, 22*, pp. 1005-1027.
[17] SCHLESINGER, W.H., 1991: Biochemistry: An analysis of global change. Academic Press, San Diego.
[18] PICKUP, G., 1996: Estimating the effects of land degradation and rainfall variation on productivity in rangelands: an approach using remote sensing and models of grazing and herbage dynamics. *Journal of Applied Ecology, 33*, pp. 819-832.
[19] PRINCE, S.D., BROWN DE COLSTOUN, E. AND KRAVITZ, L., 1998: Evidence from rain-use efficiencies does not indicate extensive Sahelian desertification. *Global Change Biology, 4*, pp. 359-374.
[20] NICHOLSON, S.E., TUCKER, C.J. AND BA, M.B., 1998: Desertification, drought, and surface vegetation, an example from the West African Sahel. *Bulletin of the American Meteorological Society, 79*, pp. 815-829.
[21] LE HOUEROU, H.N., 1984: Rain-use efficiency: a unifying concept in arid-land ecology. *Journal of Arid Environments, 7*, pp. 213-247.
[22] ZHU, Z. AND WANG, T., 1993: Trends of desertification and its rehabilitation in China. *Desertification Control Bulletin, 22*, pp. 27-30

'Hot Spot' Assessment of Land Cover Change in the Cwana Region using AVHRR Satellite Imagery

D. Celis[a] and E. De Pauw[a]

International Center for Agricultural Research in the Dry Areas (ICARDA), P.O. Box 5466, Aleppo, Syria (e.de-pauw@cgiar.org)

ABSTRACT

Remote sensing presents a valuable tool to get a grip on the highly complex issue of land degradation in dryland areas. The dataset obtained from the Advanced Very High Resolution Radiometer (AVHRR) NOAA satellite-based sensor is the only consistent one that permits the detection of trends in land use/land cover change at global and regional scales. At regional level a time series of AVHRR imagery could thus be used for delineating 'hot spots' of land use/land cover change within the last twenty years.

Ten-daily composites of 8km-AVHRR reflectance data, covering the period from January 1982 until December 2000, were downloaded from the NASA Web site, merged to form a complete coverage of North Africa, the Horn of Africa, West and Central Asia regions (the 'CWANA' region), and transformed into monthly NDVI composites. This temporal NDVI dataset was converted into a land use/land cover classification, using a hierarchical decision-tree, based on the average values of the mean and maximum NDVI. In a second stage the NDVI thresholds for different agroclimatic zones were adjusted to account for weather variability. Using these procedures 17 annual land cover maps were produced for each year of the period 1982-1999. This dataset was condensed into 'change' maps, using a procedure of identifying hierarchical levels of change patterns.

The analysis of the 1982-2000 AVHRR time series shows that most of the land in the CWANA region has remained stable during the period 1982-1999. Nevertheless, major changes occurred in land cover, especially in the Sahel, the Near East and in North Central Asia. Particularly the Near East has experienced a remarkable degree of intensification of agriculture, mainly by the conversion of rainfed into irrigated croplands. However, retrenchment of agriculture and natural vegetation, which are potential indicators of land degradation, but also intensification of natural vegetation, are other important trends throughout CWANA, with significant differences between subregions.

One of the study's main conclusions is that even after the year-to-year weather variations were compensated for, difficulties remained in interpreting the trends of land use/land cover changes across the region. The study underscores limitations of scale in the 'hot-spot' approach. Given the resolution of the AVHRR imagery only large-scale change patterns can be detected and changes occurring at smaller-scale, and associated degradation trends, can be masked by normal land use dynamics The study also highlights the importance of the time-frame in all degradation studies: base-line date and length of time series determine to a large extent whether we see deterioration, improvement, cycles or stable conditions. The main advantage of the 'hot spots' approach is that it allows zooming into 'target areas', thus achieving considerable savings in time and financial resources. However, due to the low resolution of the imagery, there are considerable limitations to what can be seen. For this reason, a second assessment stage is necessary, in which the 'hot spots' are further characterized using ground-based observation networks complemented with high-resolution satellite imagery, such as Landsat or SPOT.

1 BACKGROUND

Land degradation is a serious threat to the prosperity of rural populations in dryland areas. Its assessment is hampered by both fundamental and operational problems. First, in most cases land degradation is a creeping phenomenon: it takes time to reach a degraded state. As a result, most of the degradation has already often occurred before the start of the observation period. In addition, it is not always easy to distinguish processes related to aridity and natural climatic fluctuations from human-induced negative trends. For example, changes in biomass, salinity and sand movement may be associated with wet and dry periods rather than human influence. A second problem is one of shortage of reliable basic data on the extent and severity of land degradation, and a third one is the difficulty of harmonizing land degradation information across national and even local boundaries.

The International Center for Agricultural Research in the Dry Areas (ICARDA) deals with germplasm enhancement and natural resource management issues, including land degradation in drylands. Its current mandate region includes North Africa, West Asia, Central and South Asia, and the Horn of Africa. For convenience this area is abbreviated as CWANA (= Central Asia + West Asia + North Africa). In a dryland region, as huge and diverse as CWANA, with limited reliable ground-based resource inventories and monitoring systems, remote sensing presents a highly valuable tool to get a grip on the highly complex issue of land degradation. The main goal of this study is to use remote sensing for the detection of large-scale (regional to sub-continental) land use change trends and to assess whether any such trends can be associated with degradation. To achieve regional coverage for a substantial number of years, the system of the NOAA[1] Advanced Very High Resolution Radiometer (AVHRR) satellites has been selected.

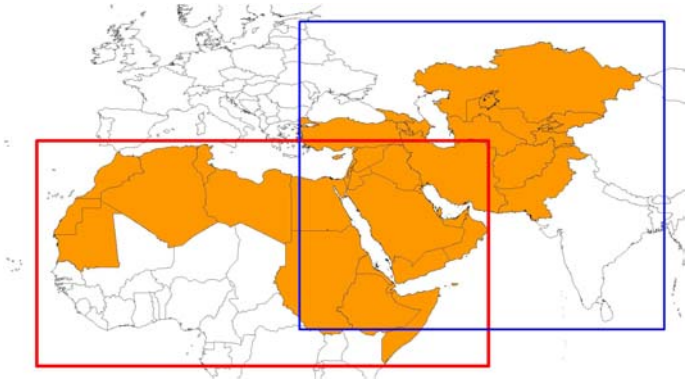

Figure. 1. Location AVHRR subsets.

2 METHODOLOGY

Six hundred and twelve 10-daily composites of 8km-AVHRR reflectance data, covering the period from January 1982 until December 2000, were downloaded from the relevant NASA Web site for band 1 (0.58-0.68 µm.) and band 2 (0.725 – 1.1 µm.). No complete time series was available for the year 1994. These data consisted of separate subsets for Africa (top left: 37.9 N, -20 W; lower right -2 S, 59.9 E) and Asia (top left 59 N, 26.5 E; lower right 4.5 S, 91 E), in 16-bit unsigned format and in Goode's Homolosine Interrupted Space projection. The data were imported as layer stacks and both subsets were mosaiced to form a complete coverage of the CWANA-region (Fig.1). The Normalized Difference Vegetation Index (NDVI) was calculated and aggregated into monthly NDVI composites in order to reduce the effects of cloud cover. Additional corrections for noise and sensor drift were made, as well as conversion to geographic projection and merger into a single CWANA-dataset.

In order to convert this temporal NDVI dataset into a land use/land cover classification, two procedures were developed. The first procedure consisted of an empirical hierarchical decision-tree, which was developed for average weather conditions [1], using as differentiating criteria the maximum and mean NDVI, the agroclimatic zone, the period of the dry season and the latitude zone (figure 2).

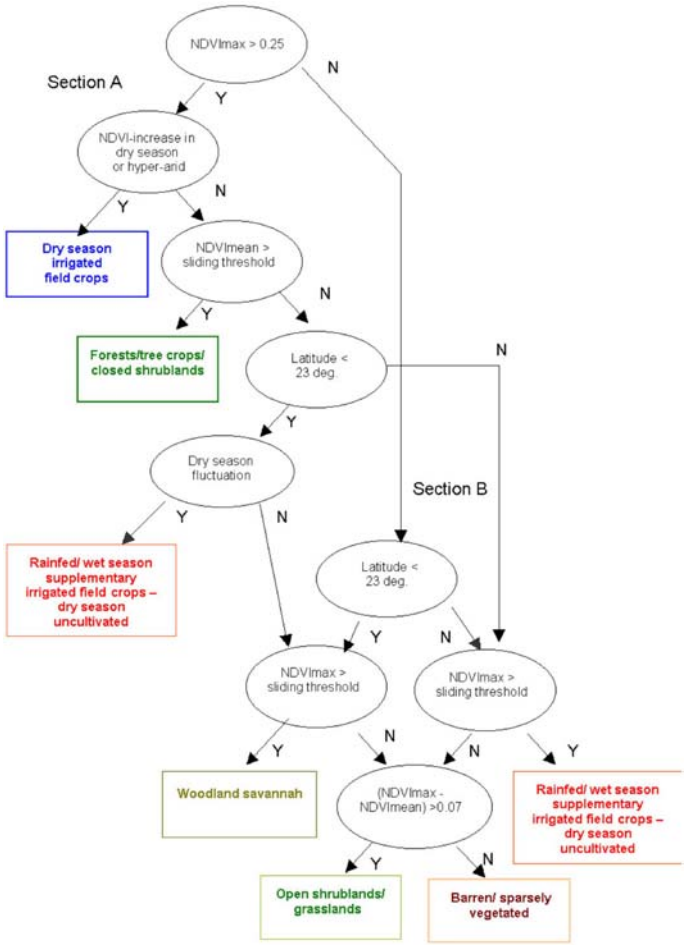

Figure 2. Hierarchical decision-tree for land use/land cover assessment.

[1] National Oceanic and Atmospheric Administration

To account also for the fact that in any particular year the actual weather can differ substantially from the average, a second procedure was developed. The NDVI is particularly sensitive to variations in weather, particularly precipitation and winter temperature (figure 3). As the NDVI thresholds used in the decision-tree apply to average climatic conditions, there is the risk that a given LULCT might be misclassified, if weather conditions at a given place deviated substantially from normal.

In order to adjust the NDVI thresholds for different weather conditions at a given location, the entire region was subdivided into 152 zones with homogeneous climatic conditions (figure 4) by using the UNESCO classification for Arid Zones [2]. For each zone the average NDVImax for the time series was determined. On this basis a threshold adjustment factor was established as follows:

$$Actual\ threshold_{\,year\ i,\ zone\ j} = Average\ threshold_{\,zone\ j} * \frac{\left[NDVI_{\max}\right]_{year\ i,\ zone\ j}}{\left[Average\ NDVI_{\max}\right]_{zone\ j}} \qquad (1)$$

Example: Zone j has an average $NDVI_{mean}$ threshold of 0.8 for the class 'Forests/tree crops/closed shrublands'. The average $NDVI_{max}$ in zone j is 0.66 and the $NDVI_{max}$ for 1982 is 0.74, which reflects better then average growing conditions. So for a correct classification the $NDVI_{mean}$ threshold also has to be higher. Following the above equation it will be equal to 0.897.

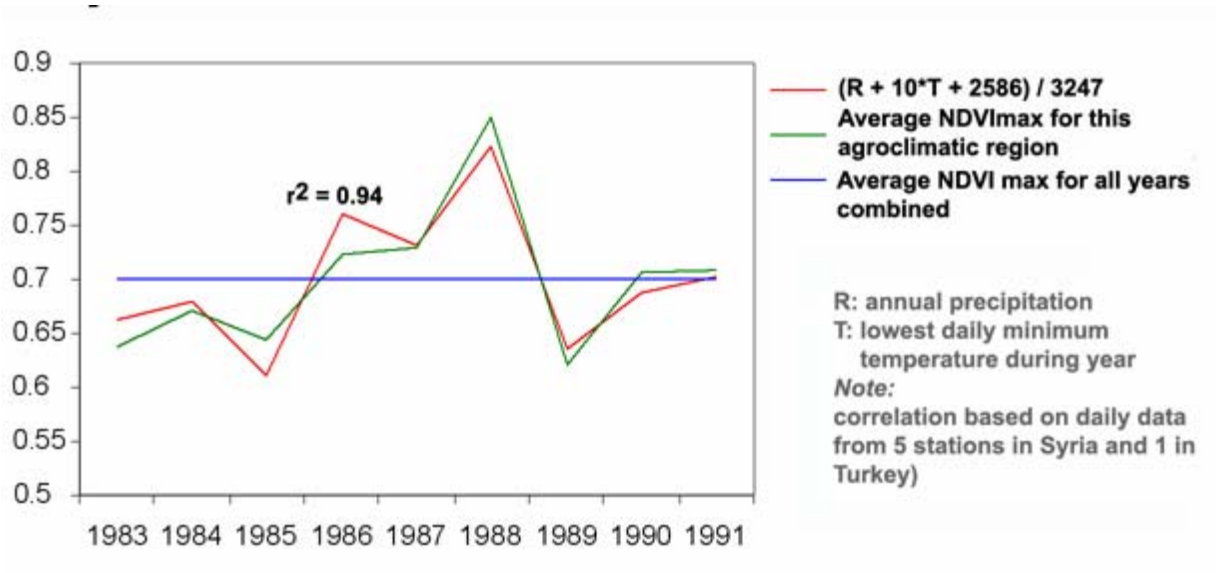

Figure 3. Agreement between average NDVImax and a linear combination of average annual rainfall (R) and minimum temperature of the coldest month (T) for 6 stations in the red-bounded agroclimatic zone of figure 4.

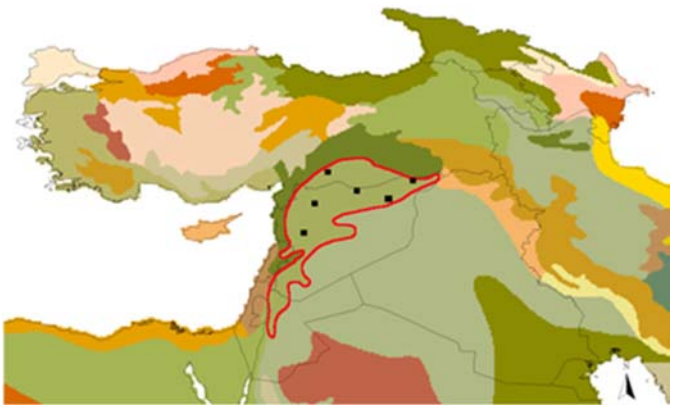

Figure 4. Local zones with homogeneous agro-climatic conditions in West Asia.

Using the above algorithm for land use/land cover classification, 17 annual land cover maps were produced by running the decision-tree algorithm with the annually adjusted NDVI thresholds for each year in the period 1982-1999. This dataset was further condensed into four maps, showing the majority land cover classes for the following three-year key periods: 1982-1984, 1987-1989, 1992-1994, and 1997-1999. For each of the sampled three-year periods the majority land cover type in each pixel was retained. If the three years had three different classes, the pixel was classified as 'noise'. Fig.5 illustrates this process for the region around Syria's northwestern border with Turkey, using the period 1987-1989.

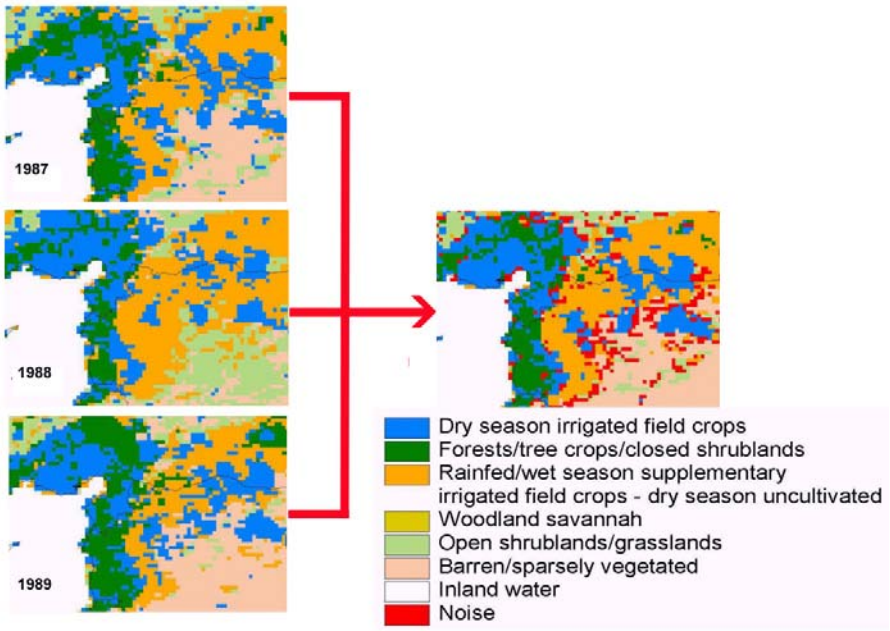

Figure 5. Majority land cover classes for different years, subset northwest Syria (on the left the land cover classes for the years 1987, 1988, 1989; on the right the majority land cover class).

Depending on the value and sequence of this majority land cover type, the following kinds of change were allocated to each pixel: *noise, stable land use/land cover, stable land use/land cover mosaic and change pattern* (table 1).

Seventeen stable classes were recognized, as well as 66 change combinations, which were regrouped into 22

Table 1. Decision rules for change detection

1) If all four classes are equal, the land cover remains stable. e.g. A A A A; B B B B
2) If a permanent change occurs from one class to another, a change class results; e.g. A B B B; A A B B; A A A B; B A A A; B B A A; B B B A
3) If the change from one class to another is not permanent, the combination is interpreted as a stable mosaic of both classes. e.g. A A B A; A B A A; A B A B; A B B A; B B A B; B A B B; B A B A; B A A B
4) If there are three or four different classes or a 'noise' class (E), the classification is 'noise'. e.g. A B C A; A B C D; A E A A; A A B E

change classes and four change trends. The 17 stable classes are shown in Fig.6. for parts of West Asia.

The 66 change combinations refer to the transition patterns from one LULCT to another between the four key periods. For example, if the LULCT "irrigated croplands" is coded "1", "Forest/Tree crops" is coded "2", and "Rainfed croplands" is coded "3", the change combination "1113" stands for "transition from irrigated to rainfed crops in the period 1992-94" and the change combination "2111" stands for "transition from forest/tree crops to rainfed crops in the period 1987-89".

At a higher level, the change combination 1113 also corresponds with the change class "Irrigated > Rainfed cropland", and the change combination "2111" with the change class "Forest > irrigated cropland".

The four change trends differentiated are: *'intensification of agriculture', 'intensification of natural vegetation', retrenchment of agriculture'*, and *'retrenchment of natural vegetation'*). Examples of 'intensification of agriculture' are the transitions from *Barren* to *Irrigated*, from *Forest* to *Rainfed*, or from *Rainfed* to *Irrigated*. Examples of 'intensification of natural vegetation' are the transitions from *Barren* to *Grassland*, or from *Savannah* to *Forest*. Examples of 'retrenchment of agriculture' are the transitions from *Irrigated* to *Barren*, from *Rainfed* to *Grassland*,

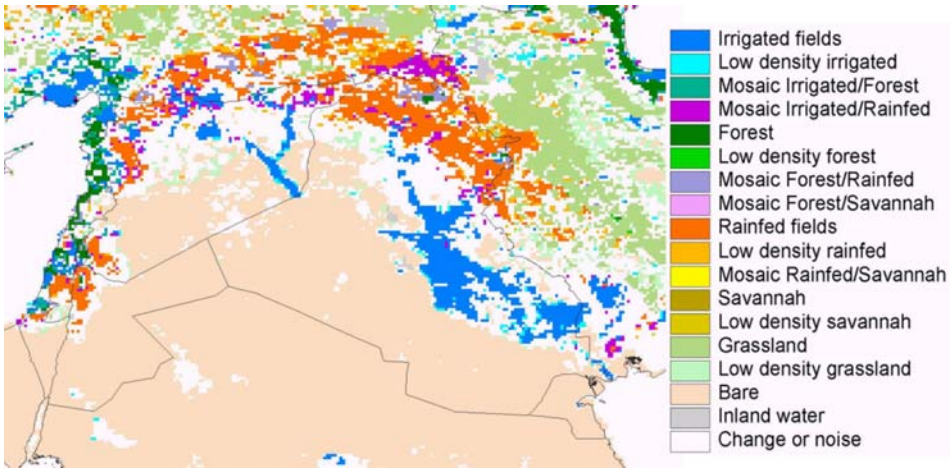

Figure 6. Stable classes for parts of West Asia.

or from *Irrigated* to *Rainfed*. Examples of 'retrenchment of natural vegetation' are the transitions from *Forest* to *Grassland*, or from *Grassland* to *Barren*.

Both *Intensification* and *Retrenchment* change trends may be associated with particular forms of land degradation. Intensification could, for example, be associated with deforestation, or be supported by depleting non-renewable water resources. On the other hand, the retrenchment trend could be associated with depleted water resources, salinization, loss of fertility, conversion of forest to grasslands etc. The large-scale change mapping will not provide specific answers, only point to areas where substantial change in the rural environment has taken place during the period 1982-1999.

3 RESULTS

On the basis of this hierarchical classification 'change maps' were prepared for eight subregions in CWANA, and areas belonging to individual change combinations, change classes and change trends were calculated. The eight sub-regions for which change maps were prepared are: the Maghreb, Northeast Africa, the Sahel and Horn of Africa, the Arabian Peninsula, West Asia and the Caucasus, Southwest Asia, South Asia and Central Asia. An

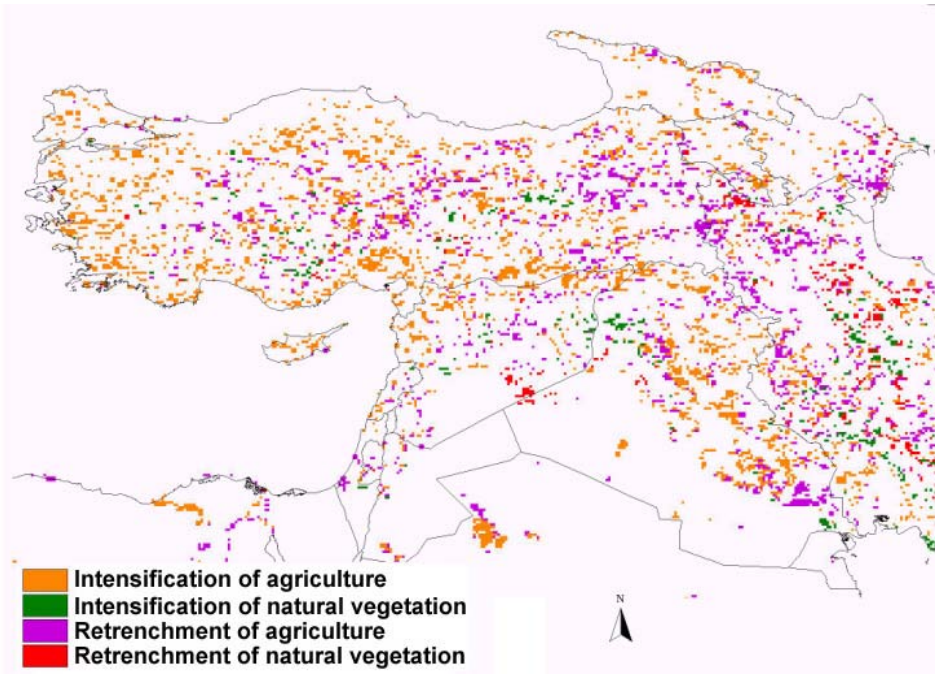

Figure 7. Spatial distribution of land cover change trends in the Near East and the Caucasus.

example of a 'change map' is shown for the West Asia and Caucasus region in figure 7. The results are also summarized in table 2.

Table 2. Summary of land cover/land use stability and change trends 1982-1999 in CWANA by sub-region (areas in sq.km).

Sub-region	Stability/Change			Change trends			
	Stable	Change	Noise	IA	RA	INV	RNV
North-West Africa	2,907,004	83,712	203,328	50,816	22,400	7,040	3,456
North-East Africa	2,554,686	19,392	21,632	6,464	11,840	256	832
Africa Sahel	4,232,252	749,824	458,368	125,504	80,768	422,592	120,960
Arabian Peninsula	2,636,992	105,408	34,240	52,928	34,048	15,360	3,072
West Asia	1,024,512	218,112	296,512	137,088	63,488	11,392	6,144
Caucasus	114,688	19,520	52,224	11,840	6,976	64	640
South-West Asia	2,810,688	368,576	444,352	116,032	159,680	56,448	36,416
Central Asia	2,754,040	431,872	272,320	147,520	125,248	111,040	48,064
TOTAL CWANA	19,034,862	1,996,416	1,782,976	648,192	504,448	624,192	219,584

Notes: IA: intensification of agriculture; RA: retrenchment of agriculture; INV: intensification of natural vegetation; RNV: retrenchment of natural vegetation.

Regional trends

In terms of land area, the most dramatic changes in land cover have occurred in the Sahel, followed by North Central Asia. In the former region approximately 750,000 km^2 changed from one land cover to another, in the latter 430,000 km^2. In relative terms, the regions where the most change occurred are the Middle East and the Sahel, where about 14% of the land cover changed. Despite these significant changes, even in the regions with the highest change in land cover, most of the land has remained stable.

Subregional trends

At the level of the sub-regions the nature and extent of the changes can be quite different.

North-West Africa

The main trend was *intensification of agriculture*. This occurred mostly through deforestation to develop irrigated and rainfed cropland in the coastal zone, and by converting bare land into irrigated croplands inland. A second trend involved a *retrenchment of agriculture*, which occurred inland, where both rainfed and irrigated fields were taken out of cultivation to become barren/sparsely vegetated areas.

North-East Africa

The only noticeably trends are *retrenchment of agriculture* on the right bank of the Nile and *intensification of agriculture* on the western part of the Nile delta due to a new irrigation development.

Sahel

The major trend detected was an *intensification of natural vegetation*, mainly in the form of a change from barren/sparsely vegetated areas to grasslands/open shrublands, but also the transition from grasslands/open shrublands into woodland savannah. The likely reason for this change was a recovery of the natural vegetation after the drought experienced in the Sahel between 1961 until 1984 was followed by a period with normal rainfall [2],[3]. The northward shift of the desert boundary after 1984, also described by Tucker [3] can therefore be interpreted as a regeneration of the grasslands/open shrublands when rainfall returned to normal after the long drought cycle. *Intensification of agriculture* occurred in Southwest Sudan and West Ethiopia, in the form of a change from rainfed field crops to tree crops or from woodland savannah to rainfed field crops. In the center of both Sudan and Ethiopia, a *retrenchment of agriculture* occurred, mainly in the form of a change from rainfed field crops to woodland savannah.

Arabian Peninsula

During the period 1982-1999 two contrasting trends of land cover change are observed. A first trend, *intensification of agriculture*, is due to the fact that since 1982 huge areas were converted into irrigated croplands, mostly in Saudi Arabia, by tapping pumping fossil water. The second trend, *retrenchment of agriculture*, is caused by the fact that large irrigated areas were also taken out of cultivation in Saudi Arabia, probably due to the depletion of the fossil aquifers and policy changes in respect of groundwater use. The observed *intensification of natural vegetation* at the edges of the Asir and Yemen Highlands, in the form of a change from barren/sparsely vegetated areas to grassland/open shrublands, is probably also related with increased rainfall after the Sahelian drought.

West Asia and Caucasus

In relation to its size, West Asia is the sub-region with the highest degree of land cover change in the period 1982-1999. Of the different change trends, *intensification of agriculture* is the most important one. Intensification occurred both towards irrigated as rainfed cropland. At the coasts of Turkey and Syria deforestation occurred to establish irrigated fields, in North-East Syria rainfed cultivation intensified to irrigated cultivation, and in Iraq barren/sparsely vegetated areas were taken into irrigation. In central Turkey, grasslands/open shrublands were taken into rainfed cultivation. *Retrenchment of agriculture* occurred mostly in inland Turkey, in the form of a change from rainfed cultivation to grasslands/open shrublands, and in Iraq in the form of irrigated fields taken out of cultivation by change to barren/sparsely vegetated areas.

In the Caucasus *intensification of agriculture* occurred mostly in the form of a change from rainfed fields to either tree crops or irrigated fields. A retrenchment of agriculture occurred mainly in the form of a change from irrigated fields to rainfed fields or from rainfed fields to grasslands/open shrublands.

South-West Asia

The main trend in Southwest Asia is one of *retrenchment of agriculture* and is particularly noticeable in Pakistan, where irrigated croplands reverted to barren/sparsely vegetated areas, whereas in Afghanistan the conversion was mostly into grasslands/open shrublands.

Central Asia

In Central Asia *intensification of agriculture* occurred mostly in the form of a change from grasslands/open shrublands into rainfed cultivation. The inverse trend, a change from rainfed cultivation to grasslands/open shrublands, is the major component of the *retrenchment of agriculture*. *Intensification of natural vegetation* is another important trend, due mostly to the change from sparsely vegetated areas to grasslands/open shrublands. This intensification trend is very noticeable in South-West Kazakhstan near the Caspian Sea. The inverse trend, a change from grasslands/open shrublands into barren/sparsely vegetated areas is particularly clear in Central Kazakhstan.

4 CONCLUSIONS

Even after the year-to-year weather variations were compensated for and taking into account the local knowledge about some large-scale change trends, it is still difficult to understand the causes of the land use/land cover changes. An intensification of agriculture is the easiest to interpret because it is always human induced, whereas a retrenchment of agriculture can have three possible causes: a long term weather change, a lack of inputs to maintain the cultivation or a degradation of the natural resource base (too intensive use of natural resources). Both the intensification and the retrenchment of natural vegetation could be either human-induced or result from a longer-term change in weather. The identification of a trend towards denser natural vegetation proves the possibility of natural regeneration and puts the issue of land degradation in a more cyclical perspective.

The study underscores some of the (unsurprising) limitations of the 'hot-spot' approach. The issue of scale is probably the most important. Given the resolution of the AVHRR imagery, with one pixel covering approximately 64 km^2, it is obvious that only large-scale change patterns can be detected. This implies that changes occurring at smaller-scale, and associated degradation trends, can be masked by normal land use dynamics (e.g. fluctuations in the land use patterns, particularly in response to rainfall fluctuations). This inability to detect small-scale changes could entail a tendency to under-estimate land use change and associated degradation trends.

The study also highlights the importance of the time-frame in all degradation studies: base-line date and length of time series determine to a large extent whether we see deterioration, improvement, cycles or stable conditions

The main advantage of the 'hot spots' approach is that it allows zooming into 'target areas', thus achieving considerable savings in time and financial resources. However, due to the low resolution of the imagery, there are

considerable limitations to what can be seen. For this reason, a second assessment stage is necessary, in which the 'hot spots' are further characterized using ground-based observation networks complemented with high-resolution satellite imagery, such as Landsat or SPOT.

REFERENCES

[1] CELIS, D. AND DE PAUW, E., 2003: Assessment of land cover/ land use in CWANA region using AVHRR imagery and agroclimatic data. Research Report. ICARDA, Aleppo, Syria

[2] UNESCO, 1979 : Map of the world distribution of arid regions. Map at scale 1:25,000,000 with explanatory note. UNESCO, Paris, 54 pp.

[3] HELLDEN, U., 1988: Desertification monitoring: Is the desert encroaching? *Desertification Control Bulletin 17*, pp. 8-12.

[4] TUCKER, C.J., DREGNE, H.E. AND NEWCOMB, W.W., 1991: Expansion and contraction of the Sahara Desert between 1980 and 1990. *Science 253*, pp. 299-301.

Wavelet time-series analysis to assess and monitor pasture condition using low resolution remote sensing data

C. De Pus[a], E.I. Ducheyne[b] and R.R. De Wulf[c]

[a] Lijn Dataproducten, VLM-Ondersteunend Centrum GIS-Vlaanderen, Gebroeders Van Eyckstraat 16,9000 Ghent, Belgium; email: Claudia.DePus@vlm.be
[b] Avia-GIS, Risschotlei 33, 2980 Zoersel, Belgium, email: educheyne@avia-gis.be
[c] Laboratory of Forest Management and Spatial Information Techniques, Ghent University; Coupure Links 653, 9000 Gent, Belgium

ABSTRACT

Remote sensing has greatly increased the potential for developing land degradation assessment methods in the vast Australian rangelands. Whereas former research mainly focused on quantitative assessment of range condition, the pasture quality plays an important role in the Mitchell grass downs, where pastures contain a mixture of annual and perennial species. Under continued heavy grazing, palatable perennial grasses can be damaged and even replaced by annual species. These annual species however loose their nutritious value quickly during the dry season and cannot protect against soil erosion.

This study aims at separating annual and perennial grasses based on their different response to rainfall events by analyzing their behaviour throughout the growing season. To this end, 9-day cloud free vegetation index composites were created for a period from 1992 until 2003. From these composites, time-series for typical annual and perennial dominated sites were derived. Seasonal parameters were extracted from these time-series and compared. Multi-resolution wavelet analysis was applied for further analysis of the signals. Small differences in the timing of the growing season were observed for annual and perennial dominated pixels when their respective benchmark areas were located close to each other. However when the benchmark areas were at some distance from each other, differences in received rainfall masked the influence of the dominant grass type. No consistent differences in NDVI amplitude could be detected, but wavelet analysis results pointed at a higher variability of the NDVI at annual sites.

Keywords: rangeland monitoring, NOAA AVHRR, time-series analysis, wavelets, TIMESAT, annual grasses, perennial grasses, pasture condition

1 INTRODUCTION

Assessment of range condition is a priority for the management of Australia's pastoral lands [1]. Rangeland monitoring using ground based methods suffers from a lack of accurate and repeatable techniques capable of separating grazing impact from both seasonal variability and landscape heterogeneity [2]. Remote sensing, offering readily available space borne data at a reasonable cost, has greatly increased the potential for developing land degradation assessment methods [3], [4].

Land degradation has been defined as a 'reduction in the capacity of landscapes to produce vegetation cover from rainfall' [2]. Assuming that cattle production is limited mainly by fodder quantity, this would directly influence the livestock production levels. This assumption does not hold for the bioregion of the Mitchell grass downs where pastures contain a mixture of annual and perennial species, with Mitchell grasses (*Astrebla* spp.) being the most abundant perennial. Under conservative grazing practices, Mitchell grass withstands extended periods of both grazing and drought. It is one of the most nutritious pasture species to be found in the Australian tropical savannas and no other grasses, in terms of productivity or hardiness, can outclass Mitchell grass. One of its most valuable attributes is that it hays off quickly while still providing nutritious fodder. Mitchell grass tussocks also recover well after the dry season grazing when the next rains arrive. However, Mitchell grass country can become degraded if stocking rates are heavy. This degradation is enhanced when there is a series of years with more than below average rainfall conditions [5]. Under continued heavy grazing the tops and root systems of palatable perennial grasses become smaller, the rate growth slows down and the remaining tillers produce less seed. The perennials will then be replaced by short-lived annuals, increasing the pressure on the remaining perennial tussocks and consequently the pasture composition changes even further [6]. Though composition change is less

obvious than a cover change, a shift between different dominant vegetation types does has a significant impact on pasture condition.

A possible means of distinguishing between annual and perennial species using remote sensing can be based on their different behaviour throughout the growing season. Annuals react on a rainfall trigger with a steep increase in greenness. They have a short growing cycle and hay off quickly. Perennials on the other hand show a slower biomass increase after rainfall and are characterized by a longer growing season. Annuals usually reach a higher greenness during their growing peak and a lower minimum at the end of the dry season than the perennials. Additionally, the growth pulse of annuals is more dependent on the rainfall quantity and therefore the greenness variability throughout the years is likely to be higher than for the perennials [7].

This study investigates if annual dominated and perennial dominated sites can be separated based on their growing characteristics through the analysis of a remote sensed derived time-series. Data from the National Oceanic and Atmospheric Administration (NOAA) Advanced Very High Resolution Radiometer (AVHRR) have shown their suitability for vegetation monitoring. Because of their daily acquisition and comprehensive record they offer the possibility of building long term time-series. Most rangeland monitoring studies use vegetation indices as the basis for their time series. The Normalized Difference Vegetation Index (NDVI) is the most widely used because of its relation with the greenness of the vegetation [8].

In the next section, the study area will be described. This will be followed by a section on image preprocessing. In the fourth section the methodology is outlined, which is then followed by the results and discussion in section 5. In the final section, the main conclusions are drawn.

2 STUDY AREA AND BENCHMARK SITES

The study area of Newcastle Waters is a 10 000 km² breeding property in the west Barkly region of Australia's Northern Territory (figure 1), located between 130 and 138° E and between 15 and 20° S. The climate is monsoonal with most of the rainfall coming in from the Gulf region. Nearly all rainfall occurs during the hot summer months, November to April, with the highest incidence in January and February. The average annual rainfall in Newcastle Waters is around 500 mm but this quantity can be highly variable in time and space.

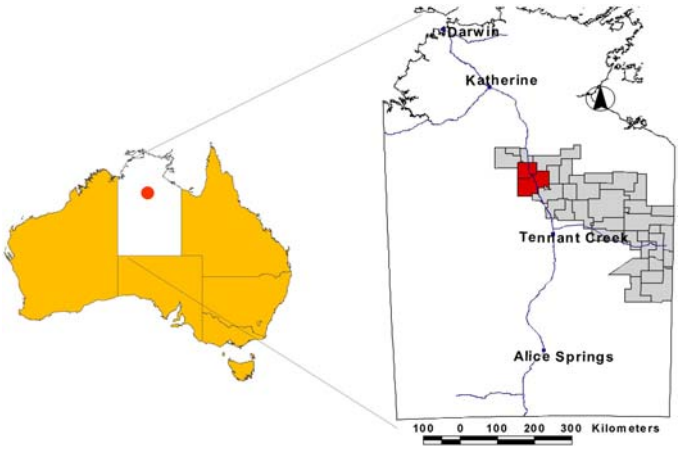

Figure 1. Study area (red) in Australia with zoom in on the Northern Territory and the Mitchell Grass Downs (grey).

The Newcastle Waters Station is situated at the edge of the Mitchell Grass Downs bioregion. Most of the bioregion features heavy cracking clay soils resulting from swamp and other alluvial depositions during the Tertiary period. Smaller areas of limestone with calcareous desert soils and lateritic plains with red earths and red sands are also present. The bioregion is dominated by Mitchell grass (*Astrebla* spp.) tussock grasslands on rolling plains with some low tree overstory of gidgee (*Acacia cambagei*) and other species although the area is generally characterized by a lack of tree and shrub cover. The Mitchell grass grassland occurs on the deep cracking clays over tertiary alluvium[5].

In order to identify benchmark areas with predominant annual or perennial species, a field survey was conducted in September 2004, to estimate total and perennial cover in the grasslands. By combining these field measurements with historical and management information four benchmark areas were delineated, two of them

dominated by annual grasses and the other two dominated by perennial grasses (figure 2). Sites A1 and P1 are located next to each other. As A1 is close to a permanent waterhole, the grazing pressure is considered to be much higher there than in P1 located further away. Site A2 is located close to an old water bore and to the old stocking route. Grazing pressure has hence always been very high resulting in a very low perennial cover. Site P2 was not visited during the fieldwork but was suggested as perennial dominated benchmark area by the station's staff.

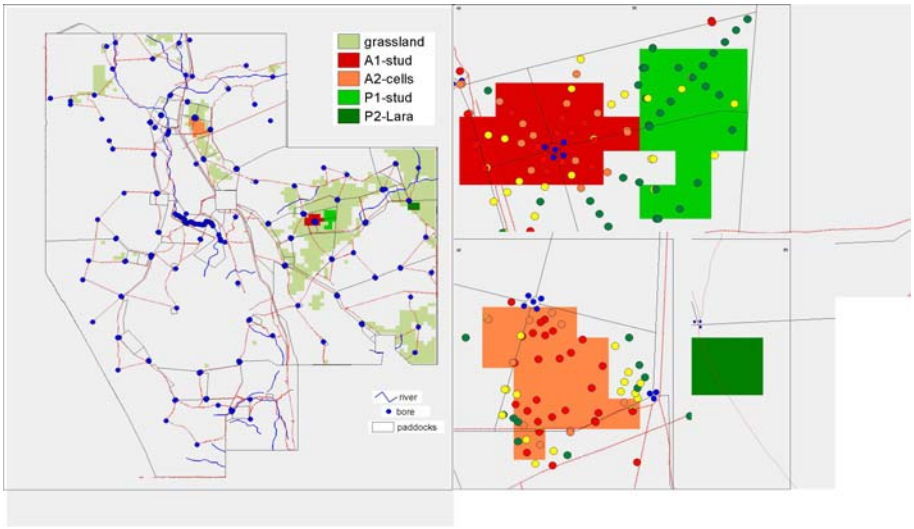

Figure 2. Selection of benchmark sites with dominant annual grasses (A1, A2) and with dominant perennial grasses (P1, P2)? Circles refer to field estimates of perennial cover (red: 0-15%, orange:15-30%, yellow 30-50%, green 50-100%).

3 SATELLITE DATA AND TIME-SERIES EXTRACTION

A series of NOAA AVHRR data was ordered from the CSIRO Earth Observation Centre. The EOC 1 km stitched dataset was georeferenced and calibrated upon delivery [9]. The data consists of daily acquisitions over a period of 12 years (table 1) and covers the complete study area. Each acquisition contains multiple bands: AVHRR band 1-5, sun and satellite view, sun zenith angle and a cloud mask.

Table 1. NOAA AVHRR dataset.

	Number of acquisitions	start date	end date
NOAA 11	1331	01/04/1992	30/08/1994
NOAA 14	3168	01/02/1995	31/10/2000
NOAA 16	1519	12/10/2000	17/07/2003

Nine-day NDVI composites were created by selecting cloud-free pixels with optimal viewing geometry and optimal atmospheric conditions. Optimal viewing geometry was defined as a satellite zenith angle smaller than 30° and a sun zenith angle smaller than 60° [10],[11]. As atmospheric disturbances tend to decrease the NDVI, optimal atmospheric conditions are met for pixels with a maximal NDVI [12]. A two step compositing algorithm first selected all cloud-free pixels with an optimal viewing geometry. Consequently, the pixel with the maximum NDVI was retained. If no cloud-free pixels with optimal viewing geometry where available for a certain period, the pixel with the smallest zenith angle was selected. During the compositing process a quality band was created for each period, assigning a quality label for each pixel depending on its cloud status and acquisition geometry. After compositing, atmospheric corrections were performed using the Simplified Method for Atmospheric Corrections (SMAC) [13].

NDVI time-series between 1993 and 2003 were extracted for all pixels in the benchmark areas. To reduce the remaining noise and to interpolate the missing data due to persistent cloud cover an adaptive Savitzky-Golay filter was applied to the time-series. The adaptive Savitzky-Golay filter method is a least-squares method that uses local polynomial functions in the fitting of a noisy time-series to the upper envelope [14]. The method was developed by by Jönsson and Ekhlund [15] and implemented in TIMESAT with the purpose of automated extraction of

seasonality information from time-series of satellite sensor data [15],[16]. The Savitzky-Golay filters in a moving window and a quadratic polynomial function is fitted to all data values within this window using a least squares method. Subsequently, the central window value is replaced with the data value of the polynomial at that position. The quality information generated during the compositing process was incorporated to determine the weight of the pixel values within the moving window, when calculating the best fitting polynomial. The half window size was set to 5 periods but can be locally reduced or increased in case of strong variation or when the amount of missing values in the window exceeds a pre-determined threshold respectively. Figure 3 shows the result of a filtered time-series.

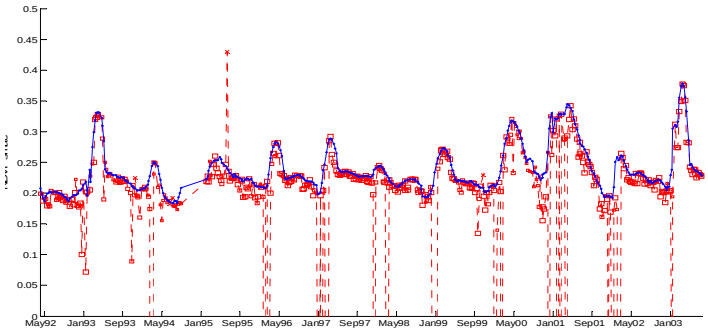

Figure 3. Filtering of raw timeseries with Savitzky-Golay Filter (raw series = red, filtered series=blue).

4 METHODOLOGY

4.1 Extraction of Seasonality Parameters

The TIMESAT program [16] was used for extraction of the seasonality parameters (Table 2). Parameters were extracted for all pixels of the benchmark sites to check for differences in seasonality between the annual and perennial time-trajectories. Mean values of the benchmark sites were compared and statistical tests were performed to check for statistical differences.

Table 2. TIMESAT growing season parameters.

Parameter	Description
Sg 1	Time for which the left edge has increased to the 10% level
Sg 2	Time for which the left edge has increased to the 90% level
Sg 3	Time for which the right edge has increased to the 10% level
Sg 4	Time for which the right edge has increased to the 90% level
Sg 5	Average of left and right minimum values
Sg 6	Time for the peak of the season
Sg 7	NDVI value for the peak
Sg 8	Seasonal amplitude
Sg 9	Asymmetry coefficient
Sg 10	Large seasonal integral
Sg 11	Small seasonal integral
Sg 12	Number of annual growing seasons

4.2 Multiresolutional Wavelet Analyis

As the annual vegetation is expected to show a sharper and shorter NDVI peak, the time-series can also be compared by looking at the spectral content. A Fourier representation reveals the spectral content of a signal but makes it impossible to recover the particular moment in time where a certain change in time has occurred. This

makes the Fourier representation inadequate when it comes to analyzing non-stationary signals. Similar to the Fourier transform, the wavelet transform performs a decomposition of a signal on a basis of elementary functions, called wavelets. The wavelet representation, however, is able to provide localization in both the time and space domain and is therefore better suited for the analysis of NDVI signals that respond to the highly variable rainfall. When performing a wavelet transform of a signal, a particular mother wavelet is chosen and shifted along the signal. At the same time the correlation of the signal with the scaled and shifted mother wavelet is determined. Correlations at large scales reveal large features, while fine signal structures are discovered at smaller scales. The shift and scale of the mother wavelet can vary continuously (continuous wavelet transform) or in discrete steps (discrete wavelet transform) [17], [18].

In this study a discrete non-decimated wavelet transform using the quadratic spline wavelet of Mallat and Zhong [19] was applied to decompose the NDVI-signal of all pixels of the benchmarks sites up to 5 scales. The quadratic cubic spline wavelet is a non-orthogonal, symmetrical wavelet with a compact support and a high number of vanishing moments, making it suitable for the analysis of smooth, continuous input signals [18],[20].

For each pixel belonging to a benchmark site the sum of the absolute values of the wavelet coefficients at the five levels (scales) was calculated. These sums were compared for pixels belonging to an annual benchmark site and pixels belonging to a perennials benchmark site.

5 RESULTS & DISCUSSION

5.1 Seasonality Parameters

The annual and perennial seasonality of sites A1 and P1 respectively show consistent patterns over the years for a number of parameters (table 3). The left 10% and 90% level, the right 10% level and the time of the peak NDVI occur later for the perennial grasses than for the annual grasses. This can be expected as annual grasses respond much stronger to rain, reach their maximum NDVI earlier, and then decline earlier than perennial grasses [7]. However the observed differences are small and not always significant statistically.

Table 3. Comparison of extracted seasonality parameters per year for A1-P1 and A2-P2.

		sg1	sg2	sg3	sg4	sg5	sg6	sg7	sg8	sg9	sg10	sg11
A1P1	1993	p>a	p>a	a>p	a>p	p>a	a>p	a>p	a>p	a>p	a>p	a>p
	1994	p>a	p>a	a>p	a>p	p>a	p>a	p>a	p>a	p>a	a>p	a>p
	1996	p>a	p>a	a>p	p>a	p>a	p>a	a>p	a>p	p>a	a>p	a>p
	1997	p>a	p>a	a>p	p>a	a>p	p>a	p>a	p>a	p>a	a>p	a>p
	1998	p>a	p>a	p>a	p>a	a>p	p>a	p>a	p>a	a>p	a>p	p>a
	1999	p>a	p>a	p>a	p>a	a>p	p>a	a>p	a>p	p>a	a>p	p>a
	2000	p>a	p>a	a>p	p>a	p>a	p>a	a>p	a>p	p>a	a>p	a>p
	2001	p>a	p>a	a>p	p>a	p>a	p>a	a>p	a>p	p>a	a>p	a>p
	2002	p>a	p>a	a>p	p>a	p>a	p>a	a>p	a>p	p>a	a>p	a>p
	2003	a>p	p>a	a>p	a>p	a>p	p>a	p>a	p>a	p>a	a>p	a>p
A2P2	1993	p>a	p>a	p>a	p>a	p>a	p>a	a>p	a>p	a>p	a>p	a>p
	1994	a>p	a>p	p>a	a>p	p>a	a>p	p>a	p>a	a>p	p>a	p>a
	1996	a>p	a>p	p>a	a>p	a>p	a>p	p>a	p>a	a>p	p>a	p>a
	1997	p>a	p>a	p>a	p>a	p>a	p>a	p>a	a>p	a>p	p>a	a>p
	1998	p>a	p>a	a>p	p>a	p>a	p>a	a>p	a>p	p>a	a>p	a>p
	1999	a>p	p>a	p>a	p>a	p>a	p>a	p>a	a>p	p>a	p>a	a>p
	2000	p>a	p>a	a>p	p>a	p>a	p>a	a>p	a>p	a>p	a>p	a>p
	2001	a>p	a>p	p>a	a>p	a>p	a>p	p>a	p>a	a>p	p>a	p>a
	2002	a>p	a>p	p>a	a>p	a>p	a>p	p>a	p>a	a>p	p>a	p>a
	2003	a>p	a>p	p>a	a>p	p>a	a>p	a>p	a>p	a>p	a>p	a>p

The differences between the A2 and P2 sites are stronger but less consequent through the years. This can be explained by the fact that A2 and P2 are at a larger distance from each other and experience a different rainfall regime. Most likely the stronger differences are caused by differences in quantity and timing of rainfall between the two sites, influencing the NDVI time trajectories more than the difference in dominant grass type. For none of the two groups consistent differences in peak or minimum NDVI were observed.

The timing of the growing season is strongly dependent on the rainfall characteristics. This method can therefore only be used to distinguish between annual and perennial vegetation if the considered pixels are located close enough to each other to assume that the received precipitation is equal. This problem could be solved by incorporating interpolated rainfall data.

5.2 Multiresolutional Wavelet Analyis

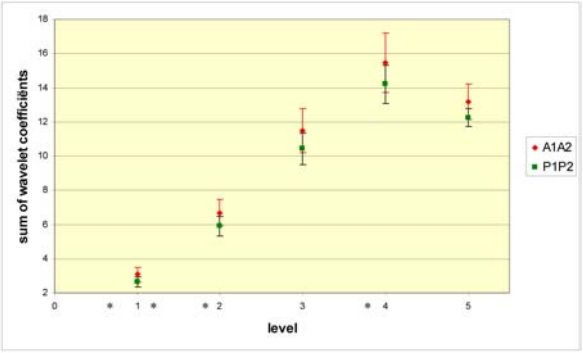

Figure 4. Mean and standard deviation of the sum of wavelet coeficients at different levels for pixels belonging to an annual benchmark site and for pixels belonging to a perennial benchmark site. Levels indicated with an asterix represent significant differences.

As apparent from figure 4, annual time-trajectories show significantly higher sums than the perennials for the first three and for the last level. This difference can be observed for different levels (scales) and points at a higher variability of the annual trajectories [21]. This is in accordance with the expected behaviour of annuals grasses. Annual grasses react stronger on rainfall events than perennial grasses, resulting in the higher variability at small scales (first levels). The size of the growth pulse through the years is more dependent on rainfall quantity than the pulse of the perennial grasses. Hence their time-series will be more variable through the years. This property is reflected in the difference at higher levels.

As the strength of the wavelet analysis is mainly in the local investigation of signals, further analysis should focus on the local analysis of the time-series, zooming in on moments of minimum and peak NDVI values.

6 CONCLUSIONS

When comparing annual and perennial dominated benchmark areas situated close to each other, small differences can be observed in the timing of the growing season. However when benchmark areas are not close, differences in received rainfall mask the influence of the dominant grass type. No consistent differences in NDVI amplitude could be detected, but wavelet analysis results point at a higher variability of the NDVI at annual benchmark sites. Further analysis should locally investigate the wavelet coefficients and incorporate multiple rainfall data for further discrimination between the two types of signals.

ACKNOWLEDGMENTS

The authors would like to thank the Consolidated Pastoral Company and the Newcastle Waters Station staff for providing accommodation during the field visits, in particular we would like to thank Miss Philippa Clarke. We would also like to acknowledge Dr. Lars Eklundh and Dr. Per Jönsson for the TIMESAT program for the post-compositing filtering of the NOAA time-series.

This work is funded under the STEREO program of the Belgian Science Policy (Belspo), contract number SR/02/30.

REFERENCES

[1] WALLACE J.F., HOLM, A.M. AND NOVELLY, P.E., 1993: Rangeland conditon assessment and monitoring using multi-temporal Landsat data. *Proc. North Aust. Remote Sensing and GIS Forum.* AURISA Monograph 8. OSS-Aurisa. Darwin.

[2] BASTIN, G.N., PICKUP G., CHEWINGS,V.H. AND PERACE, G., 1993: Land degradation assessment in central Australia using a grazing gradient method. *Rangel. J. 15,* pp. 190-216.

[3] KARFS, R.A., 2002: Rangeland monitoring in tropical savanna grasslands Northern Territory, Australia: relationships between temporal satellite data and ground data. Masters thesis, Research School of Tropical Environment Studies and Geography, James Cook University, Townsville, Queensland, Australia.

[4] PICKUP G., 1989: New land degradation survey techniques for arid Australia – problems and prospects. *Aust. Rangel. J. 11*, pp. 74-82.

[5] FISHER A., BAKER B. AND WOINARSKI J., 2002: Biodiversity Audit – Bioregional Case Study: Mitchelll Grass Downs, Northern Territory. A report to the National Land & Water audit**.** Parks and Wildlife Commission of the Northern Territory, Department of Infrastructure, Planning & Environment, Darwin

[6] PARTRIDGE I., 1999: Managing grazing in northern Australia. DPI, Queensland.
[7] ALLAN, G., JOHNSON, A., CRIDLAND, S. AND FITZGERALD, N., 2003: Application of NDVI for predicting fuel curing at landscape scales in northern Australia: can remotely sensed date help schedule fire management operations? *Int. J. Wildland Fire 12*, pp. 299-308.
[8] DI BELLA, D.M., PARUELO, J.M., BECERRA, J.E., BACOUR, C. AND BARET, F., 2004: Effect of senescent leaves on NDVI-based estimates of fAPAR: experimental and modelling evidences. *Int. J. Remote Sensing 25*, pp. 5415-5427.
[9] KING, E. A., 2003: The Australian AVHRR data set at CSIRO/EOC: origins, processes, holdings and prospects. Technical report, CSIRO EOC.
[10] GOWARD, S., MARKHAM, B., DYE, D., DULANEY, W. AND YANG, J., 1991: Normalized difference vegetation index measurements from the advanced very high-resolution radiometer. *Remote Sens. Environ*. 35, pp.257–277.
[11] LOVELL, J. AND GRAETZ, R., 2001: Filtering pathfinder AVHRR land NDVI data for Australia. *Int. J. Remote Sensing 22*, pp. 2649–2654.
[12] HOLBEN, B.N., 1986: Characteristics of maximum-value composite images from temporal AVHRR data. *Int. J. Remote Sensing 7*, pp.1417-1434.
[13] RAHMAN, H. AND DEDIEU, G., 1994: SMAC: a simplified method for the atmospheric correction of satellite measurements in the solar spectrum. *Int. J. Remote Sensing 15,* pp. 123-143.
[14] CHEN, J., JONSSON, P., TAMURA, M., GU, Z., MATSUSHITA, B. AND EKLUNDH, L., 2004: A simple method for reconstructing a high-quality NDVI time-series data set based on the Savitzky-Golay filter. *Remote Sens. Environ. 91*, pp. 332–344.
[15] JÖNSSON, P. AND EKLUNDH, L., 2004: TIMESAT - a program for analysing time-series of satellite sensor data. *Comput. Geosci. 30*, pp. 833-845.
[16] JÖNSSON, P. AND EKLUNDH, L., 2002: Seasonality extraction by function fitting to time-series of satellite sensor data. *IEEE Trans. Geosci. Remote Sensing 40*, pp.1824-1832.
[17] MALLAT, S.G.: A theory for multiresolution signal decomposition: the wavelet representation. *IEEE T. Pattern Anal. 7,* pp. 674-693.
[18] PIZURICA A., 2002: Image denoising using wavelets and spatial context modeling. Doctoral thesis submitted at the Faculty of Applied Sciences, University of Ghent, Belgium
[19] MALLAT, S., AND ZONGH, S., 1992: Characterization of Signals from Multiscale Edges. *IEEE Trans. Pattern Anal. and Machine Intel. 14*, pp.710–732.
[20] TORRENCE C AND COMPO G.P., 1997: A practical guide to wavelet analysis. *Bull. Amer. Meteor. Soc. 79*, pp. 61-78.

Monitoring of Pastoral Rangeland Condition in the Southern Northern Territory (Australia) by Remote Sensing—Status and Prospects

C. Dean[a]

[a] DNRETA, Northern Territory Government, PO Box 2130, Alice Springs, NT 0871, Australia, email: christopher.dean@nt.gov.au

ABSTRACT

The area of pastoral land to be monitored in the southern Northern Territory is presently ~242,000 km^2 and includes a wide range of environmental conditions, and minimal resources necessitate development of unique approaches, e.g. assessment based on a single image. Features seen in satellite imagery were related to corresponding manifestations on the ground, i.e. a) large barren areas resulting from overgrazing closer to watering points, b) inter-paddock differences due to overgrazing, and c) congregated cattle pads radiating from bores. Grazing effects were highlighted by the use of NDVI, NDSVI (for senescent vegetation) and specific band ratio composites converted to Intensity, Hue and Saturation then summed. One composite that was useful for Landsat imagery was 'c7': [1/9, 2/3, 3/1] with grazing effects highlighted by the band: Saturation(c7) minus Hue(c7). A composite for ASTER imagery was 'c15': [1/9, 2/3, 3/1] with grazing effects highlighted by: Intensity(c15) plus Hue(c15). To provide intuitive images the band that highlighted the grazing effect was combined with NDVI and NDVSI and rendered as a pseudo-colour image. Methods of how assessment can be automated for a collection of images (temporal and/or spatial) are discussed, including a modified grazing gradient method, and comparison of inter-paddock differences. Use of cattle track extraction from imagery is also discussed. With some preliminary work showing fruitful prospects and with the recent acquisition of more data, the subsequent increased scope for collaborative projects in turn increases the likelihood for more timely and pertinent monitoring of potential land degradation events.

Keywords: Cattle tracks, monitoring, hue, senescent, band ratios.

1 INTRODUCTION

The Northern Territory government (NTG) of Australia has a mandate to manage the environmental sustainability of rangelands in the NT, which are used by the pastoral industry, mainly for of cattle production. Monitoring of that pastoral land aims to help satisfy some governmental, legislative requirements, e.g.: sustainability for pastoral purposes, "the prevention or minimisation of degradation of or other damage to the land and its indigenous plant and animal life", and detection and assessment of changes in land condition. The jurisdiction in the southern Northern Territory (NT) is ~242,000 km^2 (24 Mha), i.e. between the size of Romania and the UK, or between Ghana and New Zealand. (With the potential inclusion of Aboriginal pastoral lands the area will be ~320,000 km^2 (32 Mha)—similar in size to Ecuador, Finland, Germany or Malaysia). It lies within a zone 800 km x 800 km centred over the tropic of Capricorn and is partitioned into 78 pastoral properties, with an average area of ~310,000 ha each. For this area in the southern NT one government employee is allocated to satellite monitoring with a budget for satellite imagery of ~AUD$4,000 (€2,380)/yr. The terrain varies from wide plains to rocky mountain ranges (even within one property), and from desert to semi-arid. The rainfall has high inter-annual variability—with up to several years of drought followed by a year of high rainfall, and with annual averages varying spatially from ~100 mm in the southeast to ~450 mm in the north. The usual NTG procedure is to assess individual properties once every three years, by spatially-limited ground-based monitoring that focuses on a set of specific zones of 50 m radius. But the unique logistic and technical hurdles have resulted, thus far, in the assessment by remote sensing of only a small subset of our jurisdiction [1],[2] and no routine. Those assessments used primarily the grazing gradient method (GGM). However there is a second and timelier requirement for monitoring: as part of a mandatory contribution by the NTG to the nation-wide Australian Collaborative Rangeland Information System (ACRIS) [3],[4] the southern NT must be assessed for change in condition, by remote sensing, by August 2006.

Due to the spatial and temporal scales involved, assessment and monitoring by remote sensing pertains primarily to characteristics of vegetative cover and to using them as indicators of effects of pastoral land management. The subject of remote sensing of vegetation covers a wide range of environments and technologies

and only those most pertinent to our jurisdiction will be mentioned here. One recommendation in a recent review [5] of the prospects for monitoring by remote sensing in arid regions was that pixel size should be less than the variability of the dominant vegetation. The properties that we monitor can have great variability in the dominant vegetation (e.g. riparian river red gums (*Eucalyptus camaldulensis*) to mulga groves (*Acacia aneura*) to grassy planes) and cattle or vehicular tracks have linear (not 2-dimensional) patterns—the pixel size must cope with all these features: a small pixel size with images of large spatial extent is ideal. Species identification would be advantageous as it would indicate directly any grazing impacts on plant biodiversity, however the process has logistical limitations: a) it necessitates ample on-ground assessment, b) considerable effort is required in developing a spectral library, and c) it requires hyper-spectral imagery (more costly per unit area than multi-spectral). A combination of high and low altitude remote sensing may be necessary [6] for monitoring and management. This is possible by using satellite imagery and aerial photography, although the latter can be costly per unit area and possibly replaced by ground-based assessment of potential trouble spots as detected from the satellite imagery—a combination that we use. A method has been reported [7] for assessing long term grazing pressure that used calibration sites along with Landsat data with a temporal resolution of about 1.3 yrs, for 12 yrs. The method required radiance corrections and a comprehensive, accurate and precise data set: which is currently beyond the financial resources of the NTG. The Queensland government [8] recently developed a similar method which gave percent vegetative cover but used an empirically-derived bare-ground index for each image and it was necessary to synchronise ground-based measurements with image acquisition. Again the NTG has insufficient resources for such intensity of on-ground calibration and for such high temporal resolution of imagery.

The GGM has long been identified by the NTG as the technique to be used for monitoring in our jurisdiction and is, in principle ideal, but it has some significant drawbacks. The essence of the GGM [1] is to compare the variation of the PD54 perpendicular-distance-index with distance from the watering point and between wet and dry years and to see if the vegetation near the watering point (the more heavily grazed area) recovers after ample rainfall. The PD54 for any single image can be mathematically distilled into a simple band subtraction: red – (constant × green) where the constant is approximately inversely proportional to the slope of the "soil line". Thus, although the comparison is theoretically fairly simple, it is complicated in practice by requiring manual, subjective measurements on spectral scatter plots, and segregation of soil types within imagery. The most significant drawbacks of the GGM in our jurisdiction are: a) only reveals degradation after the event, b) only definitive for about 68% of our jurisdiction (85% applicability × 80% reliability); c) different watering point capacities within a paddock are not discerned, d) the effect of paddock shapes and the location of watering points with respect to fences are not catered for, e) it relies on imagery from two dates—twice the cost and possibly a long wait between high rainfall events, f) our data on fences may be inadequate, g) the spatial resolution of our data on vegetation and soil types is mostly inadequate for stratification, h) placing of the soil line (without ground-based calibration) may be too subjective, and i) inverse, partial or masked gradients can be observed and potentially lead to erroneous conclusions and no quantitative result. Due to the variety of grazing gradients observed, it has been concluded [9] that vegetation gradient analysis was not a good indicator of land condition. Nevertheless, when these factors are taken into account there is a place for a GGM type analysis in our monitoring procedure: i.e. as one [qualitative] test within a series of both qualitative and quantitative tests that constitute a more automated assessment. E.g. by using a non-perpendicular-distance vegetation index and assessing each watering point's graph individually.

The prominent types of potential land degradation (which is one of the determining factors in choosing remote sensing methods), in our jurisdiction are: a) unnaturally barren areas, (Figure 1.a) where top soil can be displaced by wind or water runoff and where there are loss of traps for seeds and seedling growth[10], b) creek erosion near cattle or vehicular tracks and subsequent loss of riparian trees (Figure 1.b), c) changes in vegetation towards less palatable, nutritious or long-lived species closer to watering points, and d) potential loss of biodiversity by unnatural predominance of non-native pasture species [11]. Indicators of these seen on satellite imagery are mostly associated with: a) areas of high reflectivity such as large barren areas around watering points, b) inter-paddock differences, and c) congregated cattle pads radiating from bores amongst overstorey trees (e.g. Figures 1.c and 1.d). The density of livestock tracks has been linked with grazing pressure [12] and the erosion potential from pads is highest where tracks cross creeks or steep slopes. Generally, the altered areas need to be discerned from naturally highly reflective areas such as saltpans, bare rock and inundated areas.

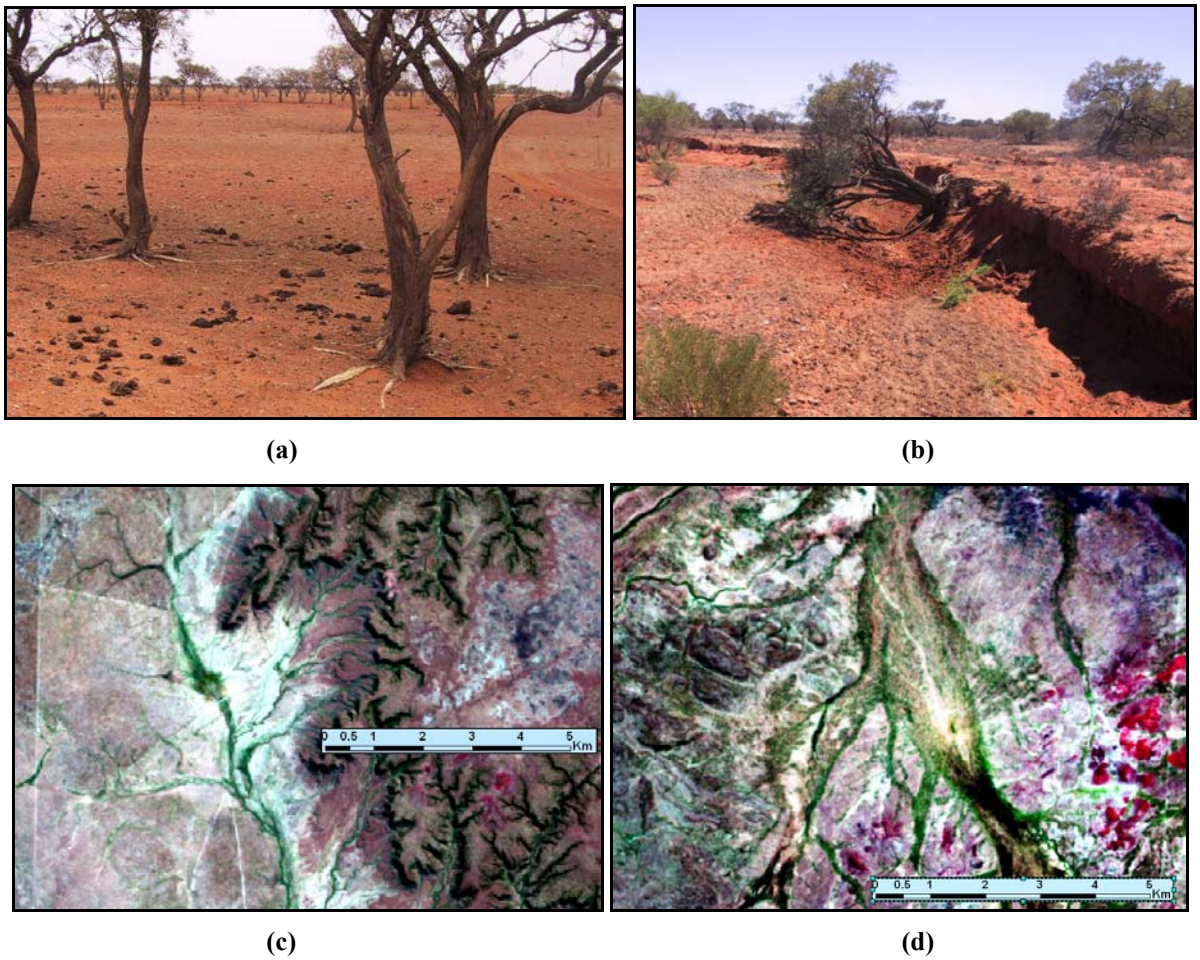

Figure 1. Examples of types of land degradation and observable effects in satellite imagery. (a) Bared tree roots owing to topsoil loss by wind erosion after overgrazing. (b) Riparian tree loss and gully erosion upstream from a vehicular track. (c) Extensive barren area (in white) due to overgrazing near a watering point, Landsat bands 5/4/3. (d) Cattle pads (in white) radiating from a watering point, Landsat bands 5/4/3.

Another major determining factor in the choice of remote sensing methods is the availability of data—dependent upon finances and available technology. Our data have been limited mostly to two sets of Landsat imagery—centred around the years 1997 and 2000, and a spatially and temporally diverse aerial photography archive with dates ranging from 1947 to about 1985. However within the last year this data set was expanded to include: a) Landsat imagery from the years 1972, 1980, 1989, 2004, and one double image from 2003, b) ASTER imagery for the year 2000 and some sparse coverage from more recent years, c) four EO1-ALI images of different dates. Other potential data are: a) Corona satellite images, which could indicate the extent of shrub and tree cover in the 1960's, b) 30 m pixel elevation data from ASTER imagery, c) LIDAR data for high resolution elevation and tree cover, d) IKONOS or QuickBird high resolution imagery.

2 METHODS USED IN TEST CASES

This section describes some methods of remote sensing analysis used in tests on different areas of potentially degraded land and vegetation, observed in satellite imagery. Anomalies were initially observed as unnatural looking (anthropogenically induced) patterns, by browsing through satellite imagery with pseudo-colour mapping. Fieldwork related image characteristics to their corresponding physical manifestations on the ground and the management practices that caused those potential problem areas were determined. Techniques were devised to highlight those features in contrast to the less disturbed landscape in the imagery. Methods that could be applied in their routine detection were devised.

2.1 Band Combinations and Discerning the Extent of Grazing Effects

The first example shows how examination of two different vegetation indices and a particular band combination can be used to visualise the extent of grazing impact and to quantitatively differentiate it. The particular watering point was distinctive in satellite imagery due to both strong inter-paddock effects and a piosphere effect, however it was necessary to prevent any non-anthropogenic features from being interpreted as resulting from management. The scenario, which at first appeared simple, was complicated by different aged watering points and different grazing periods in neighbouring paddocks, e.g. comparison with an image from three years earlier revealed that senescent vegetation (dry grass) had meanwhile gone from one paddock but was replaced by a flush of green grass after sufficient rain.

On average, owing to paucity of rainfalls, most vegetation in our jurisdiction would usually be dry rather than green. Thus, in assessing grazing pressure the presence of senescent vegetation must be accounted for (e.g. as in Ref. 13) and this was done by using the senescent vegetation index, NDSVI [14] (where a SWIR band replaces NIR in the standard equation for NDVI). This allowed a more complete picture of management practices to be observed and subsequently better interpretation of the imagery. Some separation of highly reflective surfaces into those due to bare soil that would have been vegetated if it were not due to grazing impacts, from those due to bare rock, salt pans or inundated areas etc., was possible by using different band combinations. Several combinations were trialled with Landsat imagery and the one that gave the best separation over different soil types (e.g. red or grey clay) was: [2/6, 1/5, 3/1] mapped to [r, g, b] (e.g. Figure 2.a). This combination was named ‘c7’.

To find common factors amongst the individual band ratios and to dispense with their separate influences it was decided to convert the composite ‘c7’ to Intensity, Hue, Saturation (IHS) space rather than RGB space. The Intensity image showed areas of minimal vegetation but included those of minimal grazing. The Hue image showed areas of minimal vegetation near the bore and responded well to senescent vegetation but showed no inter-paddock differences and didn’t respond well to green vegetation. The Saturation image showed areas of minimal vegetation due to grazing and showed inter-paddock differences well. To include the effect of senescent vegetation the Hue image was subtracted from the Saturation image to produce ‘c7_smh’. (To make sure they were comparable both were stretched between 0 and 255 before the subtraction). This new image c7_smh can be used to give a relative, numeric value to grazing impact, e.g. to use it in a grazing gradient graph. An intuitive representation of c7_smh can be made by combining it with NDVI and NDSVI and displaying in RGB space (a pseudo-colour image), as in Figure 2.a. For such a pseudo-colour representation it could be tempting to simply use a band ratio that showed a high contrast in vegetation in place of c7_smh, e.g. 7/5. However there was no such simple band ratio (in this instance) which differentiated as well as did c7_smh between low NDVI, low SNDVI and bare soil resulting from non-grazing effects.

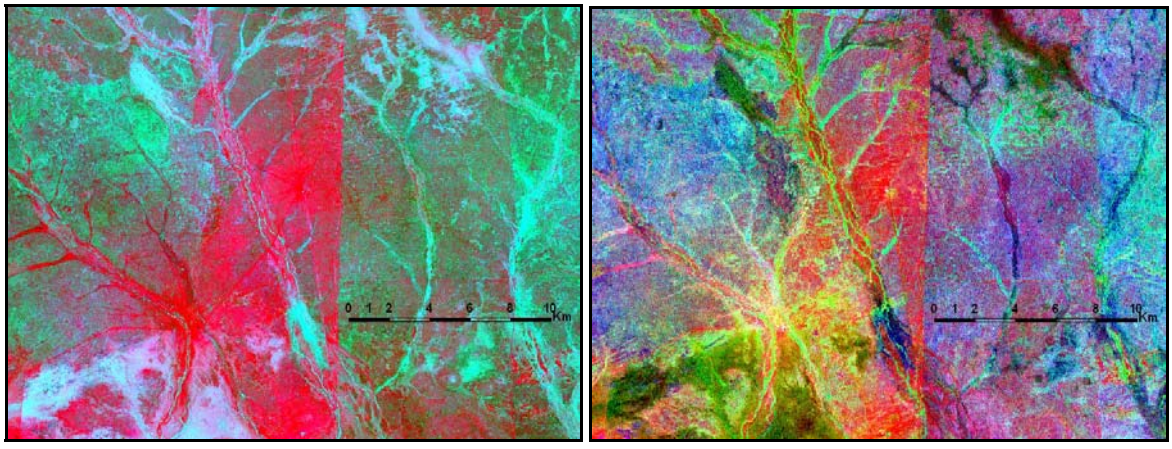

(a) **(b)**

Figure 2. Pseudo-colour images of (a) composite ‘c7’ with bands [3, 2, 1] mapped to [r, g, b], showing low vegetation areas in red (which were segregated by subtracting hue from saturation to give c7_smh), and (b) [c7_smh, NDVI, NDSVI] mapped to [r, g, b]. This combination shows green vegetation as green, senescent vegetation as blue and bare soil as red. The scale bar is 10 km long.

2.2 Band Combinations, Inter-paddock Differences and Gradients

The second example shows the use of a band combination in an image acquired after an ample rainfall but in a paddock that was previously heavily grazed and contained rocky hills, plains and sandy river beds with riparian trees. The effects were observed in an ASTER image and older Landsat imagery showed that the paddock had been heavily grazed for about 4 yrs previously. The ASTER satellite has no blue band and consequently a band ratio different to that used for Landsat, was sought, to highlight the differences in ground cover across the fences: the combination [1/9, 2/3, 3/1] (termed 'c15') mapped to [r, g, b] was found most effective (Figure 3.a). The ratio 3/1 was best at highlighting the inter-paddock differences in green vegetation, and 2/3 revealed some differences in senescent vegetation. Inclusion of more SWIR bands (e.g. 4, 5 or 7) highlighted some differences in ground cover but they made the scene more blurred due to their lower spatial resolution; also 4/5 did not discriminate between a bare, rocky slope and green vegetation on the plane. Although the NDVI was much higher in the paddock of interest (compared with the neighbouring paddock to the north), the NDSVI was marginally lower than outside the paddock. This complicated the task and required a unique solution. The modified soil adjusted NDVI, MSAVI [15] was also tested but, after stretching, it appeared identical to NDVI.

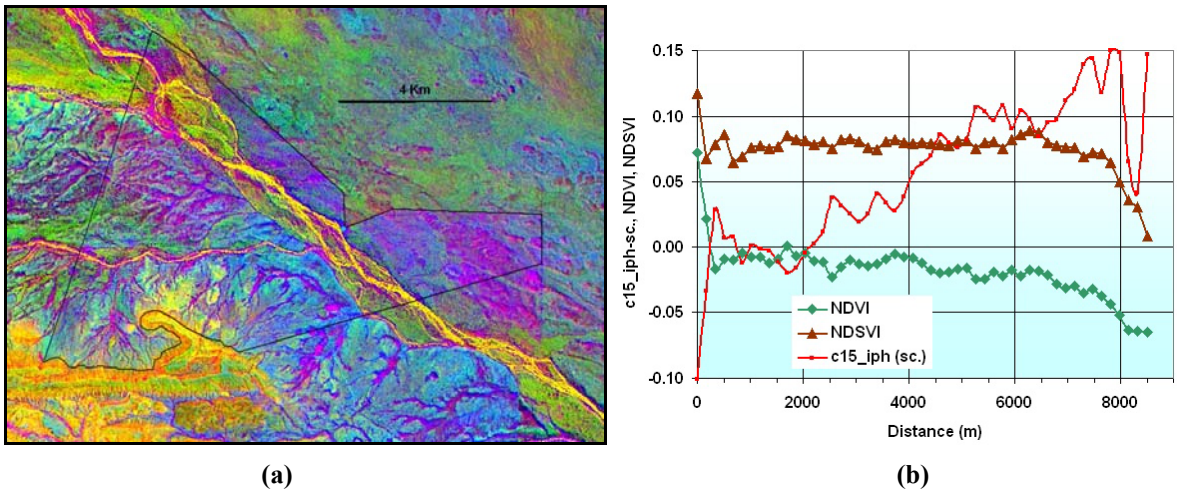

Figure 3. (a) Pseudo-colour image of combination 'c15' [1/9, 2/3, 3/1] showing inter-paddock differences. The paddock (graphed in (b)) is outlined in black, the watering point is shown as a light blue dot on the northern fence where it indents to form a triangle near the river. (b) Gradient graph of mean values every 50 metres away from the watering point (shown in (a)). The values for 'c15_iph' were scaled to fit on the same graph. The scale bar is 4 km long.

Conversion of 'c15' to IHS space revealed differences across the landscape: Saturation values showed minimal inter-paddock differences but surprisingly perhaps, revealed differences in texture: less grazed areas appeared more uniform. Hue showed the strongest inter-paddock differences, corresponding to green vegetation, and Intensity showed some differences in senescent vegetation. The values of Hue corresponding to vegetated areas were in the mid-range, with sandy creeks and rocky slopes corresponding to two extreme values of Hue. Consequently the Hue was shifted by half its range, converted to absolute values and doubled, resulting in vegetated areas having low hue. (Alternatively, this could also have been achieved by permuting the combination of band ratios used in calculating 'c15'.) After scaling, the Intensity and Hue were added together to form 'c15_iph' to show the inter-paddock differences for both the green and senescent vegetation. To produce an intuitive scene 'c15_iph' was combined with NDVI and NDVSI to give the pseudo-colour image [c15_iph, NDVI, NDVSI].

The NDVI, NDSVI and 'c15_iph' were graphed in grazing gradient format as a function of distance from the watering point (a bore) for the paddock concerned (Figure 3.b). Pixels for the sandy river beds were not included in the calculation as they merely increased variability near the bore. The graph shows that NDVI drops with distance from water—an inverse gradient (as noted in Reference 9), whereas NDSVI remains more constant but has a small dip between 500 m and 2000 m from the bore. Both NDVI and NDSVI decrease on the rocky slopes, which are prominent further from the bore. The 'c15_iph' corresponds more to a "bare soil" index as it peaks where the vegetation indices drop. Also it appears more responsive to green vegetation, although this may be due to the predominance of green over senescent vegetation in the paddock. Also noteworthy is that the 'c15_iph' has a more constant increase with distance from water. The dip in 'c15_iph' near 8,200 m is merely due to contrast between a gully and ridge in the most distant corner of the paddock, where there data points are fewer. Again, this new image c15_iph can be used to give a relative, numeric value to grazing impact.

2.3 Cattle track Detection and Usage

As cattle tracks (pads) are distinctive in much satellite imagery it was considered relevant to determine if they correspond to land degradation and what the correspondence was between features in the imagery and traits on the ground. A few networks of pads seen in imagery to be radiating from watering points were mapped on the ground with a GPS and overlaid on imagery. Attempts were made to extract cattle pads from Landsat imagery using the image analysis software eCognition [16] but the pixel width was too high and the spectra too variant for automated extraction without specific application programming. This was especially so when overstorey trees overshadowed the pads then the pixels were less bright. Nevertheless they were distinct to the human eye and could possibly be extracted from higher resolution imagery such as ASTER or IKONOS.

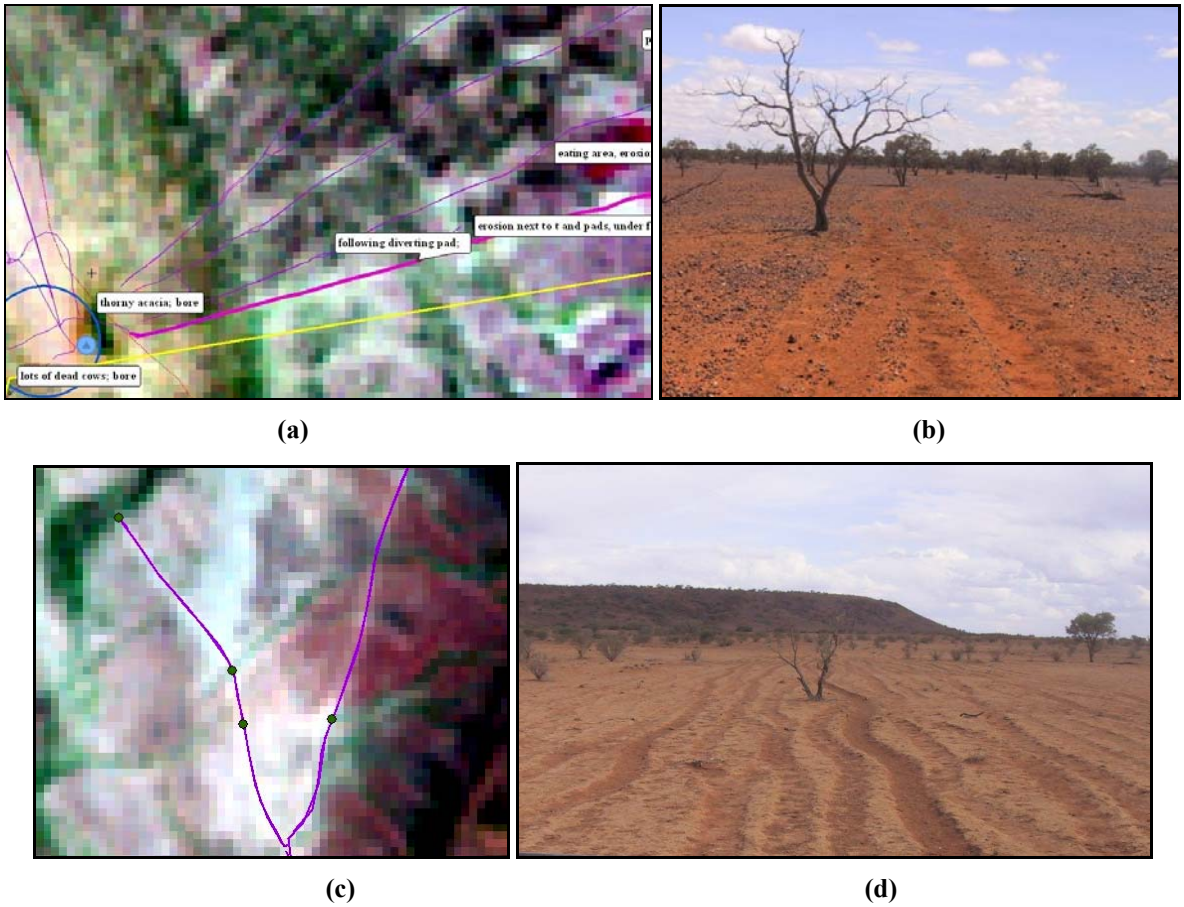

Figure 3. Examples of cattle pads as seen in Landsat imagery (pixel width ~25 m). (a), (b) A close-up of pads seen in Figure 1.d. Pads are ~3 m wide and correspond to 1 Landsat pixel or less. In (c), (d) the pads are about 50 m wide and correspond to three or less pixels (in the centre of the image in (c)). In both cases creeks had erosion damage where they met the pads.

On average, vehicular tracks were observed to produce more severe creek erosion, which was mostly upstream from the tracks where they crossed creeks, than did cattle pads. Many vehicular tracks are recorded as part of the NTG routine mapping, however new or moved tracks may only be recorded once every three yeas. There are more cattle routes crossing creeks than there are vehicular crossings. In either case the creek erosion can not be detected in satellite imagery, although steep, eroded banks are obvious in aerial photography if the sun is at a low, perpendicular angle. The aim is to overlay tracks, elevation and land type layers in order to determine vulnerable areas, therefore data on the elevation and land type is crucial. The elevation information available (in DEM format) is mainly the 90 m pixel data from the Shuttle Radar Topography Mission, which is of insufficient spatial resolution for calculating the location of creeks. The DEMs from ASTER imagery have 30 m pixels and thus would be more suitable. The ASTER DEMs can be obtained at no cost from the manufacturer in the USA but the current waiting time (in 2005) is one year. The elevations in such ASTER DEMs are not absolute and require registration using several known D-GPS readings per image—these are being obtained for our jurisdiction. Some land type data is available for most of our jurisdiction but its precision varies greatly between different locations—in some places there are errors of up to only 400 m and in other places up to 1500 m—depending on the scale of the original

mapping. Thus the extraction of tracks from imagery would yield significant information about management impacts but has several logistical hurdles to surmount before it can be routinely used in monitoring.

3 DISCUSSION AND CONCLUSIONS

The aim for the near future for enhancing the routine monitoring of pastoral leases in our jurisdiction is to automate some of the types of analysis shown in the present work. A sequence of different tests (e.g. derived from the analyses presented here) could be performed on each image. This would necessarily be done by writing specific software, whereas the image processing to-date has mainly made use of ESRI products and various freeware packages available on the internet (e.g. OpenEV). For example: edge detection of linear edges of length at least 400 m and measured 100 m away from the edge, in images of NDVI, NDSVI, c7_smh and c15_iph could yield a list of potential problem areas requiring closer scrutiny. That edge detection could be run over all imagery for our jurisdiction. Different composites may be proficient in revealing grazing effects after different types of rainfall activity. For time-series monitoring, results for each edge could be stored and the inter-paddock differences compared within images acquired at different dates. This would require a budget for future regular imagery purchases. In a similar way, using a specifically purchased high temporal resolution data set, routine monitoring has been instigated for a subset of the northern Northern Territory for dark clay areas and it uses a simple band ratio [17]. The two other developments from the present work that could be adopted for routine monitoring are the use of c7_smh or c15_iph as gradient indicators around watering points, and the vulnerability determination near cattle and vehicular tracks. Whether the gradient is negative or positive it is still an indication of possible overgrazing. There will always be reason to scan individual images though, for example to detect overgrazed areas near unmapped natural water holes, which are not near any infrastructure.

The ongoing assessment of land degradation in the southern Northern Territory using satellite monitoring is a monumental task due to the large area involved and its environmental variability, the minimal number of people employed and the limited data available. Nevertheless it is important for the environmental sustainability of the area, especially with the recent growth in the export cattle industry, and it allows much scope for further scientific and methodological developments. The preliminary work shown here in our jurisdiction appears to have fruitful prospects. With the recent acquisition of more data then the subsequent increased scope for collaborative projects in turn increases the likelihood for more timely and pertinent monitoring of potential land degradation events.

ACKNOWLEDGMENTS

The author would like to thank the NT Government for project funding and for partial funding of conference attendance along with the European Commission Directorate-General. Conversations with Greg O'Reilly yielded much useful information on local rangeland ecology. Crucial support with managing NTG protocols was provided by Ian Lancaster. Collaborative support from other NTG employees and the CRC for Greenhouse Accounting is also recognised.

REFERENCES

[1] BASTIN, G.N., PICKUP, G., CHEWINGS, V.N. AND PEARCE, G., 1993: Land Degradation Assessment in Central Australia Using a Grazing Gradient Method. *The Rangeland Journal, 15*, pp. 190-216.

[2] PEEL, L.J., 2003: Monitoring the Rangelands in Central Australia. Presented at *NT Southern Region Healthy Landscape Seminar Series*. 14th March 2003. CSIRO, Alice Springs, Australia.

[3] COMMONWEALTH OF AUSTRALIA, 2003: Managing Rangelands the key to new opportunities in northern Australia. Media Release, Hon. Warren Truss MP, Ministry of Agriculture, Fisheries and Forestry, 19th November, 2003. http://www.maff.gov.au/releases/03/03342w.html Viewed on 26th August 2005.

[4] COMMONWEALTH OF AUSTRALIA, 2005: The Australian Collaborative Rangelands Information System. Department of the Environment and Heritage. http://deh.gov.au/land/management/rangelands/acris/index.html Viewed on 26th August 2005.

[5] OKIN, G.S. AND ROBERTS, D.A., 2004: Remote Sensing in Arid Regions: Challenges and Opportunities in Ustin, S.L. (ed.): The Manual of Remote Sensing, Vol. 4, 3rd edition. pp. 111-146. John Wiley and Sons, New York.

[6] BOOTH, D.T. AND TUELLER, P.T., 2003: Rangeland Monitoring Using Remote Sensing. *Arid Land Research and Management*, *17(4)*, pp. 455-467.

[7] HOSTERT, P., RÖDER, A. AND HILL, J., 2003: Coupling Spectral Unmixing and Trend Analysis for Monitoring of Long-term Vegetation Dynamics in Mediterranean Rangelands. *Remote Sensing of Environment, 83*, pp. 183-197.

[8] BYRNE, M., HASSETT, R., TAUBE, C. AND HENRY, B., 2004: Objective Monitoring of Ground Cover Across the Desert Channels Queensland Region. Final Report to Desert Channels Queensland Incorporated. The State of Queensland, Department of Natural Resources and Mines.
[9] LIND, M., RASMUSSEN, K., ADRIANSEN, H. AND KA, A., 2003: Estimating Vegetative Productivity Gradients Around Watering Points in the Rangelands of Northern Senegal Based on NOAA AVHRR data. *Geografisk Tidsskrift, Danish Journal of Geography, 103(1)*, pp. 1-15.
[10] KINLOCH, J.E. AND FRIEDEL, M.H., 2005: Soil seed reserves in arid grazing lands of central Australia. Part 1: availability of 'safe sites'. *Journal of Arid Environments, 60*, pp. 163-185.
[11] JACKSON, J,. 2005: Is there a Relationship between Herbaceous Species Richness and Buffel Grass (Cenchrus ciliaris)? *Austral Ecology, 30*, pp. 505-517.
[12] PRINGLE, H.J.R. AND LANDSBERG, J., 2004: Predicting the distribution of livestock grazing pressure in rangelands. *Austral Ecology, 29*, pp. 31-39.
[13] MOUGENOT, B., BÉUGÉ, A., CHEHBOUNI, G., ESCADAFEL, R., HEILMAN, P., QI, J., ROYER, A. AND WATTS, C. 2000: Applications of VEGETATION data to resource management in arid and semi-arid rangelands. Presented at *VEGETATION 2000*. Lake Maggiore, Italy, 3rd-6th April 2000. http://vegetation.cnes.fr/vgtprep/vgt2000/begue.pdf. Viewed on 6th May 2005.
[14] QI, J., 2002: Improved Rangeland Information Products from Satellites. *CGEO/RA02-02/w*. Michigan State University, East Lansing, Michigan.
[15] QI, J., CHEHBOUNI, A., HUETE, A.R. AND KERR, Y.H. 1994: Modified Soil Adjusted Vegetation Index (MSAVI). *Remote Sensing of Environment, 48*, pp. 119-126.
[16] DEFINIENS, 2005: eCognition-Object Oriented Image Analysis. Definiens, Geospatial Business Unit, München, Germany http://www.definiens-imaging.com/ecognition/index.htm Viewed on 30th August 2005
[17] KARFS, R.A., DALY, C., BEUTEL, T.S., PEEL, L. AND WALLACE, J.F., 2004: VegMachine—Delivering Monitoring Information to Australia's Pastoral Industry. Presented at *The 12th Australasian Remote Sensing and Photogrammetry Conference*, Fremantle, Western Australia, 18th-22nd October, 2004.

Inter-comparison of NOAA/NASA Pathfinder and MEDOKADS AVHRR based NDVI Time Series

K. Friedrich [a], D. Koslowsky [a] and H. Billing [a]

[a] Institut für Meteorologie, Freie Universität Berlin, Carl-Heinrich-Becker-Weg 6-10, 12165 Berlin, Germany, email: kfriedrich@zedat.fu-berlin.de

ABSTRACT

The Advanced Very High Resolution Radiometer (AVHRR) instrument was designed for meteorological purposes for daily global observation at 1 km resolution. NOAA and NASA have released Pathfinder AVHRR Land (PAL) as long-term data that have been processed in a consistent manner for global change research. This data set is generated from daily data and contains amongst others NDVI for different temporal resolutions (10-day's and monthly composites) at spatial resolution of 8 km covering now a period of more than 20 years. The Mediterranean Extended Daily One-km AVHRR Data Set (MEDOKADS) is generated at the Freie Universität Berlin since 1989 and still continued in near real-time at spatial resolution of about 1 km for Mid-Europe and the Mediterranean basin. It is used as one primary remote sensing data input to the DeSurvey (A Surveillance System for Assessment and Monitoring of Desertification) research project to detect hot spots of desertification risks and trends in vegetation cover in the Mediterranean basin. NDVI time-series of the MEDOKADS based on sophisticated calibration algorithms for the short wave AVHRR channels are compared with the Pathfinder product and results are presented.

Keywords: AVHRR, MEDOKADS, Pathfinder, PAL, time series, NDVI.

1 INTRODUCTION

The AVHRR instrument operates on NOAA series Satellites.

Table 1. Orbital parameters of NOAA satellites

Orbit:	Sun synchronous, near polar
Nominal altitude:	833 km
Inclination:	98.8 degrees
Orbital period:	102 minutes
Ascending node times at launch:	14:30 (NOAA-7), 14:20 (NOAA-9),13:30 (NOAA-11), 13:30 (NOAA-14), 13:45 (NOAA-16) LST
Nodal increment:	25.3 degrees

The orbital period of about 102 minutes produces 14.1 orbits per day. Because the daily number of orbits is not an integer, the sub-orbital tracks do not repeat daily, although the local solar time of the satellite's passage is essentially unchanged for any latitude. The 110.8 degrees cross-track scan equates to a swath width of about 2700 km. This swath width is greater than the 25.3 degrees separation between successive orbital tracks and provides overlapping coverage (side-lap).

The bandwidths of the AVHRR instrument are given in table 2. The AVHRR/3 instrument used since NOAA 15 allows switching between channel 3a and channel 3b depending on day or night.

Table 2. Bandwidths of the AVHRR instrument.

Channel	1	2	3a	3b	4	5
Wavelength (micrometer)	0.58 - 0.68	0.73 - 1.10	1.58 - 1.64	3.55 - 3.93	10.3 - 11.3	11.5 - 12.5

The two channels for visible and near infrared of AVHRR instrument does not have on-board calibration facilities. Using pre-launch calibration coefficients result in unrealistic reflectances. Degradation due to the orbit injection and operation time can detected and requires a post-launch calibration. A common method to determine the calibration coefficient is to observe a surface, which is invariant in time. The degradation can be estimated with time series observations of desert targets. The duration of the time series has important effects of the results. An overestimation of degradation is possible [1]. Cloud contamination, drift to later observation time and BRDF hamper the derivation of reliable degradation coefficients.

The radiance which is measured at the satellite is influenced by the atmosphere on its path from sun to earth and earth to satellite. Different processes have to be considered for atmospheric correction. Radiant energy interacts with the atmosphere by scattering, absorption and emission. The emission for the visible and near infrared channels of AVHRR instrument form earth is negligible. The absorption by ozone is important for channel 1 and by water vapour for channel 2. Mie and Rayleigh scattering has more influence for channel 1 than for channel 2. Dark surface appear brighter when observed from space and bright surfaces darker. In each case exists a "neutral point" at which the atmosphere has no effect, the atmospheric backscatter just compensates the loss of radiation from surface. For channel 1 the "neutral point" is nearly at a reflectivity of 0.15 and for channel 2 at 0.06 and vary slightly with the turbidity of the atmosphere [2].

A complete correction for atmospheric effects for large areas is difficult because of the high variability of water vapour and aerosol load of the atmosphere in space and time.

The Bidirectional Reflectance Distribution Function (BRDF) describes the reflectivity of a target as a function of illumination and viewing geometry. The BRDF depends on wavelength and is determined by the structural and optical properties of the surface, such as shadow-casting, multiple scattering, mutual shadowing, transmission, reflection, absorption and emission by surface elements, facet orientation distribution and facet density.

The knowledge of BRDF is needed in remote sensing to remove effects caused by view and illumination geometry (for example in image standardization and mosaicking), a prerequisite for deriving albedo, land cover classification, cloud detection, atmospheric correction and other applications. It gives the lower radiometric boundary condition for any radiative transfer problem in the atmosphere and is hence of relevance for climate modelling and energy budget investigations [3].

2 PATHFINDER AVHRR LAND (PAL)

Pathfinder AVHRR Land (PAL) has been released by NOAA and NASA as a long-term data set. It has been processed in a consistent manner for global change research. This data set is generated from daily data covering now a period of more than 20 years. Pathfinder I AVHRR Land data was used for this inter-comparison. The main characteristics are shown in table 3. Figure 1 shows an example of PAL data set for the Mediterranean region.

Table 3. Main characteristics of Pathfinder AVHRR Land (PAL)

time period:	1981 - 2001
resolution:	8 km
source:	Global Area Coverage (GAC)
region:	global
projection:	Interrupted Goode Homolosine Projection
satellite:	NOAA-7, -9, -11 and -14
available data:	data for the first of each month for NDVI, channel 1 - 5, instrument scan angle, solar zenith angle, relative azimuth angle day of year and hour 10-days composite for NDVI and channel 1 – 5 monthly composite for NDVI and channel 1 - 5
distributor:	Goddard Distributed Active Archive Center (DAAC)

The PAL is based on the Global Area Coverage (GAC) data. The processor on board of the satellite samples the real-time AVHRR data to produce reduced resolution GAC data. Four out of every five samples along the scan line are used to compute one average value, and the data from only every third scan line are processed. As a result, the spatial resolution of GAC data near the subpoint is actually 1.1 km by 4 km with a 3 km gap between pixels across the scan line, although generally treated as 4 km resolution. All of the GAC data computed during a complete pass

are recorded on board the satellite for transmission to the command and data acquisition stations [4]. The 10-bit precision of the AVHRR data is retained. Resampling and averaging processes are used to produce GAC data. This is important for the inter-comparison from PAL and MEDOKADS.

The PAL daily data were spatially re-sampled, based on maximum NDVI values, from the AVHRR GAC data, which has a nominal resolution of 4 km. The GAC 4 km pixels are binned into one of the 8 km pixels of the PAL daily product. All relating channel data as well as other parameters are selected based on the location of the maximum NDVI bin. Daily data pixels with scan angles greater than 42 degrees are discarded, unless there are no pixels with scan angles less than 42 degrees. The pixels with solar zenith angle greater than 80 degrees are discarded.

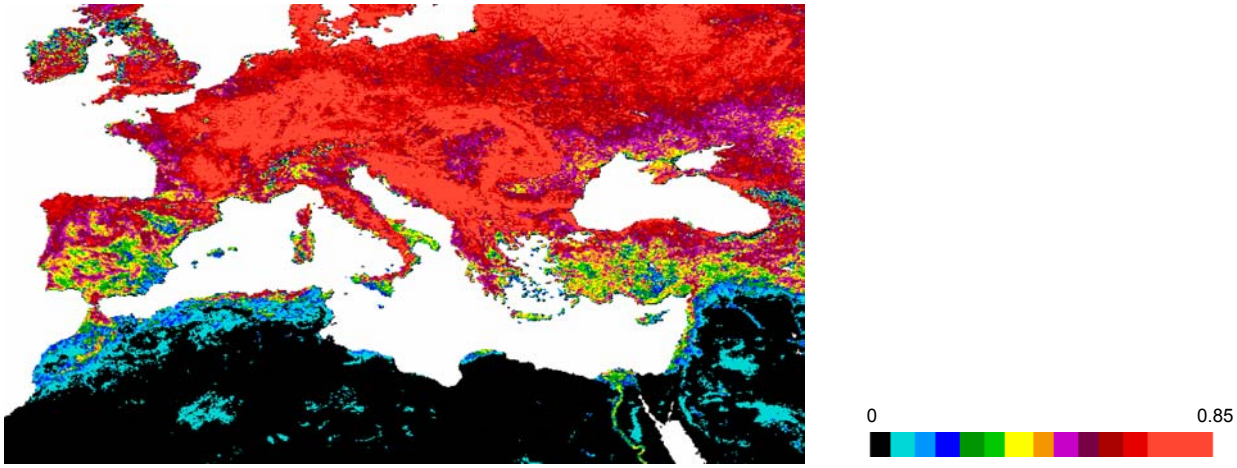

Figure 1. Example for maximum NDVI of PAL data set for the first decade of month June 2000 in geographical projection.

The data for PAL are calibrated as described in [5] for NOAA 7, 9 and 11 and for NOAA 14 described in [1]. The degradation is estimated by time series observations of desert targets over 3 years. The calibration coefficients are increasing with time (Figure).

PAL is atmospheric corrected for Rayleigh scattering and ozone absorption. The data set is not corrected for water vapour and aerosols because of their unknown concentration and high variability in the atmosphere.

3 MEDITERRANEAN EXTENDED DAILY ONE-KM AVHRR DATA SET (MEDOKADS)

MEDOKADS is generated at the Freie Universität Berlin since 1989 and still continued in near real-time at spatial resolution of about 1 km for Mid-Europe and the Mediterranean basin. Table 4 gives the main characteristics of MEDOKADS.

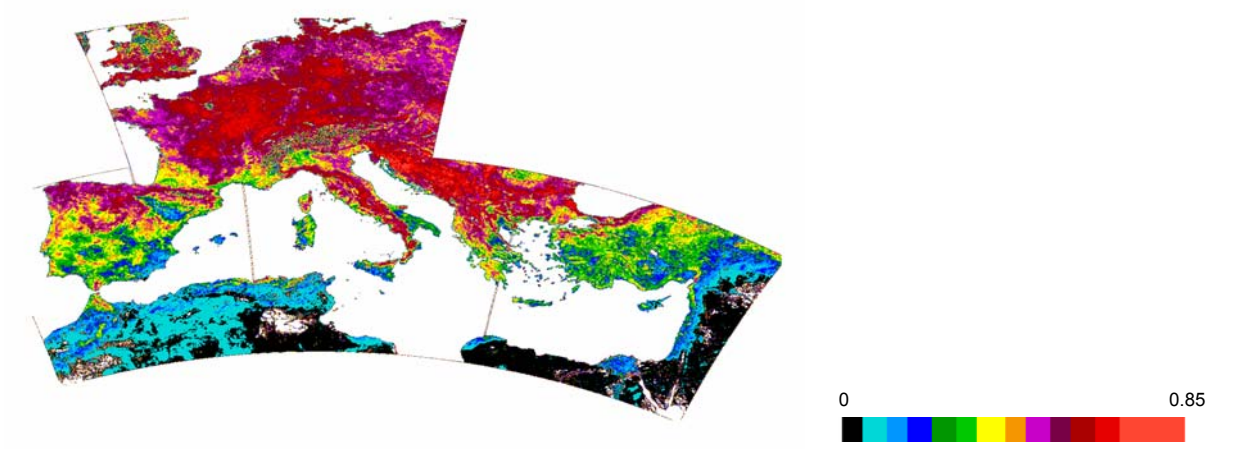

Figure 2. Example for maximum NDVI of MEDOKADS for the first decade of month June 2000 in geographical projection.

Table 4. Main characteristics of Mediterranean Extended Daily One-km AVHRR Data Set (MEDOKADS)

time period:	1989 - present
resolution:	0.01°
source:	direct read out High Resolution Picture Transmission (HRPT)
region:	west-, middle-, east- und southeast Europe, north Africa
projection:	geographical projection
satellite:	NOAA-11, -14, -15 und -16
available data:	daily data, 10-days composite and 30-days composite for channel 1 - 5, satellite/sun zenith distance, satellite/sun azimuth, broadband albedo, bitmap (origin indicator, landmask, cloudmask), NDVI, scattering angle sun satellite, SST/LST, time since equator
distributor:	FU-Berlin, Meteorologische Satellitenforschung

The AVHRR data are digitized to 10-bit precision and are transmitted from the satellite in real-time as High Resolution Picture Transmission (HRPT) data. The data for the whole reception area are converted to 16 bit integer and are remapped to polar stereographic projection with in accuracy of 3 to 10 km due to errors in orbit prediction. Areas for the MEDOKADS cut out and re-navigated to an accuracy of about 1 km and remapped to geographical projection with a nominal resolution of 0.01 degree to retain the full resolution of the AVHRR instrument. In the high latitude and at the border of each overpass the images are oversampled but all information which are collected by the satellite are included. 10-days and 30-days composite are generated based on maximum NDVI values without any constraint on satellite or sun geometry to allow studies on BRDF effects. The other channels for MEDOKADS composite data are selected according to the maximum NDVI.

The detection of calibration coefficients for MEDOKADS are described in [6]. The calibration coefficient found for NOAA 14 decrease in 1998 and nearly vanished in 1999 and 2000 (Figure).

The MEDOKADS is not atmospheric corrected because of the unknown concentration of aerosols and water vapour.

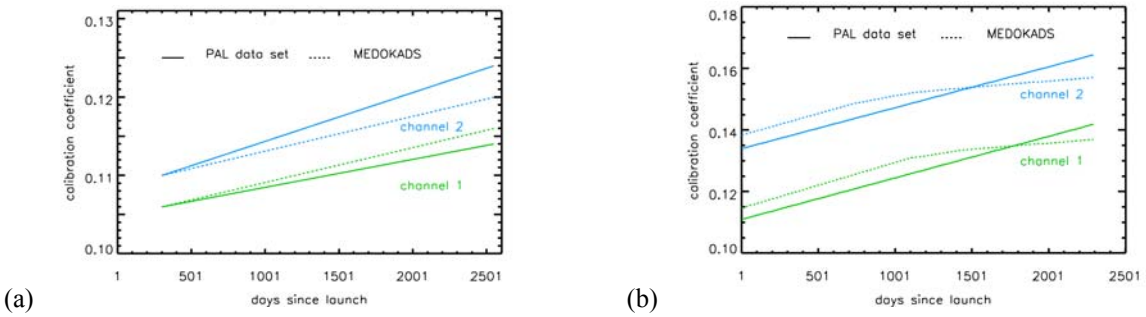

Figure 3. Calibration coefficient for NOAA 11 (a) and NOAA 14 (b) after [1], [5] and [6].

4 EFFORTS TO GET COMPARABLE SETS OF PAL AND MEDOKADS

In order to compare the both data sets it is necessary to select a projection and a resolution which is identical for both data sets. Geographical projection was chosen with a resolution of 0.04 degree. The resolution of MEDOKADS has to be reduced and the oversampling for PAL data are not so important. The management of those image files were easy.

Means, histograms and linear correlations over small and large areas are useful statistical parameters to compare different data sets. Different time slices were chosen for averaging to identify short-term and long-term phenomena.

Direct comparison of channel 1 and 2 is only possible for the first of each month because of the present data for PAL data set.

Because of the unknown parameter for atmospheric correction of PAL data a recalibration and atmospheric correction of MEDOKADS was necessary to get comparable sets of data. Recalibration has been done for MEDOKADS by using the proposed coefficient in [1], [5] and [6]. Figure 3 shows the different calibration coefficient for NOAA 11 (a) and 14 (b) which were used for recalibration.

The atmospheric correction of MEDOKADS was done with SMAC (Simplified Method for Atmospheric Corrections). SMAC is a semi-empirical approximation of the radiative transfer in the atmosphere. The SMAC requires as input the surface pressure, the ozone content, the water vapour content and the aerosols concentration. If any parameter is not transferred a certain part of the atmospheric correction will be omitted.

5 RESULTS

PAL and MEDOKADS have an overlapping time of about 13 years. In this period the mean of PAL NDVI for different regions is more than 35% higher than the mean of MEDOKADS NDVI without atmospheric correction. The variability is the same for both data sets over the displayed period. Decreasing data can be caused by increasing aerosol concentration within the atmosphere through volcano activity as the eruption of Pinatubo in 1991.

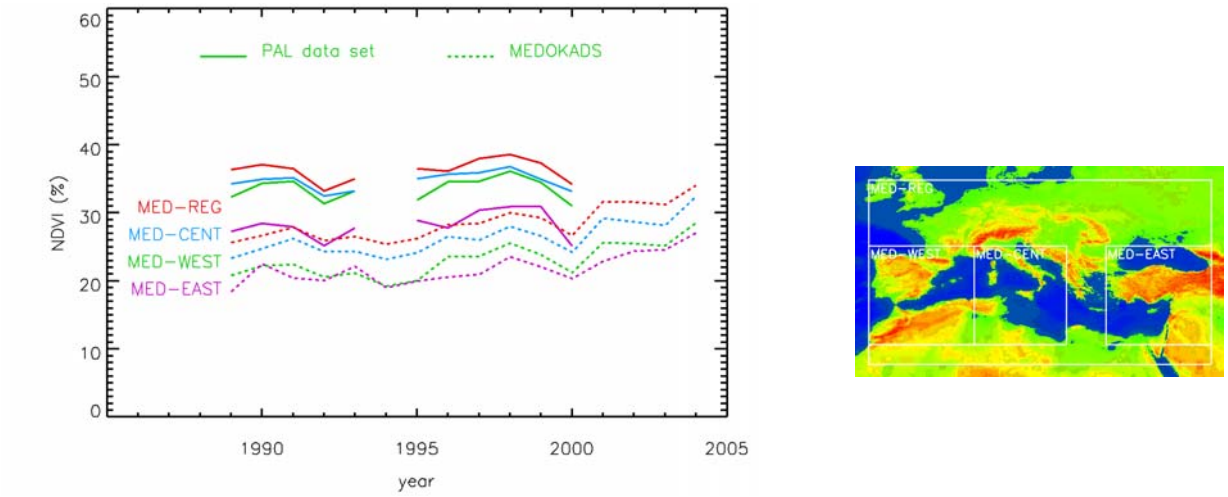

Figure 4. Annual mean of PAL and MEDOKADS NDVI for different regions.

The effect of higher NDVI for PAL data has to be searched in the original data. NDVI is defined as the result of the difference from channel 2 and channel 1 divided by the sum of channel 2 and channel 1. Tests have been made for the area of Spain. The mean of channel 1 for PAL data is up to 30 % smaller than the mean of channel 1 for MEDOKADS. The mean of channel 2 is about 10 % smaller than the mean of channel 2 for MEDOKADS. This leads to higher NDVI values for PAL data. The mean of NDVI for PAL data is 40 % greater than the mean of MEDOKADS. Other regions give the same results.

Figure 5 shows an extraction of MEDOKADS (a) and PAL (b) NDVI data after re-projection and resampling for the area of Spain. Because of the better resolution of MEDOKADS thin structures are visible which are disappeared in PAL data set. The histogram (c) shows the differences in NDVI for both data sets. The shape of both distributions are similar. The main differences is the shift between MEDOKADS and PAL data to higher values for PAL. The linear regression shows the same effect. It is characterized by an offset and by a slope less than 1.

The difference of the means of both data sets can be explained by missing atmospheric correction for MEDOKADS, different calibration coefficient and different resampling algorithms.

The PAL daily data are derived from GAC through averaging and resampling of original data. It is well known that a reduction in spatial resolution of a scene by averaging as well as resampling diminish the range of values because at least some of the minima and maxima of the data set vanish. Thus the slope of a linear regression line between original and reduced resolution data will be clearly less than 1 and the histogram of the data gets narrower. This indicates that a linear regression between PAL and MEDOKADS ever will show a slope less than 1.

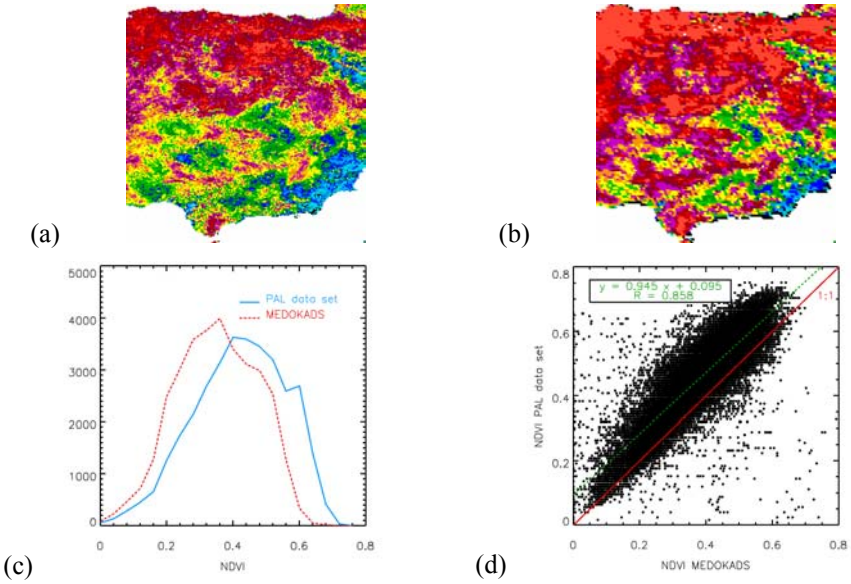

Figure 5. Inter-comparison of MEDOKADS (a) and PAL (b) NDVI with histogram (c) and linear regression (d) for the first decade of month June 2000 for the area of Spain.

Figure shows this effect of resampling and averaging. Figureb shows the resampled and Figurec the averaged image of original (Figurea). The resolution was minimised from 0.01° to 0.04°. Averaging gives a smoother image with a narrow scattering than the resampling method for linear regression (Figuree-f). Both methods are combined with loss of information. The slope of linear regression is less then 1. The histograms (Figured) changed slightly. Thin structures get lost when minimising resolution.

Koslowsky [6] found that the degradation for channel 1 of NOAA 11 is slightly higher than estimated from Rao [5] and the degradation for channel 2 is lower. This leads to higher NDVI values for PAL data. The calibration coefficient used for PAL data increase linear over the life-time for NOAA 14 [1]. Koslowsky [6] found that the degradation of AVHRR instrument is not linear during lifetime from NOAA 14. About 800 days after launch degradation process became smaller and vanish nearly completely towards end of mission.

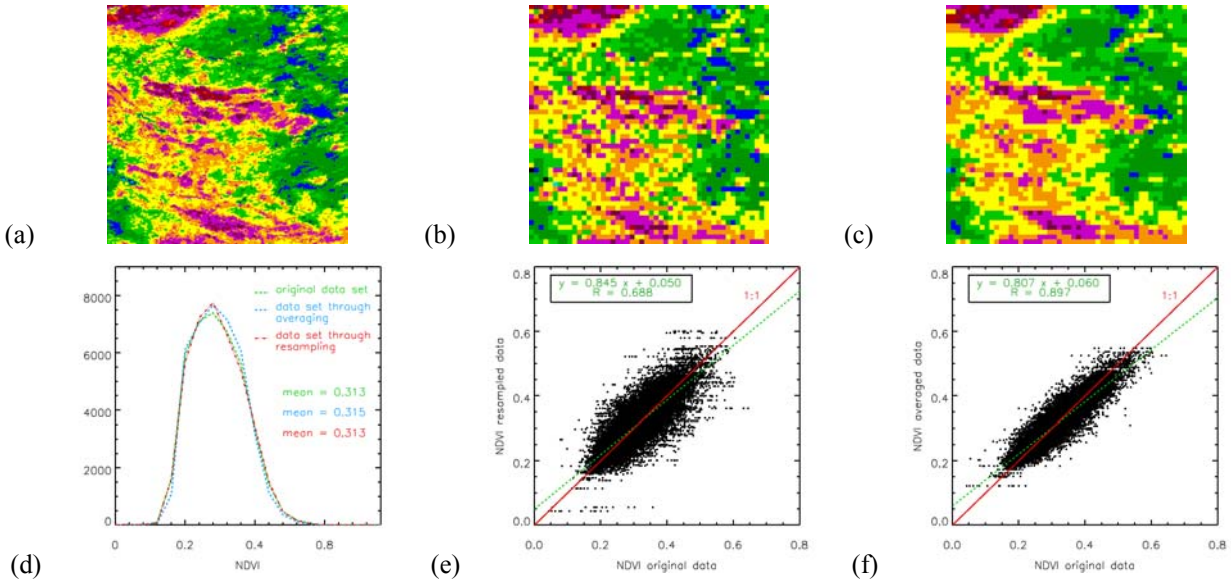

Figure 6. Effect due to resampling (b) and averaging (c) of original image (a), histogram for data sets (d), linear regression between original and resampled data (e) and averaged data (f) for an NDVI image.

This comparison shows that degradation is an ongoing process which can not be closed after a certain lifetime of sensor. Calibration for MEDOKADS is done for the whole lifetime of each sensor and changes in degradation process are considered.

The different calibration coefficients are not so important for the gap between PAL data and MEDOKDAS. The major reason for this gap is atmospheric correction.

If the atmospheric correction is made for all important processes within the atmosphere the NDVI increases because of the higher atmospheric influence of channel 2 than channel 1.

Figure 7 shows the inter-comparison for PAL data and MEDOKADS with recalibrated and atmospheric corrected data for MEDOKADS as done for PAL data. As shown in Figure c the estimated NDVI from PAL data is higher than the NDVI from MEDOKADS. This is due to the lower mean of channel 1 for PAL data (Figure a) than the mean for channel 1 of MEDOKADS. The atmospheric correction for PAL data is only made for Rayleigh scattering and ozone absorption. This correction leads to lower values in channel 1. The shape of the histogram and the mean for channel 1 (Figure a) suits very well for MEDOKADS after recalibration and atmospheric correction. The influence of channel 2 for the atmospheric correction is not as important (Figure b). Figure shows also that the effect of recalibration has less importance than the atmospheric correction. The shapes of the histograms and the means have not much changed for all channels after recalibration. The mean of NDVI for PAL data and MEDOKADS agrees good after recalibration and atmospheric correction even if the shape of the histogram differs (Figure c) due to different resampling methods during data treatment.

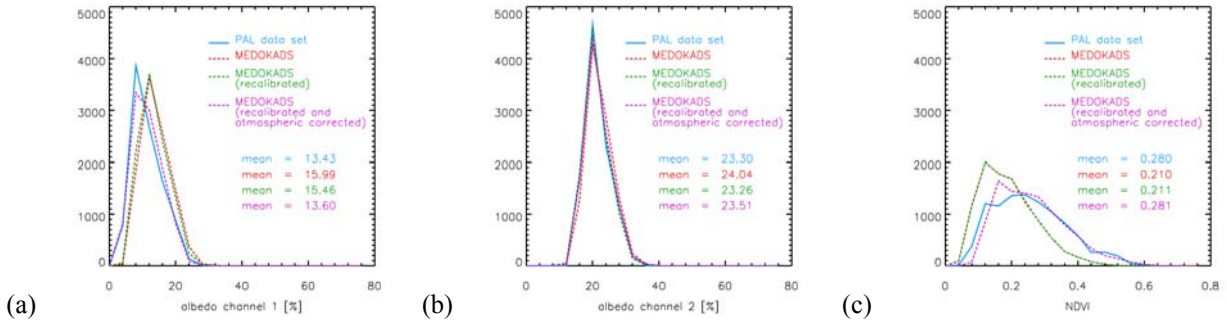

(a) (b) (c)

Figure 7. Histograms of PAL and MEDOKADS daily data (channel 1 (a), channel 2 (b), NDVI(c)) before, after recalibration and after recalibration and atmospheric correction (June 1st, 1995).

6 CONCLUSION

Incomplete atmospheric correction for PAL data set leads to considerable higher NDVI values as MEDOKADS. Through resampling and averaging the information of PAL data are reduced whereas all information are retained for MEDOKADS.

DeSurvey is a research project which will delivered a compact set of integrated procedures of desertification assessment and forecasting. High spatial resolution data sets are required to resolve local processes at the surface. MEDOKADS contains the full dynamic range of possible AVHRR data. Current data are included in MEDOKADS which is important to identify recent processes. PAL data set is an closed archive which covers 20 years of data and ends in 2001.

The results of this inter-comparison can be extrapolated to other regions which are covered by the PAL data set. When using PAL data set for inter-calibration with other satellites as SPOT, MODIS etc. those results has to be considered.

Because of all known parameter of sun and satellite geometry BRDF correction can be done for MEDOKADS. The BRDF has more influence on the data than the atmosphere. One of the next big steps to improve MEDOKADS is the implementation of BRDF correction.

REFERENCES

[1] RAO C.R.N. AND CHEN, J., 1999: Revised post-launch calibration of the visible and near-infrared channels of the Advanced Very High Resolution Radiometer (AVHRR) on the NOAA-14 spacecraft. *International Journal of Remote Sensing*, *20*, pp. 3485-3491.

[2] KOSLOWSKY, D., 1996: Mehrjährige validierte und homogenisierte Reihen des Reflexionsgrades und des Vegetationsindexes von Landoberflächen aus täglichen AVHRR-Daten hoher Auflösung; *Meteorologische Abhandlungen* : Ser. A, Monographien ; N.F., Bd. 9, H. 1.
[3] LUCHT, W. AND SCHAAF, C., 2000: BRDF Explained; http://geography.bu.edu/brdf/brdfexpl.html.
[4] KIDWELL, K., 1991: NOAA Polar Orbiter Data User's Guide. NCDC/SDSD. National Climatic Data Center, Washington, DC.(http://www2.ncdc.noaa.gov/docs/podug/index.htm).
[5] RAO, C.R.N., AND CHEN, J., 1995: Inter-satellite calibration linkages for the visible and near-infrared channels of the Advanced Very High Resolution Radiometer on the NOAA-7, -9, and -11 spacecraft. *International Journal of Remote Sensing, 16*, pp.1931 – 1942.
[6] KOSLOWSKY, D., BILLING H. AND ECKARDT, M., 2001: Sensor degradation and intercalibration of the shortwave channels of the AVHRR - NOAA 11/14/16 satellites. *Proc. of "The 2001 EUMETSAT Meteorological Satellite Data Users' Conference"*, Antalya,Turkey, 1-5 October 2001.

Analysis of the vegetation trends using low resolution remote sensing data in the Sahel (1982-1999) for the monitoring of desertification

Y.C. Hountondji[a,b], N. Sokpon[b] and P. Ozer[a]

[a] Environmental Sciences and Management Department, Liege University, Avenue de Longwy 185, B-6700 Arlon, Belgium, email: pozer@ulg.ac.be
[b] Faculty of Agronomy, University of Parakou, BP: 123 Parakou, Benin

ABSTRACT

The implementation of the United Nations Convention to Combat Desertification (UNCCD) needs the identification of areas that record declining productivity of the vegetation over long-time periods. In this scope, we analyze the state of the vegetation productivity using long-term time series (1982-1999) of NOAA-AVHRR NDVI data and compare it to rainfall data. For this, 315 rain gauges data distributed from yearly average isohyets 100 to 900 mm in five countries of West Africa (Mauritania, Senegal, Mali, Burkina Faso and Niger) are analyzed. The indicator we use here for trends analysis is the ratio between integrated vegetation index (iNDVI) during the growing period (June to October) and the May to October sum of rainfall (RR). This ratio is a proxy of the Rain Use Efficiency is the widely accepted

Overall, 91% and 94% of RR and iNDVI data recorded positive trends over the 1982-1999 period. Most stations in the Sahel were stable for the iNDVI/RR (49.5%). However, 37.8% showed strong to very strong negative change in the iNDVI/RR ratio, while only 1.3% showed positive trend. These strong negative trends recorded in more than 1/3 of the analyzed stations may reflect ongoing desertification processes in the Sahel and could be a starting point for the identification of hot-spots areas to determine where to take action within the National Action Programs (NAP) or Sub-Regional Action Programs (SRAP) to combat desertification.

Keywords: Low resolution remote sensing; integrated NDVI; Rainfall; Trend analysis; Desertification, Sahel.

1 INTRODUCTION

After about two decades of dramatic rainfall deficits that started in the late 1960s [1], the Sahel of West Africa has experienced increasing precipitation since the early 1990s [2-3]. Although increasing human pressure on the environment over the same period may have enhanced desertification processes, some authors suggested that the Sahel has been greening from the early 1980s to the late 1990s [4-5].

Since the mid-1970s, desertification benefited of a considerable interest from scientists, politics and the public. Land degradation in arid lands is now recognized as one of the major environmental problems for the 21st century [6] and the Sahel of West Africa is often quoted as the most seriously affected region. Yet, desertification processes often evoke an image of advancing desert with moving dunes threatening houses, roads, oasis and fertile lands and leaving behind a barren and sterile environment. The term desertification has been misused for a long time due to the lack of data, objective indicators and rigorous scientific studies, and because of the inexistence of a widely accepted definition [7]. Many authors have experienced a wide range of indicators in order to map the occurrence and severity of desertification [8-9]. Although many of these indicators were unsatisfactory because of their prohibitive costs and time-consuming for the process of data collection, low resolution satellite remote sensing data provide a good source of stable, reliable and long-term measurements [10-11]. Methods have been developed to assess the vegetation net primary production (NPP) from the Normalised Difference Vegetation Index (NDVI) [12, 13]. In this paper, a proxy of a remotely sensed indicator of rain use efficiency is used in order to identify areas suffering from desertification.

2 DATA AND METHODS

2.1 Meteorological station data

Monthly rainfall data were made available from an archive assembled by the “Projet Alerte Précoce et Prévision des Productions Agricoles (AP3A)” of the Centre Régional Agrhymet from station observations. Database includes

meteorological stations through the nine countries that grouped in the Inter-States Committee for Drought Control in the Sahel (CILSS). 315 rain gauges with complete monthly rainfall data from 1982 to 1999 were selected in five countries of West Africa (Mauritania, Senegal, Mali, Burkina Faso and Niger). Here we used the total rainfall records during rainy seasons (RR) that extend from May to October. The stations distribution and repartition according the bioclimatic zones [9] is shown in figure 1 and table 1.

Table 1. Selected stations in West Africa within the 100 to 900 mm isohyets.

COUNTRY	Number of selected station per climatic zone				Total
	100-300	300-500	500-700	700-900	
Burkina Faso	-	12	35	46	93
Mali	8	12	15	18	53
Mauritania	20	2	-	-	22
Niger	30	55	14	2	101
Senegal	7	20	15	4	46
Total	65	101	79	70	315

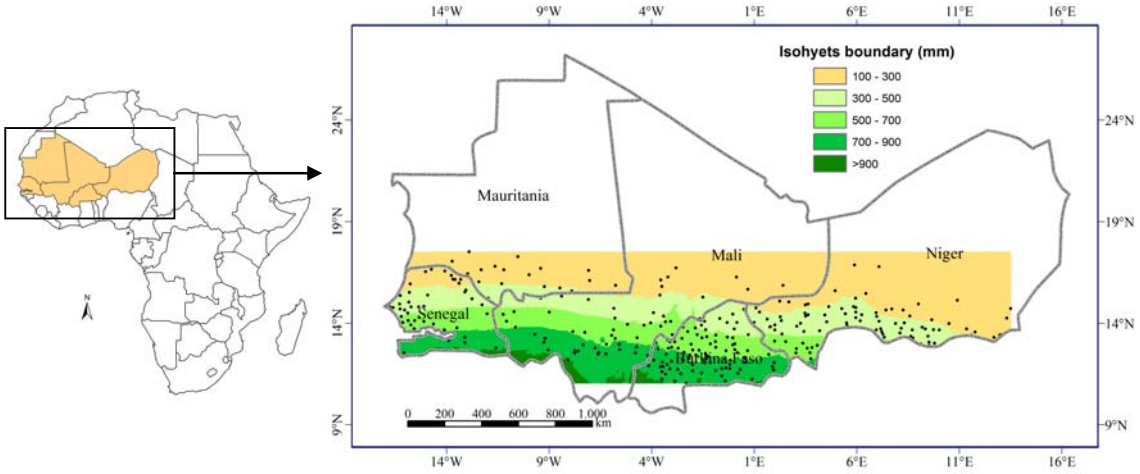

Figure 1 Geographical position of the studied stations (black dots) and bioclimatic zones (isohyets defined by kriging on average rainfall value for the 1980-2000 period).

2.2 Satellite data

For the purpose of analysing vegetation dynamics at sub-continental scale, satellite data from the NOAA AVHRR sensing system for the period 1982–1999, using the Normalized Difference Vegetation Index (NDVI) were used. The NASA/NOAA Pathfinder AVHRR Land (PAL) dataset [14] has been generated as monthly maximum value composites at a 8 km x 8 km pixel resolution. Noise levels can be very high over many areas in Africa but are comparatively low over arid to sub-humid areas where cloudiness is limited [15]. Quality issues of the Pathfinder database are discussed by Prince and Goward [16]. The NDVI has proved useful in numerous monitoring studies of vegetation and drought. It is calculated as the normalised difference in reflectance between the red band (0.55 μm - 0.68 μm) and the near infrared band (0.73 μm – 1.1 μm). This quantity is considered to be a "greenness" index. In arid and semiarid regions, it is well correlated with such parameters as leaf area index, greenleaf, biomass, vegetation cover, etc. [17].

In the present study, the time serie was restricted to the period 1982–1999 because after 1999 there was a significant shift in the NDVI values [4], probably caused by late afternoon overpass of NOAA-14. A total of 315 pixels were selected when including a rain gauge station. For all pixels, the seasonal vegetation index integral (iNDVI) covering the entire growing season from June to October were computed in order to assess the annual net primary production [18]. This approach has been preferred to the use of rasterized rainfall data obtained from satellite estimations, because of stormy features and high spatial variation of sahelian rainfall. Previous studies in

Niger [19] exhibit a significant difference in annual rainfall score within a distance of 10 km. This implies that the spatial rainfall variability on a small scale is more significant than on the survey level scale.

2.3 Method

2.3.1 Indicator of rain use efficiency

The net annual increase of biomass, or net primary production, is a measure of the production of an ecosystem. This quantity bears a direct relationship to photosynthesis and NDVI is strongly correlated with both, particularly in arid lands. Le Houérou [20] suggests that the ratio of primary production to rainfall, iNDVI/RR (rain use efficiency) is a better parameter to characterise arid and semi arid regions like the Sahel. In the Sahel, the dynamic of the vegetation is strongly linked to the rainfall evolution [10, 21-23]. For regions laying in the annual rainfall 100 mm to 900 mm, the iNDVI/RR ratio is regarded as a useful proxy for rain-use efficiency [7, 22]. As mentioned by previous studies in the West African Sahel with spatially comprehensive measurements such as these, the incidence of the individual components of desertification could be detected [24-26].

2.3.2 Trend analysis

For each station, trends from 1982 through 1999 were estimated by linear regression considering the ratio iNDVI/RR as dependant variable and time (years) as independent variable. Regression slopes were recorded for each station as parameters characterising the global trends either for the rainfall or for NDVI. Moreover, each slope was mapped in seven classes indicating very strong, strong, weak positive or negative and stable trends, adapting a procedure suggested by Eklundh and Olsson [4]. The regression procedure supplies a Student-t test and its resulting significance p-level to analyse the hypothesis that the slope is equal to 0. This p-level was used as a criterion to define the class boundaries. The trends, for the iNDVI/RR ratio, were labelled as "very strong" if the p-level exceeded 0.05 for the one-tailed t-test, "strong" if the p-level ranged between 0.05 and 0.1, "weak" if the p-level is between 0.1 and 0.2 and otherwise “stable” if the p-level is up to 0.2. These long-term linear trends for each pixel in the iNDVI/RR ratio may be understood as a combination of a number of interrelated factors including variations of biophysical and human influences. As the iNDVI/RR ratio is thought to remain stable through time, such trends can be interpreted as a measure of possible degradation or improvement of the vegetation growth.

3 RESULTS

3.1 Rainfall

A preliminary analysis of rainfall data indicates increasing rainfall in the Sahel of West Africa during the studied period (Fig 2). Overall, 91.4% of May to October rainfall recorded positive slope over the 1982-1999 period (not shown). In detail, 41.9% of the stations showed a very strong to strong positive trend, and 16.2% recorded a weak positive change. Stability characterised 41% of the analysed stations, while less than 1% recorded a weak negative trend. Stations that have recorded the most remarkable positive changes seem to follow a north-south geographic gradient and one station on two shows a stable tendency in the rainfall fringe between 700-900 mm. Such results were expected especially when considering that the drought period culminated in the early 1980s [1-3, 27] that is the beginning of the analysed dataset. In addition, these results are in accordance with recent investigations on rainfall variations in the Sahel suggesting that the drought may have ended in the early 1990s [2].

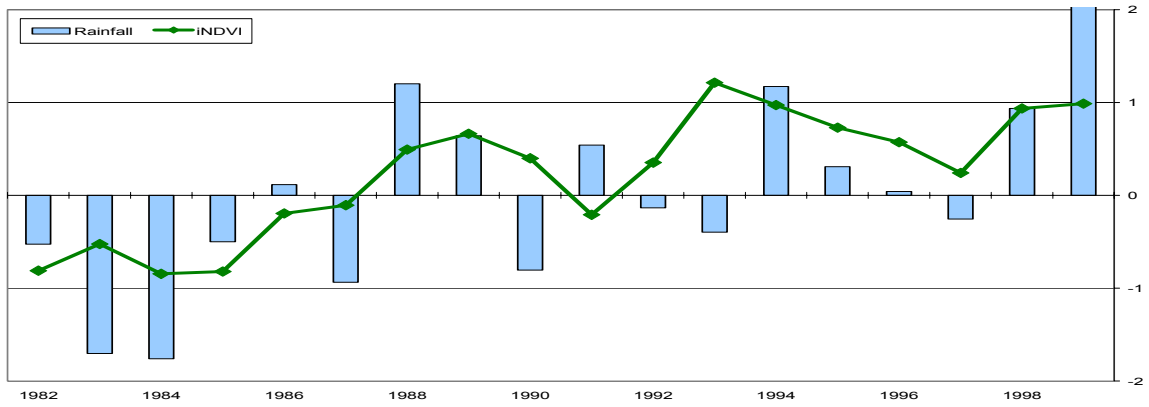

Figure 2: Average Z-scores (expressed as standard deviations) of iNDVI and rainfall for the 315 stations. The iNDVI values for the 315 stations are the mean value covering 64 km^2 centered on each climatic station.

3.2 The seasonal vegetation index (iNDVI)

Over the 315 pixels analysed in the Sahel of West Africa, 58.4% presented a very strong and strong positive change in iNDVI, while it remained stable in 30.8% of cases (not shown). These results are similar to those of Eklundh and Olsson [4] who observed a strong increase in seasonal NDVI in the Sahel since 1982 interpreted as vegetation recovery from the drought periods of the 1980s. Other detailed studies in the same area showed that after a long period of strong land degradation, vegetation recovery was observed during the 1990s [24, 28-29].

An unanswered question remains: is this vegetation recovery fully resilient with increasing rainfall?

3.3 The iNDVI/RR ratio

Trend classes for change in the iNDVI/RR ratio are summarized in Table 2 and the spatial repartition of the concerned stations is mapped in Figure 3. Overall, a negative slope is recorded in 88.6% of the 315 analyzed stations, while the remaining stations (11.4%) are characterized by a positive trend. Detailed analysis shows that, for all considered stations, most areas (54.0%) remained stable during the 1982-1999 period. However, 18.7% and 12.7% presented a very strong and strong negative change, respectively. 13.3% showed a weak negative trend and only 1.3% showed positive change. About 45% of the analyzed stations have therefore experienced decreasing trends in the iNDVI/RR ratio that may reflect possible degradation of the vegetation growth, and therefore ongoing desertification processes. The geographical distribution of downward weak to strong trends is fuzzy and may indicate localized land degradation processes in some places while few others may experience improved land management.

Differences in changes are highlighted when considering phytogeographic areas of west Africa (Figure 4). In the sahelian belt (<500 mm in annual rainfall), 50% of the stations presented a relative stability, 13.8% showed a weak negative change and 29.6.7% strongly decreased. The sahelo-sudanese zone (500-700mm) seems to have been the most affected by land degradation as vegetation resilience to rainfall is the lowest among all phytogeographic areas of the studied zone. Yet, about the half (51.9%) of the 79 stations included in this region show a stable iNDVI/RR ratio, while 20.3% experienced a very strong negative trend and 11.4% a strong negative change. In the Sudanese zone (700-900 mm), 46% of the stations appeared to be stable, while 31.5% and 8.6% suffered from a strong and weak negative change, respectively. However, it is worth mentioning that theses regions include the only stations of west Africa that display a weak positive change (2.0%). The obtained results in this southern region should be taken with precaution as previous studies mentioned that the relationship between NDVI and rainfall tends to weaken when annual rainfall is higher than 1000 mm. As primary production remains relatively constant, water being not a major limiting factor [17, 23].

Such contrasting evolutions along the bioclimatic gradients of the semi-arid belt West Africa are in accordance with recent findings of Hiernaux and Turner [28]. These authors stated that risks of environmental degradation are moderate and mainly climate-driven in pastoral systems at the drier edge, while they are serious and mainly management-driven in the crop-livestock systems of the sahelo-sudanese zone. Our results indeed show that 54% of the stations remained stable in the northern part of the studied area, while about 45% of the analyzed stations suffered from very strong, strong or weak negative changes in the sahelo-sudanese zone in the central north. As a matter of fact, Henry and colleagues [30] showed that migration flows from the northern ecologically marginal area to the sahelo-sudanese zone were partly explained by unfavorable environmental variables such as high rainfall variability, land degradation, and land availability at the origin, and favorable conditions at the destination for these variables. For this reason, there is currently less pressure in the northern part of the Sahel as people migrated because of drought while migrations are likely to contribute to negative environmental changes at the destination [31].

Recent claims that the Sahel is greening since the 1990s because of improved land management [4-5, 32-33] may be only partly true. As an example, Mazzucato and Niemeijer [32], closely studied two small areas (Bilanga and Fada-N'Gourma) in eastern Burkina Faso and suggested that these areas showed no evidence of land degradation as crop yields increased. Our results on these two stations indeed show that if the iNDVI presented positive slopes, the iNDVI/RR ratio experienced a strong negative change in Bilanga and a weak negative change in Fada-N'Gourma, suggesting that the rain-use efficiency of the vegetation has been declining over the last two decades. In northern Burkina Faso (Gorom-Gorom), Rasmussen and colleagues [29] suggested that desertification was in reverse demonstrating that vegetation was reclaiming fossil dunes revitalized during the droughts of the 1970s and 1980s. Our results at this station suggest that the iNDVI strongly increased and that the iNDVI/RR ratio remained stable during the 1980s and 1990s. In this specific case, it can be accepted that the vegetation is resilient with the rainfall increase observed during the last decade.

Table 2: Rainfall (RR), integrated NDVI (iNDVI) and rain use efficiency (iNDVI/RR) trends for 315 stations in West Africa (1982 to 1999). *[Legend: POS: positive; NEG: negative; VSNC: very strong negative change; SNC: strong negative change; WNC: weak negative change; S: stable; WPC: weak positive change; SPC: strong positive change; VSPC: very strong positive change]*.

	SLOPES				TRENDS SIGNIFICANCE														Total	%
RR	POS	%	NEG	%	VSNC	%	SNC	%	WNC	%	S	%	WPC	%	SPC	%	VSPC	%		
100<P<300	58	89,2	7	10,8	1	0,0	0	0,0	0	0,0	25	38,5	13	20,0	10	15,4	16	24,6	65	20,6
300<P<500	95	94,1	6	5,9	0	0,0	0	0,0	0	0,0	31	30,7	21	20,8	15	14,9	34	33,7	101	32,1
500<P<700	74	93,7	5	6,3	0	0,0	1	1,3	0	0,0	33	41,8	9	11,4	10	12,7	26	32,9	79	25,1
700<P<900	61	87,1	9	12,9	0	0,0	0	0,0	1	1,4	40	57,1	8	11,4	10	14,3	11	15,7	70	22,2
Total	288	91,4	27	8,6	1	0,3	1	0,3	1	0,3	129	41	51	16,2	45	14,3	87	27,6	315	100
iNDVI	POS	%	NEG	%	VSNC	%	SNC	%	WNC	%	S	%	WPC	%	SPC	%	VSPC	%	Total	%
100<P<300	63	96,9	2	3,1	0	0,0	0	0,0	0	0,0	19	29,2	5	7,7	4	6,2	37	56,9	65	20,6
300<P<500	92	91,1	9	8,9	0	0,0	0	0,0	0	0,0	35	34,7	14	13,9	8	7,9	44	43,6	101	32,1
500<P<700	73	92,4	6	7,6	0	0,0	0	0,0	0	0,0	27	34,2	8	10,1	10	12,7	34	43,0	79	25,1
700<P<900	68	97,1	2	2,9	0	0,0	0	0,0	0	0,0	16	22,9	6	8,6	6	8,6	42	60	70	22,2
Total	296	94,0	19	6,0	0	0,0	0	0,0	0	0,0	97	30,8	33	10,5	28	8,9	157	49,8	315	100
iNDVI/RR	POS	%	NEG	%	VSNC	%	SNC	%	WNC	%	S	%	WPC	%	SPC	%	VSPC	%	Total	%
100<P<300	4	6,2	61	93,8	12	18,5	13	20,0	10	15,4	30	46,2	0	0,0	0	0,0	0	0,0	65	20,6
300<P<500	9	8,9	92	91,1	22	20,8	12	11,9	13	12,9	53	52,5	0	0,0	1	0,9	0	0,0	101	32,1
500<P<700	13	16,5	66	83,5	16	20,3	9	11,4	12	15,2	41	51,9	1	1,3	0	0,0	0	0,0	79	25,1
700<P<900	10	14,3	60	85,7	9	12,9	6	8,6	7	10,0	46	65,7	2	2,9	0	0,0	0	0,0	70	22,2
Total	36	11,4	279	88,6	59	18,7	40	12,7	42	13,3	170	54,0	3	1,0	1	0,3	0	0,0	315	100

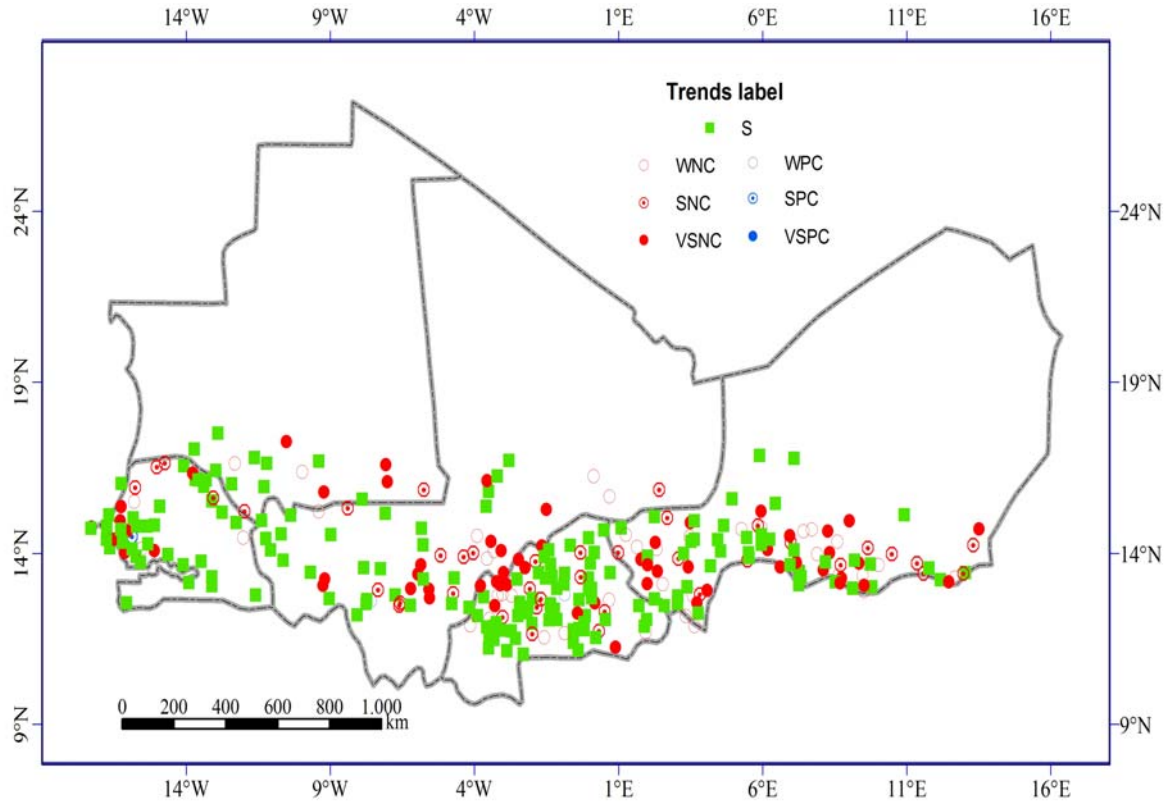

Figure 3. Trends in the iNDVI/RR ratio for 315 stations in West Africa (1982 to 1999). [Legend: VSNC: very strong negative change; SNC: strong negative change; WNC: weak negative change; S: stable; WPC: weak positive change; SPC: strong positive change; VSPC: very strong positive change].

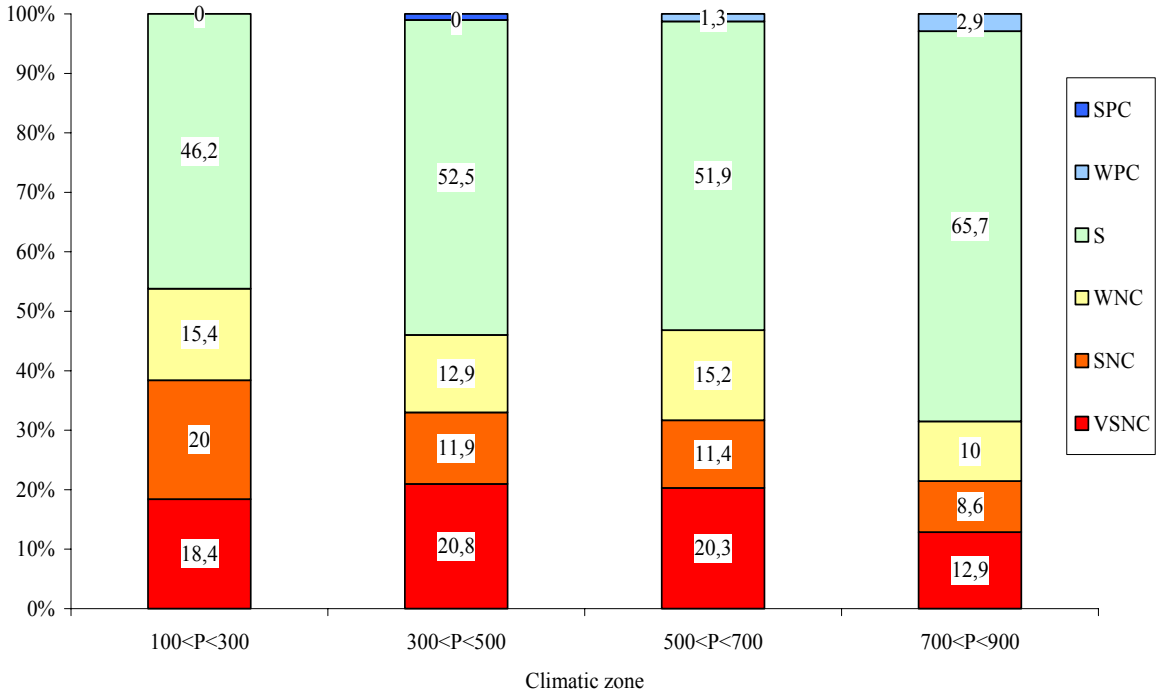

Figure 4: Relative change classes in the Rain Use efficiency considering the bioclimatic zone (100-900 mm). *[Legend: VSNC: very strong negative change; SNC: strong negative change; WNC: weak positive change; S: stable; VSPC: very strong positive change; SPC: strong positive change; WPC: weak positive change].*

As mentioned above, many biophysical and human influences may interfere in the evolution of the iNDVI/RR ratio. Increasing use of fertilizers, better water resources management and land rehabilitation measures have improved over the years. But despite such positive technical evolutions, only three stations out of 315 recorded a weak and strong positive change the iNDVI/RR ratio over the 1982-1999 periods. Another interference in the evolution of the iNDVI/RR ratio may be attributed to climate change due to the ongoing build-up of greenhouse gases. In many regions of the world, extreme precipitation events have significantly increased during the last decades [34]. Although no research on this topic is available in West Africa, a large increase in floods due to excess precipitation in short time periods has been observed lately that may suggest an increasing tendency in extreme precipitation events [35]. If this trend was confirmed, then the iNDVI/RR ratio may be negatively affected as extreme daily precipitation can not be fully used by vegetation and can further cause erosion and soil crusting.

5 CONCLUSION

Based on observations of increased crop yields and/or NDVI, recent studies have stated that desertification in the African Sahel was in reverse. However, using trends in the iNDVI/RR ratio, our results suggest that about 45% of the analyzed stations may have experienced ongoing desertification processes during the 1982-1999 periods. Our findings present an environmental situation that is probably more gloomy than recent papers stated although we are far from the concept of irreversible land degradation that was so fashionable until recently. Nevertheless, these results have to be taken with precaution because of the needs of biophysical significance of the stable trends recorded in the study. It is possible that the coarse spatial resolution of AVHRR data may hide undergoing trends that are not detectable at this scale. Otherwise, for more accurate investigations, any remote sensing-based monitoring system of land degradation in such area must be complemented by field data collection, in particular with floristic composition data which is not detectable from space, even at fine spatial resolutions. This could be a starting point for switching from empirical approaches based on vegetation indices, which suggest an improvement of the environmental situation at the regional scale, but that may not reflect real situation.

REFERENCES

[1] L'HÔTE, T., MAHÉ, G., SOMÉ, B. AND TRIBOULET, J.P., 2002: Analysis of a Sahelian annual rainfall index from 1896 to 2000; the drought continues. *Hydrol. Sc. J. 47*, pp. 563-572.

[2] OZER, P., ERPICUM, M., DEMAREE, G. AND VANDIEPENBEECK, M., 2003: The Sahelian drought may have ended during the 1990s. *Hydrol. Sc. J. 48*, pp. 489-492.

[3] DAI, A., LAMB, P.J., TRENBERTH K.E., HULME M., JONES P.D. AND XIE, P., 2004: The Recent Sahel drought is real. *Int. J. Climatol. 24*, pp. 1323-1331.

[4] EKLUNDH, L. AND OLSSON, L., 2003: Vegetation index trends for the African Sahel 1982-1999. *Geophys. Res. Lett. 30*, 10.1029/2002GL016772.

[5] PEARCE, F., 2002: Africans go back to the land as plants reclaim the desert. *New Scient. 175*, pp. 4-5.

[6] WORLD BANK, 2003: World development report 2003: Sustainable development in a dynamic world: transforming institutions, growth, and quality of life. Oxford University Press, New Delhi.

[7] NICHOLSON, S.E., TUCKER, C.J. AND BA, M.B., 1998: Desertification, drought, and surface vegetation: an example from the West African Sahel. *Bull. Am. Meteorol. Soc. 79*, pp. 815-829.

[8] MOUAT, D., LANCASTER, J., WADE, T., WICKHAM, J., FOX, C., KEPNER, W. AND BALL, T., 1997: Desertification evaluated using an integrated environmental assessment model. *Environ. Monitor. Assessm. 48*, pp. 139-156.

[9] OZER, P., 2000: Les lithométéores en région sahélienne: un indicateur climatique de la désertification. *GEO-ECO-TROP. 24*, pp. 1-317.

[10] SYMEONAKIS, E. AND DRAKE, N., 2004: Monitoring desertification and land degradation over sub-Saharan Africa. *Int. J. Rem. Sens. 25*, pp. 573-592.

[11] PRINCE, S.D., 2002: Spatial and temporal scales for detection of desertification. In: Reynolds, J.F. and Stafford Smith, D.M. (eds): Global desertification: Do humans cause deserts?, pp. 23-40. Dalhem University Press, Dalhem.

[12] JUSTICE, C.O., 1986: Monitoring the grasslands of semi-arid Africa using NOAA-AVHRR data. *Int. J. Rem. Sens. 7*, pp. 1383-1622.

[13] PRINCE, S.D. AND JUSTICE, C.O., 1991: Coarse resolution remote sensing in the Sahelian environment. *Int. J. Rem. Sens. 12*, pp. 1133-1421.

[14] JAMES, M.E. AND KALLURI, S.N.V., 1994: The Pathfinder AVHRR land data set: an improved coarse resolution data set for terrestrial monitoring. *Int. J. Rem. Sens. 15*, pp. 3347–3364.

[15] CHAPPELL, A., SEAQUIST, J.W. AND EKLUNDH, L., 2001: Improving the estimation of noise from NOAA AVHRR NDVI for Africa using geostatistics. *Int. J. Rem. Sens. 22*, pp. 1067-1080.

[16] PRINCE, S.D. AND GOWARD, S.N., 1996: Evaluation of the NOAA/NASA Pathfinder AVHRR Land Data Set for global primary production modelling. *Int. J. Rem. Sens. 17*, pp. 217–221.

[17] NICHOLSON, S.E., DAVENPORT, M.L. AND MALO, A.R., 1990: A comparison of the vegetation response to rainfall in the Sahel and East Africa, using normalized difference vegetation index from NOAA AVHRR. *Climatic Change 17*, pp. 209-241.

[18] DIALLO, O., DIOUF, A., HANA, N.P., NDIAY, A. AND PREVOST, Y., 1991: AVHRR monitoring of primary production in Senegal, West Africa. *Int. J. Rem. Sens. 12*, pp. 1259-1279.
[19] AMANI, A. AND LEBEL, T., 1997: Lagrangian kriging for the estimation of Sahelian rainfall at small time steps. *J. Hydrol. 192*, pp. 125–157.
[20] Le HOUÉROU, H.N, 1984: Rain-Use Efficiency: a unifying concept in arid land ecology. *J. Arid Environ. 7*, pp. 1-35.
[21] HESS, T., STEPHENS, W. AND THOMAS, G., 1996: Modelling NDVI from decadal rainfall data in the North East arid zone of Nigeria. *J. Environ. Manag. 48*, pp. 249-261.
[22] FOODY, G.M., 2003: Geographical weighting as a further refinement to regression modelling: an example focused on the NDVI-rainfall relationship. *Rem. Sens. Environ. 88*, pp. 283-293.
[23] DAVENPORT, M.L. AND NICHOLSON, S.E., 1993: On the relation between rainfall and Normalized Difference Vegetation Index for diverse vegetation types in East Africa. *Int. J. Rem. Sens. 12*, pp. 2369-2389.
[24] DIOUF, A. AND LAMBIN, E.F., 2001: Monitoring land-cover changes in semi-arid regions: remote sensing data and field observations in the Ferlo, Senegal. *J. Arid Environ. 48*, pp. 129-148.
[25] RASMUSSEN, M.S., 1998: Developing simple, operational, consistent NDVI-vegetation models by applying environmental and climatic information: Part I. Assessment of net primary production. *Int. J. Rem. Sens. 19*, pp. 97-117.
[26] TOTTRUP, C. AND RASMUSSEN, M.S., 2004: Mapping long-term changes in savannah crop productivity in Senegal through trend analysis of time series of remote sensing data. *Agric. Ecosyst. Environ. 103*, pp. 545-560.
[27] NICHOLSON, S.E., 1985: Sub-Saharan rainfall 1981-1984. *J. Climate Appl. Meteorol. 24*, pp. 1388-1391.
[28] HIERNAUX, P. AND TURNER, M.D., 2002: The influence of farmer and pastoralist management practices on desertification processes in the Sahel. In: Reynolds, J.F. and Stafford Smith, D.M. (eds): Global desertification: Do humans cause deserts?, pp. 135-148. Dalhem University Press, Dalhem.
[29] RASMUSSEN, K., FOG, B. AND MADSEN, J.E., 2001: Desertification in reverse? Observations from northern Burkina Faso. *Global Environ. Change 11*, pp. 271-282.
[30] HENRY, S., BOYLE, P. AND LAMBIN, E., 2003: Modelling inter-provincial migration in Burkina Faso, West Africa: the role of socio-demographic and environment factors. *Appl. Geogr. 23*, pp. 115-136.
[31] LAMBIN, E.F., TURNER, B.L. II, GEIST, H.J., AGBOLA, S.B., ANGELSEN, A., BRUCE, J.W., COOMES, O., DIRZO, R., FISCHER, G., FOLKE, C., GEORGE, P.S., HOMEWOOD, K., IMBERNON, J., LEEMANS, R. LI, X., MORAN, E.F., MORTIMORE, M., RAMAKRISHNAN, P.S., RICHARDS, J.F., SKÅNES, H., STEFFEN, W., STONE, G., SVEDIN, U., VELDKAMP, T.A., VOGEL, C. AND XU, J., 2001: The Causes of land-use and -cover change: moving beyond the myths. *Global Environ. Change 11*, pp. 261–269.
[32] MAZZUCATO, V. AND NIEMEIJER, D., 2000: The cultural economy of soil and water conservation: market principles and social networks in Eastern Burkina Faso. *Development and Change*, *31*, pp. 831-855.
[33] NIEMEIJER, D. AND MAZZUCATO, V., 2002: Soil degradation in the West African Sahel. How serious is it? *Environment*, *44*, pp. 20-31.
[34] HOUGHTON, J.T., DING, Y., GRIGGS, D.J., NOGUER, M., VAN DER LINDEN, P.J., DAI, X., MASKELL, K. AND JOHNSON, C.A., 2001: Climate Change 2001: The Scientific Basis. Cambridge University Press, New York.
[35] SENE, S. AND OZER, P., 2002: Evolution pluviométrique et relation inondations – événements pluvieux au Sénégal. *Bull. Soc. Géogr. Liège 42*, pp. 27-33.

Application of NOAA NDVI to assess vegetation distribution depending on climatic variables and anthropogenic impact: A case study in an arid region of Kazakhstan

M. Kappas[a], N.R. Muratova[b] and P. Propastin[a]

[a] Inst. of Geography, University of Göttingen, Cartography, GIS & Remote Sensing Dept.
[b] Remote Sensing Institute of Science Academy of Kazakhstan, Almaty

ABSTRACT

The territory of Kazakhstan is a perfect target for using AVHRR data in land cover – land use studies. Deserts and semi-deserts take over 80 % of the whole area. A degradation of most arid areas (60 %) of Kazakhstan cased on overgrazing during the Soviet era. The most important types of degradation in the arid pastoral areas are vegetation degradation and wind erosion. During the 20th century the area of Kazakhstan experienced two grandiose land cover changes: first was in the 1954-1960 - ploughing up the *tselina* (virgin land), being a major livestock rearing land, since then the major pasture areas were transferred from the *tselina* into desert and semi-desert zones; the second change happened during the last 10 years of 20th Century, when the Soviet economic collapsed and the agriculture of Kazakhstan creased. The decreased anthropogenic impact during this time due to a significant reduction of crop yield and stocks heads conducts to a regeneration of ecosystems and increase of vegetation activity at some areas, in spite of bad rainfall conditions. The primary objective of this study is to assess the predicting force of rainfall and temperature to spatial distribution of vegetation and the inter-annual variability of its cover in a dry region of middle Kazakhstan. Because of a high difference in elevation in this area, the relief also is a strong predicting factor. A further important predictor is anthropogenic impact. The conceptual framework for the study of the relationships between the Normalized Difference Vegetation Index (NDVI) for the growing season of every year in the study period (1985-2001) and the predicting factors is based on spatial correlation and spatial regression models. Simple, partial and multiple correlations for each of the years (1985-2001) are calculated to estimate the degree of NDVI dependence on the predicting factors. A land degradation monitoring system based on three indicators - a non-spatial indicator and two spatial indicators – is tested. Spatial multiple correlation coefficient *R* was considered to be a non-spatial indicator for land degradation. This indicator is very sensitive to the time-variations of anthropogenic impact. A lack of rainfall over a certain time and area is the second indicator. Areas below normal rainfall values and areas with plentiful rainfall values during the period 1985-2001 are determined. The above described trend in the residual values is evaluated as the third indicator for land degradation. The three indicators are then combined and this combination of indicators is used to set up an improved map of land degradation risk in middle Kazakhstan. The selected combination enables a better discrimination between land degradation induced by man and that induced by climate.

Keywords: Land Degradation Monitoring System, Kazakhstan, NOAA NDVI

1 INTRODUCTION

Satellite imagery data of NOAA AVHRR sensor have been used for assessment of green vegetation cover both at global and regional scales. The sensor gave a continuous spatial cover on a regular frequency of the photosynthetic activity, which can be expressed by indices such as Normalized Difference Vegetation Index (NDVI). The correlation between NDVI and biomass is well established [1]. NDVI and rainfall show a good correlation, both in a spatial and temporal sense [2, 3, 4, 5]. The relationship between NDVI and temperature is reported to be weaker but also significant [6].

First, the spatial relationships between vegetation and both climatic and relief predictors were examined and statistically described. We also examined a dependence of vegetation distribution on inter-annual variability of climatic factors. Then we tried to estimate how the decrease of anthropogenic impact influenced the relations. Second, an assessment of land degradation for the study area was done. We composed a set of degradation indicators which evaluate climatic, biotic, and anthropogenic processes that contribute to degradation. The used indicators enable to show the development process of degradation and then that of rehabilitation of ecosystems in the study area. All three indicators are then combined in order to identify areas that are defined as suffering from degradation. Finally the results of the degradation assessment are compared with results of field surveys for a calibration.

2 STUDY AREA

The study area is located between 46 and 50° northern latitude and 70° and 76° eastern longitude. It comprises the most *raions* (districts) of Karaganda *oblast* (province). The region is divided into two geographical sections: Sary-Arka and Betpak-Dala. The Sary-Arka occupies the northern part of the study area and includes both semi-desert zone (the thin transit zone between desert and dry steppe) that situated 120-200 km lengthways the 48° northern latitude and steppe zone. The clay desert Betpak-Dala builds the southern part of the research area.

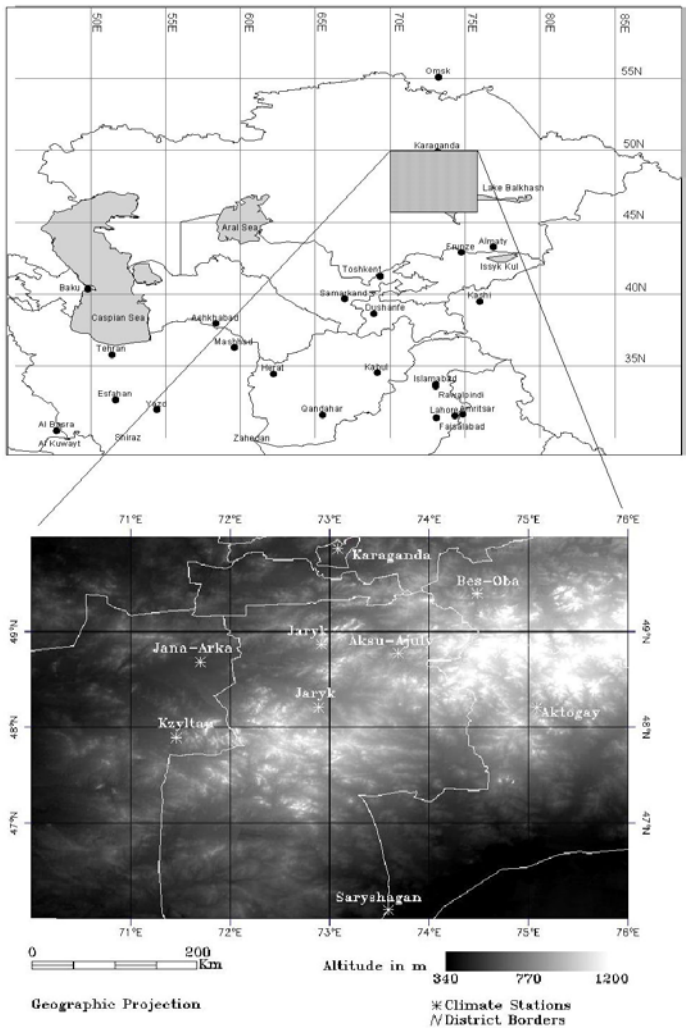

Figure 1. Study Area.

In terms of surface structure the study area is divided into two large regions: a plateau of rolling upland in the southern, western, and northern parts with average elevations 300-700 meter; hills and mountains in the central and north-eastern parts with elevations 700-1100 meter. The study area is only pure drained. The climate of the region is dry, cold and shows high continentality. Average annual precipitation is above 250 mm per year in the north of the study area, and below 150 mm in the south. The temperature amplitude is high: average January temperature is below –12° C and average July temperature is about 26-28° C. The typical vegetation classes of northern desert and steppe are represented in the study area. The vegetation of the semi-desert and desert is sparse, low-growing, and of a monotonous light grey colour. The desert zone is dominated by sagebrush and perennial saltwort associations. The most spreading vegetation species here are *Artemisia terrae-albae, Artemisia pauciflora.* In basins, were solonchak and solonetz develops, the halophytic species such as *Anabasis salsa, Salsola orientalis, Artiplex cana* and *Salsola arbusciliformis* are prevalent. The semi-desert type of vegetation is a gradual transition from desert to steppe type. The semi-desert has a complex combination of real steppe turf grasses and semi-shrubs with halophytes. This zone is occupied by shrubs such as *Artemisia pauciflora, Artemisia incana, Artemisia lessingiana*, *Festuca sulcata* and *Stipa lessingiana*. Other semi-desert plants are *Kochia prostrata, Halocnemum strobilaceum* and the saltbush *Artiplex cana* of the halophytes. The northern section of the study area lays in the dry steppe zone, were dominate short grassland species such as *Festuca sulcata, Stipa capillata, Stipa lessingiana* and *Filipendula ulmaria.* In the higher parts can be found larch and birch forests and mixed grasslands. The land resources in the desert and semi-desert zone of Kazakhstan were always used by the Kazakh people as pasture. The natural pasture use was strongly determined by climate factors and was limited by presence of water places. By this type of pasture use there is no possibility for long time overgrazing. During the Soviet period the productive steppe zone (with rainfall above 300 mm per year) was ploughed up in the 1950s. Since then, the major pastoral zones have been in the semi-desert and desert regions, and these regions began intensive to degrade.

3 DATA USED IN THE STUDY AND ITS PREPARATION

3.1 NOAA NDVI

To monitor spatial and temporal variations and trends of vegetation activities we used 10 day maximum NDVI composites of the AVHRR sensor with a spatial resolution of 8 km. The data cover the period of growing season

(April-October) from 1985 to 2001. Using a method described by Los [7, 8] NDVI data were calibrated against three time invariant desert targets located in the Big Arabian Desert, Nubia Desert and Taklamakan Desert. This method removes effects of sensor degradation and corrects drift between different sensor systems. In addition to that, we removed noisy pixel areas characterized by exceptionally low NDVI values relatively to their pixel neighbourhood. This pixels represented large cloud areas and were replaced by a mean value calculated from the temporal neighbouring NDVI layers. The 10-day NDVI composites were integrated to monthly and then to mean growing season values for each year.

3.2 Rainfall and Temperature

Climate data were retrieved from the yearly statistics by the National Hydrometeorological Centre of Kazakhstan (NHMCK). This data contain 10-day records for growing season (April-October 1985-2004) of two variables for 9 climate stations (figure 1): mean temperature (°C) and mean rainfall amount (mm). Contour maps for precipitation and temperature were build up for each year. These contour maps were transformed into raster maps. The raster maps – sum rainfall and mean temperature for growing season – were prepared for each year and integrated in the analysis process. In the interpolation process of the climatic stations a SRTM-DTM was used.

3.3 Digital terrain model

A digital terrain model for the study area with a pixel size of 3 arc second (90 m) was down loaded from the active web-site of SRTM (Shuttle Radar Topography Mission). The down loaded 16 separate files of DTM were already georeferenced.

3.4 Land cover and vegetation types

Two vegetation maps of Kazakhstan (for 1959 and 1995 years) and a digital map of Eurasian ecosystems were used to locate control sites. For each of the selected sites a temporal 10-day NDVI-profile for growing season 1992-1993 years was examined and compared with the other sites. Each vegetation association determined in the study area shows a multi-temporal NDVI-profile that was clearly different from others. This property was used to perform classification of land cover types. To determine areas occupied by the main vegetation associations and land cover types a principal component analysis (PCA) was carried out using the 63 10-day images (1985-1988). The first three principal components, which accounted about 97 % of the total variance of the 63 images, were then used for supervised classification with the maximum likelihood algorithm (MLA). The resultant land cover map was resized to 1*1 km pixel spatial resolution (figure 2).

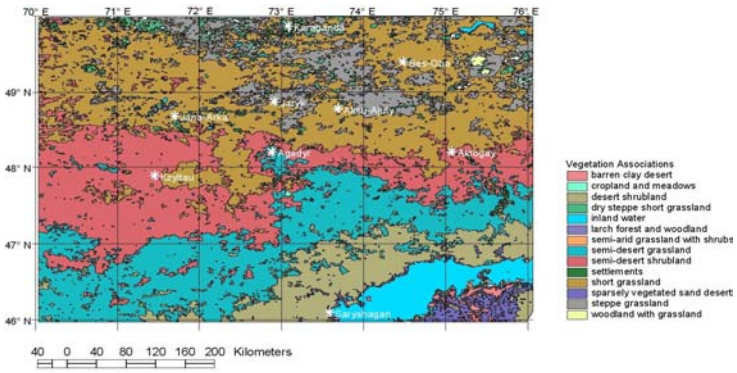

Figure 2. Vegetation Associations of the study area.

4 METHODS

A general surrogate of all vegetation characteristics (green biomass, ground covering percent, photosynthetic activity, leaves area, etc.) is NDVI. To estimate the relationships between the vegetation distribution/condition and its predicting factors we carried out the following statistical calculations.

4.1 Statistical methods

We had 4 spatial variables for statistical analysis: NDVI, rainfall amount, temperature and altitude. The NDVI was interpreted as a response variable and the others were suggested to be independent from the NDVI, but we had not excluded a possible dependence between them. Various spatial simple, partial, and multiple correlations were computed to determine a predicting value of each of the predictors and that of all together. The statistical analysis involved mean annual values of all variables for growing season and altitude. Both climatic variables vary in the space and time. Altitude is temporally constant but spatially variable. Correlation coefficients between all variables for each year were calculated. To avoid a possible multicollinearity we calculated also partial correlations. The partial correlation coefficient was calculated by using the equation:

$$r_{ab.c} = \frac{r_{ab} - r_{ac} * r_{bc}}{\sqrt{(1 - r_{ac}^{\ 2}) * (1 - r_{bc}^{\ 2})}} \quad (1)$$

where *r* is correlation coefficient; *a, b* and *c* are variables NDVI, rainfall and temperature or relief (the variable staying after point will be excluded).

Multiple correlations between NDVI and responsible variables were also calculated. The multiple correlation coefficients enable to estimate the collective influence of climatic factors on NDVI and its spatial distribution. The used equation is:

$$R_{abc} = \sqrt{\frac{r_{ab}^{\ 2} + r_{ac}^{\ 2} - 2 * r_{ab} * r_{ac} * r_{bc}}{1 - r_{bc}^{\ 2}}} \quad (2)$$

where R_{abc} is multiple correlation coefficient; r_{ab}, r_{ac} and r_{bc} are simple correlation coefficients between variables NDVI, rainfall and temperature.

A spatial multiple linear regression analysis was performed using the response variable, NDVI, and both climatic variables. For each year we fitted a multiple linear regression model that gives the NDVI value for each pixel in its dependence from the climatic predictors. The full linear model equation is expressed as:

$$\text{NDVI} = \beta + \beta 1 + \beta 1(T) + \beta 2(P) + \varepsilon \quad (3)$$

where β is the intercept, $\beta 1$ and $\beta 2$ are regression coefficients of the climatic predictors, and ε is random error.

The coefficients were estimated with the ordinary least squares procedure. The model parameters were tested sequentially: first, the term for precipitation $\beta 2$; next, the term $\beta 1$; and then the intercept β. If the two terms were evaluated as not significantly different, then these parameters were averaged and the model was refit, using the averaged parameters. We calculated a multiple regression equation for each of the 17 years (1985-2001) and the mean equation averaged for the whole period.

4.2 Identification of climatic signal

First, standard deviations of annual NDVI and of annual rainfall amounts for each pixel were calculated for the 1985-2001 period, after that a spatial correlation between the derived images was computed. Second, the same calculations for the anomalies of both variables were calculated. A high spatial correlation between these derived variables would indicate, that a spatial inter-annual variability of rainfall predicts the inter-annual variability of vegetation conditions.

4.3 Identification of areas with anthropogenic impact

In order to remove the effect of precipitation and temperature, the difference ($NDVI_{o\text{-}p}$) between the observed $NDVI_o$ and $NDVI_p$ was calculated. As a result we got 17 scenes of $NDVI_{o\text{-}p}$. Then for each pixel the temporal trend of $NDVI_{o\text{-}p}$ during the period 1985-2001 was calculated. Assuming that any trend through time present in the residuals would indicate change in *NDVI* response that is not due to climatic variables. According to this assumption, a negative trend would indicate an area liable to human induced degradation. A positive trend would indicate an area with diminishing human impact.

5 RESULTS

5.1 Relationships between spatial distribution of NDVI and spatial pattern of rainfall, temperature and relief

Rainfall during the mean growing season ranges from less than 110 mm in the southern part to more than 260 mm on the north-east. The NDVI varies between 0 and 0.45. These are typical values for dominant xerophytic formations. Values lower than 0.05 in the bare desert of the southern part indicate areas with no photosynthetic activity. These are solonchak areas or vegetation free sand masses. Values more than 0.35-0.40 in the steppe zone indicate feather-fescue-grass steppe and mixed grass steppe with birch groves. The spatial distribution of NDVI roughly corresponds to that of rainfall during the main growing season. Spatial linear correlation between these parameters is 0.80 (about 0.64 % of common variance), which is significant at the 99% level and confirms the hypothesis of a strong spatial association between rainfall and photosynthetic activity. The relation between the spatial distribution of NDVI and that of temperature is also very significant (r = -0.74). To avoid influence of other

Table 1. Spatial simple, partial and multiple correlation coefficients between NDVI and predicting variables for period 1985-2001.

Year	r_{ab} *	r_{ac}	r_{bc}	r_{ad}	$r_{ab.c}$	$r_{ac.b}$	$r_{ab.d}$	$r_{ac.d}$	R_{abc}	R_{abd}	R_{acd}	Multiple regression equation**
1985	0.76	-0.77	-0.79	0.53	0.41	-0.41	0.35	-0.11	0.81	0.77	0.79	NDVI=0.00125*P-0.0283*T+0.31
1986	0.81	-0.79	-0.69	0.60	0.59	-0.54	0.41	-0.15	0.87	0.83	0.79	NDVI=0.00164*P-0.0301*T+0.43
1987	0.76	-0.81	-0.84	0.51	0.25	-0.48	0.43	-0.29	0.82	0.77	0.81	NDVI=0.00101*P-0.0302*T+0.40
1988	0.65	-0.71	-0.57	0.58	0.42	-0.54	0.45	-0.08	0.77	0.74	0.71	NDVI=0.00102*P-0.0353*T+0.44
1989	0.81	-0.79	-0.79	0.55	0.49	-0.41	0.48	-0.19	0.85	0.82	0.79	NDVI=0.0011*P-0.0249*T+0.441
1990	0.84	0.81	-0.9	0.53	0.45	-0.18	0.43	-0.23	0.84	0.82	0.80	NDVI=0.00127*P-0.0368*T+0.45
1991	0.75	-0.71	-0.82	0.48	0.41	-0.25	0.27	-0.2	0.76	0.75	0.71	NDVI=0.00114*P-0.0257*T+0.40
1992	0.71	-0.73	-0.86	0.47	0.23	-0.33	0.37	-0.16	0.74	0.71	0.74	NDVI=0.0010*P-0.0187*T+0.261
1993	0.7	-0.79	-0.75	0.62	0.26	-0.56	0.4	-0.15	0.81	0.77	0.79	NDVI=0.0011*P-0.0184*T+0.285
1994	0.67	-0.75	-0.72	0.55	0.28	-0.52	0.38	-0.15	0.77	0.72	0.75	NDVI=0.0012*P-0.027*T+0.364
1995	0.72	-0.7	-0.7	0.38	0.45	-0.39	0.42	-0.17	0.77	0.72	0.74	NDVI=0.0016*P-0.0295*T+0.378
1996	0.83	-0.75	-0.7	0.48	0.64	-0.42	0.49	-0.1	0.86	0.83	0.81	NDVI=0.0009*P-0.0354*T+0.51
1997	0.67	-0.51	-0.71	0.29	0.34	-0.18	0.31	-0.13	0.68	0.57	0.52	NDVI=0.001*P-0.0253*T+0.36
1998	0.78	-0.76	-0.64	0.52	0.58	-0.54	0.63	-0.16	0.85	0.82	0.76	NDVI=0.0014*P-0.0349*T+0.45
1999	0.67	-0.75	-0.74	0.5	0.25	-0.51	0.28	-0.16	0.76	0.68	0.72	NDVI=0.001*P-0.0351*T+0.53
2000	0.91	-0.76	-0.61	0.48	0.86	-0.62	0.82	-0.14	0.94	0.93	0.81	NDVI=0.0011*P-0.0358*T+0.5
2001	0.83	-0.75	-0.7	0.46	0.64	-0.42	0.49	-0.1	0.86	0.83	0.81	NDVI=0.00114*P-0.031*T+0.43
Mean	0.8	-0.74	-0.81	0.51	0.51	-0.43	0.45	-0.11	0.81	0.78	0.76	NDVI=0.00125*P-0.0282*T+0.31

variables on the end results partial correlation coefficients for NDVI and all used responsible factors were calculated. The calculation of partial correlations enables to estimate "true" determination rate for each of the climatic factors on NDVI by full exclusion of the others variables used for statistical analysis. After the exclusion of temperature influence spatial relation between mean rainfall and mean NDVI values is not so high as before ($r_{ab,c}$ = 0.51n of simple, partial and multiple correlations between variables were done for each year. The results (1985-2001) are shown in table 1. The correlations coefficients vary from year to year, that proves a significant temporal variability of the spatial relationships between the NDVI and predicting variables. The mean coefficient of multiple correlations is R = 0.81, it means that more than 64 % of all spatial variations of NDVI in the research area are explained by the two climatic factors.

5.2 Multiple correlation coefficient R and anthropogenic impact

The spatial multiple correlation coefficients *R* vary from year to year and its variability is significant: the highest value (R = 0.94) was calculated for year 2000 and the lowest value (R = 0.68) for year 1997. A trend with negative slope (1985-1992) and one with positive slope (1993-2001) were detected. The positive trend after 1993 could be produced by decreasing human impact on the ecosystems. The high human influence on the desert and steppe landscapes (mostly in form of pasture grazing and efficient crops production) before the collapse of soviet economic system in 1991 was a significant predicting factor for spatial distribution and condition of natural vegetation. Since 1991 this predicting factor was considerably decreased and the role of climatic factors slowly increases. Figure 3 shows the time-series of *R* and two agricultural statistics (crops production and stocks) for the same period: since the beginning of 1990th both agricultural indexes harshly decreased, while the *R* coefficient on the contrary increased. The correlation result between the time-series of both indexes and the multiple correlation coefficient *R* shows a stronger relationship between stocks and *R* (r = -0.58) and a lower relation between crops production and *R* (r = -0.47). The reason is that most of the land is under pasture.

5.3 Relation between inter-annual variability of NDVI and annual rainfall amount

Due to the large inter-annual climatic variability in the region, it seems likely that any trend in annual NDVI may be highly correlated with trends in climatic variables. To prove this suggestion various statistical models were

tested. First, a temporal (1985-2001) variation coefficient for rainfall amounts and annual NDVI values was calculated for each pixel. A spatial correlation coefficient between these both images was determined that shows a strong relationship between the standard deviation of NDVI and that of rainfall amount (r = 0.78, about 59 % of common variance). Rainfall and NDVI deviations from period average have the highest values in the southern, western and middle parts of the study area. These areas are dominated by desert and semi-desert landscapes with tree free vegetation associations. The rainfall inter-annual variability is higher in the desert and semi-desert zone and lower in the dry steppe.

5.4 Multiple regression models

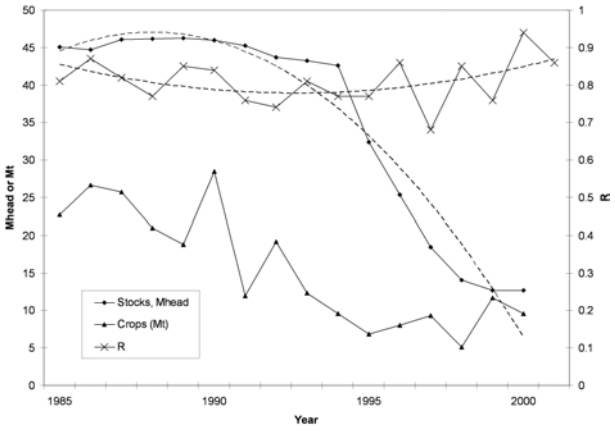

Figure 3. Time-series of spatial multiple correlation coefficient R, crops production (Mt) and stocks (Mhead) for the period 1985-2001. The dashed lines present trends for R and stocks.

A multiple linear regression equation for each year was calculated to analyse the relations between spatial pattern of climate indexes and that of average NDVI. As shown there is a high degree of correlation between both climatic variables and altitude (table 1). The presence of multicollinearity produces serious problems when making statistic inference and prediction based on the regression model. To avoid multicollinearity a regression analysis was preformed using stepwise selection of non-depended variables. In this new subset model all the predictors were significant. From 17 annual images of multiple regression surfaces (equations from table 1*)* an average multiple regression surface was calculated for the time-period 1985-2001. This $NDVI_p$ pattern shows a distribution of vegetation and its condition that depends on the spatial pattern of the climatic predictors. The multiple regression models explain about 64 % of all variations of annual *NDVI* in the study area during the period 1985-2001. Residuals from the annual multiple regression were calculated for each of the years by extracting the mean $NDVI_p$ pixel by pixel from the mean NDVI observed ($NDVI_o$).The geographical distribution of residuals shows the following pattern:

- The highest positive deviations from mean regression are to note on the coast of the Balkhash-lake, because in this sector vegetation distribution and condition are little depended from the spatial pattern of climatic factors, they are more predicted by the runoff of water streams.
- In the desert and semi-desert zones in the southern and western section of the study area also positive values are found. These areas are dominated by short grasses with shrubs.
- Negative values of residuals are to note in the middle and north-eastern parts. These areas are characterized by short grass and grassland mosaics.
- The highest negative deviations show the areas with spring wheat in this section.

On the contrary the areas with larch forest and areas covered by woods with grasses show high positive deviations. These areas are situated in the places with altitude above 900-1000 m and are to find only as little spots in the northern section of the study area.

6 ASSESSMENT OF DEGRADATION RISK FOR THE WHOLE STUDY REGION

6.1 Implementation of indicators

An assessment of the degradation risk should proof how much of the anthropogenic impact recession could lead to regeneration of the ecosystems. The human agricultural influence in the study area decreased during the last ten years of the 20th century. Another main factor is the variability of climate, in particular rainfall variability.

The time-period from 1985 to 2001 was divided into two periods: 1985-1992, and 1993-2001. During the first period the anthropogenic impact on the study area was very high, and it gradual decreased during the second period. We chose three parameters for the estimation of degradation risk. The first parameter indicates a general value of the anthropogenic impact during periods, the second parameter enables to indicate climatic impact and the third

indicator shows a reaction of vegetation spatial distribution and its productivity on a change of climatic and anthropogenic predictors.

6.1.1 Indication of anthropogenic impact

As first indicator we used the multiple correlation coefficients *R*. Its strong relationship to the value of human influence was shown above. The trend of the *R* correlates with the main trend of the agricultural indexes (stocks heads and crops production). We supposed to use this variable as a general non-spatial indicator.

6.1.2 Estimation of climatic variability impact

The second indicator was rainfall variability. Deviation (in percent) from the average rainfall was used as assessment criterion. The anomalous classes were subsequently reclassified into seven classes of rainfall change: very dry (25-18 % below the mean), dry (18-10 % below), moderately dry (10-2 % below), no changes, moderately moist (2-10 % over the mean), moist (10-18 % over) and very moist (18-25 % over). About 30 % of the entire area represents territories with very high or high degradation risk related to climatic indicator. More than 50 % of the total study area has been under dry conditions during both time-periods.

6.1.3 Identification of areas related to human induced degradation

The regression models related to climatic parameters (see 5.4) explain 46-86 % of spatial *NDVI* variations. Although climate significantly impacts *NDVI,* the large part of variations in *NDVI* is not explained by this relationship. A main reason for these unexplained variations may be anthropogenic impact. The difference $NDVI_{o\text{-}p}$ between the observed $NDVI_o$ and the predicted $NDVI_p$ by multiple regressions was calculated. As a result we got 17 scenes of $NDVI_{o\text{-}p}$ and we calculated the temporal trend of $NDVI_{o\text{-}p}$ and its slope during the period 1985-2001. Five types of trend slope can be distinguished: 1. The trend slope is close to zero, the influence of climatic factors remains constantly through the time. The area is not degraded or improved. 2. The trend slope is negative, the influence of predicting factors decreased, that means a change (reduction) of vegetation cover. 3. The trend slope is positive; the vegetation cover is improved. 4. The trend slope was positive and than turned to negative. 5. The trend slope was negative than turned to positive. Most pixels show behaviour similar to slope types 2 and 3.

6.2 Combination of indicators and set-up of a land degradation risk map

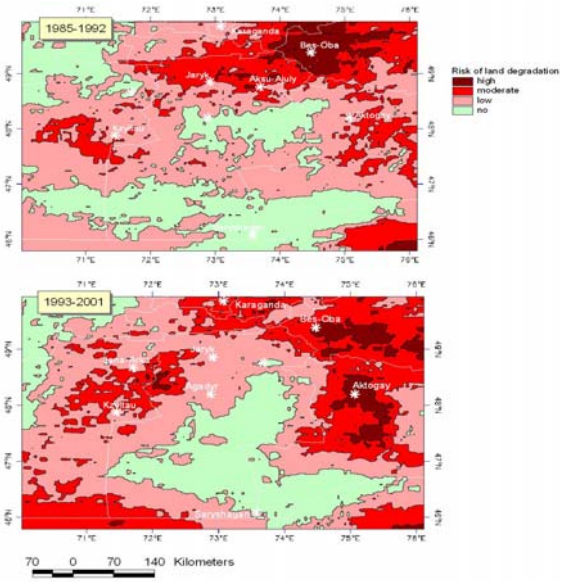

Figure 4. Final map of degradation risk reclassified to four risk classes.

Although each of the individual indicators is helpful in describing an aspect of desertification, it is useful to combine their results. The results of the above analyses – below-normal rainfall, anthropogenic impact and slope behaviour type of deviations from multiple regressions – were cross-classified to derive areas that have low or high degradation risk. First, low rainfall and negative deviation slope images were cross-classified then reclassified into four classes based on the spatial coincidence of classes from both original images. Then the reclassified product was summed with the non-spatial human pressure value. Again, the result was reclassified into four classes representing high, moderate, low and no risk of land degradation for two periods (figure 4).

There are notable changes in distribution of classes between the two time periods: In 1993-2001 areas with high degradation risk decreased from 7.3 % to only 1.1 %, and areas with no degradation risk increased from 20.8 % to 29.1 %. The other classes – moderate and low degradation risk – show no significant differences from the first period to the second (figure 4).

7 CONCLUSION

Spatial distribution of vegetation related to the geographical environment (esp. climatic conditions and terrain) is studied by correlations and regressions analysis. Sensitivity of vegetation cover to inter-annual changes of climatic conditions is also investigated. The spatial distribution of vegetation in the study area is strongly predicted by the climatic factors and terrain characteristics. But the degree of the prediction is not constant; it depends on the significance of anthropogenic impact. A decrease of anthropogenic impact in Kazakhstan since 1992 induced an increase of spatial multiple regression coefficient *(R)*. The increase of *R* means for the vegetation cover a come back to more natural conditions.

Inter-annual variability of rainfall, temperature and vegetation conditions is analysed. The results show higher variability of climatic predictors and NDVI in the desert and semi-desert vegetation zones. The terrain plays an important role in the inter-annual variability; the variability decreased with higher altitude. In the plain areas the coefficient of variation of NDVI and that of summed rainfall amounts for growing season during the period 1985-2001 is about 25-40 %. In the low hills and mountainous areas the coefficient of variation reached only 10-15 % during the same period.

Spatial multiple regressions for NDVI for each year of the period 1985-2001 were calculated. Rainfall and temperature are considered as independent variables. The regressions were used to calculate NDVI predicted values for each pixel and every year. Residuals from the predicted NDVI values are considered to be a sensitivity degree of vegetation cover related to climatic predictors. For each pixel the trend of residual was evaluated as sign of degradation or regeneration of vegetation cover. Five residuals trend types were detected. A monitoring system for land degradation was developed that used residuals trend as a main indicator.

8 REFERENCES

[1] TUCKER, C.J., VANPRAET, C.L., SHARMAN, M.J. & VAN ITTERSUM, G., 1985: Satellite remote sensing of total herbaceous biomass production in the Senegalese Sahel 1980-1984. *Remote Sensing of Environment, 17*, pp. 233-249.

[2] FOODY, G.M., 2003: Geographical weighting as a further refinement to regression modelling: an example focused on the NDVI-rainfall relationship. *Remote Sensing of Environment, 88*, pp. 283-293.

[3] CHEN, Z.M., BABIKER, I.S., CHEN, Z.X., KOMAKI, K., MOHAMED, M.A.A. AND KATO, K., 2004: Estimation of Interannual Variation in Productivity of Global Vegetation Using NDVI Data. *Int. J. Remote Sensing, 25*, pp. 3139-3159.

[4] WEISS, J.L., GUTZLER, D.S., COONROD, J.E.A., DAHM, C.N., 2004. Long-term monitoring with NDVI in a diverse semi-arid setting Central New Mexico, USA. *J. of Arid Environment, 58*, pp. 248-274.

[5] TATEISHI, R. AND EBATA, M., 2004: Analysis of phenological change patterns using 1982–2000 Advanced Very High Resolution Radiometer (AVHRR) data. *Int. J. Remote Sensing, 25(12)*, pp. 2287–2300

[6] KOWABATA, A., ICHI, K. AND YAMAGUCHI, Y., 2001: Global monitoring of interannual changes in vegetation activities using NDVI and its relationship to temperature and precipitation. *Int. J. Remote Sensing, 22*, pp. 1377-1382.

[7] LOS, S.O., 1993: Calibration adjustment of the NOAA AVHRR Normalized Difference Vegetation Index without resource to component channel 1 and 2 data. *Int. J. Remote Sensing, 14*, pp. 1907-1917.

[8] LOS S.O., 1998: Estimation of the ratio of sensor degradation between NOAA AVHRR channels 1 and 2 from monthly NDVI composites. *IEEE Transactions on Geoscience and Remote Sensing, 36(1)*, pp. 206-213.

Do Vegetation Indices Reliably Assess Vegetation Degradation?

A. Karnieli[a], Y. Bayarjargal[a] and M. Bayasgalan[b]

[a] The remote Sensing Laboratory, Jacob Blaustein Institutes for Desert Research, Ben Gurion University of the Negev, 84990, Israel, email: karnieli@bgu.ac.il

[b] National Remote Sensing Center, Ministry of Nature and Environment, Mongolia

ABSTRACT

Long-term (more than 60 years) human-induced vegetation degradation was studied by using space and ground observations in the steppe biome of Mongolia in order to explore the ability of remote sensing technique to assess the grazing effect in the range regions. In this area, several pairs of study sites were investigated – ungrazed (a fenced-off area) and heavily grazed (outside the fences). For each pair, the Enhanced Vegetation Index (EVI), computed from Landsat-7 ETM+ data, along with field-observed biophysical variables (e.g., plant density, species composite, biomass, and percent cover) and plant spectral reflectance data were collected. As expected, plant density, biomass, and percent cover were found higher in the grazed areas than in the adjacent grazed ones. However, the grazed areas have significantly higher EVI values than the ungrazed areas. The reason is that unpalatable species, having higher spectral response have invaded into the grazed areas resulting with higher EVI values.

Keywords: Mongolia, Vegetation Degradation, Grazing, Landsat-ETM+, EVI.

1 INTRODUCTION

Grazing by domestic animals is a major form of land use practices on native vegetation in rangelands all over the world. According to the FAO, permanent grasslands extend over ca. 26% of the land surface of the Earth. Therefore, range management and monitoring, especially over vast and remote areas, based on traditional field survey and measurement, might be problematic since it is an expensive, manpower demanding, and time-consuming process. Alternatively, satellite remote sensing, due to large surface cove and frequent routine observation, has been intensively used for a large number of vegetation applications in range regions. Recently the Enhanced Vegetation Index (EVI) was developed in order to optimize the vegetation signal with improved sensitivity in high biomass regions and improved vegetation monitoring while correcting for canopy background signals reducing atmosphere influences [1,2]. The EVI is based on the NDVI, SAVI, and ARVI indices, and uses functionalities from each one of them in order to overcome the soil and the atmosphere interferences. EVI is formulated as:

$$\mathrm{EVI} = \mathrm{G}\frac{\rho_{\mathrm{NIR}} - \rho_{\mathrm{red}}}{\rho_{\mathrm{NIR}} + \mathrm{C1}\rho_{\mathrm{red}} - \mathrm{C2}\rho_{\mathrm{blue}} + \mathrm{L}} \quad (1)$$

where ρ are atmospherically-corrected or partially corrected (Rayleigh and ozone absorption) surface reflectances in the respective spectral bands, L is the canopy background adjustment term, and C1, C2 are the coefficients of the aerosol resistance term, which uses the blue band to correct for aerosol influences in the red band. The coefficients adopted in the EVI algorithm are, L=1, C1= 6, C2 = 7.5, and G (gain factor) = 2.5.

Overgrazing is considered to be the key cause of *rangeland degradation* [3] while rangeland degradation is almost entirely a matter of *vegetation degradation* [4]. The latter is directly related to reduction in biomass and/or decrease in species diversity [5]. However these tendencies can be more complicated since vegetation degradation might be measured qualitatively rather than quantitatively. For instance, invasion or increase of undesirable brush species that may actually increase biomass production on degraded rangelands or loss of palatable pasture grasses and their replacement with unpalatable species [4, 6]. From the remote sensing point of view, implementing the above-mentioned vegetation applications that are related to quantitative variables is a common task and wildly used in rangelands. Bastin et al. [7], examined the potential of spaceborne systems for rangeland degradation mapping around Australian watering points, noted that there is no possibility to distinguish between different plants or change in species composition. However, only in recent years, tacking advantage of hyperspectral image spectroscopy technology, a few studies were aimed at mapping the distribution of some biological invaders [8, 9, 10] and evaluating changes in canopy chemistry and other canopy characteristics caused by invasion [11].

In Mongolia, from historic times, animal husbandry has been the main branch of the economy. 99% of the Mongolian territory has been used as natural pastures. During the last 70 years, the population density in the Mongolian drylands has increased more than 3 times and the total domestic livestock (sheep, goats, cattle, horses, and camels) have increased over 2.3 times, reaching 30 million animals. Consequently, irrational anthropogenic activities, such as overgrazing, have accelerated, causing vegetation degradation to be the main type of rangeland degradation [12, 13]. A few case studies, at plot-scale level, drew attention to sever decrease of vegetation cover due to overgrazing near settlements water sources. Yonghong and Jargalsaihan [14] noted that the plant community abundance (composition and richness) decreased as grazing pressure increased and the native vegetation were replaced by exotic species in the northeast pastureland of the country. They found that succession series along the grazing gradient were *Stipa grandis* + *Leymus chinensis* in the lightly grazed sites, *Stipa kreylovii* + *Artemisia frigida* + low grasses in the moderately grazed sites, and *Carex duriuscula* + *Artemisia scorparia* + annuals in the heavily grazed sites. Fernandez-Gimenez and Allen-Diaz [15, 16] found, based on ground observations over two years, that vegetation pattern (in species composition, biomass, etc.) changed along grazing-gradients from the watering points in response to increased grazing pressure in the Mountain-Steppe and Steppe zones of Mongolia, while no consistent changes due to grazing were observed in the Desert-Steppe. Also, it was noted that vegetation changes over degraded and eroded areas are significant and unpalatable plants or weeds fully occupied these areas. However, no shrub encroachment is associated with degradation of the Mongolia's grassland [15, 16, 17].

Advantage was taking of a unique phenomenon in Mongolia. The railway across the country, more than 1000 km in length from the northern border with Russia to the southern border with China (figure 1) was established in the 1960s. Since then, it has been protected by fences all along for avoiding animals to cross the railway and therefore no grazing is allowed inside the fences while intensive grazing characterizes the surrounding area. Since the railway passes the steppe biome, it enables to investigate the anthropogenic-induced rangeland degradation. When the train is winding the length between the fences can be as wide as 4 km, enabling remote sensing research using high resolution imagery (figure 2). This paper attempts in exploring the ability of remote sensing technique to assess vegetation degradation in the range regions of Mongolia.

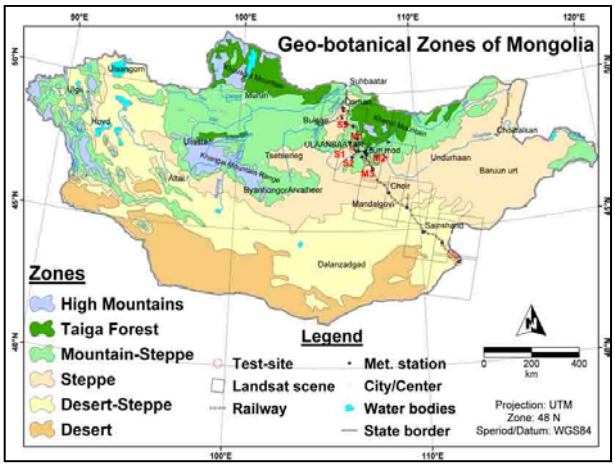

Figure 1. Geo-botanical map of Mongolia, showing the study sites along the railway that crosses the country from the northern border with Russia to the southern border with China.

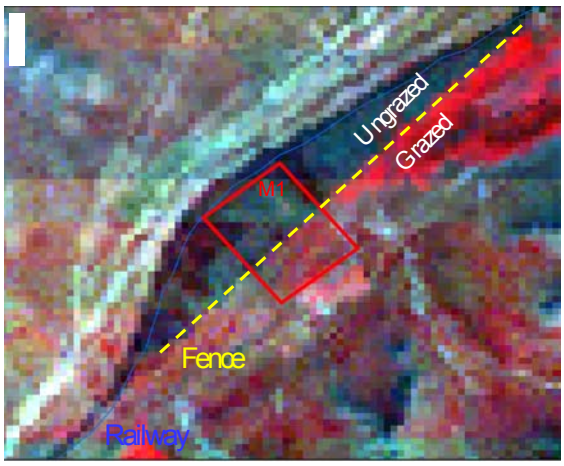

Figure 2. Example of a Landsat ETM+ image (RGB=4,3,2) showing a study site (M1). The area between the fence and the railway is the ungrazed side while intensive grazing characterized the surrounding area.

2 STUDY AREA

Mongolia has a continental climate, characterized by cold and dry winters and warm and wet (rainy) summers. The current research is focused on the Mongolian steppe biome (excluding the desert steppe) (Figure 1). The area occupies ca. 4.5*108 hectares. Mean annual precipitation ranges between 150 to 300 mm and the mean annual temperature between -3 to +3 Cº. The aridity index (ratio of precipitation to potential evapotranspiration) ranges between 0.2 to 0.5, indicating semi-arid environment. The southern part of the region is characterized by flat plains and rolling hills covered in feather grass and shrubs. Typical species of grass include *Stipa krylovii* and *Agropyron cristatum*, and unpalatable shrubs such as *Caragana* spp. and *Artemisia* species are abundant. Mountains that exist

in the northern are characterized by coniferous forests on the northern slopes, while the southern slopes are covered by open steppe vegetation. The vegetation is therefore a combination of Siberian taiga forest and Mongolian steppe flora, including species such as pine (*Pinus sylvestris*), aspen (*Populus tremula*) and edelweiss (*Leontopodium ochroleucum*).

3 METHODOLOGY

The research was conducted in six study-sites selected along the railway (Figure 1). Three of them are located at the Mountain-Steppe zone (denoted hereafter as sites M1, M2, and M3) and the other three in the Steppe zone (S1, S2, and S3). Each site consists on pairs of study polygons – ungrazed (the fenced-off area) and heavily grazed (outside the fences). All sites are large enough in term of the spatial resolution of Landsat images, e.g., 30 x 30 meter and characterized by flat topography.

Four Landsat-7 Enhanced Thematic Mapper Plus (ETM+) images, acquired in early 2000s were used. In order to reduce image-to-image variations that are related to sun angle, differences in atmospheric condition, and vegetation phenology, all images were selected during the vegetation growing season, when the possibility to discriminate between vegetation and soil covers is the highest. In addition, cloud covers are minimal in all images. Digital number values were converted to radiance, and ground-leaving reflectances were created from the radiances using the 6S algorithm. Later, the four images were merged to create a continuous scene. The Enhanced Vegetation Index (EVI) (equation 1) was computed from the reflectance values. This index was selected in order to reduce the uncertainty in soil background and atmospheric effect along the entire study area. Approximately the same number of pixels was sampled in the grazed and the adjacent ungrazed polygons.

Ground-truth activities were conducted during two field-campaigns in the summers of 2002 and 2003 in framework of the Joint Russian-Mongolian Complex Biological Expedition in participation of the University of Moscow, Remote Sensing Laboratory (Blaustein Institute for Desert Research, Ben-Gurion University of the Negev), the Institute of Botany (Academy of Science of Mongolia), and the National Remote Sensing Center (Ministry for Nature and Environment of Mongolia). Biophysical variables of dominant and co-dominant plants species, including plant density (i.e., number of plants per unit area), composition, dry biomass, and percent of vegetation cover, were sampled and measured. The study polygons were precisely located by a Global Positioning System (GPS).

In conjunction with the above, spectral reflectance measurements were implemented with the FieldSpec-HandHeld Spectroradiometer (manufactured by Analytical Spectral Device [18]) at wavelengths of 325-1075 nm with a spectral resolution of 2 nm. A High Intensity Contact Probe device with a fiber optic was attached to the spectroradiometer. This device has an independent light source (about two fold of the solar intensity) and made it feasible to measure under all-weather conditions. The contact probe was attached to clipped plants and soil samples. Measurements of a white reference panel (Spectralon plate, Labsphere Inc.) were taken immediately before each spectral measurement.

4 RESULTS AND DISCUSSION

It was hypothesized that intensive grazing will reduce the plant density, biomass, and plant cover. It is further assumed that the EVI will have lower values outside the fences due to vegetation degradation. Table 1 summarized the results of the field campaigns and the image processing along with the descriptive statistics and significance. As expected, between 23 to 34 plants per unit area were measured inside the fence while 12 to 25 plants outside. As expected, figure 3A confirms that a higher plant density characterizes each ungrazed polygon than the adjacent grazed ones. Similarly, it is shown In Figure 3B that inside the fences the average dry biomass is twice as much than outside. This ratio is higher in the Mountain Steppe polygons than in the Steppe ones. The same trend can also be observed in the plant cover (figure 3C). Higher cover observed in the ungrazed polygons than the ungrazed. However, a revised trend was revealed by analysis of the spaceborne data (figure 3D). Landsat-ETM+ derived EVI shows significant higher values outside the enclosures than inside. This phenomenon exists in each of the study sites as illustrated in figure 4. These unlikely results, i.e., negative correlation between the biophysical variables and the vegetation index, should lead for further discussion about the plant composition, phenology, and palatable characteristics of the plants.

Table 1. Biophysical variables at the study sites, in the grazed and ungrazed polygons, descriptive statistics, and significance.

Polygon	Plant density		Biomass (g/m^2)		Cover (%)		EVI	
	Ungrazed	Grazed	Ungrazed	Grazed	Ungrazed	Grazed	Ungrazed	Grazed
M1	23	12	216.7	32.2	99.9	59.0	0.21	0.28
M2	29	25	126.4	81.2	58.5	52.0	0.26	0.30
M3	34	25	188.6	43.7	62.6	48.5	0.20	0.28
S1	30	12	53.6	19.2	73.0	50.0	0.25	0.27
S2	20	14	66.1	61.4	55.0	56.0	0.21	0.27
S3	25	20	122.8	114.6	48.0	45.5	0.22	0.27
Average	26.83	18.00	129.03	58.72	66.17	51.83	0.22	0.28
SD	5.12	6.16	64.70	35.00	18.50	4.97	0.02	0.01
t-test significance (one tail)	0.004		0.036		0.037		0.001	

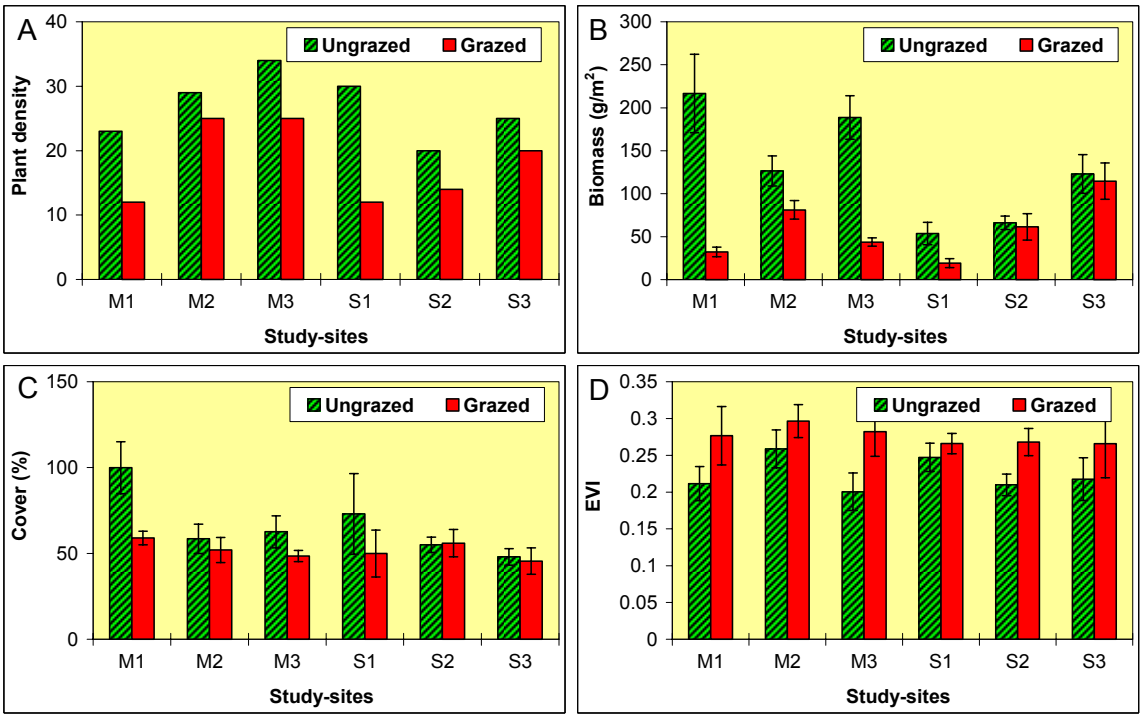

Figure 3. Values of the biophysical variables (density, biomass and cover) and the Enhanced Vegetation Index in the study sites, separated by the grazed and ungrazed polygons. Bars indicate one standard deviation from the mean.

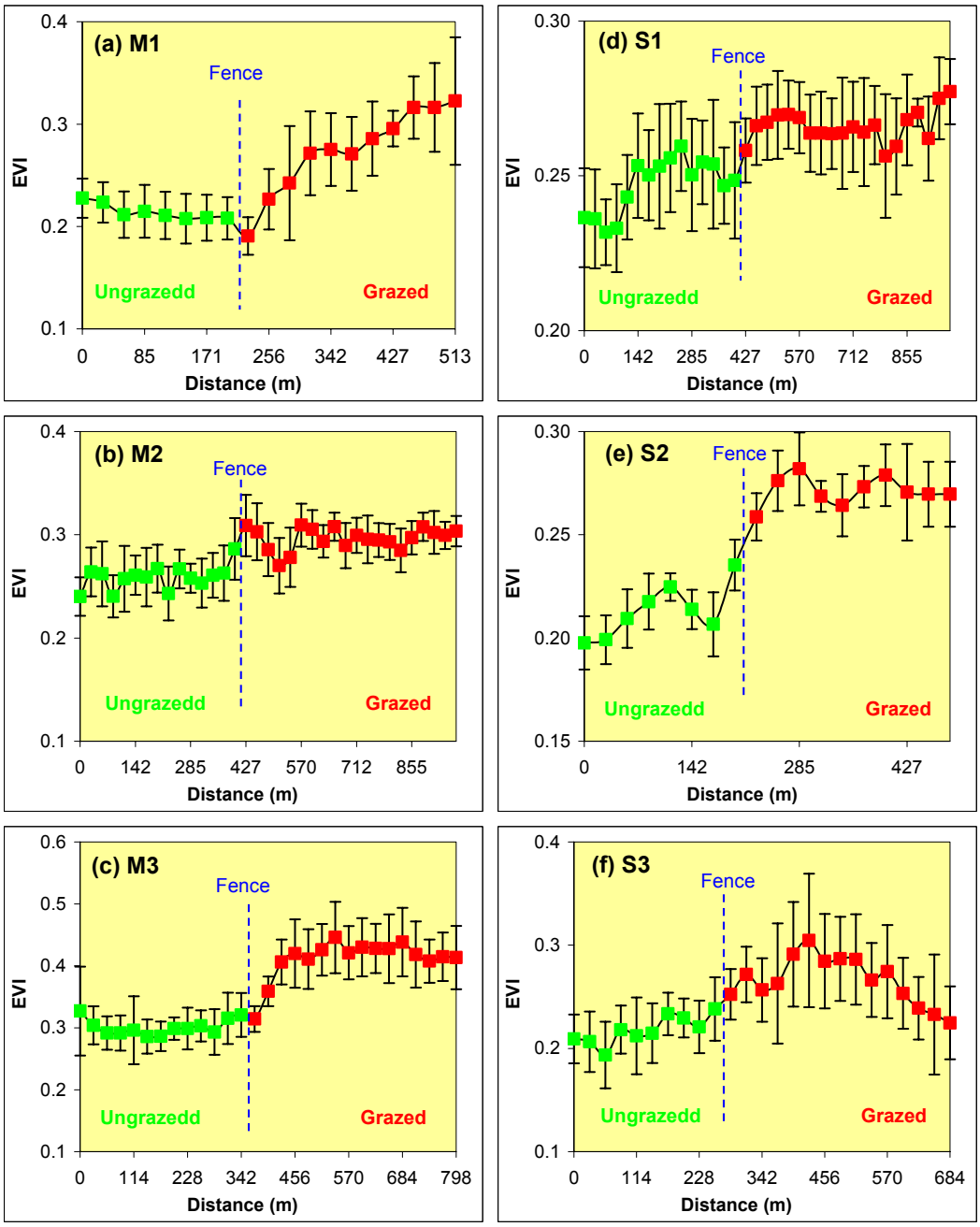

Figure 4. EVI values along a cross section perpendicular to the railway fence in the study sites. Bars indicate one standard deviation from the mean.

Mountain-Steppe Zone

Different perennial grasses are dominated the ungrazed areas while mostly forbs with little contributions of grasses were dominated the grazed areas. The species composition of the ungrazed areas consists of *Stipa krylovii*, *Halerpestes salsuginosa*, *Leymus chinensis*, *Agropyron cristatum*, *Poa attenuata*, *Galium verum,* and *Agrostis mongolica*. These perennial native grasses have good palatable value for the animals during the summer, especially *S. krylovii* and *A. cristatum* are highly nutritious and very good digestible plants to all livestock throughout the year [19]. They bloom in early August and have seed matures in September. Also, communities such as *P. attenuata*, *L. chinensis*, and *A. mongolica* have very high palatability to all livestock especially to small animals (i.e., sheep and goats) during the whole season, and those are high-costly and main contributor plant for Mongolia's pastureland [17] in addition to the other native *Poaceae* grasses. During the blooming period in August, main

perennial grasses (e.g., *S. krylovii, L. chinensis* etc.) have bright-gray and brown-gray flowers with 1-1.5 cm wide at the top of spikes and very straight tall about 30-70 cm. Since these needle grasses grow relatively uniform and cover about 20-30% of the fenced-off areas in each study-site, the surface looks relatively brighter for the human eyes (figure 5A). In the false color composite of the Landsat image the ungrazed area looks dark and no indication for photosynthetic activity is observed (Figure 2). In the grazed areas, *Artemisia frigida*, *Artemisia dracunculus*, *Potentila acaulis*, *Glaux maritime*, *Bupleurum scorzonerifolium*, *Allium bidentatum*, *Agrostis mongolica Caragana pygmaea*, *Leymus chinensis*, *Koeleria cristata*, *Gallium verum*, *Potentila acaulis*, and *Iris bungei* are dominant. Livestock, especially sheep, can hardly graze these perennial forbs and sub-shrubs in summer while goats moderately grazed them in autumn. Because of indigestibility value during the mid summer of those unpalatable perennial forbs (e.g., *A. frigida* and *A. dracunculus*), weedy annuals (e.g., *P. acaulis*), and subshrubs (e.g., *C. pygmaea*), the areas under the control of these plants are shown relatively green (figure 5A). Nevertheless, these dense bunch-forming semi-shrubs are very nutritious for livestock in early summer and late autumn when toxic values might be low (Mandakh Bayart, personal communication). Gunin et al. [20] noted that several species such as *Artemisia* (*A. scoparia, A. frigida*) and *Echinopsilon divaricatum* are indicators for rangeland degradation and human-induced desertification processes.

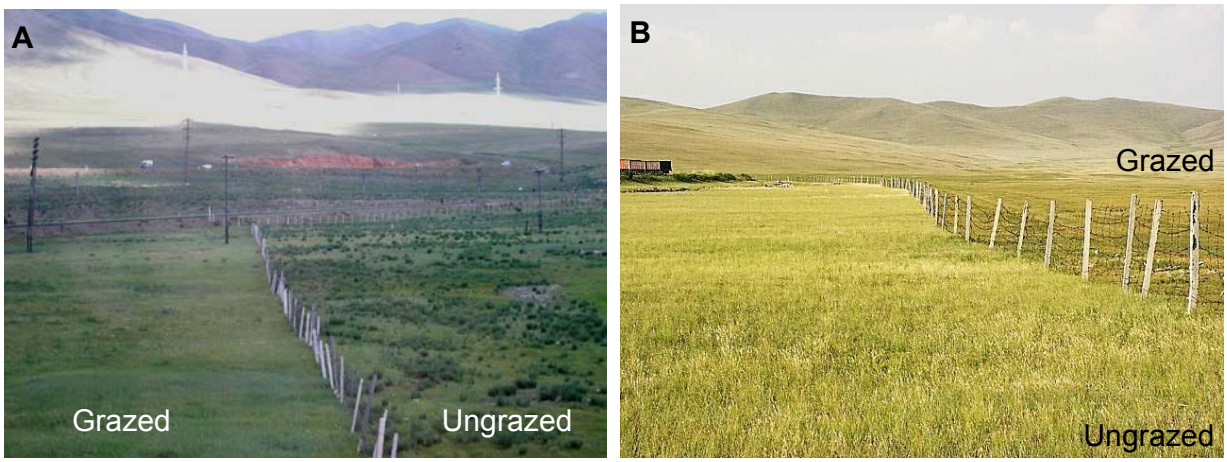

Figure 5. General view of the research sites: (A) Mountain Steppe site (M1): association in the ungrazed area –*Halerpestes salsuginosa+Agrostis mongolica*; grazed area – *Glaux maritima+Agrostis mongolica*. Note the darker tones in the grazed area are due to the wide spread of *Iris bungei*. (B) Steppe site (S1): association in the ungrazed area – *Stipa krylovii+Buplerum scorzonerifolium+Cleistogenes squarrosa*; grazed area – *Carex duriuscula+Artemisia adamsii*. Note the brighter tones in the fenced-off area due to the *S. krylovii***.**

Steppe Zone

In the three selected study-sites of the Steppe zone, communities of *Stipa krylovii*, *Allium senescens*, *Agropiron cristatum*, *Festuca sibirica*, *Stipa grandis*, *Cleistogenes squarrosa*, and *Buplerum scorzonerifolium* are dominant the ungrazed areas. All these perennial grasses have very high nutritious values, so they are invaluable forage plants [19]. In contrast, *Carex duriuscula*, *Artemisia adamsii*, *Artemisia frigida*, and *Potentilla acaulis* were dominant in the grazing allowed areas. As noted by Fernandez-Gimenez and Allen-Diaz [15, 16], these species response in different levels of degradation in the Steppe zone of Mongolia. Visually, ungrazed areas in the Steppe are shown as brighter than the grazed areas due to the wide spread of the *S. krylovii* (Figure 5B).

Based on the above-mentioned hypotheses, one-tail t-test was performed for each of the variables (table 1). It can be seen that there is a significant difference between the grazed and the ungrazed data series, and, indeed, grazing had the expected significant effect on the biophysical variable but the EVI.

Figure 6 illustrates the spectral reflectance graphs of different species in the steppe biome of Mongolia. It can be seen that most of the dominant species in the fenced-off area, mostly good palatable plants such as *S. krylovii*, *B. scorzonerifolium*, *A. senescens*, and *A. mongolica* have lower reflectance levels in the NIR part of the electromagnetic spectrum. On the contrary, other unpalatable species, such as *G. maritime*, *L. chinensis*, *P. acaulis*, and *I, bungei* that occupy the grazing areas have higher reflectance levels in the NIR. Figure 7 demonstrates these differences with two representatives. *S. krylovii* is a good palatable grass that represents the protected area. In the middle of the summer the grass turn yellow, therefore its cells losses water, the refractive index decrease, and hence

reflectance in the NIR decrease. *I. bungei* represents the grazed area. This is a succulent plant and therefore it characterizes by high refractive index that produces high reflectance values.

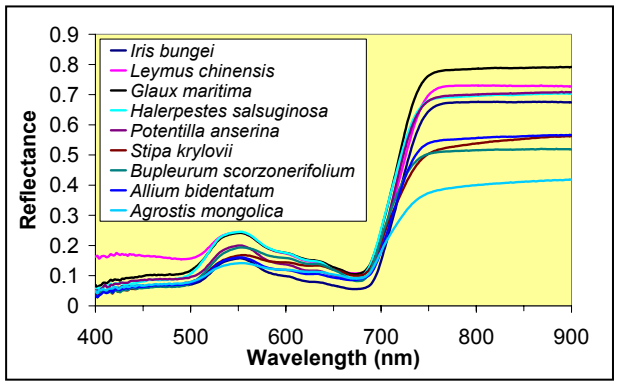

Figure 6. Spectral reflectance graphs of different species in the steppe biome.

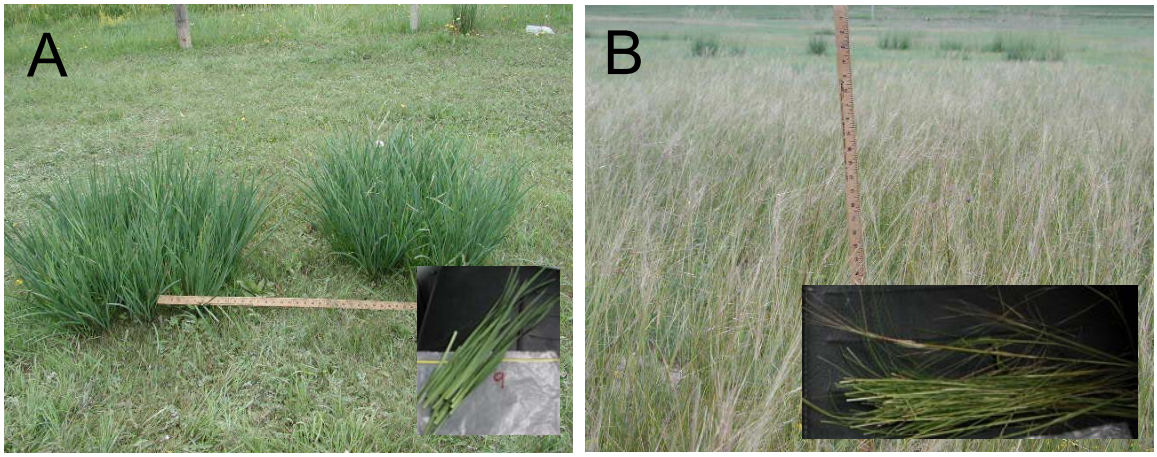

Figure 7. Dominant species in the Mountain Steppe zone. (A) *Iris bungei*, a succulent plant characterized by high refractive index that produces high reflectance values; (B) *Stipa krylovii,* a good palatable grass representing the protected area. In the middle of the summer the grass turn yellow, therefore its cells losses water, the refractive index decrease, and hence reflectance in the NIR decrease.

5 CONCLUSIONS

Ground observations along the Mongolian railway confirms previous range condition model of vegetation dynamics (e.g. [21]). The model predicts that as herbivore numbers increase, plant biomass and cover decline and species composition shifts from dominance by perennial grasses and forbs (`climax' species) towards dominance by unpalatable forbs and weedy annuals. When grazing is decreased or removed, biomass and cover are predicted to increase, and species composition shifts back towards late-successional stages. Although the common remote sensing based vegetation indices models assumed higher index values as biomass and cover increase, the current observations show the oposite. The reason is the difference in leaf structure and phenological stage between the palatable specice inside the fenced-off area and the unpolatable species outside the fences. The palatable species are mainly grasses that turn yellow in the mid summer, while the rodual species can be succulent plants characterize by high refractive index that produces high reflectance values.

REFERENCES

[1] LIU, H.Q. AND HUETE, A.R., 1995: A feedback based modification of the NDVI to minimize canopy background and atmospheric noise. *IEEE Transactions on Geoscience and Remote Sensing 33*, pp. 457– 465.
[2] HUETE, A., 1988: A soil-adjusted vegetation index (SAVI). *Remote Sens. Environ. 25,* pp. 295-309.
[3] THOMAS, D.S.G. AND MIDDLETON, N.J., 1994: *Desertification: Exploring the myth*. John Wiley & Sons, Chichester.
[4] DREGNE, H.E. AND CHOU, N-T., 1992: Global desertification dimensions and costs. In: *Degradation and restoration of arid lands*. Lubbock: Texas Tech. University.
[5] ESWARAN, H, BEINROTH, F.H. AND VIRMANI, S.M., 2000: Resource management domains: a biophysical unit for assessing and monitoring land quality. *Agric. Ecosys. and Environ. 81 (2)*, pp. 155-162.
[6] BROWN, J.R. AND ARCHER, S., 1999: Shrub invasion of grassland: Recruitment is continuous and not regulated by herbaceous biomass or density. *Ecology 80(7)*, pp. 2385-2396.
[7] BASTIN, G.N., PICKUP, G. AND PEARCE, G., 1995: Utility of AVHRR data for land degradation assessment - a case-study. *Int. J. Remote Sens. 16 (4)*, pp. 651-672.
[8] LASS, L.W., THILL, D.C., SHAFII, B. AND PRATHER, T.S., 2002: Detecting spotted knapweed (*Centaurea maculosa*) with hyperspectral remote sensing technology. *Weed Technol. 16*, pp. 426–432.
[9] LASS, L.W., PRATHER, T.S., GLENN, N.F., WEBER, K.T., MUNDT, J.T. AND PETTINGILL, J., 2005: A review of remote sensing of invasive weeds and example of the early detection of spotted knapweed (*Centaurea maculosa*) and babysbreath (*Gypsophila paniculata*) with a hyperspectral sensor. *Weed Science 53 (2)*, pp. 242-251.
[10] UNDERWOOD, E., USTIN, S. L. AND DIPIETRO D., 2003: Mapping nonnative plants using hyperspectral imagery. *Remote Sens. Environ. 86*, pp. 150–161.
[11] ASNER, G.P. AND VITOUSEK, P.M., 2005: Remote analysis of biological invasion and biogeochemical change Proceedings of the National Academy of Sciences of The United States of America 102 (12), pp. 4383-4386.
[12] ADYASUREN, TS., 1998: State of drought and desertification in Mongolia. In: *Environment and development issues in Mongolia*. Ulaanbaatar, Mongolia, 96 p.
[13] BATJARGAL, Z., 1999: Desertification in Mongolia. In: Icelandic Agricultural Research Service (RALA). Report 200, Reykjavik, Iceland, pp. 107-113.
[14] YONGHONG, L. AND JARGALSAIHAN, L., 1993: Grazing dynamic of *Stipa grandis* steppe in the northeast Mongolia plateau. In: *Proceeding of the International Symposium on Grassland Resources*. Huhehot, Inner-Mongolia, China. 25 p.
[15] FERNANDEZ-GIMENEZ, M.E. AND ALLEN-DIAZ, B., 1999: Testing a non-equilibrium model of rangeland vegetation dynamics in Mongolia. *Journal of Applied Ecology 36 (6),* pp. 871-885.
[16] FERNANDEZ-GIMENEZ, M.E., 2000: The role of Mongolian nomadic pastoralists' ecological knowledge in rangeland management. *Ecological Applications 10 (5)*, pp. 1318-1326.
[17] TSERENBALJID, G., 2002: *Colour atlas of antropophilus plants of Mongolia*. Admon printing House, Ulaanbatar, Mongolia, 251.
[18] ASD, 2000: *Hand Held Spectrometer User's Guide*. FieldSpec UV/VNIR. Analytical Spectral Devices Inc. Boulder, USA.
[19] JIGJIDSUREN, S. AND JOHNSON, D.A., 2003: Forage Plants in Mongolia. Ullanbaatar. Mongolia.
[20] GUNIN, P., VOSTOKOVA, E.A., DOROFEYUK, N.I., TARASOV, P.E. AND BLACK. C.C., 1999: Assessing present day plant cover dynamics. In: GUNIN, P., VOSTOKOVA, E.A., DOROFEYUK, N.I., TARASOV, P.E. AND BLACK, C.C. (eds.). Vegetation Dynamics of Mongolia. Kluwer Academic Publishers, Dordrecht, The Netherlands. pp. 131–163.
[21] DYKSTERHUIS, E.J., 1949: Condition and management of range land based on quantitative ecology. *J. Range Management 2*, pp. 104-115.

MEDOKADS: A Long-term Data Set for Detection and Monitoring of Desertification Risks in the Mediterranean

D. Koslowsky[a], H. Billing[a] and K. Friedrich[a]

[a] Freie Universität Berlin, Institut für Meteorologie, C.-H.-Becker-Weg 6-10, 12165 Berlin, email: kosze@zedat.fu-berlin.de

ABSTRACT

Research supported by the EC in the last decade gained basic new knowledge in regional and large scale land-surfaces processes in the Mediterranean basin. Time series like MEDOKADS (*Me*diterranean *E*xtended *D*aily *O*ne *K*m *A*VHRR *D*ata *S*et) including reflectances and radiances in different spectral regions as well as derived quantities like albedo, vegetation index, land and sea surface temperatures, cloud cover and classification have been generated and prolonged to cover now climatological relevant periods. Discussions are still going on whether AVHRR based time series are suited to give reliable results in near real-time monitoring and trend analysis of desertification risks in the Mediterranean basin. Additional efforts in calibration, normalisation and harmonisation are still required to fulfil this task not only as a prerequisite to contribute to an early warning system in the Mediterranean basin, but also to establish a long-term normalisation standard for inter-comparison with results of new sensors like MODIS, AATSR and SEVIRI. Inter-comparison with the global pathfinder data set provided by NOAA are ongoing to extrapolate results globally. In the appendix some practical information is given for automatic access to the data for pre-registered users.

Keywords: Global Change, AVHRR, NDVI, time series

1 INTRODUCTION

The Advance Very High Resolution Radiometer (AVHRR) flown on the NOAA satellites originally was designed for use in weather analysis and forecast. At the time of its first operation on the NOAA 6 satellite in 1978 only a limited number of stations was capable to process and store the huge amount of data. In the meantime new storage media and high speed computer facilities became available at low prices and enabled a larger number of institutions to handle and process AVHRR data. Simultaneously the successful compromise of temporal and spatial resolution, processing and storage requirements extended the application towards land surface investigations.

More than 25 years of operation without major changes now offer the possibility to use the data for studies of environmental changes. On the other hand this opportunity causes additional efforts to pre-processing, validation and harmonisation of these long-term data sets. Especially the detection of non-periodic changes of the earth's surface requires the removal of all possible contributions, which are caused by changing observation conditions and changes due to the instrument's characteristics. For users, who are not interested in these processing steps, but want to retain as much as possible information, an intermediate product has been compiled at the Free University of Berlin (FUB): the Mediterranean Extended Daily One-Km AVHRR Data Sets (MEDOKADS) [1].

Multiple evaluations of long-term data sets are only possible if they are stored on random access storage devices. An initial stage to built up such a large storage system was given in 2000 by participating the research project GLOWA-Elbe (BMFB) [http://www.glowa-elbe.de]. Internal funds as well as contributions by SISCAL (IST-2000-28187 (EU)) [2] and now DeSurvey [http://www.desurvey.net] together with declining costs enabled an extension to about 10 Tbyte capacity, which now allows not only to store the full MEDOKADS data set but also higher level products as well as results of different evaluation algorithms.

2 GENERAL DESCRIPTION OF THE MEDOKADS

2.1 Design of the MEDOKADS

Interactively supervised fine-navigated sub-areas from directly received and pre-processed HRPT data are used to create the MEDOKADS product, the “Mediterranean Extended Daily One-km AVHRR Data Set”. This data set consist out of full resolution AVHRR channel data and collateral data in „geographic“ projection, i.e. latitude - longitude presentation, with a resolution of 0.010 in both directions.

The area of interest for the studies in the Mediterranean is defined by its corner coordinates

55^0N/10^0W 55^0N/42^0E
27^0N/10^0W 27^0N/42^0E

and amounts to 2800 lines by 5200 columns with 14,560,000 raster positions. The geographic extent is shown in Fig. 1. Each of the four sub-regions marked in Fig. 1 forms a special storage unit covering the Iberian Peninsula (S), Italy (I), the Balkans (B), and the Eastern Mediterranean area (E) respectively. The stripes S and I have the same size of 2800 lines and 1536 columns, while B and E consist of 1900 lines by 1536 pixel. Smaller windows regardless to the stripe boundaries can be selected and are completely defined by the geographic coordinates of the upper left corner and the number of lines and columns. These data sets are easy to merge, if larger areas or the whole Mediterranean have to be considered. Areas for which data are not yet available in supervised form are kept blank. The coordinates of the upper left corners of the sub-areas are:

S:	Iberian Peninsula	55 0 N/10 0 W
I:	Italy	55 0 N/ 5 0 E
B:	Balkan Peninsula	46^0 N/15^0 E
E:	East Mediterranean	46^0 N/27^0 E

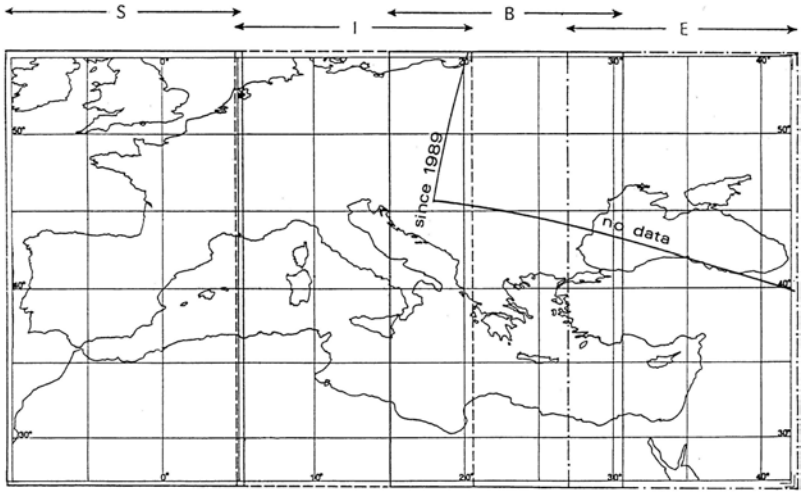

Figure 1. Area covered by the MEDOKADS. S, I, B and E shows the four subset stripes for the Iberian Peninsula, Italy, Balkan, and Eastern Mediterranean. No data are processed so far for the north-east corner covering eastern Europe and the northern Black Sea.

There is some overlapping between the stripes to cover the four main land surface sub-areas. To avoid problems of digital data representation, all values are converted to signed 16-bit integers. The formal digital resolution is 0.01 of units (i.e. for reflectances, degree for temperatures (Celsius) and angles) multiplied by a factor of 100 without any offset. The calibrated data of the five AVHRR channels at top of atmosphere (TOA) form the first five files. Channel 1 and 2 data are corrected for sun height and sun-earth distance. A number of pseudo-channels are added containing collateral data or derived products coincident pixel by pixel: local satellite and sun zenith distance and azimuth, local scattering angle, broadband albedo, NDVI, SST/LST, local time and a bitmap. The upper byte of the bitmap channel represents the *origin indicator*, a 6 bit bitmap inserted into the spare bits of each AVHRR super-pixel at data reception time, which allows to identify the date and the orbit number of each individual pixel, even in the case of multi-day composites like the maximum NDVI. It allows to recover the original digital counts and to apply sophisticated calibration and correction algorithms later on to each individual pixel without a loss in digital resolution. The other byte contains a land/water bit and a cloud mask and allows to switch between different evaluation algorithms for land and water surfaces. Thus the MEDOKADS build up a 15 channel pixel-congruent data set (Table 1). Daily as well as ten day composite data sets according to the maximum NDVI are generated. As a sample the 16 year's mean NDVI (January to December) is shown in figure 2.

Table 1. Channels and pseudo-channels of the MEDOKADS data bank

No.	Content	No.	Content
1	Calibrated AVHRR-CH1	9	local sun azimuth
2	Calibrated AVHRR-CH2	10	local scattering angle sun to satellite
3	Calibrated AVHRR-CH3	11	"origin indicator" and bitmap
4	Calibrated AVHRR-CH4	12	TOA broad-band reflectance
5	Calibrated AVHRR-CH5	13	NDVI
6	Local satellite zenith distance	14	Sea/land surface temperature
7	Local sun zenith distance	15	local time since ascending node
8	Local satellite azimuth	16	Cloud classification (in preparation)

The west to east extent of the area is 52^0 according to about 4400 km. Thus 2 to 3 adjacent satellite passes are necessary to cover the whole region with the result that the absolute time difference can be up to 3½ hours between the western and eastern part. The total amount of data for a complete set with 16 pseudo-channels for one day of the whole basin is about 580 Mbyte. Thus up to now the MEDOKADS of more than 16 years from 1989 to 2005 amounts to about 3Tbyte.

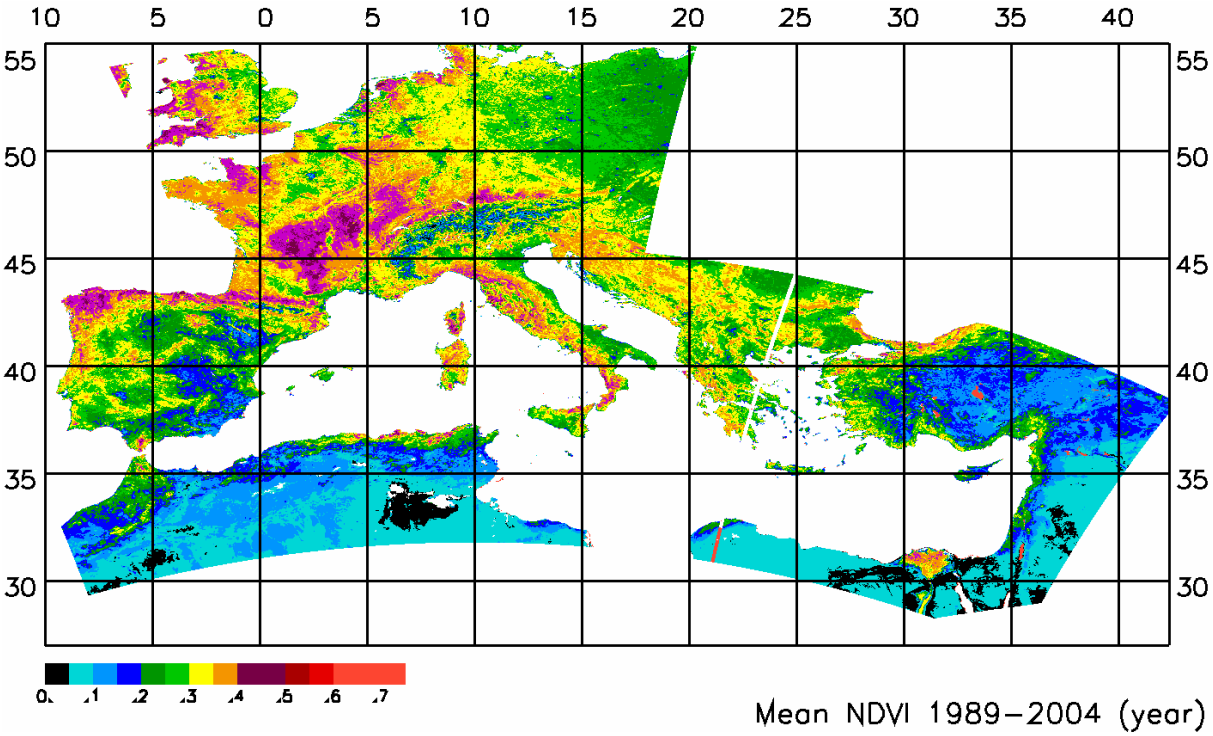

Figure 2. Sample of a MEDOKADS derived product. Annual mean of the period 1989 to 2004 showing the region covered with data.

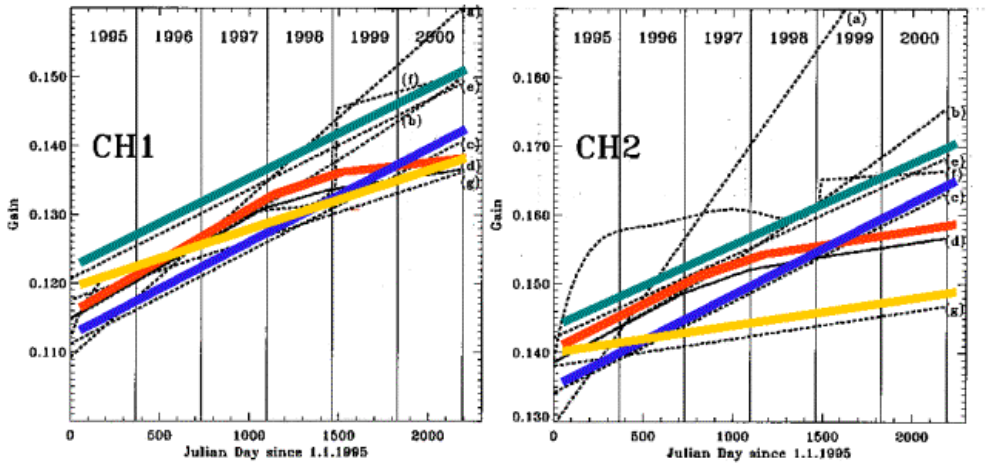

Figure 3. Signal degradation of channel 1 and 2 of the AVHRR of NOAA 14 by different authors.

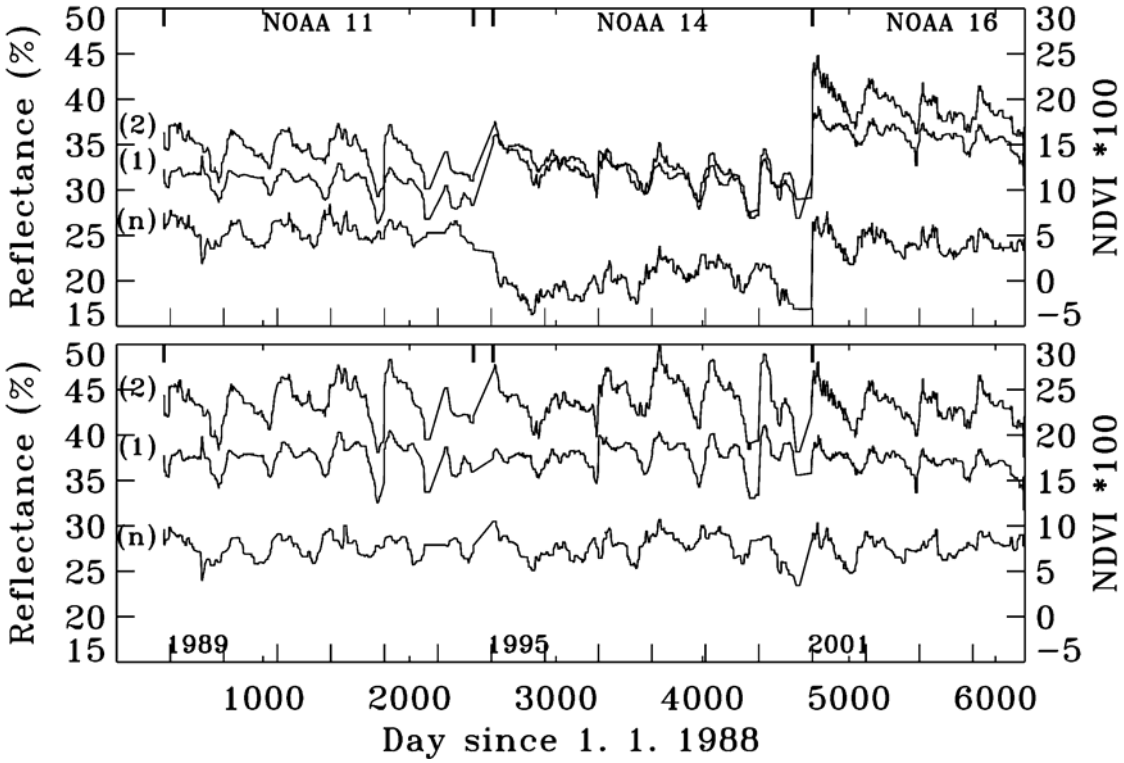

Figure 4. Time series of daily BRDF corrected reflectances derived from AVHRR channel 1 (1), channel 2 (2) and NDVI (n) of the satellites NOAA 11 to NOAA 16 of a calibration test site in the Great Erg Occidental in Algeria before (upper panel) and after inter-calibration (lower panel).

2.2 Calibration of the short-wave channels and changes in spectral response

While internal calibration targets can be used to calibrate the thermal channels of the AVHRR instrument [3,4] external targets have to be used to monitor the gain of the shortwave channels. Starting with carefully evaluated post-launch calibration coefficients for the NOAA 11 satellite [5] a test site in the Western Great Erg was monitored by FUB to derive degradation coefficients for the AVHRR instrument using time series corrected for BRDF (Bidirectional Reflectance Distribution Function) and inter-calibration of the instruments of the successive satellites NOAA 11, NOAA 14 and NOAA 16 [6]. This work resulted in somewhat different degradation and calibration coefficient than used for the Pathfinder (PAL) data set. As an example of different approaches for deriving degradation coefficient for NOAA 14 refer to Fig. 3. A broad spread can be found with the curves of FUB in the middle for the early years of operation. The slope of the degradation functions of FUB for the years 1998 to 2000 in comparison to others decreases as in 2000 nearly no degradation could be found. Fig. 4 shows plots of the reflectances of the calibration target without (upper panel) and with inter-calibration for the 16 year from 1989 to 2004.

Starting with NOAA 15 the AVHRR/3 instrument is flown on the polar orbiting satellite, which shows a sharper separation between the red and near infrared channel resulting in derived higher NDVI data. The correction functions presented by Trishchenko et al. [7] were used to normalise the data series to NOAA 9 standard. But it is felt, that the corrections for the AVHRR/3 instrument are not sufficient for most part of the MEDOKADS area.

REFERENCES

[1] KOSLOWSKY, D., 2003: The MEDOKADS data set as a substantial part of a remote sensing data network for a Mediterranean research and application network. In: Bolle, H.-J. (ed.): Mediterranean Climate, pp. 165-177. Springer-Verlag Berlin Heidelberg New York.

[2] FELL, F. ET AL., 2003: SISCAL project: establishing an internet-based delivery of near-real-time data products on coastal areas and lakes from satellite imagery. Ocean Remote Sensing and Applications. In: Frouin, R.J., Yuan, Y., Kawamura, H. (eds.): Proceedings of the SPIE, Volume 4892, pp. 566-576.

[3] KIDWELL, K.B., 1991: NOAA polar orbiter data users guide, (TIROS-N, NOAA-6, NOAA-7, NOAA-8, NOAA-9, NOAA-10, NOAA-11, NOAA-12, National Oceanic and Atmospheric Administration National Environmental Satellite, Data, and Information Service National Climatic Data Center Satellite Data Services Division, Washington, DC.

[4] GOODRUM, G., KIDWELL, K.B. AND WINSTON, W., 2000: NOOA KLM user's guide. U.S. Department of Commerce National Oceanic and Atmospheric Administration, National Environmental Satellite, Data and Information Service, Washington, DC.

[5] RAO, C.R.N. AND CHEN, J. ,1994: Post-launch calibration of the visible and near infrared channels of the Advanced Very High Resolution Radiometer on NOAA-7, -9, and -11 spacecraft, TR 78, NOAA/NESDIS, Washington, D.C..

[6] KOSLOWSKY, D., BILLING, H. AND ECKARDT, M., 2001: Sensor degradation and inter-calibration of the shortwave channels of the AVHRR - NOAA 11/14/16 satellites Proceedings of the 2001 EUMETSAT Meteorological Satellite Data Users' Conference, Antalya, Turkey, 1-5 October 20001, pp. 107-113. ISBN 92-9110-044-7.

[7] TRISHCHENKO, A.P., CIHLAR, J. AND LI, Z., 2002: Effects of spectral response function on surface reflectance and NDVI measured with moderate resolution satellite sensors. *Rem. Sens. Env. 81*, pp 1-18.

I APPENDIX

I.1 Using the Origin-Indicator

Even when floating values are converted to 16 bit integer depending of the computer platform used, it might be necessary to swap the byte order. All data in the MEDOKADS use the “little-endian” data representation, which means that bytes of lower significant have lower address. The same is true for the bit-order: the 16th bit (B15) is the most significant (MSB) and B0 the least significant one.

The meaning of the bits of pseudo-channel "I" of the MEDOKADS is:

B15...../.....B0
(MSB)...../.....(LSB)
higher (second) byte lower (first) byte

B15	= land/water-bit	land	= 0;	water	= 1
B14	= cloudmask	clear	= 0;	cloudy	= 1
B13 ...B6	= spare				
B5/0	= origin-indicator				
B5/4	= orbit-offset (0 = 1. Orbit ; 3 = 4. orbit of ingestion period)				
B3/0	= day-No. in decade (1 ... 10)				

The origin-indicator allows to recover date and orbit-number of each pixel even in the case of 10-day-max-NDVI composites or other logical combinations which select pixel out of a period but alter its value. In the case of 10-day-max-NDVI composites all remaining possible pseudo-channels correspond to the same AVHRR superpixel.

I.2 Naming Conventions

I.2.1 Internal names

The initial creation of MEDAKADS in the beginning of the early nineties of the last century when names data on PC systems must not exceed 8 characters plus 3 characters extension still defines the internal names. Further separation of the data is achieved by sub-directories. To allow a simple ordering of time series data names should include date and/or time like YYMMDD or HHMMSS. The next character to the right indicates the above mentioned area and coordinates of upper corner:

S:	Iberian Pensins.	(55 N/10 W;	2800 lines; 1536 pixel)
I:	Italy	(55 N/ 5 E;	2800 lines; 1536 pixel)
B:	Balkans	(46 N/15 E;	1900 lines; 1536 pixel)
E:	Eastern Mediterranean	(46 N/27 E;	1900 lines; 1536 pixel)

The last character of the file name characterises the channel or pseudochannel number:

1 ... 5	:	calibrated AVHRR channel 1 ... 5
6	:	satellite zenith distance according to pixel location
7	:	sun zenith distance according to pixel location
8	:	satellite azimuth according to pixel location
9	:	sun azimuth according to pixel location
P	:	scattering angle according to pixel location
A	:	broad-band albedo
N	:	NDVI
I	:	bit maps, including origin-indicator
T	:	local time in pixel position since ascending node
S	:	sea/land surface temperatures (split window)

MAX(NDVI) composite data are provided in the same manner. The first 6 characters of the names are of the form YYnnNV (YY = year, nn = no. of decade in the year, NV= identification for MAX(NDVI) data set. Decades are not synchronised to the first day of a month and are running continuously. The assignment of decade number and date can be found in MEDOKADS_DİR:NDVI_CD_LABEL.yyyy (yyyy:year).

Possible values of the origin-indicator:

1. Orbit:	1.....10 (decimal)	1 ..... 12 (octal)
2. Orbit:	17 26	21..... 32
3. orbit:	33 42	41..... 52
4. orbit:	49 58	61..... 72

Example: 100052_8 (octal): this is a pixel over land; pixel is cloud free; data of day No. 10 of the decade and of the 3. swath of the ingestion period.

I.2.2 External names by automatic access

The external file names are derived from the internal ones but contain information about the location, size and resolution of the product. The terms are explained for an example given in chapter 3.2.1.2:

050502_L700_S800_P4700_X1200_R100_S.MYAREA_I16

050502:	Date 02-MAY-2005
L700:	700 lines
S800	800 samples
P4700:	latitude of the upper left corner is 47.00^0 N
X1200	longitude of the upper left corner is 12.00^0 E
R100:	relative resolution factor is 1.00 (that means: actual resolution is 0.01^0)
S:	type of pseudo-channel is LST/SST (split window surface temperature)
MYAREA:	name given with AREA keyword in request file
I16:	Interger*2 (16 bit digital resolution)

I.3 Automatic Access to MEDOKADS

I.3.1 Basics of the automated data access system

A demon has been developed and installed for automatic access to data of arbitrarily defined windows of the Mediterranean basin to provide DeSurvey participants with archives and near real-time data derived from daytime NOAA AVHRR data. While archive data can be used evaluate time-series and to establish a climatological basis of earth surface quantities, access to near real-time (NRT) data is possible with a delay of about four weeks necessary to provide fine-navigated products. This extension of the MEDOKADS is as long possible as the receiving equipment of FUB is functioning or on-line access to raw HRPT data from other sources is granted.

The MEDOKADS data reside in the protected area of the computer network of the university. Thus only registered user can get access to the data. The following steps have to be done:

1) Send a non-formal request to kosze@zedat.fu-berlin.de including the IP name or adress of the computer which will be used for the data access.
2) Then an agreement of scientific use of the data will be prepared which has to be signed by both parties.
3) The IP-number will be inserted to the data base to allow FTP access to the server.
4) The remote user has to fill in a ASCII form and send it to the FTP server in directory MEDOKAD_CMD. The request form must have the ".medokads_req" (not case sensitive).
5) The demon checks the directory MEDOKADS every minute for newly arrived request forms.
6) If one or more requests arrived, the forms are renamed from "*.medokads_req" to "*.medokads_bsy" indicating that the request is being processed. To allow a identification of subsequent requests with the same name, a identification using date and time is added to the name of the request.
7) A log-file with the extension "*.medokads_log" is created and can be accessed during the processing phase in the directory MEDKADS_LOG to monitor the processing steps and to identify error conditions.
8) A syntax check is performed and in case of errors remarks are included.
9) When the syntax check has succeeded the full request form is added to an accounting data base.
10) If the request form does not contain all parameters, missing values are added from

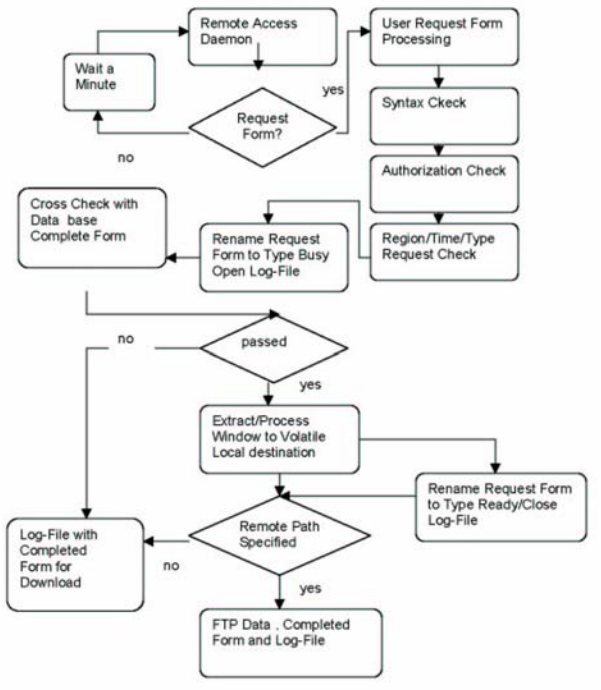

the accounting data base, if the specified request data window has been used before.

11) The defined data window will now be processed, the maximum window size is 9.000.000 pixel per pseudo-channel .
12) The results are written to directory MEDKADS_DATA with the subdirectory extracted from the e-mail address, mandatory in each request, before "@" on the server.
13) At end of the data extraction the "*.medokads_bsy" is renamed to "*.medokads_rdy", indicating data are ready for download. If an FTP address and directory is included in the request file, data are sent automatically to this destination.

Data request can be ordered for single product channel or for all 15 pseudo-channels. For the testing period, as long as disk space is available, all resulting data windows are saved to recover problems and errors. Later on data will be available for download for one week. The processing steps are summarised in Fig. 5.

I.3.2 Details of Processing the Data Window

Requested windows can be located anywhere in Europe and the Mediterranean and can have any size (max. 4500 lines by 5236 columns), maximum total 9.000.000 pixel). A patchwork programme checks, which areas (stripes) can contribute data to the specified window. Parts of the window that cannot be provided with data are left blank.

The filling strategy is first to use the Spain (S), Italy (I), Balkans (B) or Eastern Mediterranean (E) stripe of the MEDOKADS data set and not to select data with smallest zenith distance of the satellite. Thus in the case of single dates the Iberian, Italy and Balkans Peninsula as well as the East Mediterranean area are covered by data from one satellite swath and do not show variable cutting lines.

Figure 5. Flow chart of the automated access system.

I.3.3 Template of a ASCII request form

```
FORM=RASTER                     ;Request form for RASTER image data
AREA=TEST_WINDOW                ;specify  unique names for different locations
TYPE=OVER                       ;OVER (others are not yet implemented)
COMP=DAY                        ;DAY,C10, (daily, 10-day's composite)
MOS=MOS                         ;MOS: MOSAIK OF ACTUAL RECEPTION PERIOD or ""
SAT=N11                         ;N11,N14,N16 (N11:1989-94; N14: 1995-2000; N16: since 2001)
CHAN=ALL                        ;ALL,SST,CH1...H5,ALB,NDVI,CLOUD,TIME,SUNZNT,SATZNT,SUNAZ,SATAZ
MCHAN= 15ANS                    ; Selection out of "123456789AINPST" (overwrites CHAN)
DATE=15-AUG-1993                ;DD-MMM-YYYY
TIME=PM                         ;for daytime data
FROM=10-FEB-1993                ;time series, together with mandatory TO overwrites DATE
TO=30-Jun-1993                  ; s. FROM, FROM ... TO must not cross year boundary
LAT_UPL=42.0                    ;LATITUDE UPPER LEFT CORNER (DEGREE)
LON_UPL=-09.0                   ;LONGITUDE UPPER LEFT CORNER (DEGREE, E: positive)
PROJ=GEO                        ;GEO (others not yet implemented)
RES=1.                          ;Resolution-factor (ever = 1.)
PIXEL=350                       ;NUMBER
LINES=200                       ;NUMBER
EMAIL=user@site.de              ;REQUIRED FOR AUTHORIZATION CHECK (mandatory)
IPNUM=mycomputer                ;IP-NUMBER or NAME (not checked for errors)
IPDIR=mydirectory               ;RETURN PATH for anonymous ftp (not checked for errors)
;
; the ordering of the keywords is variable
; text following ";" interpreted as comment.
; each line should contain at least one ";" and/or carriage return/linefeed
;
;  to be sent to        130.133.7.26
;                       cd MEDOKADS_CMD
; IP address of sending computer has to be previously registered
;
```

Fifty years of landscape evolution in southwestern Mauritania by means of aerial photos. Land degradation continues…

A.J. Niang[a], A. Ozer[a] and P. Ozer[b]

[a] Department of Geography, Liege University, Allée du 6 Août 2, B-4000 Liège, Belgium, email: ajeniang@yahoo.fr

[b] Environmental Sciences and Management Department, Liege University, Avenue de Longwy 185, B-6700 Arlon, Belgium

ABSTRACT

Southwestern Mauritania is located in a semi-arid environment exposed to large rainfall variations and affected by a severe drought since the mid-1960s. The studied area includes the right bank of the Senegal River and the southern extension of the Saharan sandy dunes. The study is based on the analysis of climatic data (daily rainfall, wind speed and dust related conditions), field studies, and four aerial surveys realized in 1954, 1972, 1992 and 2003. We analyze the climatic evolution since 1951 and monitor landscape evolution over the last 50 years.

The climatic analysis shows that, after a strong decline of yearly rainfall started in the mid-1960s, a significant increase is observed from the early 1990s. In the meantime, dust storms frequency has dramatically increased while the threshold wind speed declined as a result of vegetation contraction. The comparison of the four mosaics of aerial photos reveals the major impact of both drought and human on recent environment changes. Three land cover types were selected for the analysis: forest, active dunes, and rice fields. Most forests disappeared during the last fifty years, declining from 2837 to 76 ha from 1954 to 2003. Active dunes were absent from the 1954 aerial photos, limited to 10 ha in 1972, and then increased to 672 ha in 1992. While no rice fields existed before the 1980s, their surface was 1097 ha in 1992 and 1987 ha in 2003 and with a total of 4300 ha ready to be used.

If the increase of active dunes activity is likely to be a consequence of the persisting drought, forest decline is more likely to be attributed to fuel wood collection in a first time, then to the creation of rice fields since the late 1980s. Although the 2003 aerial photos show a timid return of vegetation in very limited and specific areas, field surveys show that wind erosion is still very important and water erosion is developing very rapidly because of the absence of vegetation cover. Land degradation in this area of Mauritania is therefore continuing despite better rainfall conditions.

Keywords: Land cover change, Wind erosion, Desertification, Aerial photos, Senegal River Valley, Mauritania

1 INTRODUCTION

Southwestern Mauritania is located in a semi-arid environment exposed to large rainfall variations. During the Quaternary, the study area has experienced a long morphodynamic evolution submitted to very different paleoclimates. Soils are characterised by sandy dunes that developed during the latest arid phase of the ogolian period (from 18000 to 12000 BP). These sandy formations are oriented in a North-East to South-West direction.

This sandy dunes scheme is abruptly stopped by the alluvial plain of the Senegal River which appears like a 10 to 25 kilometers wide depression covered by alluvial deposits with a very low relief. The geomorphological evolution is linked to climatic variations and sea level changes because of the very flat slope of the Senegal River.

The rainfall regime of the study area is characterized by great variability in both time and space. Even within short distances, rainfall may be very different [1]. Climate is characterized by a short rainy season, largely limited to the months of July, August and September, as well as the North–South gradient of the mean annual rainfall [2]. Over the last decades, the Sahel of West Africa has been affected by a severe drought [2, 3, 4]. These long-time rainfall shortages have not only affected natural vegetation and stream flows but also, and probably defitively, socio-economical activities. In Mauritania, above 90% of the population was rural fourty years ago, dominated by agriculture in southern Mauritania and by pastoralism in the central and northern zones of the country, most inhabitants being nomads. From the mid-1960s, the long-term drought killed most of the livestock and forced nomad population to sedentarise creating new villages or enlarging small cities [5, 6]. Many others moved towards the capital Nouakchott with a population that increased from 6000 in 1962 to 535 000 in 1988 and to about one million currently [7, 8].

The precarity of hydroclimatic conditions has led to the large hydrological works conducted to optimize water ressources management of the Senegal River basin for agricultural purposes. Large dams were constructed in the late 1980s. One upstream, Manantali, in order to allow irrigated agriculture in all seasons. The other one downstream, Diama, to impead the intrusions of salted sea water.

The area on which we focus here is the central part of the Trarza region (figure 1) and is delimited between 15°30' and 14°40' W, and 17°50 and 15°30 N. The northern part of the study area is charcasterized by desert-like conditions. The southern area is part of the traditionnally called "sahelian belt" that is exposed to desertification processes.

Recent papers suggested that the Sahel of West Africa has been greening during the last decade [9, 10, 11]. This greening would be due to increasing rainfall recorded during the 1990s [12] but the resilience of vegetation to rainfall is not evident everywhere and the idea of "greening Sahel" has been challenged by some authors [13, 14]. In this paper, environmental evolution is analyzed over the last 50 years with climatic data (daily rainfall, wind speed and dust related conditions), field studies, and four aerial surveys realized in 1954, 1972, 1992 and 2003 in order to estimate latest trends in land cover.

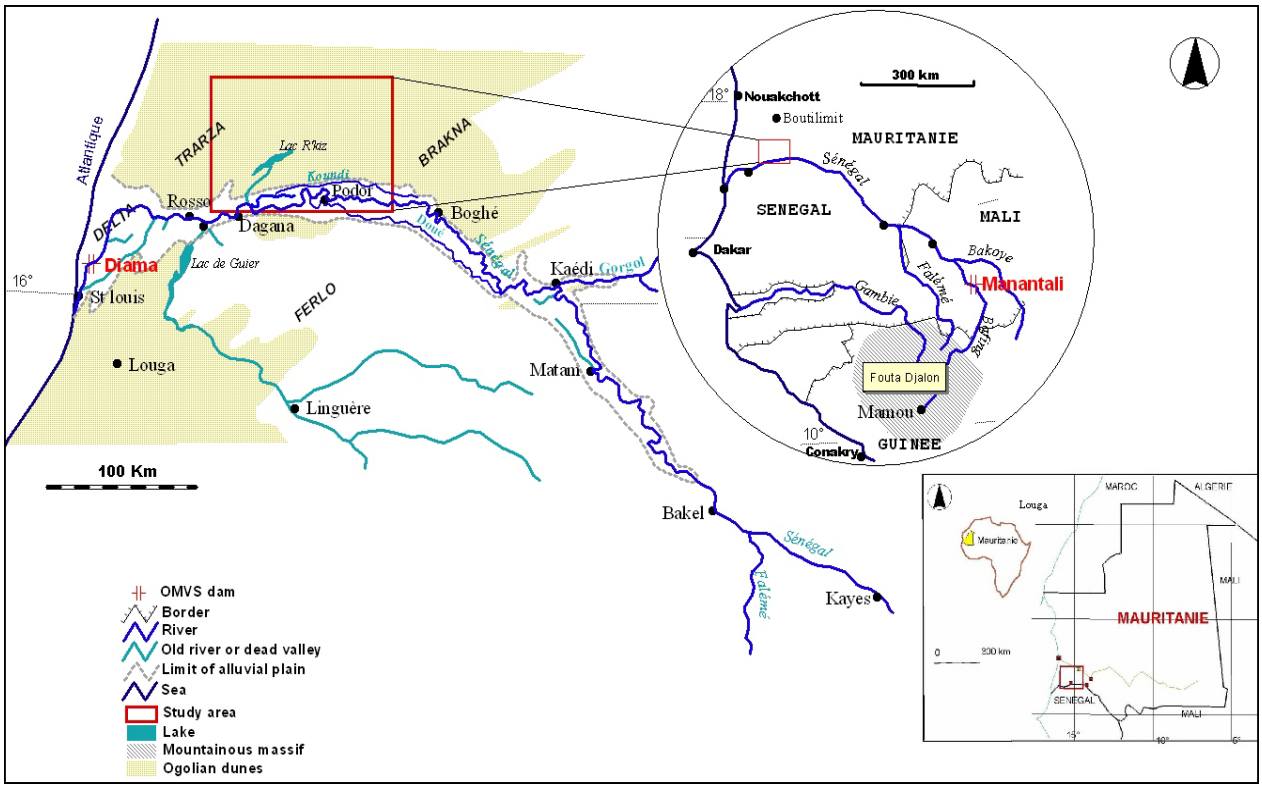

Figure 1. Geographical position of the study area.

2 DATA AND METHODS

2.1 Climate data

Daily rainfall data from the origin of the station until 2001 for the station of Boutilimit were made available from an archive assembled by the Agrhymet representation in Mauritania.

The meteorological horizontal visibility is one of the elements world-widely identifying air mass characteristics. In synoptic stations, it is observed on a 3-hourly basis and defined as the greatest horizontal distance at which a black object of suitable dimensions, located near the ground can be seen and recognized when observed against a background scattering of hydrometeors (rain, snow, fog, mist) or lithometeors (dust processes) [15]. The international synoptic surface observation code (SYNOP code) [16] allowed the identification of four classes of dust-related conditions:

1] dust being raised from the ground at the time of the observation (07, 08) and reducing horizontal visibility to less than 5 km (blowing dust);

2] dust storms, resulting of turbulent wind systems entraining particles of dust into the air, at various degrees of intensity (09, 30, 31, 32, 33, 34, 35, 36) reducing horizontal visibility to below 1 km;

3] dust suspended in the air but not being raised from the ground at the time of observation (06), remnants of earlier deflation events reducing horizontal visibility to less than 5 km. Dust deposition is noticed at the time of the observation; and

4] haze (05, presumably caused by dust) reducing horizontal visibility to less than 10 km. In this case, no dust deposition is observed which suggests that the dust particles have been raised from the soil at a considerable distance away.

Data on dust related conditions were digitized from the 3-hourly time-scale synoptic observations made in Boutilimit and archived at the meteorological office of Mauritania. They cover the 1951 to 1998 period. Later records were not used as they are not reliable due to the absence of observers since the late 1990s. Each day was qualified as (i) without dust if the horizontal visibility was greater or equal to 5 km, (ii) with suspended dust only in case of haze and/or dust suspended in the air with a visibility below 5 km; or as (iii) with deflation (or wind erosion) for days with observed blowing dust and/or dust storm.

Data on wind speed recorded at 10 meters height were also digitized from the 3-hourly time-scale synoptic observations. Here, the highest wind speed of the day was automatically selected. The data at the station of Boutilimit cover the 1951 to 1998 and later records are not reliable due to the bad conditions of the anemometer [2].

2.2 Airborne data

The study has drawn upon various sources of information, including topographical map, aerial photos and satellite pictures. In addition, field observations and collection of data has been carried out. The most important data sources are briefly listed in table 1.

Table 1. Aerial photos and satellite pictures used for this study.

Year	Mission	Reference	Characteristics	Scale/Resolution	Type and origine
March 1954	AOF 1954	088	Grey scale	1 : 50000	Aerial photos (IGN France)
May 1972	CORONA 1116-1	DS1116-1075DA043	Grey scale	1 :37000	Satellite pictures (USA)
November 1992	MAU 1992	014/400	Grey scale	1 :40000	Aerial photos (IGN France)
December 2003	OMVS	n/a	RGB	0.5 meter	Aerial photos (Canada)

3.3 Methodology

3.3.1 Climate

Climate data were analysed using classical methods and the non parametric Pettitt statistical test [17] in order to identify potential abrupt changes in the series. In addition, in order to retrieve the threshold wind speed at Boutilimit, the daily maximum wind speed and the associated observed deflation events were plotted in the form of frequency diagrams for each station. A 10% frequency of the deflation events was chosen to estimate the threshold wind speed.

3.3.2 Aerial photos

Differences in the time of year of aerial photo coverage, as well as in quality and processing, make quantitative analysis of changes between the four set of photos difficult. However, certain objects and features may be identified visually on the basis of pattern and shape. These include:

- Dense individual trees over a certain size that may be called “forest”.
- Active aeolean surface morphology.

• Human habitations.
• Rice fields that clearly appear of aerial photos with well-defined linear boundaries.

All topographical map, aerial photos and satellite pictures have been scanned and comparisons were realized in *Erdas imagine* et *Arcview*. After a geometric correction, aerial photos and satellite pictures were mosaiced. Digitalisations made on different data sources have superposed in order to quantify land use cover changes.

4 RESULTS AND DISCUSSIONS

4.1 Climatic evolution

4.1.1 Rainfall

The analysis of rainfall shows the very high variability of yearly totals that vary from about 10 mm in 1987 to above 400 mm in 1955 (figure 2). We applied the non parametric statistical test of Pettitt [17] in order to find any abrupt changes in the 1923-2001 series of rainfall. Results show a first abrupt change in 1969 indicating that an intense precipitation deficit started in 1970 and ended in 1990. Yet, the 1923-1969 period recorded average yearly rainfall of 191 mm while the drought of the 1970s and 1980s recorded 103 mm, that is a deficit of 46%. Since 1991, average rainfall is 181 mm, very near pre-drought conditions.

These results correspond to the trends observed elsewhere in the Sahel of West Africa, with the start of the drought in the late 1960s [2, 3, 4] and wetter conditions in the early 1990s [12].

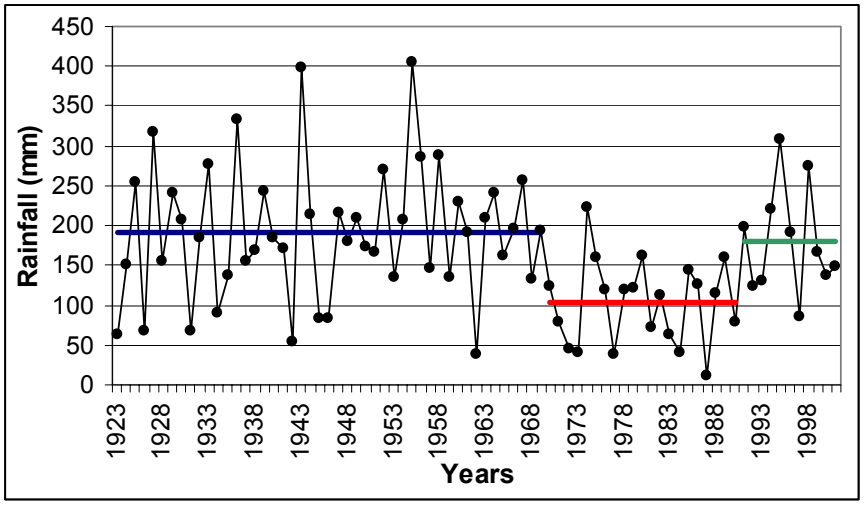

Figure 2. Rainfall at the station of Boutilimit from 1923 to 2001. Horizontal lines indicate average rainfall value recorded during the three homogeneous periods of rainfall indicated by the non parametric statistical test of Pettitt [17]:

4.1.2 Dust processes and threshold wind speed

Dust processes have strongly increased during the 1951-1998 period (not shown). From about 20 events per year before the drought, dust events reached an average of above 100 events per year during the drought and remained stable during the 1990s. This trend is similar to those found anywhere else in West Africa [2].

The association between dust-raising events and wind speed were calculated for the three climatic periods identified above (1951-1969, 1970-1990 and 1991-1998). The frequency of occurrence of deflation events at Boutilimit is shown in figure 3.

The threshold wind speed calculated for dust raising events at the 10% frequency decreased from 8 m s^{-1} during the 1951-1969 period, to 6 m s^{-1} during the drought and 5 m s^{-1} during the 1990s. The same trend is observed when analyzing wind speed associated with deflation events at the 50% frequency. From above 12 m s^{-1} during the pre-drought period, it declines to the 8-9 m s^{-1} interval during the drought and to 7 m s^{-1} during the 1990s. A similar trend was observed in other stations of Mauritania [2] and can be explained as a result of the degradation of the soil cover enhanced by the drought, overgrazing, wood collection, livestock stepping, and many other reasons that lead to this higher capacity of the wind to provoke erosion. Such assumption will be verified later on when analyzing aerial photos.

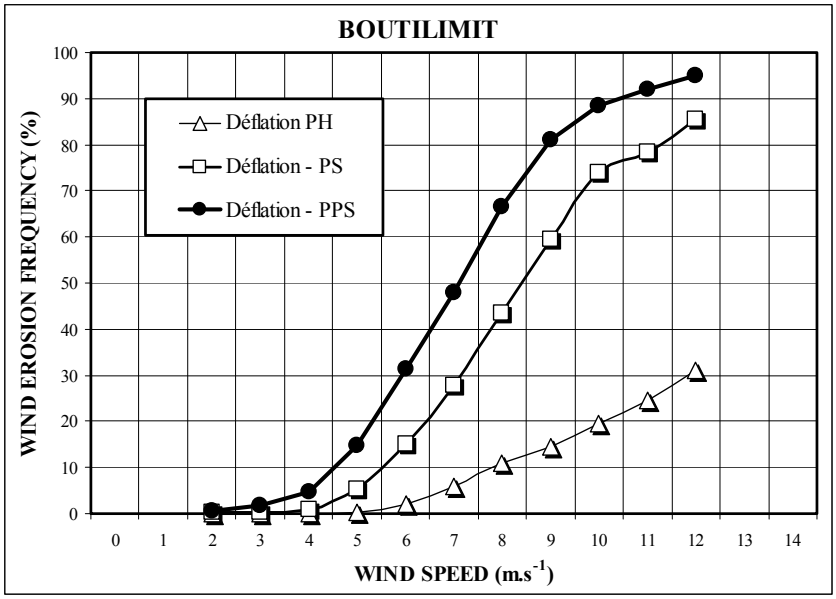

Figure 3. Frequency of deflation events vs wind speed at Boutilimit during the 1951-1969, 1970-1990, and 1991-1998 periods

4.2 Landscape changes

4.2.1 Land use change in southwestern Mauritania, 1954-1992

A common area was selected from the airborne data of 1954, 1972 and 1992 in order to estimate changes in environmental features (figure 4). Superposition of airborne data shows that the most important changes are observed in the dune morphology. All dunes were fixed by vegetation in 1954. In the early 1970s, very little areas were on the move suggesting that a few years of rainfall shortages are not enough to radically change the landscape. However, 20 years of drought and human pressure were fatal to solid dunes and wind erosion has become the major morphodynamic process. Vegetation disappeared, from 17.0% in 1954 to 1.6% in 1992, and most dune crests visible from the white spots of the 1992 aerial photo are active (figure 4). Despite what has been noted in other places of West Africa, ogolian fossil dunes have been reactivated but none moved southwards.

Our findings are similar to those observed in other areas of the Sahel, that is a strong degradation of the environment during the early 1980s due to the intensification and the persistence of the rainfall deficit [2,11]. In addition, they fit very well with the evolution of the frequency of dust processes noted in Boutilimit and in the semi-arid belt of West Africa [2].

4.2.2 Land use change in the Senegal Valley, 1954-2003

In order to estimate the environmental evolution consecutive to the rainfall increase, the analysis is focused on the Senegal Valley, an area of 13075 ha covered by all four aerial photos from 1954 (Fig. 5) to 2003 (Fig. 6).

The analysis of all four airborne data clearly shows the continuous disappearance of forest cover from 2837 ha (21.7%) in 1954 to 76 ha (0.6%) in 2003. If the forest reduction was of the order of 50% between the 1950s and the early 1970s, major changes occurred between 1972 and 1992 with surfaces declining from 1356 ha to 92 ha. An hypothesis that has been confirmed by local people is that forest contracted during the 1950s and the 1960s due to wood collection as fuel or for construction. Between 1972 and 1992, forest did not decline because of the drought but were cleared to welcome new rice fields. These were created thanks to the construction of two large dams realized to optimize water ressources management of the Senegal River. Yet, inexistant before the dams, rice fields covered 1097 ha (8.4%) in 1992 and 1987 ha (15.2%) in 2003, with a total of 4300 ha (32.9%) ready to be used.

Regeneration of vegetation can be observed in very limited areas where human pressure is small such as in fields protected by fences. But the most interesting process in the last 10 years is the development of several types of water erosion that clearly appear in red on figure 6 such as backward erosion, gullying (figure 7), bank erosion and the creation of badlands that did not existed before. These new processes are favoured by the low vegetation cover and the return of rainfall characterized by heavy events.

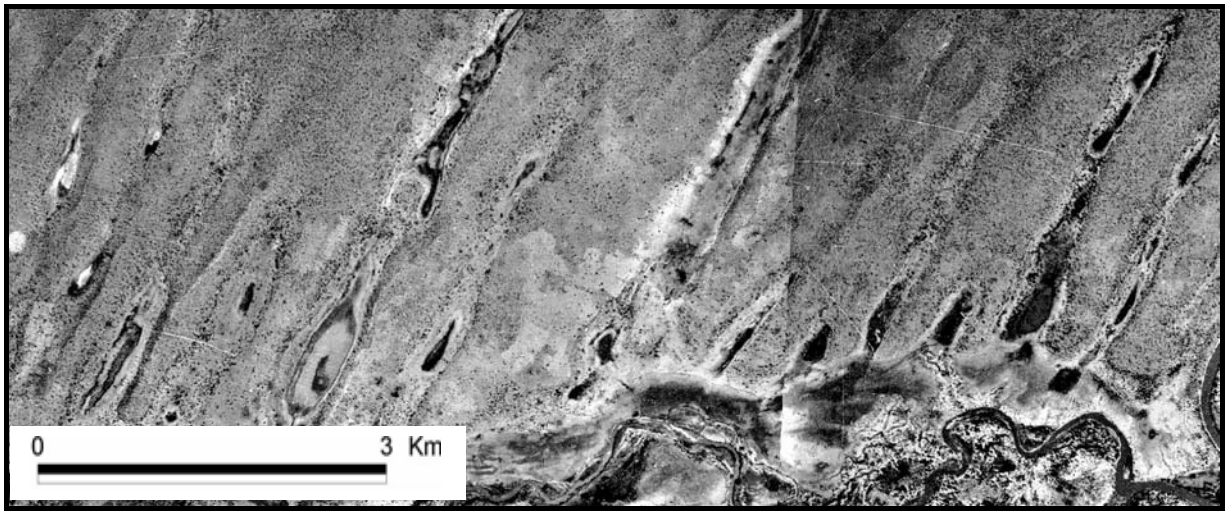

1954

1972

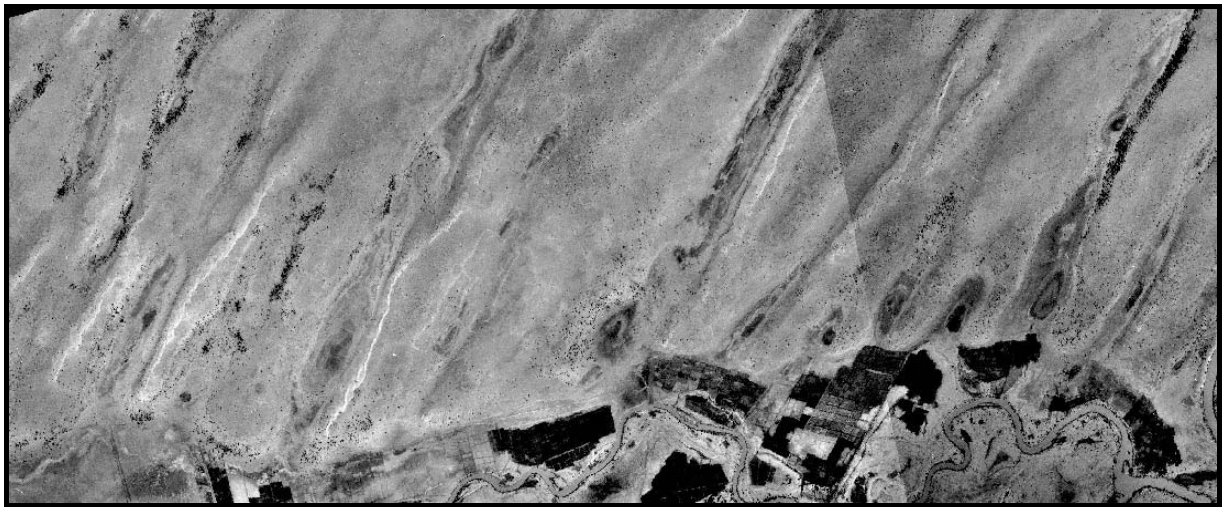

1992

Figure 4. Aerial photos of southwestern Mauritania in 1954, 1972 and 1992.

Figure 5. Aerial photo of the Senegal Valley in 1954.

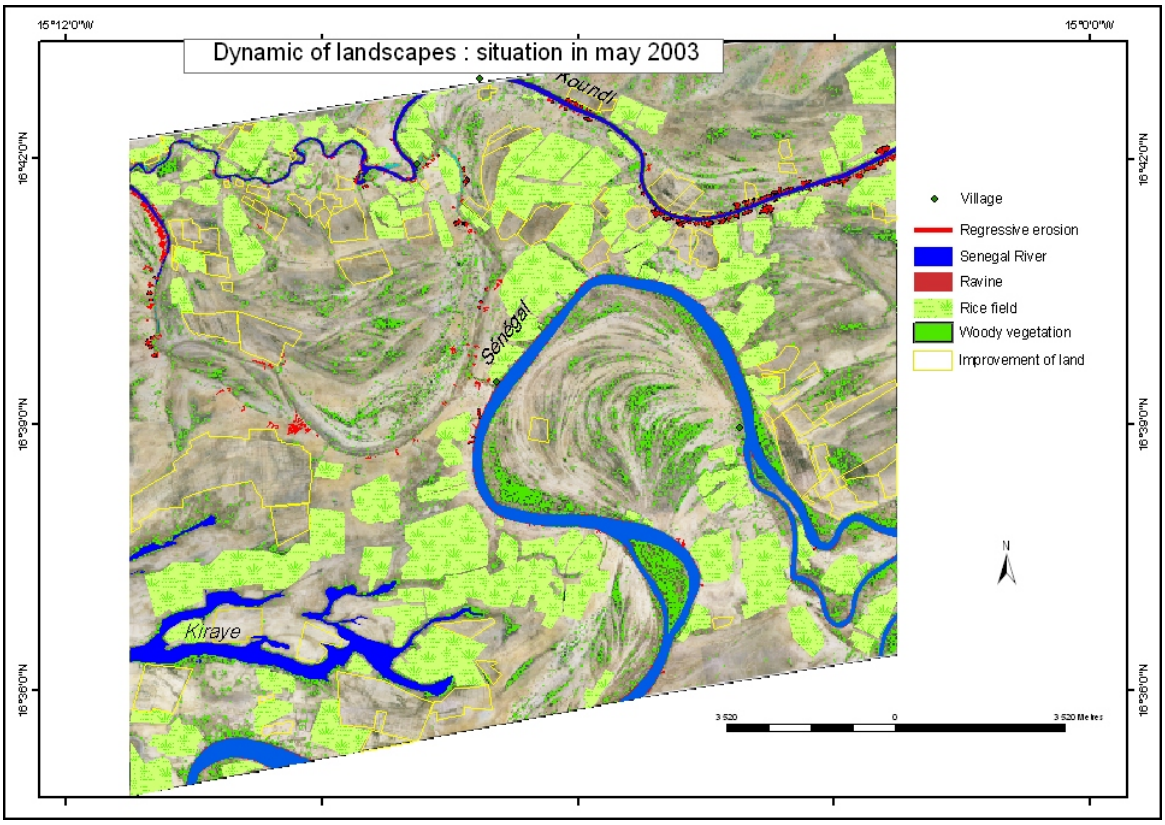

Figure 6. Aerial photo of the Senegal Valley in 2003 and classification of selected land cover.

5 CONCLUSION

This multitemporal analysis realized from climatic and airborne data allowed us to understand the landscape evolution in an area of southwestern Mauritania during the last 50 years.

As observed in most other places of the Sahel, land degradation did not start directly with rainfall shortages but later on due to the intensification and the persistence of the precipitation deficit. In addition, increasing human pressure has been a constant during the period of analysis. Crests of fixed dunes have been reactivated during the 1980s, vegetation contracted during the same period, and forests almost disappeared during the second half of the 20th century. A clear return to more normal precipitation did not provoked a significant greening of the natural features of the landscape. This explains why wind erosion still remains a major environmental parameter in the dune area North of the Senegal Valley. In addition, this low vegetation cover created perfect conditions for water erosion (gullying, badlands) that did not exist previously.

However, destruction of the forests and other features did not give place to bare desert-like soils. At the contrary, most of these areas have been replaced by rice fields after the construction of two dams to optimize water ressources management of the Senegal River. These areas may therefore show a good resilience of vegetation from space when the analysis is realized based on low resolution satellite data such as the Pathfinder series of NOAA-AVHRR [9,18-19] but do not represent the true evolution of the environment. In other words, man continues land degradation except when large enterprises well financed allow land improvement, but at the detriment to protected forests...

REFERENCES

[1] SIVAKUMAR, M.V.K. AND HATFIELD, J.L., 1990: Spatial variability of rainfall at an experimental station in Niger, West Africa. *Theor. Appl. Climatol. 42*, pp. 33-39.
[2] OZER, P., 2000: Les lithométéores en région sahélienne: un indicateur climatique de la désertification. *GEO-ECO-TROP. 24*, pp. 1-317.
[3] L'HÔTE, T., MAHÉ, G., SOMÉ, B. AND TRIBOULET, J.P., 2002: Analysis of a Sahelian annual rainfall index from 1896 to 2000; the drought continues. *Hydrol. Sc. J. 47*, pp. 563-572.
[4] DAI, A., LAMB, P.J., TRENBERTH K.E., HULME M., JONES P.D. AND XIE, P., 2004: The Recent Sahel drought is real. *Int. J. Climatol. 24*, pp. 1323-1331.
[5] GRAVIER, M., 1996: De la tente à l'habitation en banco, sédentarisation et déforestation : l'exemple du Tagant en Mauritanie. *Sécheresse 7*, pp. 195-202.
[6] GRAVIER, M., 1996: Nomadisme et sédentarisation au Tagant (Mauritanie). *Cahiers d'Outre-Mer 195*, pp. 227-246.
[7] SALAMA, M., DECONINCK, J.N., LOFTY, M.F. AND RISER, J., 1991: L'ensablement de Nouakchott: exemple de l'aéroport. *Sécheresse 2*, pp. 101-109.
[8] http://mauritania.unfpa.org/datarim.htm (last access: 31/08/05)
[9] EKLUNDH, L. AND OLSSON, L., 2003: Vegetation index trends for the African Sahel 1982-1999. *Geophys. Res. Lett. 30*, 10.1029/2002GL016772.
[10] PEARCE, F., 2002: Africans go back to the land as plants reclaim the desert. *New Scient. 175*, pp. 4-5.
[11] RASMUSSEN, K., FOG, B. AND MADSEN, J.E., 2001: Desertification in reverse? Observations from northern Burkina Faso. *Global Environ. Change 11*, pp. 271-282.
[12] OZER, P., ERPICUM, M., DEMAREE, G. AND VANDIEPENBEECK, M., 2003: The Sahelian drought may have ended during the 1990s. *Hydrol. Sc. J. 48*, pp. 489-492.
[13] HIERNAUX, P. AND TURNER, M.D., 2002: The influence of farmer and pastoralist management practices on desertification processes in the Sahel. In: Reynolds, J.F. and Stafford Smith, D.M. (eds): Global desertification: Do humans cause deserts?, pp. 135-148. Dalhem University Press, Dalhem.
[14] HOUNTONDJI, Y.C., SOKPON, N. AND OZER, P., 2005. Analysis of the vegetation trends using low resolution remote sensing data in the Sahel (1982-1999) for the monitoring of desertification. This RGLDD Congress.
[15] WORLD METEOROLOGICAL ORGANIZATION, 1992: *International Meteorological Vocabulary.* WMO, Geneva.
[16] WORLD METEOROLOGICAL ORGANIZATION, 1992: *Guide to meteorological instruments and methods observations, WMO n°8*. WMO, Geneva.
[17] PETTITT, A.N., 1979: A non-parametric approach to the change-point problem. *Appl. Statist. 28*, pp. 126-135.
[18] NICHOLSON, S.E., TUCKER, C.J. AND BA, M.B., 1998: Desertification, drought, and surface vegetation: an example from the West African Sahel. *Bull. Am. Meteorol. Soc. 79*, pp. 815-829.
[19] PRINCE, S.D., BROWN DE COLSTOUN, E. AND KRAVITZ, L.L., 1998: Evidence from rain-use efficiencies does not indicate extensive Sahelian desertification. *Global Change Biol. 4*, pp. 359–374.

Assessment of NDVI and NDWI spectral indices using MODIS time series analysis and development of a new spectral index based on MODIS shortwave infrared bands

A. Palacios-Orueta[a,b], S. Khanna[b], J. Litago[c,b], M. L. Whiting[b] and S. L. Ustin[b]

[a] E.T.S.I. Montes. Universidad Politécnica de Madrid, email: alicia.palacios@upm.es
[b] Calspace, University of California, Davis
[c] E.T.S.I. Agrónomos. Universidad Politécnica de Madrid

ABSTRACT

We put forward a new spectral index, Shortwave Angle Normalized Index (SANI), based on the NIR and SWIR MODIS bands. The new index parameterizes the general shape of this part of the spectrum by measuring the angle at SWIR1 and the normalized index between NIR and SWIR2. Preliminary results show that it performs well in tracking moisture and discriminating between soil, vegetation and dry vegetation. We use Time Series Analysis to explore the temporal evolution of NDVI, NDWI and SANI and climatic data for the years 2000 to 2005. Our analyses show that SANI is synchronized with precipitation in grasslands but not in irrigated cropland where irrigation is a major source of moisture. NDVI does not follow precipitation closely in either of the two regions. SANI also shows an overall negative trend, which corresponds to the overall positive trend in precipitation levels from 2000 to 2005. Thus, this index seems to be a powerful tool for uncovering subtle sources of variability, inter-annual trends in environmental variables and dynamic relationships between soil and plant variables.

1 INTRODUCTION

In the last few decades, climate change has begun to affect the responses of natural and cultivated vegetation. Although ecosystem response to the climatic trends can be subtle and difficult to detect, changes can have a strong impact on ecosystem health at medium to longer time periods. It is crucial to assess such impacts in order to design effective management strategies. Long-term ecosystem variability can change abruptly due to land use or disturbance or slowly and cumulatively, as in the case of climate change. On the other hand, non-permanent inter-annual variability occurs with annual climate anomalies [1] or land management, e.g., crop rotation and it is important to be able to distinguish between small but significant trends versus natural inter-annual variability. Time series data acquired through remote sensing instruments can provide information about ecosystem dynamics at medium (decadal) time scales and at a frequency that makes it possible to study both abrupt and gradual change in response to short and longer term variability. Such information will allow assessment of multivariate relationships between climate and remote sensing variables as well as among those variables.

Spectral indices are one of the most common techniques used for analyzing remote sensing data [2]. Indices are based on combinations of a small number of bands that enhance specific spectral properties. In vegetated environments spectral indices focus on emphasizing vegetation characteristics. When working with multispectral data only a few bands can be used, therefore indices are usually indicators of general characteristics such as plant cover, greenness, or amount of exposed soil.

The most universal index, NDVI (Normalized Difference Vegetation Index) has been used extensively to monitor ecosystems; in both the spatial and temporal domains [3] because it is proven to be a good indicator of ecosystem parameters like biomass, LAI and FPAR [4] among others. While NDVI derived indices are based on plant pigment absorption there are other indices which try to discriminate vegetation parameters such as water content and the amount of non-photosynthetic vegetation. The NDWI, (Normalized Difference Water Index) is a good indicator of soil and vegetation water content [5]. There are also several indices that characterize non-photosynthetic vegetation, (NPV) [6]. Plants function within a constrained range of biochemical variation. For example, a healthy plant will have high pigment content and also high water and nitrogen contents. Thus indices used to measure these different characteristics are frequently physiologically correlated. Most indices are also constructed using red (R) and/or near-infrared (NIR) bands, which means that they are mathematically correlated.

The principal advantage of indexes is their ease of use and potential to measure specific bands having known functional properties. Their disadvantage is a reduction in information content due to the decrease in the data dimensionality. Nevertheless, this becomes advantageous when significant information remains and is integrated in

a framework for exploitation. For instance, the availability of R and NIR bands on the AVHRR sensor has made it possible to make the first temporal analyses spanning a long time period, showing for the first time, global responses to inter-annual and multi-decadal climate patterns [7].

The MODIS sensor has 7 bands in the optical domain which allow parameterization of the general shape of the reflectance spectrum, providing valuable information about vegetation greenness, moisture conditions, and presence of bare soil and dry vegetation. These data combined with the near-daily acquisition make it possible to use multidimensional schemes such that subtle changes in the spectral shape can be monitored over time for individual pixels and images can be monitored for spatial variation. At present, MODIS provides two vegetation indices; NDVI and EVI (Enhanced Vegetation Index) [8], both of them are based on the R and NIR bands. The use of the SWIR, which is not affected by the path radiance and is highly sensitive to moisture has been largely unexploited.

Several remote sensing studies have explored the relationships between temporal spectral profiles and seasonal dynamics to assess general trends and phenological parameters [9]. Benedetti [10] found a high correlation between NDVI and wheat phenology in Emilia Romagna, Italy, including an exponential increase in NDVI corresponding to maximum spring biomass. Runtunuwu [11] calculated the length of growing season as the period when the vegetation index exceeds a threshold. Although these and other studies have used time series data, analyses have rarely included specific statistical tests for time series. In time series analysis (TSA), a stochastic model is fitted to explain the data dynamics and predict future evolution. These statistical methodologies can uncover subtle relationships and trends contained in the temporal data that offer significant value for research on ecosystem response to climate change. Piwowar and Ledrew [12] proposed the use of the Auto Regressive-Moving Average (ARMA) model to analyze NDVI temporal data. ARMA has been used in ecology and recently also in remote sensing. These methods are appropriate for parameterizing temporal relationships and locating them in a spatial context.

The objective of this research was to assess the potential of three spectral indices to monitor the temporal variability of ecosystems and the relationships between climatic variables and ecosystem change, using two TSA techniques. We also investigated whether indexes not based on R and NIR can provide new information about phenological evolution. We tested two common indices, NDVI and NDWI, and a third index that we introduce in this paper, termed Shortwave Angle Normalized Index (SANI). We tested whether these indexes contain distinct information that can complement each other. In the first part we describe the new index, SANI and explore the spectral variability contained in MODIS bands over the year. In the second part we use TSA to examine the relationships among several indexes and the response of indexes to climatic variables.

1.1 The SANI Index

The SANI index is based on a combination of NIR, SWIR1 and SWIR2 MODIS bands. Whiting et al. [13] demonstrated that the SWIR region could be fitted by an inverted Gaussian function that was highly correlated with moisture content in soils. SANI emulates the general shape of this part of the spectrum as it would be shown by a hyperspectral sensor. To accomplish this we evaluate a triangle with three vertices at NIR, SWIR1 and SWIR2 in terms of the size of the angle at SWIR1 (α_{SWIR1}) and the inclination of the line that connects the NIR reflectance with SWIR2 (L_{NS}) (see figures 1, a and b).

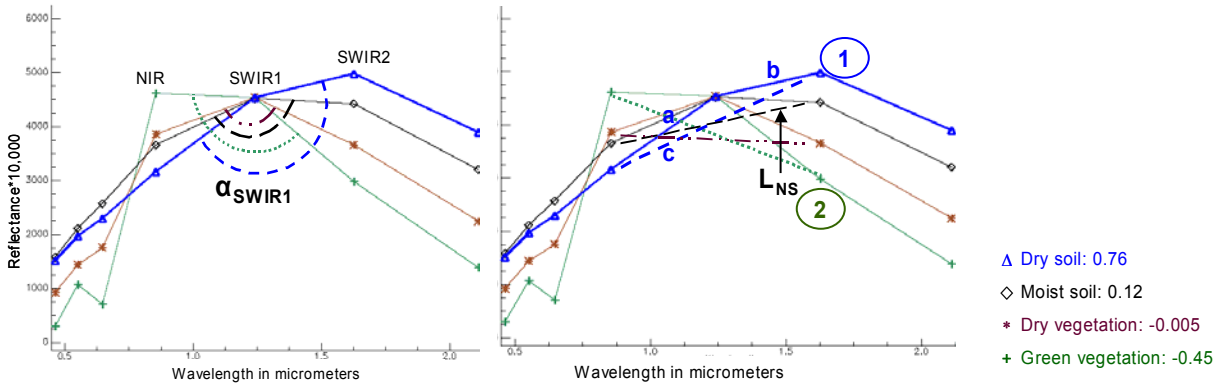

Figure 1. (a) Angle α_{SWIR1} formed at vertex, SWIR1 of the triangle formed by NIR-SWIR1-SWIR2 bands of MODIS and (b) Line L_{NS} that passes through NIR-SWIR2 with sides a, b and c of the triangle.

The angle α_{SWIR1} is large in dry soils and in healthy photosynthetic vegetation (PV), it decreases in NPV and moist soils. The line L_{NS} tilts towards NIR when moisture content increases and towards SWIR2 as the moisture content decreases. As a consequence, the normalized ratio between SWIR2 and NIR is negative in vegetation and positive in soils and is intermediate with different levels of moisture. The extreme negative and positive slopes of L_{NS} are coincident with large α_{SWIR1} in healthy vegetation and dry soil respectively (positions 1 and 2 in figure 1b). Thus, by multiplying the angle, α_{SWIR1} and the normalized difference between NIR and SWIR2, the discrimination of soil, NPV, and PV is emphasized by assigning high positive values to dry soils and high negative values to healthy vegetation. In the case of NPV both, α_{SWIR1} and the normalized ratio are small, so that SANI is close to zero. For moist soils the normalized index is still positive but α_{SWIR1} is smaller with low positive values. It is expected that the main source of error in SANI will be discriminating between NPV and moist soils. Since the index is based on bands sensitive to moisture and not to photosynthetic activity we expect that it to show different dynamics than NDVI. Due to the construction of the index, it is observed that when NDVI is high SANI is low. For example, in healthy full cover vegetation, NDVI is highly positive and SANI is highly negative. We expect that SANI is efficient when discriminating soil and NPV at low NDVI values.

2 DATA AND METHODOLOGY

We used MODIS surface-reflectance (MOD09) 8-day composite images. Two-hundred forty-seven (247) images from February 2000 to July 2005 were downloaded from the MODIS website (http://redhook.gsfc.nasa.gov/) and re-projected to latitude and longitude using the MODIS reprojection tool. Time series data were compiled for each of the seven bands using IDL programming language. Three spectral indices, NDVI, NDWI, and SANI were computed from these bands. We downloaded daily climatic data from the California Irrigation Management Information System (CIMIS) network (http://www.cimis.water.ca.gov/cimis) and summarized them into 8-day values. For solar radiation we calculated the average and precipitation was summed for the 8-day period. Dynamic relationships were studied using TSA using both frequency and temporal domains. Fourier methods [14] are commonly used to measure periodicities and dynamic relationships. We applied Fourier Spectral Analysis (FSA) to search for hidden periodicities in each time series index and determine the dynamic relationships between index and climate variable periodicities. In the temporal domain, we tested the stationarity of the time series using the "Unit Root Test" [15]. All analyses were performed in SAS v8.2. The study areas were located in Central California and consisted of two distinct ecosystems, annual grasslands and summer-irrigated crops. The objective was to determine if we could observe dynamic relationships between indices and climatic variables by studying two distinct phenological cycles in the two land-cover types.

3 RESULTS AND DISCUSSION

3.1 Annual profiles of precipitation and spectral indexes

We describe the annual evolution of the NDVI, NDWI, SANI and precipitation during 2002 for annual grasslands located in the foothills of the Sierra Nevada Range and summer irrigated crops located in the San Joaquin Valley. To assess the functioning of the indexes we also explore typical spectral profiles from the annual grassland site.

3.1.1 Annual Grasslands

In annual grasslands at this latitude (37 N) with a Mediterranean climate, maximum moisture and photosynthetic activity happen during fall, winter and beginning of spring due to precipitation patterns. The grasslands become dry by mid-spring and by late spring soils become the dominant spectral component of the pixel until the following fall. Figures 2 a, b, c, and d, show the evolution of the spectral profiles from January to December 2002. The asterisks in the index values indicate a significant change from the previous date. The reflectance profiles show a transition from full green cover in January to bare soil in September. In January the spectral shape corresponds to fully green vegetation so NDVI is high (0.77) and NDWI is low but positive (0.05). The NIR reflectance is much larger than SWIR2 and therefore SANI is highly negative (-0.7). By mid-April the spectral profile approaches the typical NPV shape. The decrease in moisture is captured by NDWI, which becomes negative (-0.07) but is even more evident in SANI which increases to -0.02. On the other hand NDVI decreases only slightly (0.65). In contrast, during the rest of April there is a significant decrease in NDVI, while NDWI and SANI barely change. It appears that the drop in moisture is reflected by the rapid change of NDWI and SANI early in the month and the corresponding gradual decrease in green vegetation is evident by the lagged decrease of NDVI. By the beginning of June, the spectral profile is typical of dry soil; NDVI has decreased at a constant rate while SANI has increased significantly, becoming positive. This sign change indicates that the surface residue component is decreasing and soils represent the largest fraction of the pixel. Throughout the summer, reflectance profiles have the typical shape of dry soil, with

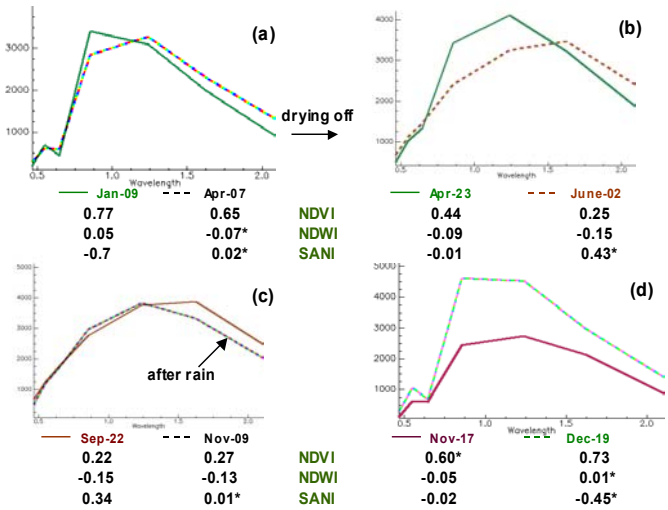

Figure 2. Spectral Profiles at different times of the year for the grassland pixel in the Sierra Nevada foothills. **(a)** January and April, **(b)** April and June, **(c)** September and November and **(d)** November and December.

low NDVI and NDWI and high SANI. By mid-November, after the first week of rains, SANI has decreased markedly due to soil moisture but NDVI and NDWI do not change significantly until late in November when vegetation starts growing due to the available moisture. There is a sharp increase in NDVI (0.33) and SANI becomes negative due to the presence of green vegetation. By mid-December, the pixel is again dominated by green vegetation, NDWI becomes slightly positive (0.01), NDVI increases to 0. 73, and SANI decreases to -0.45.

Figure 3 shows the annual evolution of the indices and precipitation for this site. The letters on the graph indicate the spectral profile of dates shown in figures 2.a, b, c, and d. NDVI has continuous high values during fall, winter and early spring and low values in summer. NDWI shows the same trend as NDVI, but with the inflection points happening earlier in spring (March) and later in autumn (October), so that it has a longer period of low values. Also, at the inflection points this index changes sign, so that a threshold at zero could be used as an indicator of the beginning of the dry season. SANI is highly negative during the growing period and highly positive during summer due to the dominance of dry soil. It fluctuates more than NDVI and NDWI during the whole year especially in winter due to its higher dynamic range and its quick response to soil moisture, so that declines in index values are coupled to rain events. At the end of the wet period there is a three week plateau with near zero values due the presence of NPV which is consistently observed in all grassland pixels.

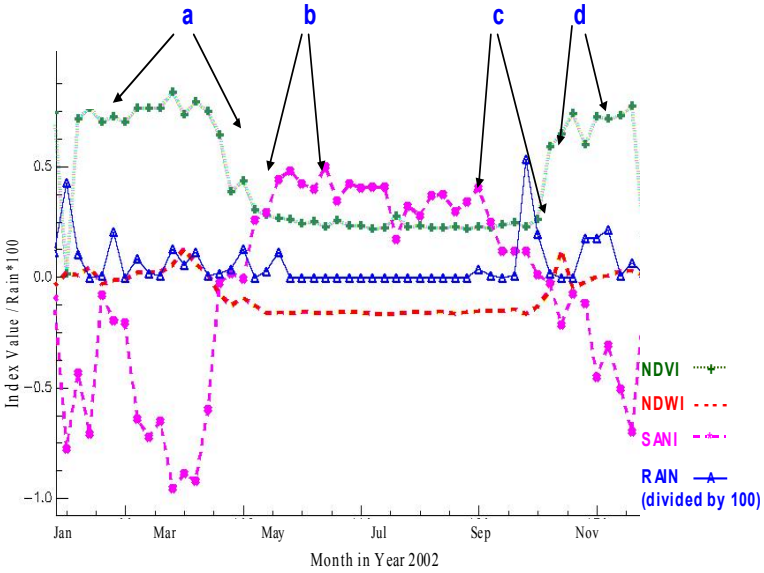

Figure 3. Annual Profile of NDVI, NDWI, SANI and precipitation in the year 2002 for Annual Grasslands.

3.1.2 Summer-Irrigated Cropland

For the summer irrigated crops (figure 4) the indexes follow opposite trends. The cropping practices define the temporal evolution, so that phenological periods are distinct. Irrigation provides enough moisture throughout the year that water is not limiting. During summer there is full vegetation cover, while in winter soil is the main component, except for some greenness due to weeds. There are two distinct short periods, one in spring when green cover is incomplete and one at the end of summer when NPV is present before harvesting. As expected, NDVI is

highest during the growing season and lowest but still positive during winter. NDWI is negative except for a short period in the middle of the growing season (56 days). SANI has the highest dynamic range being negative during summer (i.e., active crop growth) and positive during winter when soil is bare or has minor weed cover. From the end of January to June, NDVI and NDWI are nearly constant while SANI is more variable due to varying soil moisture. SANI decreases sharply in May, which is the beginning of the crop irrigation. Both NDVI and SANI rapidly change at the beginning of the growing season. These indexes reach maximum and minimum values respectively in mid-July.

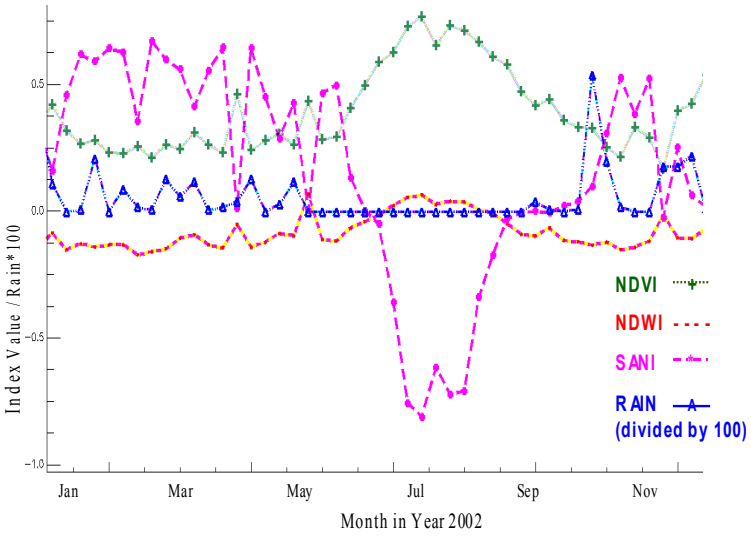

Figure 4. Annual Profile of NDVI, NDWI, SANI and precipitation in the year 2002 for Summer-Irrigated Cropland.

NDVI and SANI change at the end of the growing season at a slower rate than at the beginning. While at the beginning of the growing period, green cover is growing over bare soil, at the end, green cover is changing to NPV. NDVI keeps decreasing monotonically until November but SANI shows an inflection point in mid-September forming a plateau with near zero values until the end of the month. These low SANI values can be due to either moist soil or presence of NPV. Since this is cropland, we can assume that at the end of the growing season, these values indicate NPV, not high moisture content. This plateau lasts while the dry crop canopy stays on the field. NDWI on the other hand reaches negative values 21 days before SANI when the crop starts to dry out. This indicates that NDWI can be a good indicator of mild desiccation, signifying the early stages of the dry season.

3.2 Time Series Analysis for the 5-year period

To analyze the dynamic relationships among indexes and climatic variables we applied TSA to data from February 2000 to July 2005. Figures 5 and 8 show the time series of precipitation, solar radiation, NDVI and SANI for the annual grasslands and the summer-irrigated crop, respectively.

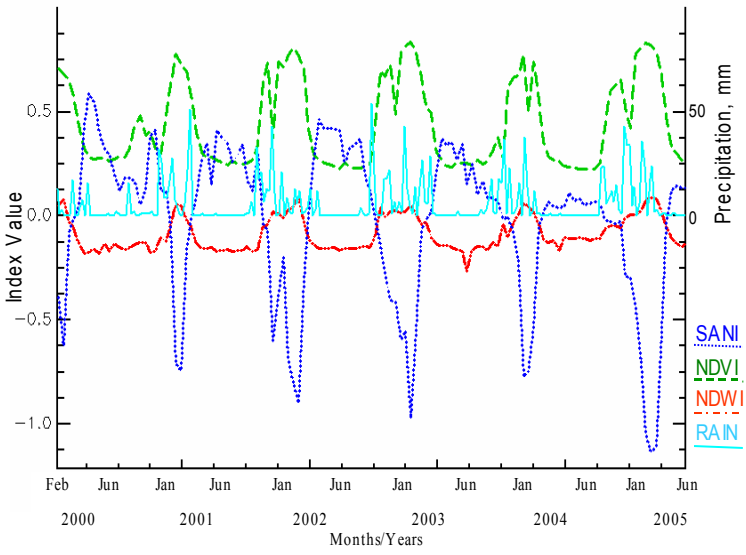

Figure 5. Five year time series of precipitation, NDVI, NDWI and SANI for annual grasslands.

3.2.1 Annual Grasslands

A Fourier Spectral Analysis was performed on both indexes at the two study sites**.** Figure 6a shows the periodogram for NDVI and SANI in the annual grasslands. Time series of both indexes exhibit a highly significant and dominant peak at period 49.4 (fundamental frequency). This period corresponds, in terms of Fourier frequencies, to the annual cycle of 46 8-day periods. The SANI periodogram shows significantly higher values than NDVI in all frequencies, and especially in the fundamental frequency. This indicates that the sum of squares explained by the SANI model in terms of the variance (13.18) is higher than that explained by NDVI (2.44). The first difference periodograms suggest the same result.

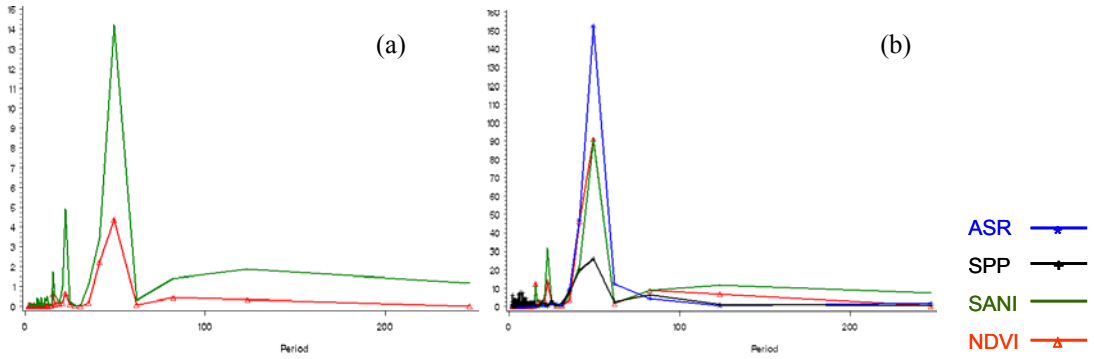

Figure 6. (a) Periodograms for NDVI and SANI five-year time series and (b) Periodograms for standardized values of time series of SPP, NDVI, NDWI and SANI.

In annual grasslands, SANI reaches its minimum value at the Fourier period 27.44 and begins its increasing trend in the next period 30.88, while NDVI reaches its minimum value at Fourier period 30.88 and begins its increasing trend with a lag at period 35.29. The SANI trend precedes NDVI, which is verified by the analysis of first differences of both series. Comparison of periodograms obtained from standardized values of NDVI, SANI, annual solar radiation (ASR) and cumulative precipitation (SPP) as shown in Figure 6b, reveals that the increasing trend for SANI and SPP begins at period 30.88 while for NDVI and ASR that trend begins at period 35.29. Thus SANI closely follows precipitation while NDVI closely follows the dominant annual cycle. Ecologically, by the end of the dry summer, the grasslands are almost bare soil. The first rains bring moisture to the soil, which are tracked efficiently and immediately by SANI. The moisture initiates vegetation growth, which is followed by slowly increasing NDVI. Thus it is observed that NDVI and ASR are simultaneous and lag behind SPP and SANI.

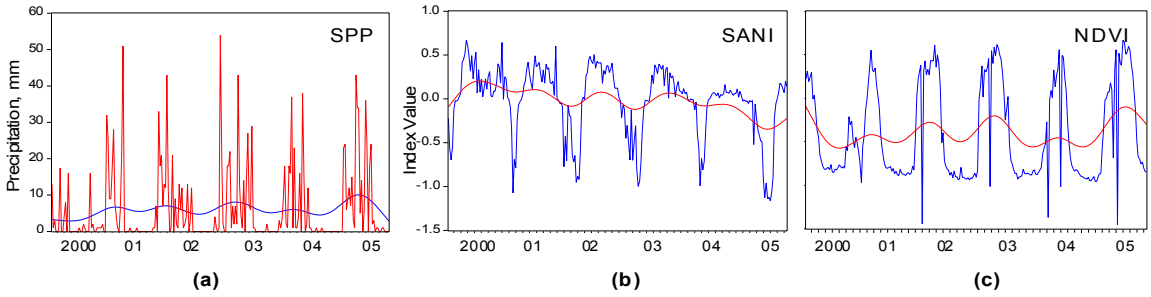

Figure 7. Hodrick-Prescott trends overlaid on the five-year time series of (a) precipitation, (b) SANI and (c) NDVI.

Periodograms of SANI, NDVI, ASR and SPP (levels and standardized values) also suggest the presence of long-term trends, particularly in SANI. A stationarity test [15] (Table 2) was applied to investigate the presence of a stochastic trend (unit root) in the time series. The test rejected the presence of a stochastic trend in NDVI (-4.192 < -3.459) but could not reject it for SANI (-0.586 > -2.576). The estimated coefficients of the test indicate a negative stochastic trend in SANI, which is also observed in its time series plot (figure 7b). As precipitation increases, soil and vegetation moisture increases leading to a decrease in SANI. Thus a trend in increasing precipitation from 2001 to 2005 (figure 7a) will manifest itself as a decreasing trend in SANI. This is the pattern observed (figure 7b). However, no such trend is evident for NDVI as shown in figures 7c. The trend line is overlaid on the time series after applying an adaptation of the Hodrick-Prescott filter [16].

3.2.2 Summer-Irrigated Cropland

Figure 9a shows the periodograms for NDVI and SANI in the irrigated summer crop. General trends are similar to those found in grasslands but some significant differences occur in the dynamics of SANI and NDVI. The periodograms of the standardized values of ASR, SPP, NDVI and SANI (Figure 9b), indicate that the last three variables essentially follow the dominant annual cycle. However, SPP, NDVI and SANI begin the increasing trend at the same Fourier period (30.88). This fact seems to indicate that precipitation influences the start of the cycles in both indexes. Since in irrigated croplands (especially summer crops) water is not a limiting factor both SANI and NDVI are simultaneous (Figure 9b).

Table 1. Augmented Dickey-Fuller (*ADF*) test values for three spectral indices measured in two California sites with the null hypothesis (H_0): the variable has a unit root. k is the number of lags included in the test regression. The AIC2 rule was used to choose the optimal lag length for all tests [17]. Number of observations, N=247.

Site	NDVI	k	SANI	k
Annual Grassland	-4.192*	9	-0.586	45
Irrigated Summer Crop	-4.548*	8	-5.792*	33

* Reject H_0 at the 1% critical value.

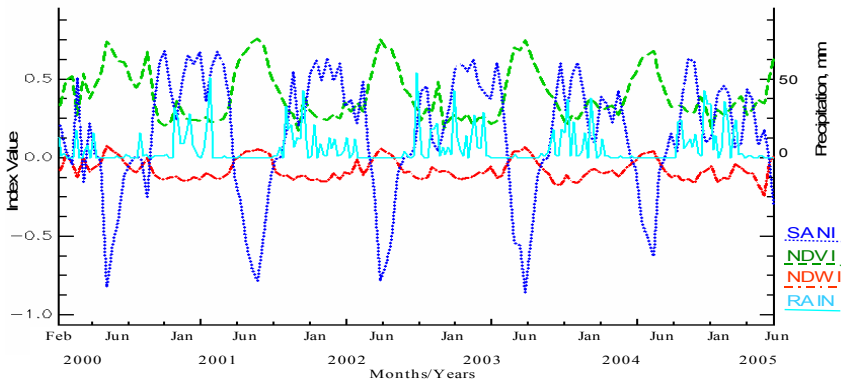

Figure 8. Five year time series of precipitation, NDVI, NDWI and SANI for summer-irrigated cropland.

Periodograms of SANI, NDVI, ASR and SPP (levels and standardized values) suggest the lack of long-term trends in these series (figures 9 a and b). The Dickey-Fuller test rejects the presence of stochastic trends in both indexes (for NDVI the test value was -4.548<-3.459 and for SANI the test value was -5.792<-3.462, Table 1) and confirms the previous result. As NDVI and SANI both are largely independent of precipitation in summer-irrigated crops, it is expected that the long-term trend of increasing precipitation will not manifest itself in either time-series index. Thus the rejection of trends, especially in the SANI time series only strengthens the argument that SANI is a good indicator of moisture evolution patterns for different land-cover types. The temporal evolution of three indexes has been analyzed from both the spectral perspective and with TSA. Results show that although the main temporal evolution of these indexes follow similar patterns they show differences that provide useful information about ecological functioning and potential for discrimination. The dynamic relationships of these indexes with climatologic time series, as well as variability among them, have been evaluated. SANI is demonstrated to be a good indicator of NPV and soil. It has been shown to be a better indicator of moisture than photosynthetic activity. Its major drawback is that it can confuse wet soil and NPV, which can affect the estimate of soil cover in certain periods of the year. Nonetheless, if the type of vegetation is known (e.g. cropland, grassland, etc.), the temporal context be used to improve discrimination between these two elements.

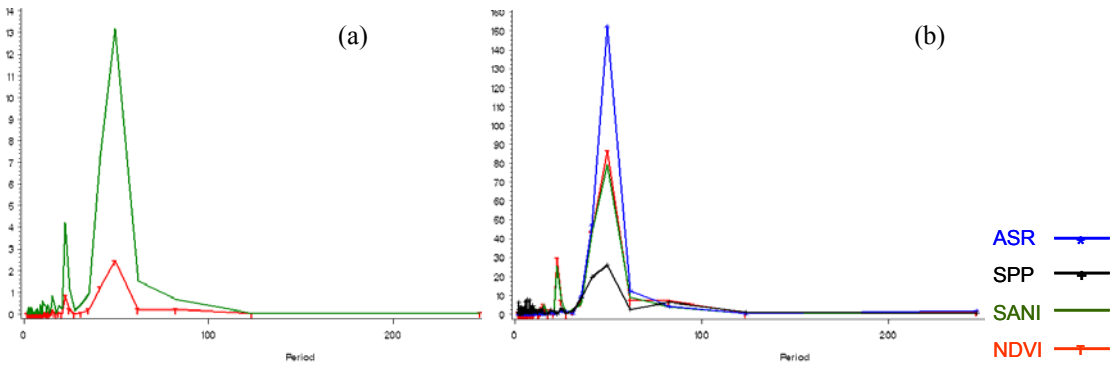

Figure 9. (a) Periodogram for NDVI and SANI five-year time series and (b) Periodograms for standardized values of time series of SPP, NDVI, NDWI and SANI.

4 CONCLUSIONS

While these are preliminary results we observe that SANI is the more sensitive at tracking moisture. This index shows a temporal profile distinct from the other indexes, having higher dynamic range and quicker response time to precipitation. In addition, SANI shows good potential for deriving clear thresholds that discriminate land cover classes. It seems to be a good indicator of NPV and soil. TSA like Fourier spectral analysis and trend detection are proven to be powerful tools for uncovering subtle variations and analyzing dynamic relationships. Future research will explore validating the new index as an indicator of moisture in soils and vegetation.

ACKNOWLEDGEMENTS

This study was funded by the NASA Modis project, "Modis Global Estimate of Canopy Water Content", Grant No. NNG04GQ42G. We are grateful to George J. Scheer and Lawrence Ross for their IT and data management support.

REFERENCES

[1] BRADLEY, B.A. AND MUSTARD, J.F., 2005: Identifying land cover variability distinct from land cover change: Cheatgrass in the Great Basin. *Remote Sens. Environ. 94*, pp. 204-213.
[2] HUETE, A.R., LIU, H.Q. ET AL., 1997: A comparison of vegetation indices global set of TM images for EOS-MODIS. *Remote Sens. Environ. 59(3)*, p. 440-451.
[3] DEFRIES, R.S., TOWNSHEND, J.R.G. AND HANSEN, M.C., 1999: Continuous fields of vegetation characteristics at the global scale at 1 – km resolution. *J. Geophys. Res. 104(D14)*, p. 16911-16923.
[4] BARET, F. AND GUYOT, G., 1991: Potentials and limits of vegetation indices for LAI and APAR assessment. *Remote Sens. Environ. 35*, p. 161-173.
[5] FENSHOLT, R. AND SANDHOLT, I., 2003:Derivation of a shortwave infrared water stress index from MODIS near- and shortwave infrared data in a semiarid environment. *Remote Sens. Environ. 87*, p. 111-121.
[6] BIARD, F., BANNARI, A. AND BONN, F., 1995: SACRI (Soil Adjusted Corn Residue Index): un indice utilisant le proche et le moyen infrarouge pour la detection des residue de culture de mais. Proceedings of the 17th Canadian Symposium on Remote Sensing, Saskatoon, Canada, p. 413-419.
[7] ANAYAMBA, A. AND TUCKER, C.J., 2005: Analysis of Sahelian vegetation dynamics using NOAA-AVHRR NDVI data from 1981–2003. *J. Arid Environ. 63*, p. 596-614.
[8] HUETE, A., DIDAN, K., MIURA, T., RODRIGUEZ, E.P., GAO, X. AND FERREIRA, L.G., 2002: Overview of the radiometric and biophysical performance of the MODIS vegetation indices. *Remote Sens. Env. 83*, p. 195-213.
[9] CUOMO, V., LANFREDI, M. ET AL., 2001: Detection of interannual variation of vegetation in middle and southern Italy during 1985-1999 with 1 km NOAA AVHRR NDVI data. *J. Geophys. Res. - Atmospheres 106(D16)*, p. 17863-17876.
[10] BENEDETTI, R. AND ROSSINI, P., 1993: On the Use of NDVI Profiles as a Tool for Agricultural Statistics: The case study of Wheat Yield Estimate and Forecast in Emilia Romagna. *Remote Sens. Environ. 45*, p. 311-326.
[11] RUNTUNUWU, E. AND KONDOH, A., 2001: Length of the growth period derived from remote sensed and climate data for different vegetation types in Monsoon Asia. *Indones. J. Agric. Sci. 1*, p. 1-4.
[12] PIWOWAR, J.M. AND LEDREW, E.F., 2002: ARMA time series analysis modelling of remote sensing imagery: a new approach for climate change studies. *Int. J. Remote Sens. 23(24)*, p. 5225-5248.
[13] WHITING, M., LI, L. ET AL., 2004: Correcting soil spectra for moisture: I. modeling moisture content. *Remote Sens. Environ. 89*, p. 535-552.
[14] PRIESTLEY, M.B., 1981: Spectral Analysis and Time Series. Academic Press, London.
[15] DICKEY, D.A. AND FULLER, W.A., 1979: Distribution of the estimators for Autoregressive Time Series with a unit root. *J. Am. Stat. Assoc. 74*, p. 427-431.
[16] HODRICK, R.J. AND PRESCOTT, E.C., 1997: Postwar U.S. Business Cycles: An Empirical Investigation. *J. Money Credit Banking. 29*, p. 1-16.
[17] PANTULA, S.G., GONZALEZ-FARIAS, G. AND FULLER, W.A., 1994: A comparison of Unit-Root Test Criteria. *J. Business Econ. Stat. 12*, p. 449-459.

Environmental change monitoring applying satellite and airborne remote sensing data in the Taita Hills, Kenya

P.K.E. Pellikka[a], B.J.F. Clark[a], T. Sirviö[a] and K. Masalin[a]

[a] Department of Geography, University of Helsinki, P.O. Box 64, 00014 Helsinki, Finland, petri.pellikka@helsinki.fi

ABSTRACT

This paper presents environmental change monitoring in the Taita Hills, Kenya applying SPOT XS satellite imagery, aerial photography and digital camera data. The paper presents the data, methods for atmospheric correction, and results from land cover change detection and soil erosion change detection. The results indicated that gully density has doubled in the test sites during the observation period since 1955 and the area of Mwatate reservoir has decreased 25% due to siltation. SPOT satellite image analysis indicates that erosion areas have increased 33% (10 km^2) and built-up areas, indicating urban growth, have doubled between 1987 and 2002. The area of coniferous plantation forests has increased 32%, while the area of broad-leaved forest types (indigenous and plantation) has decreased 3% (1.6 km^2). Based on the results, the gully erosion and land degradation is an on-going process in the area, while forest cover does not show such a dramatic trend.

Keywords: land use change, soil erosion, satellite and airborne remote sensing

1 INTRODUCTION

Climate changes and population growth cause increasing pressure on the East African highlands. The results of the pressure are manifold: urban growth, intensified agriculture, decrease of forested areas, loss of biodiversity, accelerated land degradation and soil erosion. The consequences introduce great demands on land use planning. Remote sensing data and techniques, and geographic information systems (GIS), provide efficient methods for analysis of land use and tools for modelling and planning. By understanding the driving forces of land use development in the past, managing the current situation with modern GIS tools, and modelling the future, we are able to develop plans for multiple uses of natural resources and nature conservation.

The Taita Hills in SE-Kenya is one of the risk areas in East Africa. Many research groups have been studying the biodiversity and population dynamics [1] as well as urban growth in the area [2]. The TAITA project, entitled *Development of land use change detection methodology applying geographic information systems in East African highlands,* aims to develop a practical land use change detection methodology and to create a geographic database for the land use and its changes in the area. The aim of this multidisciplinary project is divided into four sub-objectives: studies in land use change, urban growth, spatio-temporal changes in land degradation, and development of the management systems for naturally protected forests. The aim of this paper is to present the preprocessing of the satellite imagery, land cover change detection methods and results, and preliminary results of the gully erosion studies. The data and results from the project are available for regional decision-makers in the Taita Taveta district in Kenya.

2 STUDY AREA

The Taita Hills (Latitude 3°25´, longitude 38°20´) cover an area of 1000 km^2 and are surrounded by both western and eastern sections of Tsavo National Park (figure 1). While the surrounding dry savannah grassland is at an elevation of 700 m, the average height of Taita Hills is 1500 m, the highest peak, Vuria, being at 2208 meters (figure 2). The annual rainfall varies from 500 mm in the plains to 1500 mm in the hills and there are two rainy seasons: the long rains in March-May/June and the short rains in October-December. Variability of precipitation from year to year is high, especially in lower altitudes. A great number of ecological regions are based mainly on the relief and climatic conditions in the area.

Being part of the Eastern Arc, the Taita Hills are very valuable and rich in biodiversity and have many endemic mammal, bird, and butterfly species. The hills were once covered with cloud forest, but after 1960s the forests have suffered substantial loss and degradation. To date, less than 400 ha of original forest is retained in a scatter of three larger remnants, Chawia (50 ha), Ngangao (92 ha) and Mbololo (220 ha), and nine tiny remnants embedded in a

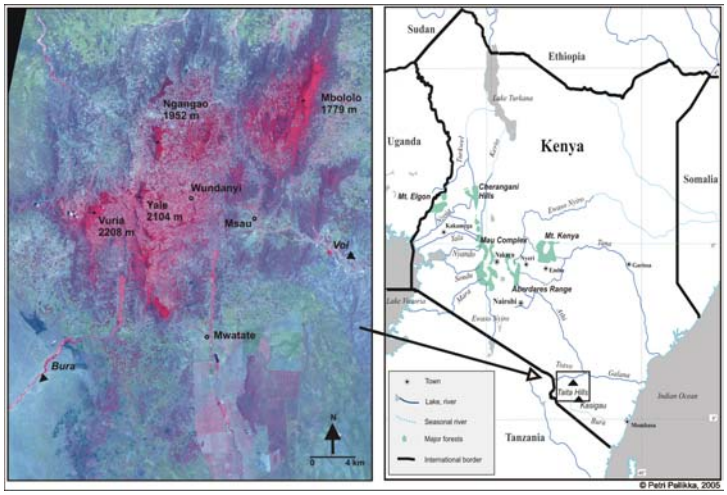

Figure 1. Taita Hills in Kenya. SPOT XS satellite image in false colour composition, Oct. 15, 2003 presents the area under investigation.

Figure 2. Taita Hills rise from the plains at 700-1000 m to 2208 m a.s.l. (Photo: P. Pellikka, 2004).

mosaic of human settlements, small-holder cultivation plots and exotic plantations. The characteristic tree species in the indigenous forests are *Magaranga conglomerata*, *Ochna holstii* and *Newtonia buchannii* and various *Acasia* species in the lowlands. The population of the whole Taita-Taveta district has grown from 90 146 (1962) persons to slightly over 300,000, of which 42,000 are residing in urban areas. The spatial distribution of population in the area closely follows climatic and other ecological conditions.

Land use in the Taita Hills is dominated by intensive agriculture, the typical crops being maize, peas, sugar canes, beans, tomatoes and banana in the highlands. Extensive agriculture with sorghum and millet cultivation and grazing are dominant land use types on the foothills and plains. The scarcity of arable land has forced the local communities to take more land under agriculture, which has caused dynamic changes in land use patterns and has led to serious land degradation (e.g. deforestation & soil erosion). Due to poor agricultural management, erodible soils and the large relative height differences of the hills, the foothills especially are subject to land degradation and accelerated soil erosion.

3 DATA

3.1 Cartographic Data

Nine 1:50 000 scale Survey of Kenya topographic paper map sheets were digitally scanned and utilized in the generation of a GIS database, including layers such as a road network, hydrography and administrative borders. The digital elevation model (DEM), used for the topographic correction and orthorectification of the satellite imagery, was generated from the scanned maps. The 50-feet interval contour lines were captured automatically from the nine map sheet areas and merged together in ArcGIS. Utilising the TOPOGRID function in ArcINFO workstation, a 20-metre planimetric resolution raster DEM for the Taita Hills study area was interpolated. As a final stage in the DEM preparation, the attribute values were converted from feet to metres to ensure compatibility with other metric measurements. The outcome of this process was a raster DEM in a UTM Zone 37 projection with a Clarke 1880 Spheroid, a planimetric accuracy of +/- 50 meters and an altimetric accuracy of 8 metres [3]. Raster models of slope and aspect were derived from the 20-metre DEM utilising ERDAS IMAGINE.

3.2 Remote Sensing Data

SPOT XS satellite imagery from 1987, 1992, 1999, 2002 and 2003 form the main data for land use change detection (table 1). The data have a 20-metre spatial resolution and are orthorectified, calibrated, and corrected for topographic effects [4, 5]. Also, black and white aerial photography from 1955, 1986 and 1993 has been scanned

Table 1. SPOT satellite data in the TAITA project. θ_{VA} = Sensor Azimuth Angle, θ_{ZA} = Solar Azimuth Angle, θ_V = Sensor View Angle (+/- 27° for SPOT), θ_Z = Solar Zenith Angle.

Date	Image	Sensor	Bands	θ_V	θ_{VA}	θ_Z	θ_{ZA}
July 1, 1987	143-357	SPOT 1 HRV 1	Green, Red, NIR	R 10.3°	98.91°	36.35°	41.37 °
Mar. 25, 1992	142-357	SPOT 2, HRV 1	Green, Red, NIR	R 13.8°	98.9°	26.5°	79.0°
Mar. 25, 1992	143-357	SPOT 2, HRV 2	Green, Red, NIR	R 9.3°	98.9°	26.0°	78.7°
Feb. 12, 1999	143-357	SPOT 4, HRVIR 2	Green, Red, NIR, MIR	L 4.2°	278.7°	27.7°	113.7 °
June 6, 2002	142-357	SPOT 4, HRVIR 1	Green, Red, NIR	L 20.2°	278.6°	32.4°	36.9°
Oct. 15, 2003	143-357	SPOT 4, HRVIR1	Green, Red, NIR, MIR	R 10.4°	98.8°	21.0°	104.3 °

and orthorectified using an elevation model generated as part of the correction process (table 2). The ground resolution varies between approximately 0.14 and 0.46 m depending on the flight altitude above ground, photo scale and scan resolution. New airborne digital camera data were acquired in March 2003 and January 2004 using a true-colour NIKON D1X digital camera. The digital camera data were used in EnsoMOSAIC software to construct digital image mosaics over several study sites [6, 7].

In this study, the land use change between 1987 and 2002 was analyzed in an area of 1000 km^2 covering the hills and the sisal plantations in the south. The soil erosion was studied in the south-western foothills in the communities of Msau and Mwatate using airborne remote sensing data from 1955, 1986, 1993, 2003 and 2004. The areas studied are depicted in figure 1.

Table 2. Characteristics of the airborne remote sensing data.

Sensor	Photogrammetric Camera	Photogrammetric Camera Leica RC10	Photogrammetric Camera Leica RC10	Small Format Digital Camera NIKON D1X
Year	1955	1986	1993	2003, 2004
Date	Jan.- Feb.	Feb.		March 23-25, 03 Jan. 25-28, 04
Mode	Black & white	Black & white	Black & white	Blue, Green, Red
Camera focal length	152.3 mm	151.68 mm	151.21 mm	14 mm
Scale/ ground resolution	~1:30000	~1:10000	~1:10000	~0.26-0.64 m
Scan resolution	14 µm	21 µm	21 µm	
Ground resolution	~ 0.46 m	~ 0.21 m	~ 0.21 m	

4 METHODS

4.1 Preprocessing of SPOT Imagery

4.1.1 Topographic normalization and orthorectification

Topographic normalization is used for correcting the so called slope and aspect effect. Given a uniform land cover, the brightness values in the remote sensing data are higher on sun-exposed slopes than on the slopes oriented away from the sun since they receive more direct solar radiation. Although the effect is not so serious with the small solar zenith angles in the tropics, it causes misclassification and hampers multi-temporal analysis and has to be corrected. In the several correction methods developed [5], slope and aspect models derived from the DEM are used in the normalization. In this study, the C-factor correction is used [8]. Orthorectification is also necessary for precise registration of the satellite imagery with a national or international coordinate system.

4.1.2 Atmospheric correction applying the Historical Empirical Line Method (HELM)

Accurate land-use classification and change detection in a set of multi-temporal SPOT XS data is dependent on the ability to successfully relate differences in corrected radiance or reflectance measurements to actual changes in

vegetative state or land-cover on the ground. Consequently, the initial processing stage was to make the imagery spatially and spectrally comparable. It was also necessary to retrieve surface reflectance (P_s) from the imagery and therefore an *absolute* radiometric calibration, as opposed to a relative normalization, was required. However, no detailed overpass concurrent atmospheric measures were available for the TAITA project SPOT data. The Historical Empirical Line Method (HELM) was developed to account for these circumstances and limitations.

The basic premise behind HELM is that the reflectance properties of a spatially extensive, spectrally bright and invariant-in-time calibration ground target can be measured in the field, using a spectrometer, and utilized in conjunction with image derived dark object radiance values to calibrate the at-sensor radiance (L_{SAT}) at the various image dates to a stable surface reflectance (P_s). Where the calibration targets are spectrally pseudo-invariant over time, the measurement of P_s need not coincide with the image data acquisition [9]. To account for the variable off-nadir view angle of the SPOT sensors it is necessary to capture the Bidirectional Reflectance Distribution Function (BRDF) of the calibration site. The main assumptions of HELM are that the atmosphere is approximately homogenous throughout the image area and that there is a linear relationship between L_{SAT} and P_s. Although this relationship is quadratic for the full range of reflectance (0-100%), it is sufficiently linear over the range 0-70% to allow linear interpolation with negligible error (all P_s for the Taita Hills were less than 70%).

Because of this near-linear relationship, the empirical line correction can be implemented utilizing a standard linear regression equation in the form $\boldsymbol{y = ax + b}$; where $\boldsymbol{a}$ is the slope of the regression line, representing the atmospheric attenuation, and $\boldsymbol{b}$ is the intercept with the x-axis, representing the atmospheric path radiance. A separate correction is derived for each spectral band in the data (figure 3). For HELM it is argued that an accurate estimation of the correction line can be obtained using detailed field measurements of only *one* appropriate within-scene "bright" calibration target, and image based measures of radiance for an assumed 1% reflectance "dark" target. Field measurements at further ground sites are recommended, however, for verification and accuracy assessment purposes. The objective of HELM is, therefore, to (re)construct the historical linear relationship between L_{SAT}, as recorded by the multi-temporal satellite imagery, and P_s for the Pseudo-invariant Pixels (PIPs), as measured in the field.

The main difficulty with applying HELM to SPOT data is to identify calibration targets that are large enough to counter the contaminating effects of the point spread function on the instantaneous field of view of the sensor. The calibration and validation targets need to be at least three times the pixel size (60 x 60m for 20m resolution SPOT 1-4 XS data) to derive "true" L_{SAT} pixel values [10]. For the TAITA project, a roadside quarry was chosen as the main bright calibration target and half-day long measurements were made in an attempt to measure changes in P_s with $\boldsymbol{\theta_z}$ and $\boldsymbol{\theta_v}$ (+/- 27° for SPOT) [11]. In the event, it was found that the noise level of the handheld spectrometer measurements exceeded the signal of variation in P_s with $\boldsymbol{\theta_z}$ and $\boldsymbol{\theta_v}$, so it was not possible to quantify these relationships. However, it can be inferred from this that these variations must be relatively small and therefore that the calibration target exhibited near-Lambertian reflectance behaviour. It was thus considered that the average nadir reflectance characteristics of the target had been accurately captured and that the SPOT imagery with varying $\boldsymbol{\theta_v}$ could be normalized to this data with minimal error, given the measurement noise (coefficient of variation 12.7%).

The spectrometer derived P_s data were processed to synthesis the SPOT response for the PIPs at each date based on the specific spectral sensitivities of each band (obtained from the SPOT website) for the SPOT sensor involved. The L_{SAT} values for the darkest in-scene object and the bright calibration site were determined for each spectral band from the SPOT images and regressed to the synthesized P_s to derive a correction equation which was then applied to the whole scene (figure 3). The HELM technique has been successfully applied to the TAITA project multi-temporal SPOT XS dataset and, as is shown in table 3, it gives more accurate results than using either simple image based correction methods (DOS and COST), 6S with generalized atmospheric parameters, or no correction at all (uncorrected top-of-atmosphere reflectance - P_{TOA}). The main disadvantage of applying HELM was that the SWIR band available for the 1999 and 2003 images had to be left out of correction, as the spectrometer used for the field measurements only covered the 0.325 to 1.075 μm (VIS/NIR) range.

4.3. Land Cover Change Detection

4.3.1 Classification method

The land cover classification methodology utilized for the SPOT data was a stepwise process combining both unsupervised ISODATA and supervised maximum-likelihood classification stages within ERDAS IMAGINE. In the first step, the 2002 image was classified into 100 clusters using the ISODATA algorithm. Then, in conjunction with GPS referenced land cover field data from the Taita Hills, four spectral clusters best representing each of the desired output land cover classes were identified and written to a signature file. This signature file was then used as the basis for a supervised maximum-likelihood (re-)classification of the image. As a final stage, the related spectral

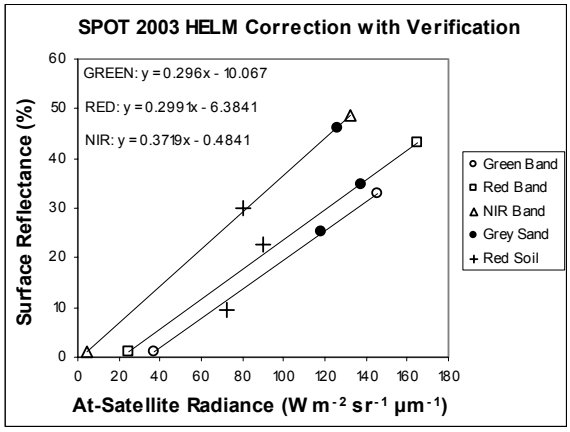

Figure 3. 2003 SPOT-4 Image HELM correction.

Table 3. Average RMSE % P_s for all field sites, all bands and all dates.

Method	Accuracy
P_{TOA}	8.05%
DOS	10.18%
COST 1	7.99%
COST 2	9.10%
6S	7.01%
HELM	1.80%

clusters (such as agriculture-1, agriculture-2, agriculture-3, and agriculture-4) were grouped and merged to give the finalized 8 land cover classes, as listed below. Subsequent to the classification of the 2002 image, the edited signature file was then applied directly to the 1987 scene as well to derive a maximum-likelihood classification, followed by the same spectral class grouping and merging process to give the finalized 8 land cover classes. Given the image-to-image orthorectification and radiometric calibration pre-processing steps, this enabled direct comparisons for the same land cover classes to be made between the 1987 and 2002 SPOT images.

Additionally, it should be noted that the sisal plantations located on the plains to the south of the Taita Hills were masked out from the rest of the image area and classified separately, because of the similar spectral characteristics they shared with rest of the land cover. The classes identified within the sisal plantations were water, agriculture, young sisal, middle-aged sisal, mature sisal, erosion areas, thicket, grasslands and bushlands. The sisal plantations covered 108.3 km^2 and the rest of the area 905.8 km^2.

The rest of the image area, including the Taita Hills and lowlands, was classified into 8 classes: forest, coniferous forest, agriculture, erosion areas, barren land and built-up areas, thicket, bushlands and grasslands. The forest class includes indigenous closed canopy forests and other dense broad-leaved forests, which are mainly exotic eucalyptus and grevillea forests. In addition, riverine forests with typical species *Acacia xanthophylla*, *A. eliator* and *Newtonia hilbrandtii*, belong to the forest class. Coniferous forests are pine (mostly *Pinus patula*) and cypress (*Cypressus lusitanica*) plantations. The differences in grasslands, bushlands and thickets are caused by tree height and density. The same species can be found in each of these three classes, but the characteristic tree and shrub species in the bushlands typically belong to *Acasia* ssp., *Grewia* ssp. and *Commiphora* ssp., and the tree species in the thickets typically belong to *Euphorbia* ssp. and *Commiphora* ssp. The grasslands are normally 20 to 50 cm high and their spectral characteristics vary strongly according to precipitation.

4.3.2 Results

The land cover changes within the sisal plantation express mainly management changes of the plantation and phenological differences. Some aspects, however, are interesting from the land management and land degradation point of view. Based on personal communication with the plantation owner the whole area of the world's largest plantation is 9800 ha [12]. Based on the classification, 6 985 ha was under sisal management in 1987 and 5 913 ha in 2002 showing a decrease of 15%. The area of grasslands has increased 134% from 1987 to 2002, and erosion areas 121%, while agricultural areas other than sisal plantations decreased 75% and area of Mwatate reservoir 37%. The changes in areas for the sisal plantations indicate the management practices and rotation cycle of the sisal plant. The area of the reservoir fluctuates strongly according to yearly rainfall and the use of water upstream from the reservoir. Overall, the reservoir has been shrinking steadily year by year. The changes in percentages and absolute areas are shown in table 4.

The land cover changes in the rest of the image area show that the agricultural area has decreased by 35%, while coniferous forests have increased by 32%, thickets by 35%, grasslands by 31%, erosion areas by 33% and built-up areas and barren land by 171%. Broad-leaved closed canopy forests have decreased by only 3% during the observation period of 15 years. The growth in area of coniferous forests evidently relates to maturing of the trees and therefore strengthening of the reflectance signal from the trees. The changes in percentages and absolute areas are shown in table 5 and the classification in figure 4. From table 5 it can be seen that the decrease in agricultural land is strong, from 29 359 ha to 19 019 ha, while thickets have been expanding from 15 724 ha to 21 170 ha and grasslands from 17 241 ha to 22 536 ha. The reasons for the strong decrease in agricultural fields might lie partly in

the phenology of agricultural plants and natural vegetation. The large agricultural areas in the south and south-west of the 1987 image (figure 4) may have been misclassified as agriculture instead of grasslands. Since there is no field data from 1987 this cannot be ascertained conclusively. In addition, the small fields and mixed crop systems cause a lot of mixed pixels and the growth cycle of various crops affects the reflectance. The expansion of grasslands from 1987 to 2002 may be explained by this misclassification in the 1987 scene.

Table 4. The area (ha), percentage and change of land cover types within sisal plantations.

Year/Class	Water	Agriculture	Sisal mature	Sisal young	Sisal middle-aged	Thicket	Grass-land	Bush-land	Erosion areas	Total
1987 ha	28	133	3314	1721	1950	1631	410	1171	473	10831
1987 %	0.3	1.2	30.6	15.9	18	15.1	3.8	10.8	4.4	100.1
2002 ha	18	33	1701	1904	2308	1206	959	1660	1044	10833
2002 %	0.2	0.3	15.7	17.6	21.3	11.1	8.9	15.3	9.6	100
1987-2002 %	-37	-75	-49	11	18	-26	134	42	121	

Table 5. The area, percentage and change of land cover types in the Taita Hills and lowlands.

Year/Class	Coniferous forest	Forest	Agriculture	Thicket	Grass-land	Bush-land	Erosion areas	Barren & built-up area	Total
1987 ha	988	4815	29359	15724	17241	19196	3178	75	90576
1987 %	1.1	5.3	32.4	17.4	19.0	21.2	3.5	0.1	100
2002 ha	1301	4655	19019	21179	22536	17456	4228	202	90576
2002 %	1.4	5.1	21.0	23.4	24.9	19.3	4.7	0.2	100
1987-2002 %	32	-3	-35	35	31	-9	33	171	

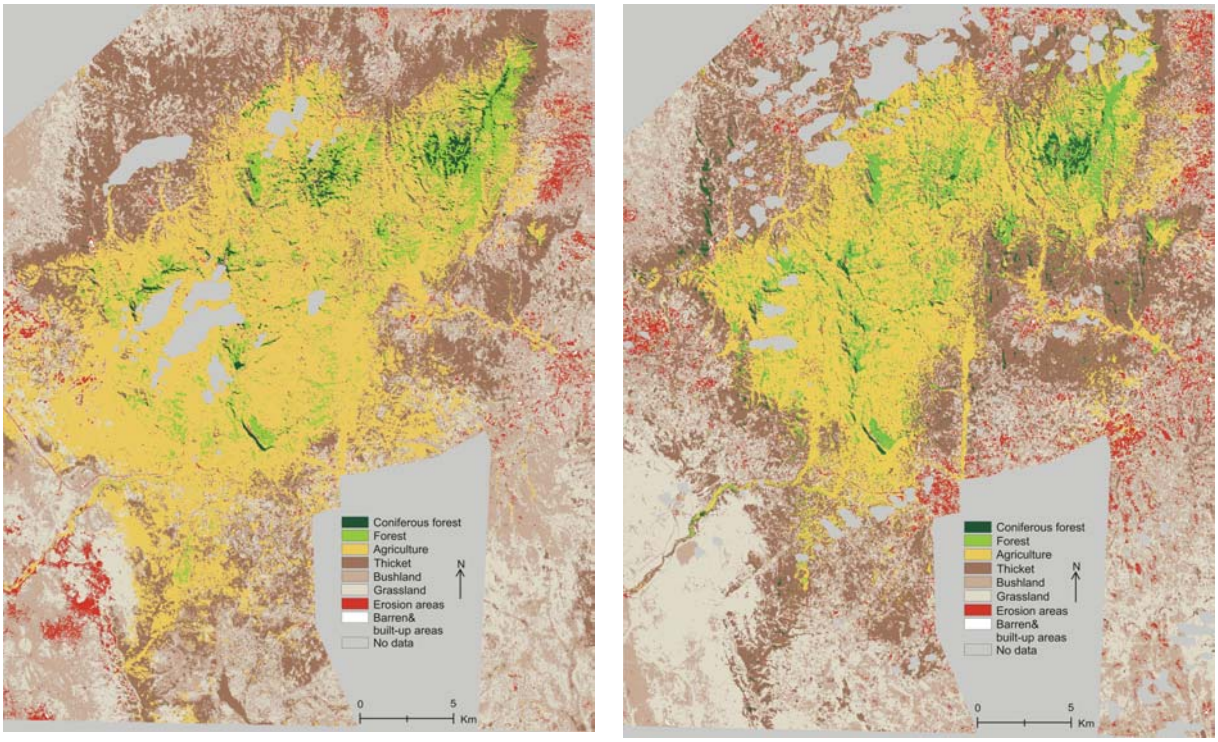

Figure 4. Land use in the Taita Hills in 1987 (left) and 2002 (right). The area of sisal plantation is masked by legend.

4.4 Gully Erosion Changes between 1955-2004

4.4.1 Introduction

Gullies (figure 5) are "relatively permanent steep-sided watercourses, which experience ephemeral flows during rainstorms" [13]. Gullies normally have a distinctive propagating head [14], which extends upslope due to three main processes: 1) slumping, 2) piping or tunnelling and 3) incision of rills due to excessive overland flow. Gully erosion is a very serious form of water erosion causing severe on-site effects, such as damage to the productive land (e.g. agriculture, forests, grazing land) and constructed sites (e.g. roads and bridges). Off-site effects of gully erosion consist of siltation of rivers and reservoirs and damage to the local soil-water balance (e.g. lowering of ground water table) [15].

Figure 5. Gully erosion site in Mwatate (Photo: T. Sirviö, 2004).

Land degradation and gullying are caused by vegetation loss, inadequate land management and non-sustainable land use. During recent years gully erosion has been studied within a wide range of environments [16, 17, 18]. According to these studies, the contribution of gully erosion on water erosion varies significantly between 10-94%, ranging from 0.1-64.9 tons $ha^{-1}y^{-1}$ [15].

Gully erosion is studied in two different locations within the Taita Hills foothills; in Mwatate and Msau (figure 1). Land use types within these areas typically range from squatter homesteads to abandoned sisal plantations, and from cultivated fields to overgrazed degraded forests. Except for 1) detection of gully erosion changes and rates within the Taita Hills between 1955-2004, the general objectives of the gully erosion studies within the area include 2) determination of the main factors affecting gully growth in the area [19, 20, 21] and development of the GIS-based methodologies for erosion hazard assessments.

4.4.2 Methods

All the airborne remote sensing data over the gully study sites were processed into projected and seamless ortho-rectified mosaics representing the study areas, utilizing bilinear interpolation and histogram matching techniques. The final mosaic is geometrically and spectrally accurate due to the application of a camera calibration model, and an ortho-correction process including corrections for light falloff and for bi-directional effects conducted for each individual image in the mosaic [3]. The resolution of the final mosaics was set to 0.3 m. The high resolution (1 m) DEM was produced from the digital aerial images based on air GPS –coordinates and elevation values calculated for each tie point used in image rectification and block adjustment. The DEMs are corrected by filling the sinks with *fill* –function (ArcGIS® 9.0) to derive hydrologically sound DEMs [22].

All the gullies in the study areas are identified and digitized using the digital or scanned aerial images and subjected to manual stereoscopic investigation. Single gullies and their branches with IDs and gully length (meters) form a basis for the GIS gully database. Gully densities (m/ha) are calculated with basic GIS-tools using one-hectare-grid with IDs as a reference (figure 6). Finally, gully densities within each year and within the grid cells are compared to each other showing the density changes during the last 50 years.

4.4.3 Preliminary Results

Gully erosion density has increased remarkably in the Taita Hills from 60.6 m/ha to 126.9 m/ha during the last fifty years (1955-2004) and the highest densities are found in the middle parts of the Mwatate study area (figure 6). Density changes and accelerated erosion in the area are related to the increased population density, and especially construction and poor management of land. At the same time the total length of the gullies in the area has grown from 55.62 to 110.29 km. The average length of the gullies has remained almost at the same level (slight increase from 97.9 to 99.0 meters), but the total number of gullies has increased from 568 to 1 114. Figure 7 shows rapid gully head propagation in Mwatate triggered by a road cutting. Accelerated erosion is also revealed by the rapid siltation of the reservoir (figure 6), the size of which has decreased from 25.84 to 20.27 ha during the last 50 years.

5 DISCUSSION

The processing chain developed for the SPOT data included orthorectification, HELM atmospheric correction, and topographic normalization applying C-correction factors. While the orthorectification and topographic corrections

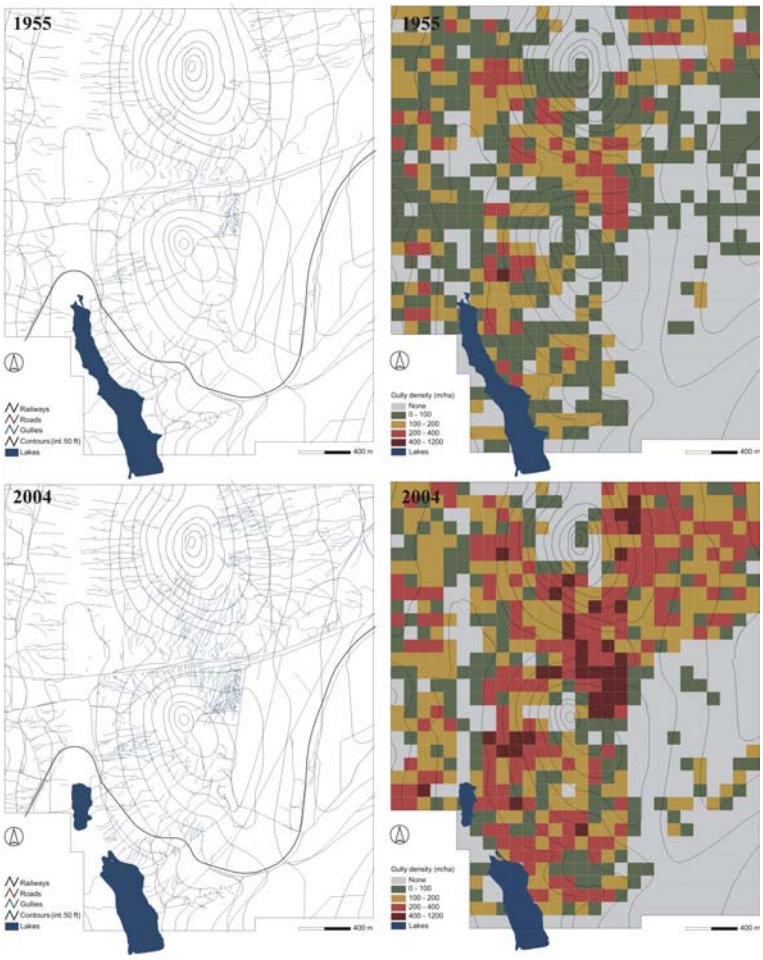

Figure 6. Gully extension (left) and gully density maps (m/ha) (right) within Mwatate study area between 1955 and 2004.

are "off-the-shelf" techniques, the HELM is a first of a kind developed for SPOT XS data. It proved to be most suitable for SPOT data where no detailed overpass concurrent atmospheric measurements are available for absolute radiometric correction. In order to further validate HELM and to provide quantified BRDF measurements for a main calibration ground target, further research has been carried out in the Helsinki metropolitan area. With the assistance of the Finnish Geodetic Institute, BRDF measurements have been made at a large car park using a goniometer, and additional verification points have been taken using a handheld ASD spectrometer. Multi-temporal SPOT imagery and detailed atmospheric data will be acquired for the Helsinki metropolitan area and an in-depth accuracy assessment and comparison of HELM will be undertaken.

The land cover change in the area showed only a small decrease of 1.6 km^2 in forest cover in the Taita Hills. This represents a 3% loss, which is much less than that presented by Ward et al. in 2004, who used Landsat TM data from 1987 and 1999 and calculated a 37% loss of closed canopy forest in the same study area [23]. The main reason for this big difference is that the TM data were not atmospherically or topographically calibrated and the data were from different seasons. The SPOT data utilized in this study are from July (1987) and June (2002), both acquired during dry seasons, but recently after long rains. The growth in area of coniferous forests evidently relates to maturing of the trees and therefore strengthening of the reflectance signal from coniferous tree species, like pine and cypress. Although the data was carefully pre-processed for this study, the classification still includes misclassifications caused by phenological differences of natural and agricultural plants. This is the case especially with grasslands and agriculture and this misclassification is very difficult to avoid.

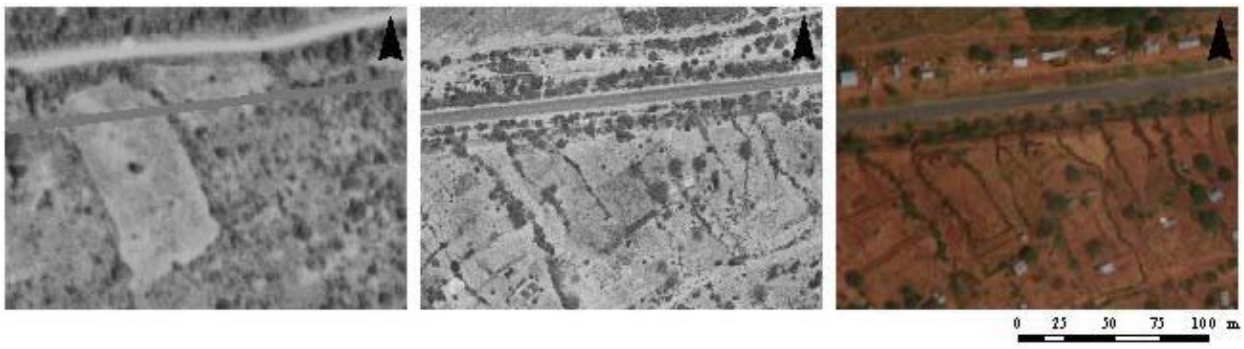

Figure 7. Rapid gully headcut propagation in Mwatate, as shown in aerial photographs in 1955 (left), 1993 (centre) and 2004 (right).

The change detection also indicates a small increase of erosion areas and built-up areas and a decrease of water surface. The decrease in water surface seems to be taken place during the last 15 years. Within the sisal plantations the study revealed an increase of bushlands, grasslands and soil erosion areas and less land under sisal management.

The gully erosion studies expressed significant land degradation in the area. Extremely high densities of gullies in the area are related to the poor soil conservation practices and ill-managed construction. Rapid degradation of the landscape is shown by both the large increase in number and total length of the gullies in the area during the last fifty years.

ACKNOWLEDGMENTS

The study is funded by the Academy of Finland, Council for Development Studies and the University of Helsinki. The local cooperation partners University of Nairobi, Department of Geography, World Agroforestry Centre (ICRAF) and East African Wildlife Society are acknowledged for the field work assistance and cooperation. The Ministry of Education of the Republic of Kenya and the Taita Taveta District Office are acknowledged for the research permit and local assistance. Mr. Christopher Cheseny from Voi helped us with the plant identification. Dr. Petri Pellikka is the principal investigator of the TAITA project. Mr. Barnaby Clark has been responsible for the data preprocessing, Ms. Katja Masalin for the land use classification and Mr. Tommi Sirviö for the land degradation studies.

REFERENCES

[1] LENS, L., DONGEN, S. V., NORRIS, K., GITHIRU, M. AND MATTHYSEN, E., 2002: Avian persistence in fragmented rainforest. *Science 298*, pp. 1236-1238.

[2] HURSKAINEN, P., 2005: *Change Detection of Informal Settlements Using Multi-Temporal Aerial Photographs – the Case of Voi, Kenya*. Unpublished M.Sc. thesis. University of Helsinki. 124 p. + 8 app.

[3] PELLIKKA, P., CLARK, B., HURSKAINEN, P., KESKINEN, A., LANNE, M., MASALIN, K., NYMAN-GHEZELBASH, P. AND SIRVIÖ, T., 2004: Land use change monitoring applying Geographic Information Systems in the Taita Hills, SE-Kenya. *Proc. 5th AARSE conference*, 18-21 October, 2004, Nairobi, Kenya. CD-publication, no page numbers.

[4] PELLIKKA, P., 1998: Development of correction chain for multispectral airborne video camera data for natural resource assessment. *Fennia 176(1)*, pp. 1-110.

[5] SANDMEIER, S. AND ITTEN, K.I., 1997: A physically-based model to correct atmospheric and illumination effects in optical satellite data of rugged terrain. *IEEE Transactions on Geoscience ad Remote Sensing 35*, pp. 708-717.

[6] HOLM, M., LOHI, A., RANTASUO, M., VÄÄTÄINEN, S., HÖYHTYÄ, T., PUUMALAINEN, J., SARKEALA, J. AND SEDANO, F., 1999: Creation of large mosaics of airborne digital camera imagery. *Proceedings of the 4th Airborne Remote Sensing Conference and Exhibition*, 21-24 June 1999, Ottawa, Canada.

[7] HURSKAINEN, P. AND PELLIKKA, P., 2004: Change detection of informal settlements using multi-temporal aerial photographs – the case of Voi, SE-Kenya. *Proc. 5th AARSE conference.*, 18-21 October, 2004, Nairobi, Kenya. CD-Publication, no page numbers

[8] TEILLET, P.M., GUINDON, B. AND GOODENOUGH, D.G., 1982: On the slope-aspect correction of multispectral scanner data. *Canadian Journal of Remote Sensing 8*, 84-106.

[9] SMITH, G.M. AND MILTON, E.J., 1999: The use of the empirical line method to calibrate remotely sensed data. *International Journal of Remote Sensing 24(5)*, pp. 1143-1150.

[10] KARPOUZLI, E. AND MALTHUS, T., 2003: The empirical line method for the atmospheric correction of IKONOS imagery. *International Journal of Remote Sensing 20(13)*, pp. 2653-2662.

[11] MORAN, M.S., BRYANT, R., THOME, K., NI, W., NOUVELLON, Y., GONZALES-DUGO, M.P., OI, J. AND CLARKE, T.R., 2001: A refined empirical line approach for reflectance retrieval from Landsat-5 and Landsat-7 ETM+. *Remote Sensing of Environment 78*, pp. 71-82.

[12] PELLIKKA, P.K.E., 2005: *Taita Journal, January 19 – February 2, 2005*. Unpublished.

[13] MORGAN, R.P.C., 1995: *Soil Erosion and Conservation*. Longman Group Ltd., Essex, England

[14] REBEIRO-HARGRAVE, A., 2000: *Large Scale Modelling of Drainage Network Evolution in a Tectonically Active Environment*. Ph.D. Thesis. University of London. 323 pp.

[15] POESEN, J., NACHTERGAELE, J., VERSTRAETEN, G. AND VALENTIN, C., 2003: Gully erosion and environmental change: importance and research needs. *Catena 50*, pp. 91-133.

[16] VANDEKERCKHOEVE, L., POESEN, J., OOSTWOUD WIJDENES, D., GYSSELS, G., BEUSELINCK, L. AND DE LUNA, E., 2000: Characteristics and controlling factors of bank gullies in two semi-arid Mediterranean environments. *Geomorphology 33*, pp. 37-58.

[17] MORGAN, R.P.C. AND MNGOMEZULU, D., 2003: Threshold conditions for initiation of valley-side gullies in the Middle Veld of Swaziland. *Catena 50*, pp. 401-414.
[18] VANVALLEGHEM, T, VAN DEN EECKHAUT, M., POESEN, J., DECKERS, J., NACHTERGAELE, J., VAN OOST, K. AND SLENTERS, C., 2003: Characteristics and controlling factors of old gullies under forest in a temperate humid climate: a case study from the Meerdaal Forest (Central Belgium). *Geomorphology 56*, pp. 15-29.
[19] SIRVIÖ, T., REBEIRO-HARGRAVE, A. AND PELLIKKA, P., 2004: Geoinformation in gully erosion studies in the Taita Hills, SE-Kenya, preliminary results. *Proceedings of the 5th AARSE conference*, 18-21 October, 2004, Nairobi, Kenya. CD-publication, no page numbers.
[20] SIRVIÖ, T. AND REBEIRO-HARGRAVE, A., 2004: Hazardous foothills – An overview of gully erosion within the Taita Hills. *In*: Pellikka, P., J. Ylhäisi & B. Clark (eds.): *Taita Hills and Kenya, 2004*. Expedition Reports of Department of Geography, University of Helsinki 40, Department of Geography, University of Helsinki, pp. 79-86.
[21] SIRVIÖ, T., REBEIRO-HARGRAVE, A., PELLIKKA, P. AND SHEPHERD, K.: Controlling factors of gully erosion with special reference to the land use and soil spectral properties, the Taita Hills, South-eastern Kenya. Unpublished manuscript.
[22] TARBOTON, D.G., BRAS, R.L. AND RODRIGUEZ-ITURBE, I., 1991: On the Extraction of Channel Networks from Digital Elevation Data. *Hydrological Processes 5*, pp. 81-101.
[23] WARD, J., DULL, C., HERTEL, G., MWANGI, J., MADOFFE, S. AND DOUCE, K., 2004: Monitoring for Sustainable Forestry and Biodiversity in the Eastern Arc Mountains of Tanzania and Kenya. *The International Archives of Photogrammetry, Remote Sensing and Spatial Information Sciences, Vol.34, Part XXX*. ALSO: USDA Forest Service, 1999, Monitoring Changes in Forest Condition, Land Fragmentation and Conversion: Eastern Arc Mountains of Tanzania and Kenya http://www.easternarc.org/landchange/arcfinal1100_files/frame.htm *cited in SOINI, E., 2005. Livelihoods, capital, strategies and outcomes in the Taita hills of Kenya. Unpublished project report, 34 p.*

Land-cover change and vegetation dynamics across Africa and Europe

P. Rowhani[a], M. Linderman[b], D. Benz[a], S. Serneels[a] and E.F. Lambin[a]

[a] University of Louvain, Department of Geography, Place Pasteur 3, Louvain-la-Neuve, Belgium, email: rowhani@geog.ucl.ac.be
[b] University of Iowa, Department of Geography

ABSTRACT

While previous studies have examined broad-scale trends in phenology or provided more detailed estimates of land-cover conversion, less is known of the year-to-year dynamics of vegetation. Significant shifts in the timing and overall vegetation activity have considerable implications for a variety of processes including vegetation/climate interactions, hydrology, ecological systems, and food security. Using improved metrics, as developed by [1], and recently available MODerate resolution Imaging Spectrometer (MODIS) data, we examined the magnitude, extent, and nature of changes in photosynthetic activity and its timing across the European and African continent. This approach to study the dynamics of terrestrial ecosystems has the potential to provide one step in the development of practical applications of land-cover change analyses.

In this paper we quantified the overall changes in vegetation activity for each year between 2000 and 2005 and examined the proportion linked to differences in phenology and overall photosynthetic activity. In addition, we examined the nature of these changes in terms of frequency and duration and identified areas of intensive change. "Hotspots" of interannual change were defined as areas which underwent extreme change. Categorizing the direction and the duration of change between years identifies temporal patterns and measures land degradation processes and ecosystem response to perturbations.

Keywords: Land-cover change, Interannual change, Modis.

1 INTRODUCTION

The planet's land surface has been altered in many ways, either by converting natural landscapes for human use or by changes in land-cover with a natural cause. As shown in several studies, these transformations affect in various ways different environmental issues such as local, regional and global climate change, implications in the carbon and hydrological cycles, loss of biodiversity, food security of societies using these ecosystems [2][3][4][5][6][7]. Changes in surface attributes are the result of the combination of different processes occurring at a continuum of temporal and spatial scales [8][9]. Thus, knowledge in the magnitude, distribution and processes of changes in landcover across spatial and temporal scales is needed to better understand the interactions and potential impacts that changes in the characteristics of the terrestrial surface may have.

Remote sensing data has been widely used in the past to measure the extent and effects of land-cover change [10][11][12][13]. But previous datasets have limited our ability to perform detailed analyses of inter-annual change. The disadvantage of fine resolution data is obviously its inability to provide high temporal resolution which results in a focus on long-term conversions from one land-cover category to another. At a regional to global scale, the most widely used satellite sensor with high temporal resolution, NOAA's Advanced Very High Resolution Radiometer (AVHRR), is known to have some issues as well. Widely reported georeferencing, sensor calibration and satellite-orbit drift problems limited the utility of early datasets [14][15][16][17]. Improvements and corrections in the processing were made to overcome these problems and the new, more consistent datasets [18][19] have allowed essential regional to global analyses of inter-annual to long term vegetation trends [20][3][21][22]. Nevertheless, some inherent sensor and data constraints continue to limit the utility of these datasets.

The current MODerate resolution Imaging Spectrometer (MODIS) sensors aboard the Terra and Aqua platforms provide data with improved radiometric and geolocation accuracy well suited for detailed regional to global studies of land-cover change [23]. A recent study used 1-km spatial resolution MODIS data to monitor the response of vegetation phenology to seasonal variation in rainfall across Africa [24]. The same data was used in another study to establish improved indices of interannual change and measure year-to-year changes in seasonality and overall vegetation activity across Sub-Saharan Africa from 2000 to 2004 [1]. We present here the application of these new indices and methodologies adapted to a slightly longer time series and to all of the African and European

continents. These new tools allow to determine the magnitude of the overall change in landcover as well as the proportion due to differences in phenology compared to differences in annual photosynthetic activity. The distribution of all these changes are also analysed across different ecosystems. The resilience and the long-lasting effects

2 METHODOLOGY

2.1 Data

The data used for this study, MODIS collection 4 Nadir Bi-directionally Adjusted Reflectance (NBAR) visible bands (MODIS product MOD43B4) from February 2000 to March 2005, provide significant improvements for vegetation dynamics and land cover change monitoring relative to AVHRR data. As Ref. 25 suggest, using satellite data to monitor changes in the terrestrial surface requires that the repeated measures precisely reflect the surface conditions. For example, measuring temporal trends or changes requires that the measurements be taken repeatedly of the same area. Average geolocation errors for AVHRR data are typically greater than 1 pixel (> 1000 m). The geolocation error for 1-km MODIS products is estimated to be less than 50 m [26]. This allows precise resampling of the same areas and reduces contamination of adjacent pixels. In addition, the spectral characteristics and preprocessing are significant improvements over previous sensors.

The MODIS sensor contains 36 bands distributed from the visible to the thermal spectral wavelengths. Using this array of information, atmospheric properties can be collected real-time and allow enhanced atmospheric corrections [27]. The Bidirectional Distribution Reflectance Function (BRDF) modeling developed by Ref. 28 uses 16 atmospherically and georeferenced daily images to estimate nadir reflectance values for that period, hence removing directional effects from the composited images. Finally, the spectral characteristics of MODIS were specifically designed to improve upon previous sensors and provide increased sensitivity for vegetation monitoring.

The NBAR values were used to derive corresponding Enhanced Vegetation Index (EVI) values for each 16 day period. EVI is a spectral index similar to the widely-used Normalized Difference Vegetation Index (NDVI). Like NDVI, EVI has been shown to be sensitive to vegetation characteristics. However, where NDVI is more linked with chlorophyll activity, EVI was designed to be responsive to variations in Leaf Area Index (LAI), canopy type, canopy structural, plant physiognomy [29]. EVI was specifically designed to reduce atmospheric and soil contamination. In a comparison, done by Ref. 1, a strong linear relationship was found between EVI and NDVI. They also found that the soil background for NDVI was 70% higher and had twice the standard deviation of the EVI data. In addition, in comparisons across a range of vegetation types and densities, EVI has been shown to saturate at higher LAIs allowing more accurate change detection in high density vegetation [23].

2.2 Preprocessing

Preprocessing of the MODIS data included mosaicking, interpolating clouded pixels and obvious noise, and masking unsuitable data. The individual tiles of spectral bands and quality flags were mosaicked and georeferenced using IDL ENVI software. The mosaicked bands were converted to EVI values:

$$\mathrm{EVI} = \mathrm{G}\frac{\rho_{\mathrm{nir}} - \rho_{\mathrm{red}}}{\rho_{\mathrm{nir}} + \mathrm{C}_1 \times \rho_{\mathrm{red}} - \mathrm{C}_2 \times \rho_{\mathrm{blue}} + \mathrm{L}} \tag{1}$$

Here, G is the gain factor of 2.5, pnir, pblue, and pred are the near infrared, blue, and red band surface reflectances, respectively, C1 are C2 are aerosol correction factors of 6.0 and 7.5, respectively, and L is the canopy background adjustment factor of 1.0 [23].

Clouded pixels and uncertain pixels were determined based on the provided cloud mask and BRDF inversion quality flags. These dates were interpolated using a quadratic interpolation of the previous two and following two suitable pixels. A mask of anomalous one-period noise spikes was developed from the difference between the raw data and the median of five periods. Only the most obvious values (<0.1% of the values) were flagged as noise (difference > 0.2 EVI) and interpolated. The combination of the cloud mask, quality flags, and noise values provided the overall status map. Any pixel where more than 3 consecutive periods between the first previous and first following non-cloud pixels and 7 periods between the second previous and the second following non-cloud pixels were interpolated was excluded from the analysis.

To account for the range of seasons as a result of latitudinal and ecosystem differences, start of the year dates were calculated across the continent. For this purpose, we calculated a median year for each pixel and the Start Of the Year (SOY) was defined as the midpoint between start of the growing season and the end of the previous

growing season of this median year. Growing season dates were calculated based on thresholds based on the senescence values and peak growing season EVI. The thresholds were set at 20% of the seasonal range above the senescence values. Four to five full growing seasons for each pixel were extracted from the full set of data.

A reference year was extracted from the three full years for each pixel. The reference year was defined as the median value of the three yearly EVI values for each period. Three years is not an optimal time period for reference year archiving. As more data become available, a more representative reference can be computed. However, as we were interested in year-to-year changes across the three years, the reference provided an adequate comparison.

2.3 Indices of change

The processed data were used to derive indices of interannual change. The basic concept of the indices is based on the temporal Change Vector (CV). The CV is the difference between two annual profile vectors, **I**, (Eq. 1) where **I** is a temporal profile of the annual vegetation index.

$$\mathbf{CV} = \mathbf{I}_2 - \mathbf{I}_1 \tag{2}$$

To summarize change, [30] calculated an index called the Change Vector Magnitude (CVM). The CVM is the Euclidean distance of the CV and offered a concise representation of total change. However, since the CVM is non-linear it is sometimes sensitive to noise and abrupt changes. Here we use two modified versions of this index to examine total change (timing and overall activity) and overall activity alone. To measure total change we calculated the Sum of the absolute values of the Change Vector (SCV).

$$\mathrm{SCV} = \sum_{i=1}^{n} \mathrm{abs}(I_2 - I_1)_i \tag{3}$$

The SCV provides a linear measure of the difference in both the magnitude and timing of vegetation activity. To measure changes in just the magnitude of vegetation activity we calculated the Difference in the Integrated Vegetation indices (DIV). DIV is given as:

$$\mathrm{DIV} = abs\left(\sum_{i=1}^{n} (I_2)_i - \sum_{i=1}^{n} (I_1)_i \right) \tag{4}$$

where *n* is the number of time steps in one year and I is the vegetation index value at each given time step. DIV does not take into account the timing of the vegetation activity and only measures the difference between years. Using the SCV and DIV, we could then estimate the amount of change due to just seasonal shifts or differences in timing of vegetation activity. Subtracting the DIV from the SCV leaves only the change due to timing differences. The difference is referred to as the SSI.

$$\mathrm{SSI} = \mathrm{SCV} - \mathrm{aDIV} \tag{5}$$

2.4 Analyses

To identify areas of change across Africa, the SCV was calculated for each of the years [1]. The portion of change for each year was calculated as the SCV divided by the integrated vegetation index of the reference year. This normalized index provided an annual relative percent change. Areas of 20%, 33% and 50% change relative to the reference year were identified. The total area of change over all three years was calculated as those pixels undergoing change during at least one of the three years. The total change irrespective of the direction of change was measured to examine the overall change occurring. Directional change, increases or decreases of the various indices, was calculated to examine the temporal and spatial aggregation of these changes. Continental statistics were derived for all areas. To partition the total change according to differences in timing (e.g. seasonal differences) and vegetation activity, the relative change in the DIV and SSI were used. The percent change of the DIV relative to the reference gave an indication of the change in amount of vegetation activity. The relative percent change of the SSI, on the other hand only reflected changes due to timing of the vegetation activity.

The distribution of these changes relative to broad ecotypes was examined. The relationship between the changes and the vegetation types where they occur was examined by extracting statistics for continent-wide ecotypes. The MODIS land-cover product, which include the 17 land-cover classes following the International

Geosphere-Biosphere Programme (IGBP), was used to examine this distribution of. Six major ecotypes were derived from this dataset. Closed and open shrubland were joined into one general shrubland ecotype. The savanna ecotype included the savannas, the woody savannas and the grasslands. Desert and sparsely vegetated areas made up the desert ecotype. The crop ecotype is comprised of the croplands and the cropland/natural vegetation mosaic. We separated the forests into two categories. The needle-leaf included evergreen and deciduous needle-leaf forests as well as the mixed forest. Broad-leaf was made of evergreen and deciduous broad-leaf forests.

To test the ephemeral nature of change, two decision tree analyses were used to classify the direction and duration of change. Both analyses were based on the evolution of the integrated vegetation index over the four to five years. First, in the case of a five year pixel, we compared the averaged value of the first three and the last three years (if only four years were available, the average of the first two years and the last two years was taken). Six different categories were defined: an increase or decrease by five to 10%, an increase or decrease by ten to 20% and an increase or decrease by more than 20%. The second decision tree was used to classify more extreme situations. Only four different classes were defined in this case: pixels which have a yearly variation of less than 4% in integrated EVI were defined as constant, those that remain constant but experience one abrupt drop or rise of integrated EVI by more than 15% were regrouped in another class and finally, the pixels which experienced an increase or decrease of more than 4% a year, each year were also joined into one class.

3 RESULTS

This methodology was applied on two different continents, Africa and Europe. To quantify the area of change, the normalized change per pixel was categorized by 20, 33 and 50% change of the integrated EVI of the reference year. Table 1 shows the results of the these categories for the three indices. We can see the yearly evolution of these indices and compare them from continent to continent

Table 1. Percent of vegetated pixels with changes greater than 0.20, 0.33 and 0.50 relative to the integrated EVI (iEVI) of the reference year.

	EUROPE					AFRICA			
	2000/1	2001/2	2002/3	2003/4		2000/1	2001/2	2002/3	2003/4
	%SCV					%SCV			
20%	14.00	21.56	20.34	24.01	20%	2.87	3.44	5.08	4.32
33%	4.62	7.23	7.51	8.25	33%	0.34	0.37	0.45	0.41
50%	1.84	2.68	2.68	2.81	50%	0.06	0.06	0.05	0.06
	%DIV					%DIV			
20%	5.70	7.90	8.20	12.99	20%	1.50	1.26	3.72	2.43
33%	1.86	2.28	2.57	3.68	33%	0.21	0.20	0.33	0..27
50%	0.78	0.79	0.82	0.69	50%	0.03	0.03	0.02	0.04
	%SSI					%SSI			
20%	3.64	6.44	5.51	4.76	20%	0.25	0.38	0.17	0.27
33%	1.03	1.97	0.61	1.71	33%	0.02	0.03	0.01	0.02
50%	0.33	0.65	0.51	0.63	50%	0.01	0.01	0.00	0.01

The European continent shows clearly a higher percent of interannual change than in Africa and this interannual change seems to increase each year. It reaches a peak value in the fourth year and over 24% of the area changes by more than 20% in SCV compared to the reference year. Focusing on more intense changes, over 8.2% of the continent changed by more than one third of the iEVI and 2.8% changed by more than half of the total photosynthetic activity of a median year during the four/five years. Looking at just the effects of phenology, we find extensive temporal variability. The %SSI values were relatively inconsistently distributed over time. They reach a peak value of over 6.4% of change greater than 20% in 2001/2 and then decrease regularly afterwards. Larger phonological changes were still quite important. Just looking at the changes in annual integrated vegetation

index (iEVI), we find that considerable portions of the continent underwent changes in iEVI each year. Regions of high change resulting from differences in iEVI were consistently more prevalent than areas affected by phenological changes

Analyzing the overall change in Africa we can see that in 2002/3, a peak value of over 5% of the continent change by more than one fifth of the iEVI of the reference year. More intense change were much less frequent than in Europe. Considering only changes in phenology we see that it is mainly the 2001/2 period that experiences the most change in %SSI. However, changes in photosynthetic activity seem to be very low that year and reach a maximum in 2002/3, with over 3.7% changing by more than 20%.

4 SUMMARY

A method to monitor land-cover change and vegetation dynamics on a regional to global scale using improved metrics and recently available MODerate resolution Imaging Spectrometer (MODIS) data is proposed. We examined the magnitude, extent, and nature of changes in photosynthetic activity and its timing across the European and African continent.

The methodologies outlined above describe a comprehensive approach to study long-term broad trends to detailed analyses of interannual differences. The approaches have the potential to provide timely and informative information on interannual change relevant to several scientific and practical areas of need. The quantification and characterization of land-cover change patterns should help develop practical applications of land-cover change outputs.

ACKNOWLEDGMENTS

This work was performed in the research program on satellite remote sensing for the Belgian Federal Science Policy Office (GLOVEG project) and the FP5's Environment and Sustainable Development Program of the European Commission (CYCLOPES project). Marc Linderman would like to gratefully acknowledge the financial support of the National Science Foundation (International Research Fellowship Post-Doctoral Program). We would also like to thank Boston University's MODIS Land Cover group for the provision of the MODIS data.

REFERENCES

[1] LINDERMAN, M, ROWHANI, P., BENZ, D., SERNEELS, S. AND LAMBIN, E.F., 2005: Land-cover change and vegetation dynamics across Africa. *Journal of Geophysical Research, 110*.

[2] CHASE, T.N., PIELKE, R.A., NEMANI, R. AND RUNNING, S.W., 1996: Sensitivity of a general circulation model to global changes in leaf area index. *Journal of Geophysical Research, 101*, pp. 7393-7408.

[3] BOUNOUA, L., COLLATZ, G.J., LOS, S.O., SELLERS, P.J., DAZLICH, D.A., TUCKER, C.J. AND RANDALL, D.A., 2000: Sensitivity of climate to changes in NDVI. *Journal of Climate, 13,* pp. 2277-2292.

[4] GALVIN, K.A., BOONE, R.B., SMITH, N.M. AND LYNN, S.J., 2001: Impacts of climate variability on East African pastoralists: linking social science and remote sensing. *Climate Research, 19*, pp. 161-172.

[5] GUILLEVIC, P., KOSTER, R.D., SUAREZ, M.J., BOUNOUA, L., COLLATZ, G.J., LOS, S.O. AND MANHANAMA, S.P.P., 2002: Influence of the inter-annual variability of vegetation on the surface energy balance - A global sensitivity study. *Journal of Hydrometeorolgy, 3*, pp. 617-629.

[6] PARMESAN, C. AND YOHE, G., 2003: A globally coherent fingerprint of climate change impacts across natural systems, *Nature, 421*, pp. 37-42.

[7] LAWRENCE, D.M. AND SLINGO, J.M., 2004: An annual cycle of vegetation in a GCM. Part II: global impacts on climate and hydrology. *Climate Dynamics, 22*, pp. 107-122.

[8] LAMBIN, E.F. AND EHRLICH, D., 1997: Land-cover changes in Sub-Saharan Africa (1982-1991): Application of a change index based on remotely sensed surface temperature and vegetation indices at a continental scale. *Remote Sensing of Environment, 61*, pp. 181-200.

[9] GEIST, H. AND LAMBIN, E., 2002: Proximate causes and underlying driving factors of tropical deforestation. *Bioscience. 52*, pp. pp. 143-150.

[10] NEMANI, R.R., RUNNING, S.W., PIELKE, R.A. AND CHASE, T.N., 1996: Global vegetation cover changes from coarse resolution satellite data. *Journal of Geophysical Research*, *101*.

[11] MYNENI, R.B., KEELING, C.D., TUCKER, C.J., ASRAR, G. AND NEMANI, R.R., 1997: Increased plant growth in the northern high latitudes from 1981 to 1991. *Nature, 386*, pp. 698-702.

[12] ZHANG, X.Y., FRIEDL, M.A., SCHAAF, C.B. AND STRAHLER, A.H., 2004: Climate controls on vegetation phenological patterns in northern mid- and high latitudes inferred from MODIS data. *Global Change Biology, 10*, pp. 1133-1145.

[13] LEPERS, E, LAMBIN, E., JANETOS, A., DEFRIES, R., ACHARD, F., RAMANKUTTY, N., AND SCHOLES, R., 2005: A synthesis of information on rapid land-cover change for the period 1981-2000. *BioScience., 55*.
[14] GUTMAN, G., 1994: Normalisation of multi-annual global AVHRR reflectance data over land surfaces to common sun-target geometry. *Advances in Space Research, 14*, pp. 121–124.
[15] VERMOTE, E. F. AND KAUFMAN, Y. J., 1995: Absolute calibration of AVHRR visible and near-infrared channels using ocean and cloud views. *International Journal of Remote Sensing, 16*, pp. 2317-2340.
[16] CIHLAR, J., LY, H., LI, Z., CHEN, J., POKRANT, H., & HUANG, F., 1997: Multitemporal, multichannel AVHRR data sets for land biosphere studies: Artifacts and corrections. *Remote Sensing of Environment, 60*, pp. 35-57.
[17] GUTMAN, G., 1999: On the use of long-term global data of land reflectances and vegetation indices derived from the Advanced Very High Resolution Radiometer. *Journal of Geophysical Research, 104*, pp. 6241-6255.
[18] JAMES, M.E. AND KALLURI, S.N.V., 1994: The Pathfinder Avhrr Land data set - An improved coarse resolution data set for terrestrial monitoring. *International Journal Of Remote Sensing, 15*, pp. 3347-3363.
[19] TUCKER, C.J., NEWCOMB, W.W. AND DREGNE, H.E., 1994: AVHRR data sets for determination of desert spatial extent. *International Journal of Remote Sensing, 15*, pp. 3547-3566.
[20] MYNENI, R.B., TUCKER, C.J., ASRAR, G. AND KEELING, C.D., 1998: Interannual variations in satellite-sensed vegetation index data from 1981 to 1991. *Journal of Geophysical Research, 103*, pp. 6145-6160.
[21] GOETZ, S.J., PRINCE, S.D., SMALL, J. AND GLEASON, A.C.R., 2000: Interannual variability of global terrestrial primary production: Results of a model driven with satellite observations. *Journal of Geophysical Research, 105*, pp. 20077-20091.
[22] ANYAMBA, A., TUCKER, C.J. AND MAHONEY, R., 2002: From El Niño to La Niña: Vegetation response pattern over East and Southern Africa during the 1997-2000 period. *Journal of Climate, 15*, pp. 3096-3103.
[23] HUETE, A., DIDAN, K., MIURA, T., RODRIGUEZ, E.P., GAO, X. AND FERREIRA, L.G., 2002: Overview of the radiometric and biophysical performance of the MODIS vegetation indices. *Remote Sensing of Environment, 83*, pp. 195-213.
[24] ZHANG, X., FRIEDL, M.A., SCHAAF, C.B. AND STRAHLER, A.H., Monitoring the response of vegetation phenology to precipitation in Africa by coupling MODIS and TRMM instruments. *Journal of Geophysical Research, 110*.
[25] CIHLAR, J., CHEN, J.M., LI, Z., HUANG, F., LATIFOVIC, R. AND DIXON, R., 1998: Can interannual land surface signal be discerned in composite AVHRR data? *Journal of Geophysical Research-Atmospheres, 103*, pp. 23163-23172.
[26] WOLFE, R.E., NISHIHAMA, M., FLEIG, A.J., KUYPER, J.A., ROY, D.P., STOREY, J.C. AND PATT, F.S., 2002: Achieving sub-pixel geolocation accuracy in support of MODIS land science. *Remote Sensing of Environment, 83*, pp. 31-49.
[27] VERMOTE, E.F., ELSALEOUS, N., JUSTICE, C.O., KAUFMAN, Y.J., PRIVETTE, J.L., REMER, L., ROGER, J.C. AND TANRE, D., 1997: Atmospheric correction of visible to middle-infrared EOS-MODIS data over land surfaces: Background, operational algorithm and validation. *Journal of Geophysical Research, 102*, pp. 17131-17141.
[28] SCHAAF, C.B., GAO, F., STRAHLER, A.H., LUCHT, W., LI, X., TSANG, T., STRUGNELL, N.C., ZHANG, X., JIN, Y., MULLER, J.-P., LEWIS, P., BARNSLEY, M., HOBSON, P., DISNEY, M., ROBERTS, G., DUNDERDALE, M., DOLL, C., D'ENTREMONT, R.P., HU, B., LIANG, S., PRIVETTE, J.L. AND ROY, D., 2002: First operational BRDF, albedo nadir reflectance products from MODIS. *Remote Sensing of Environment, 83*, pp. 135-148.
[29] GAO, X., HUETE, A.R., NI, W.G. AND MIURA, T., 2000: Optical-biophysical relationships of vegetation spectra without background contamination. *Remote Sensing of Environment, 74*, pp. 609-620.
[30] LAMBIN, E.F. AND STRAHLER, A.H., 1994: Change-vector analysis in multitemporal space - a tool to detect and categorize land-cover change processes using high temporal-resolution satellite data. *Remote Sensing of Environment, 48*, pp. 231-244.

Use of the NOAA AVHRR NDVI-Ts feature space to derive vegetation cover estimates from long term time series for determining regional vegetation trends in the Mediterranean

M. Stellmes[a], S. Sommer[b] and J. Hill[a]

[a] Remote Sensing Department, Faculty of Geography/Geosciences, University of Trier, D-54290 Trier, stellmes@uni-trier.de

[b] Institute for Environment and Sustainability, Joint Research Centre, I-21020 Ispra

ABSTRACT

The aim of this study was a comparison of NOAA AVHRR NDVI data with vegetation cover fractions derived from this SMA approach and testing their usability for vegetation change detection in the Mediterranean area. Vegetation fractions were derived for the Iberian Peninsula from the 1 km NOAA AVHRR MEDOKADS data archive covering a time period from 1989 to 2004 [1] [2]. For validation purposes NDVI-Ts derived vegetation abundance was compared with green vegetation fraction (GVF) obtained from classical spectral mixture modelling applied to the reflectance channels of Landsat TM data. Single date comparisons indicate that there is higher coherence and consistency of unmixing derived vegetation fractions of the two systems than in the comparison of normalised NDVI values alone [3]. This could open new doors for a more consistent validation of regional scale vegetation change detection by comparing the NOAA AVHRR results more systematically with the results of Landsat TM time series analysis, which are available through projects such as DeMon-II and GeoRange.

Keywords: time series, change detection, NOAA AVHRR, NDVI, vegetation fraction, SMA, Mediterranean

1 INTRODUCTION

Semi-arid areas like the Mediterranean region are sensible and vulnerable eco-regions, which are susceptible to land degradation. It is widely accepted that changes of the vegetation density over time bear important information of land degradation dynamics either caused by natural or man-made processes. For monitoring the development of vegetation cover on a regional to global scale, archives of satellite data with coarse geometric but high temporal resolution are the preferable choice. These data allow a better geographical coverage and temporal monitoring of the area of interest due to their high repetition rate than high resolution data from i.e. Landsat TM. The currently longest back-dating times series of simple bio-physical variables i.e. for NDVI and land surface temperature are provided by NOAA AVHRR sensors.

The NDVI is a commonly used indicator for monitoring the vegetation cover. Unfortunately, this index is not only determined by the vegetation cover but is also influenced by the background signal by i.e. soil and rock. Thus, soils can show NDVI values up to 0.3 [4]. Especially areas with low vegetation cover, typically the dry land regions in the Mediterranean, are affected by the limitation of detecting thin vegetation cover. Furthermore the relationship between NDVI and other measures of vegetation cover was proved to be not linear [5]. Additionally the NDVI shows sensitivity to several parameters such as the atmosphere, the illumination and the observation geometry, which is supposed to be eliminated through a temporal maximum value compositing of the data [6]. Moreover, the NDVI values are platform dependant due to different spectral properties as well as the observation geometry which complicates a direct comparison among different sensors.

Due to these problems, it is preferable to find a measure for vegetation cover which proves to be independent from external factors. In this context spectral mixture analysis (SMA) has become known as one of the most promising approaches for vegetation cover estimates [7, 8]. This method admits the derivation of vegetation cover fraction on the basis of multi-spectral image data which allow a characterisation of different surface materials. But due to the spectral limitation of the NOAA AVHRR data the classical SMA cannot be simply applied.

To overcome these limitations the potential of alternative by using mixture analysis techniques (MA) has been explored. A modified approach basing on the inverse relationship between NDVI and land surface temperature was implemented. Generally, surface temperature (Ts) is observed to be inversely proportional to the amount of vegetation canopy cover and thus to the NDVI. Due to a variety of factors including latent heat transfer through evapotranspiration, the lower heat capacity and thermal inertia of vegetation compared to soil [9, 10, 11]. Although

this relationship may be weakened under wet surface conditions [12], seasonal trajectories of both NDVI and Ts have shown to characterise land cover in a more comprehensive and climatically resistant manner than multitemporal NDVI data alone [13].

The implemented SMA technique thus acts on the assumption, that vegetation cover should predominantly control the position of an AVHRR land surface pixel within the feature space spanned up by NDVI and surface temperature. In this advanced concept, SMA is expected to improve the vegetation cover estimation in low vegetated areas because of diminishing the effect of the background signal on the NDVI.

2 BACKGROUND – SPECTRAL MIXTURE ANALYSIS

The concept of the classical linear spectral mixture analysis (SMA) is based on the assumption, that the measured surface reflectance of a pixel is equivalent to the sum of the single reflectances from a limited number of pure materials - the so-called endmembers - depending on their pixel fraction [14]. Mathematically, this assumption can be expressed as:

$$\rho_j = \sum_{i=1}^{m} F_i \cdot \rho_{i,j} + \varepsilon_j \quad , \tag{1}$$

where ρj denotes the reflectance of a pixel in band j, Fi the fraction of an endmember i of the pixel, $\rho_{i,j}$ the reflectance of endmember i in channel j and εj is the residual error in band j.

At the same time the proportions of the endmember have to fulfil the sum-to-unity constraint, which can be expressed as:

$$\sum_{i=1}^{m} F_i = 1 \tag{2}$$

If the reflectance values of the endmembers are known, their fractions can be estimated for every pixel by solving the linear system of equations.

The difficulty encountered in the application of SMA to NOAA AVHRR data is related to the limited number of reflectance channels recorded and hence, restrict the separability of different surface materials. Therefore, it seems to be preferable to implement an approach which is not depending on the surface reflectance but rather bases on the inverse relationship between the vegetation cover and the surface temperature under dry conditions. Due to factors like the latent heat transfer through evapotranspiration, the lower heat capacity and the thermal inertia of vegetation compared to soil, the surface temperature is inversely proportional to the amount of vegetation canopy [9, 11], which itself is proportional to the NDVI [15]. On small spatial scale the variations of different vegetation species and soil classes can show a high variability [10], while on coarse geometric resolution the variation in surface temperature seems to be mainly caused by vegetation fraction [12]. Thus, linear approximations to explain NDVI as well as surface temperature of mixed AVHRR pixel (vegetation and non-vegetation) in relation to vegetation have been given (figure 1).

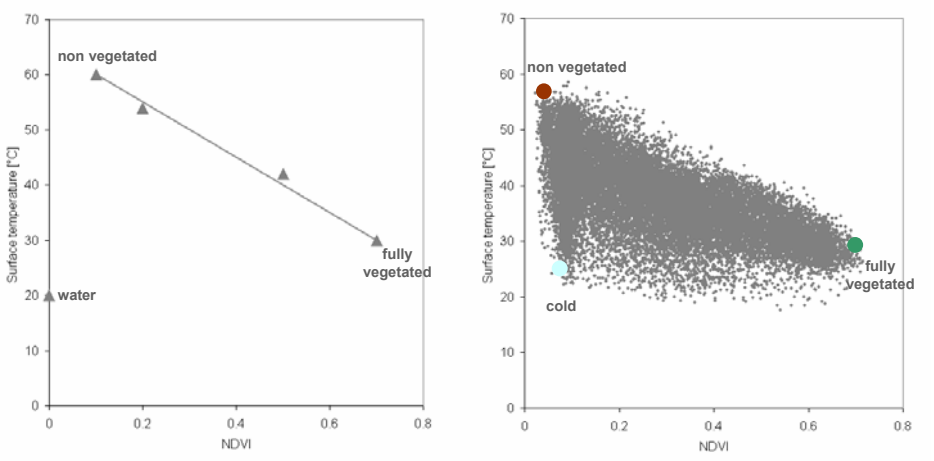

Figure 1. left: simplified illustration of the NDVI–Ts relationship [16]; right: NDVI-Ts relationship for the Iberian Peninsula derived from 1km-MEDOKADS NOAA AVHRR time series, August 1991.

Price [4] expressed the NDVI of a mixed NOAA AVHRR pixel as a function of the vegetation cover fraction as

$$NDVI_{pixel} = f \cdot NDVI_{veg} + (1-f) \cdot NDVI_{non-veg}, \quad (3)$$

where $NDVI_{pixel}$ is the NDVI of a given pixel, f is the vegetation fraction, $NDVI_{veg}$ is the NDVI value for full vegetation and NDVInon-veg is the NDVI value for a non vegetated surface.

Likewise, the relationship between vegetation cover fraction and surface temperature was stated by Caselles and Sobrino [17] as

$$T_{pixel} = f \cdot T_{veg} + (1-f) \cdot T_{non-veg} \quad (4)$$

where T_{pixel} is the surface temperature of a pixel, f is the fraction of vegetation, T_{veg} the surface temperature for full vegetation and $T_{non-veg}$ denotes the surface temperature of a non vegetated surface.

According to these relationships, the implemented spectral unmixing approach acts on the assumption that vegetation cover should predominantly control the position of an AVHRR land surface pixel within the feature space formed by NDVI and surface temperature [3], which is illustrated by figure 1.

3 METHODOLOGY

3.1 Datasets and Preprocessing

The MEDOKADS NOAA AVHRR with a geometric resolution of 1 km comprises a time period from 1989 to 2004. The archive provides the five original spectral channels, derived thematic parameters such as the NDVI and the surface temperature and additionally, subsidiary information concerning the observation geometry.

The pre-processing of the NOAA reflectance channels [1, 2] included the correction of the sensor degradation as well as the intercalibration of the different AVHRR sensors. Furthermore the provided reflectance values are the at-satellite reflectance where the sun zenith angle and the distance between sun and earth is regarded to determine the irradiation for every pixel. The TOA surface temperature was derived via the split window approach.

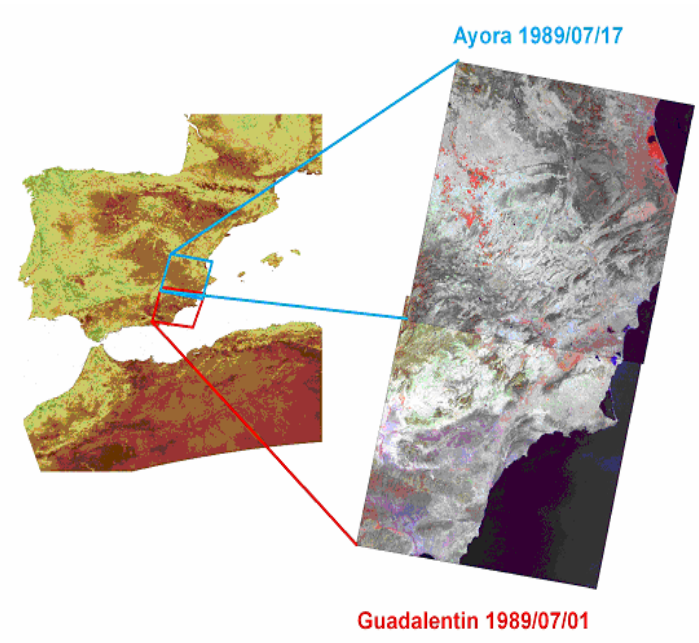

Figure 2. MEDOKADS NOAA AVHRR, monthly composite NDVI, July 1989 and RGB-false-colour-composites of the test sites .of Ayora and the Guadalentin.

For validation purposes Lansat TM images were utilised which were already pre-processed in the run of former projects (GeoRange) (EVK2-CT-2000-00091). Two test sites around Ayora (acquired at 17th July 1989) and the Guadalentin (acquired at 1st July 1989) were examined and compared to the results of the NOAA AVHRR. The Lansat TM images were automatically co-registered with the NOAA AVHRR data to improve the geometric matching and the atmospheric correction was performed based on the modelling procedure developed by Hill and Mehl [18]. Furthermore the TOA surface temperatures were derived following the equations given by Chander and Markham [19].

3.2 Endmember selection

Based on the considerations in section 2 an endmember model was defined comprising three endmembers which represent “fully vegetated (100% vegetation coverage), “non-vegetated” (0% vegetation cover) and “cold” pixels. These endmembers represent the edges of the space spanned up by NDVI and surface temperature and therefore build a spectrally distinct and robust model to estimate the vegetation cover.

Thereby the cold endmember works similar to the shade endmember in the common unmixing approach. It is supposed to compensate effects that lower the surface temperature of the surface, as there are local gradients related to altitude and exposition, temperature variations due to soil moisture, variable evaporation and evapotranspiration respectively and remaining cloud artefacts.

The crucial point of MA approaches is the elaborate definition and selection of the endmembers. As mentioned before, three endmembers are needed for the implemented approach, which represent the pure "corners" of the mixture triangle. The spectral mixture analysis was calculated for the whole time series. Due to variable climatic conditions and changing observation geometry the NDVI-Ts relationship is not constant in time and space. Therefore the mixture triangle has to be adapted from time to another to enable a better vegetation cover fraction estimate. In a former approach the endmembers were chosen image-based [21]. As these endmembers can underlie distortions, i.e. caused by external effects like droughts, and, moreover, as it cannot be guaranteed that the image-based endmembers represent the extreme edges of the mixture analysis (MA) triangle, an automated approach for the statistical selection was driven forward. Thereby synthetic endmembers defined upon theoretical considerations and statistical methods were favoured.

The endmembers' NDVI should represent the extreme values for dense vegetation and soil respectively. The maximum value of vegetation can reach values up to 0.7 for not atmospherically corrected NOAA AVHRR data [21]. Several studies [22, 23] have examined external effects on the reflectance and thus, on the NDVI calculated from the NOAA AVHRR sensor. Holben [22] as well as Singh [23] showed that the NDVI is strongly dependant on the sun zenith angle (Θ_S). With increasing Θ_S the NDVI adversely decreases (for $\Theta_S > 30°$). The influence is much stronger with increasing vegetation density, thus bare soils are almost not affected by the Θ_S. In practical terms this means that the observed maximum values for the NDVI around winter solstice are lower than at the summer solstice. The examination of the time series under this aspect revealed the described effects with a minimum value of the NDVI for maximum Θ_S in December and vice versa maximum values for NDVI with low Θ_S in June. As a consequence the vegetation cover especially for dense vegetation is underestimated in winter in comparison to summer.

The dependency of the NDVI on the Θ_S was considered when defining the NDVI for the fully vegetated endmember. As the Θ_S was provided with the NOAA AVHRR archive as a subsidiary information, a correction that estimates the maximum possible NDVI for every pixel at every time step was implemented. Since the soil is almost not affected by the sun zenith angle, its NDVI was extracted statistically at the lower edge of the monthly NDVI distribution. The NDVI of the cold endmember was equalled with the non vegetated endmember value as the cold endmember was predefined as representing a cold bare soil.

The temperature for the fully vegetated and the non vegetated endmember were defined via the NDVI-Ts relationship extracted by implementing the automated approach described by Nemani [12], which was followed by a linear regression. With the derived regression parameters the temperature for the two endmembers could be

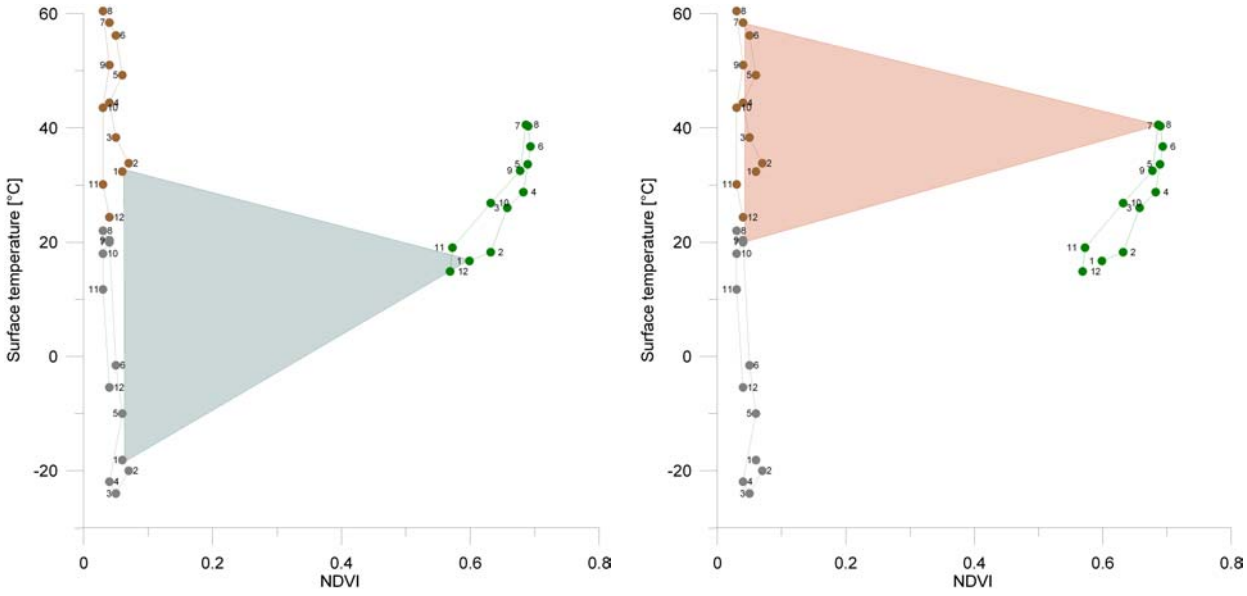

Figure 3. Extracted NDVI-Ts mixture triangle for January 1990 (left) and July 1990 (right).

estimated. The surface temperature strongly varies from North to South and from West to East respectively. This phenomenon is occurred especially in the winter season, leading to different NDVI-Ts relationships for different regions. To avoid mistakes in the vegetation fraction estimation the scene was segmented into different areas and for each one the NDVI-Ts-line was extracted separately. Moreover, to avoid sharp transitions a linear interpolation was implemented.

As the cold endmember should represents a cold bare soil, the temperature of the cold endmember was defined statistically at the lower edge of the temperature values present at the already before determined NDVI value. Figure 3 illustrates exemplary the extracted NDVI Ts MA triangle for January and July 1990.

3.3 Validation

For validation of the implemented approach, Landsat TM scenes were utilised. As this sensor features besides six reflective channels also a thermal one, the realisation of both the "classical" SMA and the NDVI-Ts MA was possible. On the one hand the SMA was performed implementing a three-endmember-model comprising soil, vegetation and shade on the 30 m resolution. On the other hand NDVI and surface temperature were derived to perform the NDVI-Ts MA at a geometric resolution of 120 m.

In a following step the TM data were degraded to 1 km to allow a comparison of the two MA approaches, SMA and NDVI-Ts MA, and to compare the results from Landsat TM and NOAA AVHRR.

Preceding this comparison, the derived vegetation abundances were normalised under the assumption that the shade component does not change the ratio between the other derived components, which means that the abundance of the cold endmember is apportioned to the remaining endmembers according to their fractional abundances trough following factor [24]:

$$F=1/(1-F_{cold}) \quad (4)$$

4 RESULTS

At first the results of the two mixture analyses performed on the Landsat TM scenes were compared. As the analyses brought similar results for the two sites, only the results for Ayora are presented in this study. Figure 4 (left) shows a scatter plot between the SMA and the NDVI for the test site of Ayora. It can be clearly seen that the relationship is non-linear and the vegetation abundances are more sensible for low vegetation cover than the NDVI. The NDVI is characterised by the steep slope for lower values, while for increasing vegetation cover the vegetation abundances saturate. The relationship between the results of the SMA and the NDVI-Ts MA is shown in figure 4 (right). This figure illustrates that the two measures are connected linearly, almost 1:1. Thus, it can be concluded that the vegetation abundances derived via the two approaches provide the same information.

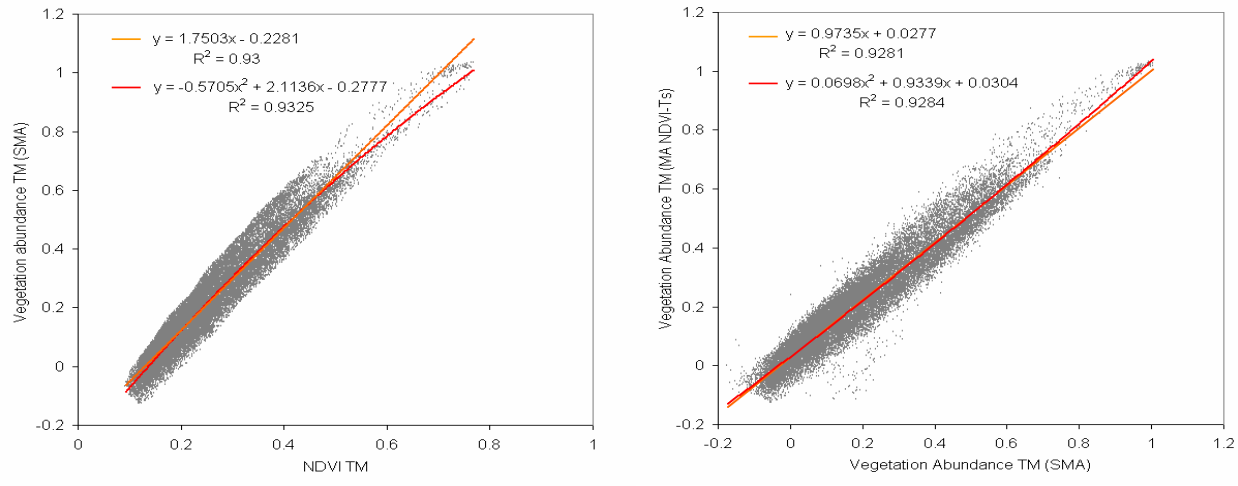

Figure 4. Scattergrams for the region of Ayora. Parameters derived from a degraded Landsat TM scene (July 1989), left: NDVI – vegetation abundance (SMA reflectance), right: normalised vegetation fraction (SMA reflectance) – normalised vegetation abundance (SMA NDVI-Ts).

In a second step, the results derived from the two sensors Landsat TM and NOAA AVHRR were compared. Figure 5 (left) shows the scatter plot between the NDVI derived from NOAA AVHRR and the NDVI derived from

Landsat TM respectively. The relationship is not linear as the spectral properties of the sensors' channels differ in position and width. The scatter plot of the vegetation abundance derived for the two sensors (figure 5 (right)) show an almost linear relationship, even though this relationship is not 1:1.

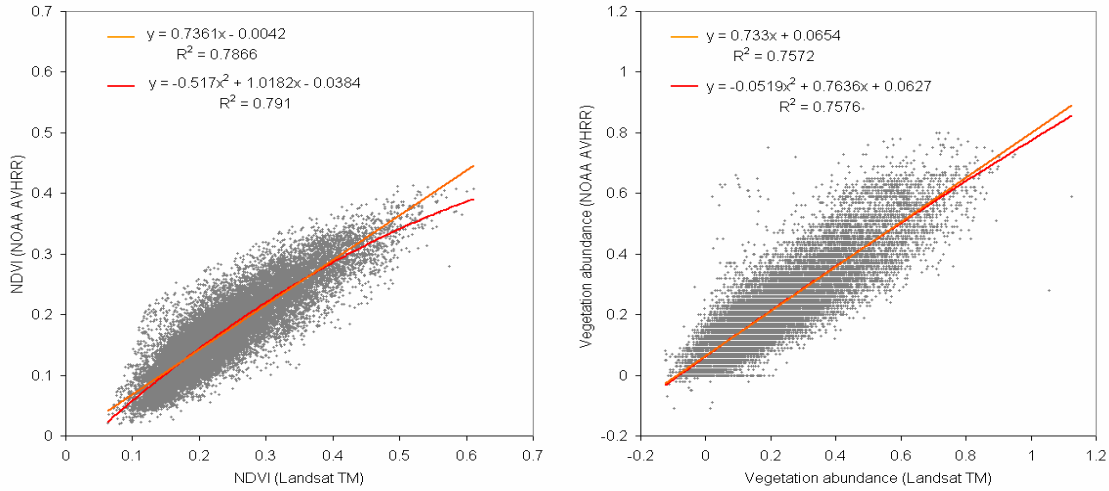

Figure 5. Scattergrams for the region of the Guadalentin. Parameters derived from a degraded Landsat TM scene (July, 1989) and the corresponding NOAA AVHRR monthly composite, left: NDVI (TM) – NDVI (AVHRR), right: vegetation fraction (TM) - vegetation fraction (AVHRR).

The NDVI and the derived vegetation abundances for January 1989 are presented in figure 6. At first view it is apparent that the vegetation abundances show a higher dynamic for areas with low as well as high vegetation cover than the NDVI. The NDVI utilises only a range from 0.05 to 0.7, where the limitation of the lower values is caused by the background signal and the upper boundary results from the saturation of the NDVI with dense vegetation cover. In addition, the NDVI values for non vegetated areas like the Sahara are significantly above zero.

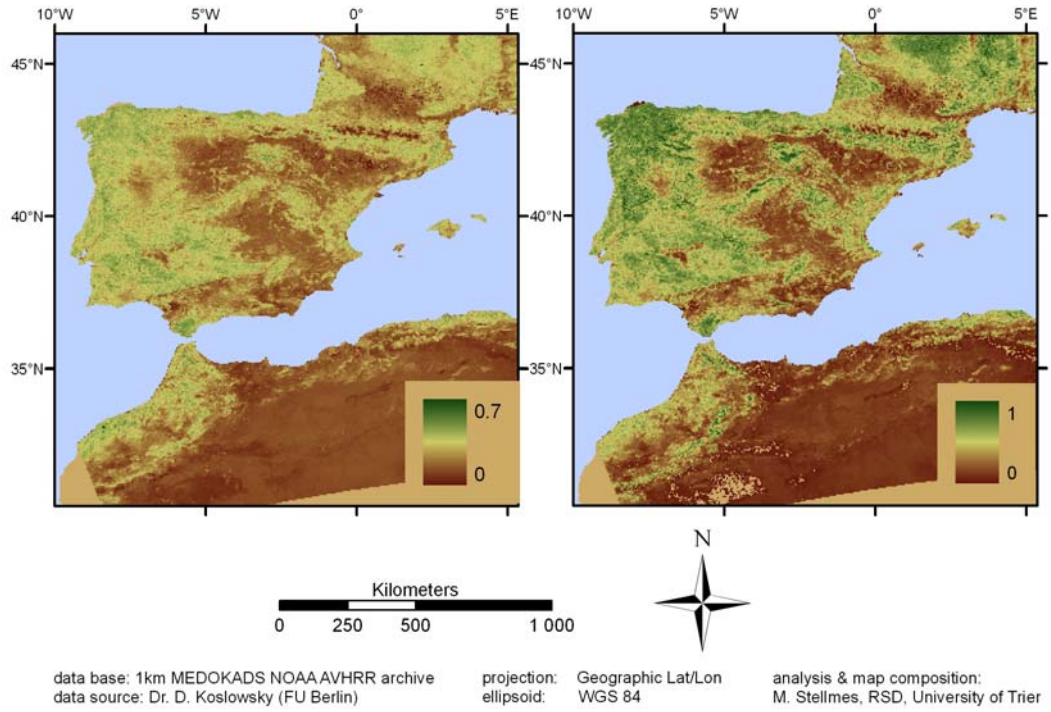

Figure 6. NDVI (left) and derived vegetation abundances (right) in January 1989 for the Iberian Peninsula.

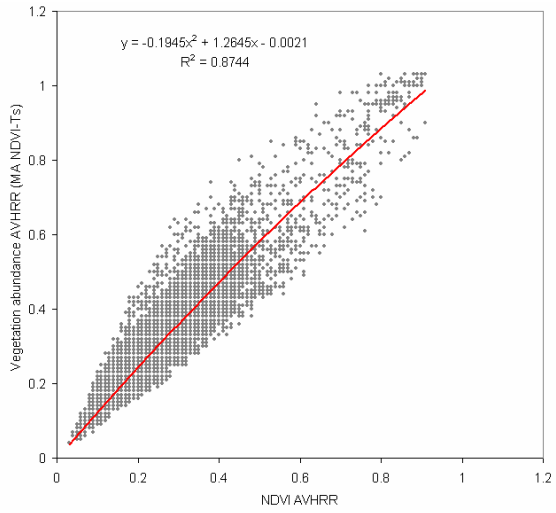

A comparison of the NDVI and the vegetation abundances derived from the 1 km NOAA AVHRR data (figure 7) bears resemblance to the results obtained from Landsat TM. Compared was the South-Eastern part of Spain, which comprises the two test sites examined in this study. Also this example shows the higher sensitivity of the vegetation abundances than the NDVI for low vegetation densities. However, the values scatter stronger, which can presumably be ascribed to the bigger area represented in the scattergram.

Figure 7. Scattergram of NDVI and vegetation abundance (NDVI-Ts MA) for South-Eastern Spain. Parameters derived from a NOAA AVHRR scene (July 1989).

5 CONCLUSIONS

Aim of this study was the implementation of an enhanced vegetation density layer performed on the 1 km MEDOKDAS NOAA AVHRR archive. Instead of using reflectance characteristics like in the classical SMA approach, the implemented method bases on the inverse relationship of vegetation cover and surface temperature. Based on the analyses of Landsat TM scenes, it was shown that the vegetation abundances delivered by the "classical" SMA and the NDVI-Ts MA show a strong linear relationship and thus, it can be concluded that they provide the same information on a coarse geometric resolution. Furthermore, the inter-comparison of the normalised vegetation abundances derived from Landsat TM and NOAA AVHRR also showed a linear relationship whereas the comparison of the NDVI was proved to be not linear. Therefore it can be assumed that the derived vegetation abundances allow a better inter-comparison of different sensors than the NDVI alone. An inspection of the NDVI and the NDVI-Ts MA vegetation abundance estimation from both sensors showed that the vegetation abundances show a higher sensitivity for lower vegetation densities. Thus, the derived vegetation abundances are more sensitive and significant for sparse vegetation covers below 30% than the NDVI [16].This is from special importance as low vegetation covers are often present in semi-arid areas like the Mediterranean which are susceptible to land degradation processes.

A consideration of the sun zenith angle could reduce the effect of an underestimation of the vegetation cover in winter time opposite to the summer season. Here it should be pointed out that this correction does no replace a bidirectional atmospheric correction. But as by now this desirable kind of data are recently not available, we consider this to be an improvement for vegetation estimation especially for the relation of vegetation cover between summer and winter.

Furthermore, the study demonstrated that the vegetation abundances show a higher dynamic than the NDVI. In addition the vegetation abundances supply better estimates for non vegetated areas due to the reduction of the background's influence. However, extreme temperature gradients caused by the geographic position, i.e. elevation gradients in mountainous regions, lead to an overestimation of vegetation abundances. These effects could be reduced by stratification techniques. Other problems occur mainly for surfaces which are affected by wet conditions like for example rice fields, because the NDVI-Ts-relationship strictly exists only under dry conditions. The cold component can compensate differences in moisture, but only to a certain extent, which appears as an overestimation of vegetation cover abundances for this kind of land covers. Thus, further research is needed to refine the methods of the endmember selection, especially for the cold endmember as correction parameter.

ACKNOWLEDGMENTS

This work was financially supported through the 5th framework program of the EU within the project LADAMER. This is gratefully acknowledged. The authors like to thank Dirk Koslowsky (FU Berlin) for providing us with the NOAA AVHRR MEDOKADS archive, Achim Röder (University of Trier) for supporting the work with Landsat TM data for validation purposes and Wolfgang Mehl (JRC, Italy) for providing the registration tool "findgcp".

REFERENCES

[1] KOSLOWSKY, D., 1998: Daily extended 1-km AVHRR data sets of the Mediterranean, Proceedings 9th Conf. Sat. Meteor. and Oceanogr. UNESCO, Paris; France, 25-29 May, AMS, Boston, MA, 38-41.

[2] KOSLOWSKY, D., 2003: 12 years Mediterranean satellite data set and analysis. In: H.-J. Bolle (ed.): Mediterranean Climate, , Berlin Heidelberg New York, Springer-Verlag, pp. 165-177.

[3] EUROPEAN COMMISSION, 1998: An Integrated Approach to Assess and Monitor Desertification Processes in the Mediterranean Basin (DeMon-II). Final Report, European Commission, Directorate General Joint Research Centre, Ispra, Contract No.: 11589-95-12 A2 FP ISP B.

[4] PRICE, J.C., 1993: Estimating of leaf area index from satellite data. *IEEE Transactions on Geoscience and Remote Sensing, 31(3)*, pp. 727-734.

[5] ASRAR, G., FUCHS, M., KANEMASU, E.T. AND HATFIELD, J.L., 1984: Estimating absorbed photosynthetic radiation and leaf area index from spectral reflectance in wheat. *Agronomy Journal, 76*, pp. 300-306.

[6] HOLBEN, B., 1986: Characteristics of Maximum Value Compositing Images from Temporal AVHRR Data. *International Journal of Remote Sensing, 7*, pp. 1417-1434.

[7] SMITH, M.O., ADAMS, J.B. AND SABOL, D.E., 1994: Mapping sparse vegetation canopies. In: Hill, J. and Mégiers, J. (eds.): Imaging spectrometry – a tool for environmental observations, pp. 221-235. Kluwer Academic, Dordrecht.

[8] HILL, J., HOSTERT, P., TSIOURLIS, G., KASAPIDIS, P. AND UDELHOVEN, T., 1998: Monitoring 20 years of intense grazing impact on the Greek island of Crete with earth observation satellites. *Journal of Arid Environments, 39*, pp. 165-178.

[9] GATES, D. M., 1980: Biophysical Ecology. Springer-Verlag , New York, Heidelberg, Berlin.

[10] CHOUDHURY, B.J., 1989: Estimating evaporation and carbon assimilation using infrared temperature data: vistas in modelling. In: Asrar, G. (ed.): Theory and Applications of Optical Remote Sensing, New York, Wiley and sons, pp. 628-690

[11] GOWARD, S.N. AND HOPE, A.S., 1989: Evapotranspiration from combined reflected solar and emitted terrestrial radiation: preliminary FIFE results from AVHRR data. *Advances in Space Research, 9*, pp. 239-249.

[12] NEMANI, P, PIERCE, L., RUNNING, S.W. AND GOWARD, S., 1993: Developing satellite derived estimates of surface moisture status. *Journal of Applied Meteorology, 32*, pp. 548-557.

[13] EHRLICH, D. AND LAMBIN, E. F., 1996: Broad-scale land-cover classification and interannual climatic change, *International Journal of Remote sensing, 17*, pp. 845-862.

[14] SETTLE, J.J. AND DRAKE, N.A., 1993: Linear mixing and the estimation of ground cover proportions. *International Journal of Remote Sensing, 14*, pp. 1159-1177.

[15] HUETE, A.R., JACKSON, R.D. AND POST, D.F., 1987: Spectral response of a plant canopy with different soil backgrounds. *Remote Sensing of Environment, 17*, pp. 37-53.

[16] SOMMER, S., 1999: Regional desertification indicators. In: MEDALUS III Project 3 Final Report, Contract ENV4-CT95-0121, pp. 39-82. http://www.kcl.ac.uk/kis/schools/hums/geog/medalus/medalus.html

[17] CASELLES, V. AND SOBRINO, J.A., 1989: Determination of frosts in orange groves from NOAA-9 AVHRR data. *Remote Sensing of Environment, 29*, pp. 23-26.

[18] HILL, J. AND MEHL, W., 2003: Geo- und radiometrische Aufbereitung multi- und hyperspektraler Daten zur Erzeugung langjähriger kalibrierter Zeitreihen. *Photogrammetrie Fernerkundung Geoinformation, 1*, pp. 7-14.

[19] CHANDER, G. AND MARKHAM, B., 2003: Revised Landsat-5 TM Radiometric Calibration Procedures and Postcalibration Dynamic Ranges. *IEEE Transactions of Geoscience and Remote Sensing, 41(11)*, pp. 2674-2677.

[20] STELLMES, M., SOMMER, S. AND HILL, J., 2005: Regional vegetation monitoring based on the NOAA AVHRR time series in the Mediterranean Area. In: Erasmi, S., Cyffka, B. and Kappas, M. (eds.): GGRS 2004 - 1st Göttingen GIS & Remote Sensing Days - Environmental studies. *Göttinger Geographische Abhandlungen, 113*, pp. 124-130.

[21] CZAJKOWSKI, K.P., GOWARD, S.N., MULHERN, T., GOETZ, S.J., WALZ, A., SHIREY, D., STADLER, S., PRINCE, S.D. AND DUBAYAH, R.O., 2004: Estimating environmental variables using thermal remote sensing. In: Quattrocchi, D.A. and Luvall, J.C. (eds.): Thermal remote sensing in land surface processes, CRC Press, pp. 11-32.

[22] HOLBEN, B. AND FRASER, R. S., 1984: Red and near-infrared sensor response to off-nadir viewing. *International Journal of Remote Sensing, 5(1)*, pp. 145-160.

[23] SINGH, S.M., 1988: Simulation of solar zenith angle effect on global vegetation index (GVI) data. *International Journal of Remote Sensing, 9(2)*, pp. 237-248

[24] ADAMS, J.B., SMITH, M.O. AND GILLESPIE, A.R., 1993: Imaging Spectroscopy: Interpretation Based on Spectral Mixture Analysis, In: Pieters, C.M. and Englert, P. (eds.): Remote Geochemical Analysis: Elemental and Mineralogical Composition. Cambridge University Press.

Surface degradation and recovery indicators in the Eastern Mediterranean region derived from long-term monthly 1 km AVHRR/NDVI data

T. Udelhoven[a], T. Jarmer[a], B. Katlan[b], M. Al-Abed[c], N. Assad[c], Z. Makhamreh[a] and J. Hill[a]

[a] Remote Sensing Department, Trier University, email: udelhove@uni-trier.de
[b] Center for research and studies pertaining to the development of the arid and semi-arid areas of the Arab World (ACSAD), Syria
[c] General Organisation for Remote Sensing (GORS), Damascus, Syria

ABSTRACT

The present study addresses long-term variation in vegetation cover in the Eastern Mediterranean area, particularly in Syria and Lebanon. The analysis is based on monthly 1 km AVHRR/NDVI data from the MEDOKADS data archive (Free University, Berlin) and is covering the time period from 1989 to 2004. For trend analysis two non-parametric methods were applied, the Modified Seasonal Kendal test and the Kendall slope. The analysis of seasonal components was accomplished by discrete Fourier transform and continuous wavelet transform (CWT). Selected hot and bright spots were further evaluated by visual interpretation of Landsat TM images from the beginning and the end of the monitoring period. The results from time-series analysis were subject of uncertainty, unless other, additional information sources were used for verification such as geo-physical as well as socio-economic data. For both countries observed trends in vegetation abundances cannot be understood without reference to local and national policies.

Keywords: Trend analysis, CWT, DFT, Syria, Lebanon, degradation

1 INTRODUCTION

The problem of degradation received worldwide attention with the United Nation Convention to Combat Desertification (UNCCD). Using their definition "Land degradation means a reduction or loss, in arid, semi-arid and dry sub-humid areas, of the biological or economic productivity […] resulting from land uses or from a process or combination of processes […], such as: (1) soil erosion caused by wind and/or water; (2) deterioration of the physical, chemical and biological or economic properties of soil; and (3) long-term loss of natural vegetation." [1]. For discriminating between short-lived fluctuations in surface reflectance and long-term trends as indicators of enduring environmental pressure, high temporal resolution remote sensing data are required such as provided by the NOAA/AVHRR sensors. By time-series analysis degradation and development tendencies can be detected in terms of changes in vegetation abundances. With regard to the almost exclusively vegetation-related signal in the archived global environmental satellite data it is an essential requirement that the available data series is covering a time span as along as possible. Inter-annual climatic changes such as temperature and precipitation profoundly influence plant phenological status such as the onset green-up, the rate of biomass accumulation, and the onset and rate of vegetation senescence [2]. Significant trends derived from short series lead to misinterpretations especially if no climatically reference data are available.

Following the UNCCD definition bright spots indicate areas which are or have been taken up positive development incentives leading to improvements in the health of ecosystems or economic improvements in compliance to criteria of sustainable development. Hot spots in turn flag areas suffering from various types of degradation processes; these might be triggered from changes in natural factors and/or socio-economic conditions.

The objective of the present study is to investigate time-series characteristics such as trends and frequency components in vegetation abundances in Lebanon and Syria using NDVI data from the 1 km AVHRR-Medokads data set [3] and to discuss the impact of local and national policies on the observed results. This point will be elaborated by taking a closer look at identified hot spots and bright spots in the two countries.

2 MATERAL AND METHODS

The NDVI data used in this study derive from the "Mediterranean Extended Daily One Km AVHRR Data Set" (MEDOKADS) [3]. All time-series calculations were carried out using the TimeStats software package [4]. For this study two non-parametric trend tests were used: The significance of long-term variations was assessed by the Modified Seasonal Mann-Kendall (MSK) test which is suited for monotonic trend detection independent from its functional type (e.g. linear, quadratic) [5,6]. The Seasonal Kendall (SK) slope estimator represents a non-parametric alternative for the slope coefficient in a linear trend analysis and is applied to describe the magnitude and inclination of a trend [7]. TimeStats offers also tools to describe cyclic components in a series. Methods applied in this study include the phase spectra from NDVI series and the continuous wavelet transform (CWT). The CWT can provide indications for significant changes in a time-series. It describes a time series in terms of wavelet coefficients, each of which representing the amplitude of the wavelet function at a particular location within the data vector and for a particular wavelet scale. The result of the CWT for each series is the scalogram which describes the wavelet power of Fourier frequencies in dependence of the time. Integrated over time the global wavelet is obtained from the scalogram, which can be used for power spectrum estimation. The scalogram can also be integrated over a selected band of Fourier frequencies, resulting in a curve showing the development of the power of the frequency band in time [8].

3 RESULTS

3.1 Lebanon

In Lebanon there exist many reasons for land degradation including deforestation, over-grazing, urbanization, bad agricultural techniques, and rural exodus. Because most of the country being on slope terrain relief, rainfall intensity and runoff contribute to severe water erosion and soil loss, especially where the vegetation cover is reduced or lost [9]. The average NDVI values in Lebanon vary between 0.05 and 0.20 in North-East Lebanon and along the Lebanon and Anti-Lebanon Mountainous, whereas in the Bekaa valley average NDVI up to 0.55 are common.

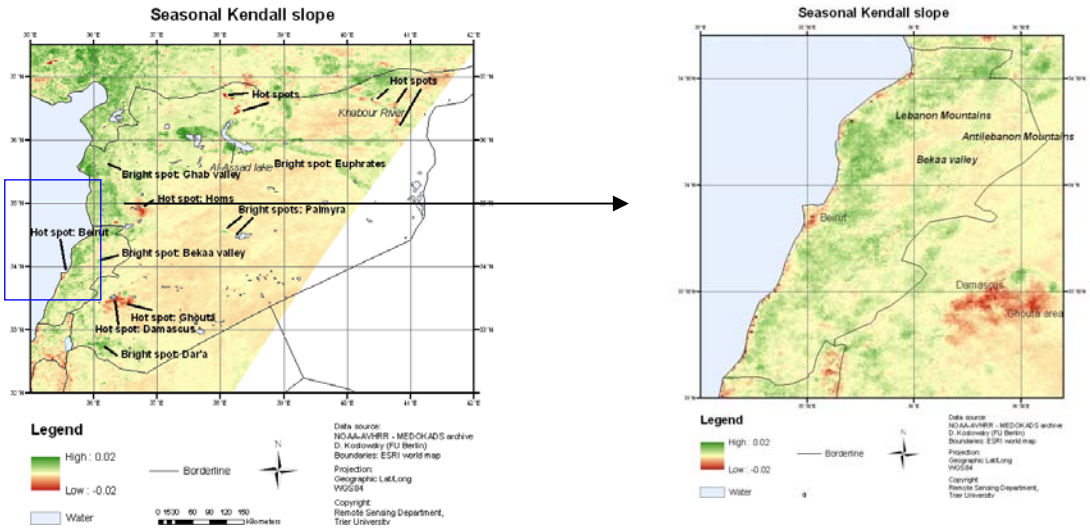

Figure 1. Results from the Seasonal Kendall-Slope statistics indicating the inclination of long-term NDVI trends in Lebanon.

One approach to describe the degradation risk in Lebanon was the implementation of the CoDeL-project (Combating Desertification in Lebanon) which was funded by the German Agency for Technical Cooperation (GTZ). CoDeL has elaborated a map of priority areas for combating desertification [10]. Regions severely exposed to desertification in the CoDeL map are the plains and valleys of areas in Baalbeck and El-Hermel, which are located in the Bekaa Valley and in North Lebanon, respectively. Regions partially affected by desertification are the regions around the big cities along the coastal line such as Beirut, the West-Bekaa valley and in the South of Lebanon.

While the CoDeL-approach addresses the degradation risk in Lebanon it does not account for the actual state of degradation. Figure 1 and 2 illustrate the trend inclinations of the NDVI expressed by the Kendall-slopes and the significances from the MSK test. Figure 3 shows the mean TOA-NDVI levels from 1989 to 2004. The coastal zone which consists of a continuous urbanized belt from Damour, south of Beirut, to Berbara (north of Jbeil) is characterized by negative Kendall slopes, although most of the negative trends are not yet significant ($\alpha < 5\%$).

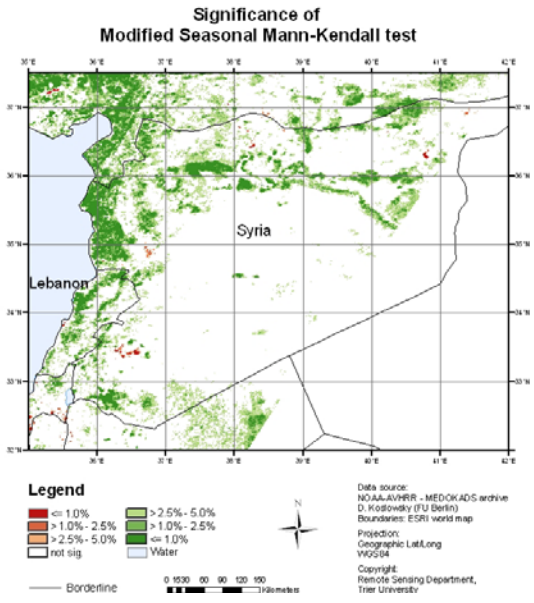

Figure 2. Significance for the MSK test for trend analysis for Syria and Lebanon. Lower percentages indicate highly significant trends.

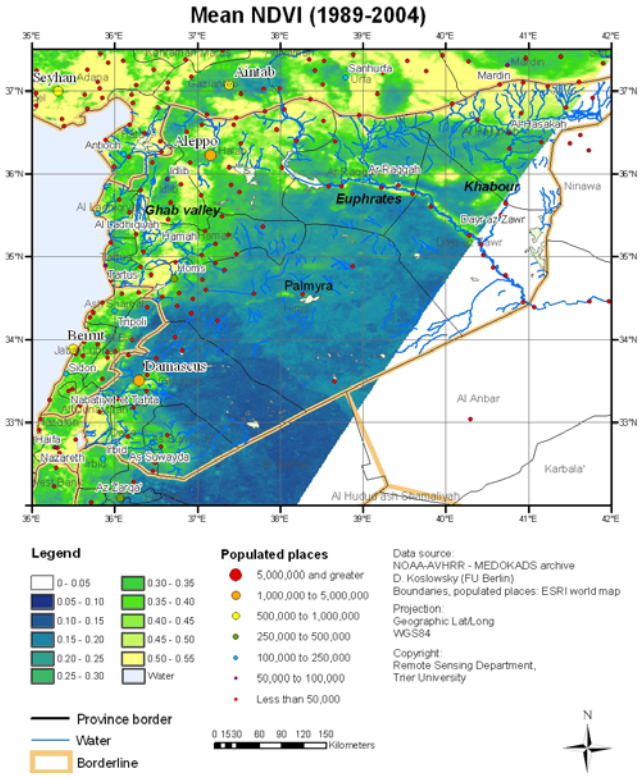

Figure 3.: Mean top-of-atmosphere (TOA) NDVI levels (1989-2004).

About one third of Lebanon's total population resides in Beirut and its suburbs. Also the economic activities are concentrated along the coastal zone, contributing about 73 percent of Lebanon's Gross Domestic Product [11]. The current expansion of developed areas along the Lebanese coast is triggered by the restoration of national economy growth in the postwar period (1990-present, [12]). A comparison of the two Landsat scenes in figure 4 showing the Beirut area in 1987 and in 2000 distinctly highlights the increasing pressure in urbanization during the last two decades. Facing with declining land resources along the narrow coastal line Lebanons government supports the specialization of high quality agricultural produce in this area. It is feared that the disappearance of agricultural land

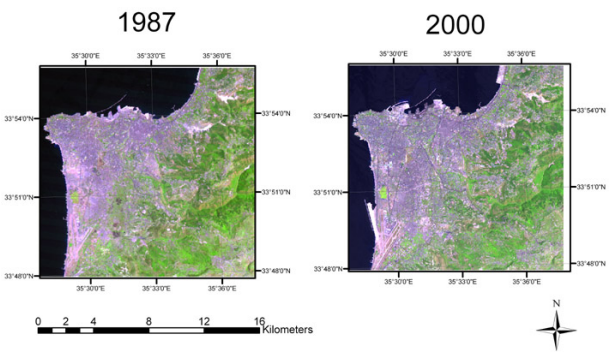

Figure 4. Landsat TM images (5-4-3) from 26.5.1987 (left) and 21.5.2000 (right) from Beirut.

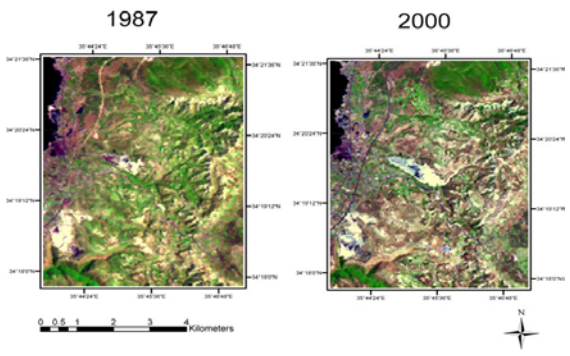

Figure 5. Landsat TM (5-4-3) sub-scenes from Lebanon (left: 26.5.87, right: 26.5.2000).

in the coastal area will lead to reduced water infiltration in the soil, faster runoff of rainwater in the urbanized belt, flooding in the lower coastal plain in case of heavy rainfall and soil erosion [11, 13].

This development also threatens the floristic richness of the Lebanese coastal zone which was described in a recent study by Talhouk et al. [14]. Although most of the NDVI series along the coast have no significant decreasing trends, local degradation tendencies exist such as illustrated by the two Landsat scenes in figure 5 showing a stripe of the coastal areas North of Beirut in 1987 and 2000, respectively.

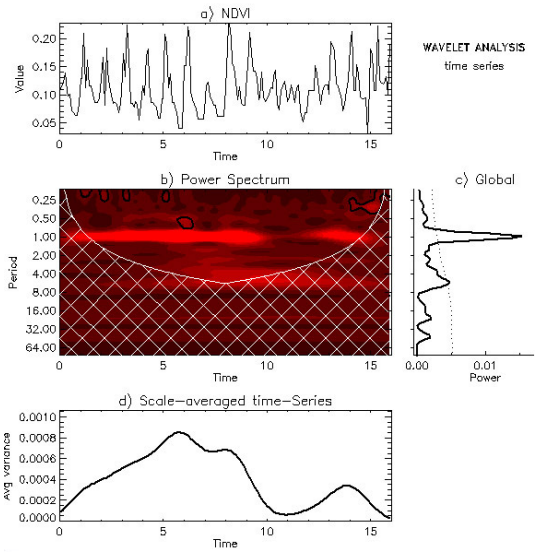

Figure 6. CWT results form a monthly NDVI series (Bekaa-valley). The scale average wavelet power (d) correspond to the annual vegetation growth cycle.

A distinct bright spot area is the Bekaa valley between the Lebanon and Anti-Lebanon Mountains which is of extraordinary importance for food production in Lebanon. Although the valley is characterized by significantly increasing vegetation abundances in the MSK map and mean TOA-NDVI values exceed 0.5 its western part is flagged as risk area in the CoDeL map.

Almost 42 percent of Lebanon's exploitable agricultural land is located in the Bekaa. It hosts 62 percent of the total area used for industrial crops (including sugar beet, tobacco, and vineyards) and 57 percent of the total area used for cereal production [11].

Since not irrigated areas are subject to episodic droughts agriculture is also increasingly shifting to irrigated production, thereby putting added pressure on dwindling water resources. In figure 6 the results of CWT analyses are presented for a NDVI series collected from a pixel in the Northeast part of the Bekaa. The NDVI graph and the scalogram show that after eleven years of observation time in 1999 there was a distinct decline in the NDVI and the related wavelet power of the annual cycle in the scalogram drops almost to zero. 1999 was a severe drought year in Lebanon and Syria. But in spite of better weather conditions in 2000 a significant rebound in the annual NDVI cycle is not visible from the scalogram not before 2001. Severe droughts have a lasting effect in non-irrigated areas for rainfed cultures and thus the expansion of irrigation areas is propagated to overcome these problems.

2.2 Syria

Being a Mediterranean country, the Syrian climate is characterized by rainy winters and hot dry summer with two short transitional seasons in between. The largest part of the country representing about 45% of the total area is falling below the 200 mm isohyets and is designated as 'badiah' or steppe and where cultivation is outlawed. Rainfed agriculture is historically practiced in northern and western plateaus and plains. Irrigation is mainly practiced in the large river valleys of Euphrates, Khabour and Orontes [15,16]. Forest is generally confined to the coastal mountains. Syria's largest agricultural products include grain crops, cotton, sugar beet and olives. According to the annual rainfall amount Syria can be divided into several zones (figure 7). The dry central steppe area is dominated by Aridisols while the surrounding Inceptisols indicate areas outside the central steppe with rainfalls amounts between 250 and 600 mm. Entisols occur in the coastal area and along the terraces of Syria's rivers and Vertisols can be found in the South of the country. The annual NDVI phases which are shown in figure 8 can also be used to differentiate between the central steppe where the green peak is already reached in February after the winter rain while the phase is shifted toward March to May in the surrounding rainfed areas. The latest green peak in the year belongs to cotton along the Euphrates River which is characterized by annual phases between July and September.

Hot-spot areas

The inter-annual rainfall pattern in Syria varies considerably from one year to another making rainfed farming system extremely risky, especially in the South of the 36th latitude, the 250 mm isohyet. Facing the rising demand of water the Syrian government has initiated several huge dam projects along its major rivers. Since the agriculture production in Syria mainly depends on rainfall amounts, the dams are mostly aimed at sustaining cereal cropping.

The MSK and the Kendall slopes maps show negative NDVI trends along the Euphrates river upstream the Al-Assad lake and along the Khabour river. The two Landsat scenes in figure 9 illustrate that the declining NDVI trends along the Euphrates are caused by flooding the lower river terrace between Ash Shajarah, situated on the northern edge of Lake Assad, and Jarabulus, located near the Turkish border by a new dam.

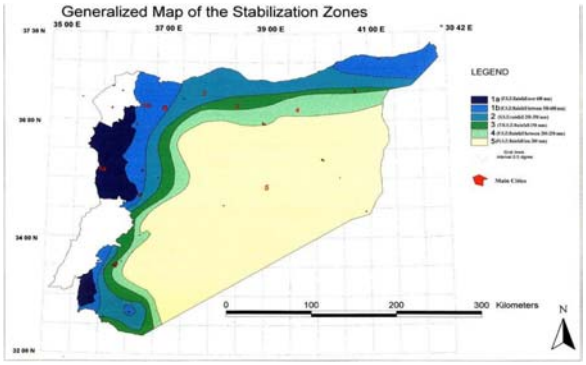

Figure 7. Stabilisation zones of Syria [17].

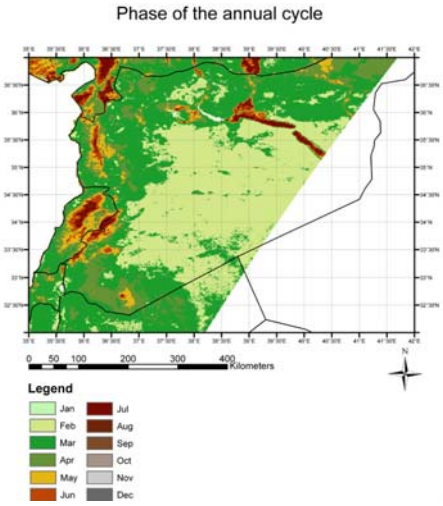

Figure 8. Annual NDVI phase (1989 to 2004).

A similar situation is found along the Khabour river where during the observation period a new dam was finished (figure 10). But here also downstream NDVI trends have negative inclinations due to a shortage of water after closing the dam. One other dam project which has not yet been realized is a dam on the Yarmouk River with 225 million cubic meter capacity which was agreed between Syria and Jordan in 2002 [18].

Two other areas with significantly declining NDVI are located in the western part of Syria around Damascus and Homs cities. The *hot spot* area around Damascus can be separated into two parts reflecting two different aspects of degradation: The first area indicates the urban encroachment of Damascus and its suburbs during the last two decades. The second area in the eastern part belongs to the Ghouta region of Damascus in which orchards and horticultures are grown [15].

The two Landsat sub-scenes in figure 11 give some indication about a land-use change from 1987 to 2000. The lower greenness in 2000 was probably additionally influenced by the severe drought in 1999. Because annual rainfall amount does not exceed 350 mm in the average in the area and the population of Damascus is further growing, agricultural production is supported by wells and surface irrigation. Irrigation water mainly origins from the Barada River which forms two table lakes in the East, Bahr el Aateibe and Bahret Hijjane. By excessive irrigation in the Ghouta area during the last decades the lake regularly dries out completely during the dry seasons and groundwater pumping led to salinity build-up in the soil matrix.

The situation of the hot spot area around Homs is similar to Damascus. The southern area is characterized by urban encroachment while the horticulture region in the North is suffering from a shortage of water. Due to excessive irrigation in the past the ground water tables has been significantly lowered. The land use change in both areas was also confirmed by a distinct shift of the annual green peak's phase during the last 16 years which is illustrated in figure 12. While in the first years of observation time the maximum of the green peak was in between April and June, the phases shifted at the end to January to March and occurred just after winter rainfall.

The Kendall slope map shows one other potential hot spot area which is located in the Northeast of Syria around Qameshly city but which is yet not significant. Also here the increased irrigation is triggered by the enhanced food demand in the growing city which may cause problems in the near future.

Areas with increasing NDVI trends

The MSK map also highlights regions with significant increasing NDVI trends. Referring to figure 3 most of these areas correspond to places with high mean (TOA-) NDVI values between 0.35 and 0.55. One important region experiencing growing vegetation abundances is the lower Euphrates terrace with its fertile soils (Torrifluvents, a suborder of Entisols) downstream the Al-Assad lake. Together with its two major tributaries, the Balikh and Khabur

(Nahr al Khabur) rivers in the northeast, the Euphrates is the Syrian major irrigation source. An about 200 km long stripe along the Euphrates were cotton is grown has significant positive NDVI trends and is characterized by annual phases between June and July.

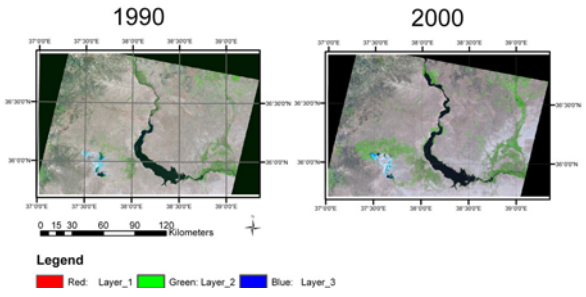

Figure 9. Landsat scenes in 1990 and 2000 showing the artificial Al-Assad Lake.

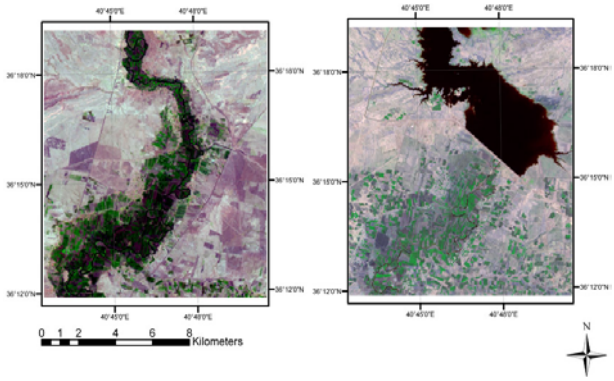

Figure 10. Landsat sub-scenes from 19.5.1990 and 29.5.2001 showing the Khabour river dam project before and after construction the dam.

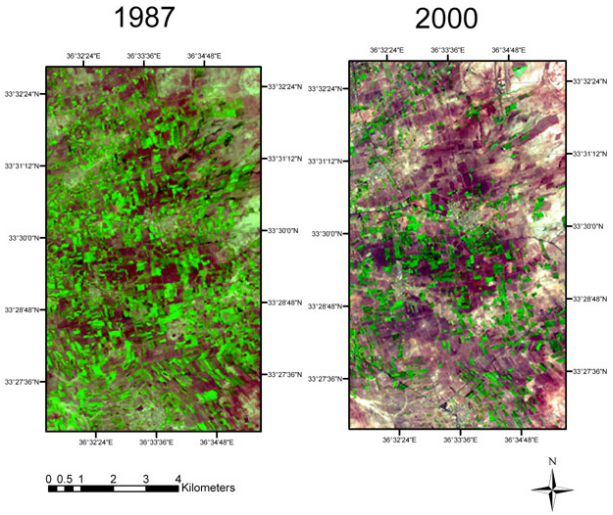

Figure 11. Landsat TM sub-scenes (26.5.1987 and 21.5.2000) from the Ghouta area of Damascus (RGB channels: 5-4-3).

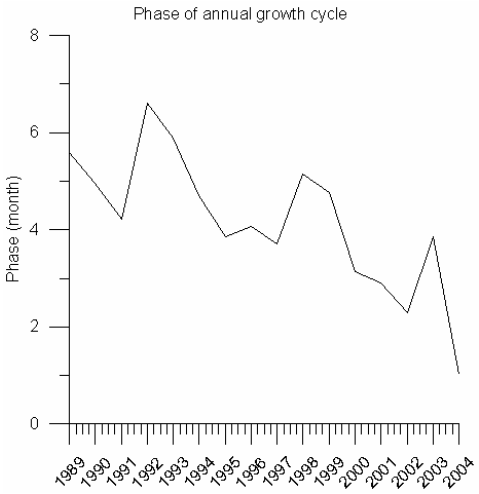

Figure 12. Results from a windowed FFT: Development of the annual growth cycle's phase in the Ghouta region.

In the western parts of Syria positive trends correspond to the coastal area and the ridges of the coastal mountains. Belonging to stabilization zone 1 this region receives more than 600 mm annual precipitation providing good conditions for cultivation of citrus trees, crops, tobacco and tomatoes. Also greenhouse cultivation and plastic cultures have experienced accelerated growth in the last years. Forested areas along the lower and upper stages in this sub-humid or humid climate mainly consist of Quercus Calliprinos, Quercus Infectoria, Cedrus Libani and Juniperus Excelsa and irregularly experience wild. Reliable indicators for forest fires could however not be identified at 1 km resolution from the Medokads data.

One important bright spot area is located in the Al Ghab Valley East of Homs. Since 1954 the government had reclaimed land from this swampy area, where periodically the Orontes River overflowed its banks in destructive floods [15]. Although the region is characterized by significant positive NDVI trends locally some salinization problems have arised. They are caused by a high ground water table and the usage of untreated brackish water for irrigation.

In the central part of the steppe area there are two small neighboured bright spots visible from the MSK map. The spot in the East is the Palmyra oasis and the area in the west is located along the road from Damascus to Palmyra and is irrigated by ground water. The comparison of the Landsat images in figure 13 shows that this area has grown up during the 1990ies. In 1990, the location is rarely visible in the Landsat scene, but in 2000 the irrigated field occupied a size of about 5650 ha. Also the irrigated area around Palmyra has extended. Two auxiliary

bright spot areas are located in the South of Syria. The first are the hills of the Jebel-ed-Drouz Mountains which belong to stabilization zone 1b. The area is cultivated with fruit trees and grapes. The second area is located in the west of the Mountains in the Dar'a province. Belonging to stability zone two, this area receives 250-350 mm annual precipitation. The most important limiting factor for rainfed agriculture is a high density of stones in the top soil. In 1994, the Syrian Government initiated a project to clean the top soils from stones. This improvement led to a distinctly enhanced agricultural productivity which in turn resulted in increasing NDVI trends. The most important agricultural products in this area nowadays are olives, crops, wheat, lenses, and chick peas.

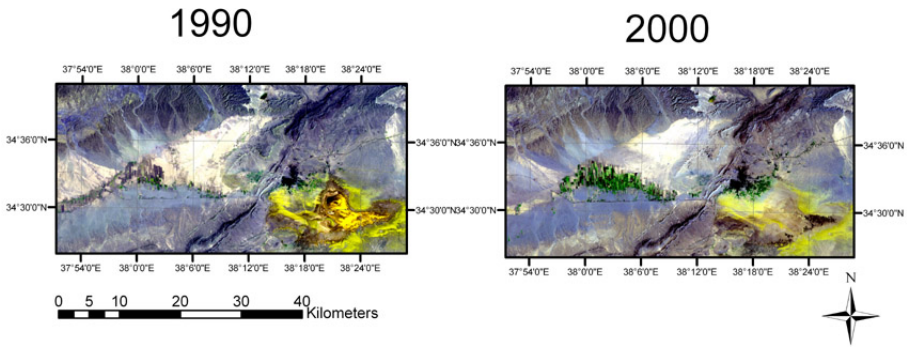

Figure 13. New irrigated area along the road between Tiyas and Tadmur (Palmyra).

3 DISCUSSION

Results from time-series analysis in Lebanon and Syria show that in general degradation tendencies as measured by long-term trends in vegetation abundances is not the overall impression in Lebanon and Syria. In contrast, large areas are characterized by positive trends which are related to improved management systems in forestry, grazing and irrigation, and by land reclamation schemes. Modern agricultural trends include expanding greenhouse and plastic cultures (which is not visible by the NDVI), less fallow, greater use of herbicides and deeper tillage. In rotation systems with cereals to a greater extent legumes are used as self-regenerating pasture plants [19]. Crop production in dry areas is increased by the development of drought resistance breeding lines and by the use of early-maturing genotypes as a way of withstanding drought and high temperatures during the grain-filling and cropping period [20]. Additionally, different phenologies are mixed to maximize grain yield in wet and dry environments.

The main reasons for identified hot spots are the expansion of the irrigation system, soil erosion, crusting and salinization, the depletion of biomass and vegetation cover, the destruction of wetlands, explosive expansion of urban agglomerates, and forest fires. Indeed development incentives leading to the reclamation of so far unused lands for agricultural production becomes easily detectible through the changing vegetation signal, initially efficient reclamation schemes may later enter a phase where undesired effects (such as soil salinizsation) become so important that the overall success of the action is doubtful. Potential risk areas are currently the Ghab and the Bekaa valleys. In some areas such as in the Ghouta area of Damascus and in the Homs area degradation tendencies by exhaustive irrigation are visible by significantly declining NDVI trends.

By new dam projects the irrigated area in Syria is significantly increased, but dams have also considerable downstream environmental and economic impacts which are also visible by negative vegetation abundances downstream the new dam at the Khabour River. The ground water level change and temporal and spatial dynamics of flooding has impacts on riparian ecology including flood-recession agriculture and shallow-groundwater irrigation. [21].

In Syrian's steppe, which is largely considered to be degraded no negative NDVI trends were identified during the last two decades. Reasons for this finding might be that the NDVI at low vegetation abundances and at a coarse resolution is not sensitive to detect further decline in vegetation abundances or toward subtle changes in the steppe flora [22]. In the meantime there is also some evidence to suggest that a certain amount of grazing pressure on arid rangelands maintains or even enhances floral species diversity [23].

ACKNOWLEDGMENTS

We would like to thank Dirk Koslowksy (Free University Berlin) who provided the 1 km AVHRR Medokads set. Furthermore we are very grateful to C. Torrence and G. P. Compo for their CWT software tool which is used in TimeStats. Their source code is available at http://paos.colorado.edu/research/wavelets.

REFERENCES

[1] UNCCD, 2003: United Nations Concention to Combat Desertification. http://www.unccd.int/convention/convention.php.

[2] LEE, R., YU, F. AND PRICE, K.P., 2002: Evaluating vegetation phonological patterns in inner Mongolia using NDVI time series analysis. *Int. J. Remote Sensing, 23*, pp. 2505-2512.

[3] KOSLOWSKY, D., BILLING, H. AND ECKARDT, M., 2001: Sensor degradation and inter-calibration of the shortwave channels of the AVHRR - NOAA 11/14/16 satellites. Proceedings of the 2001 EUMETSAT Meteorological Satellite Data Users' Conference, Antalya, Turkey, 1-5 October 20001, 107-113

[4] UDELHOVEN, T., 2005: TimeStats: a software tool for analyzing spatial-temporal raster data archives. International Conference on *Remote Sensing and Geoinformation Processing in the Assessment and Monitoring of Land Degradation and Desertification*, Trier, 2005.

[5] SCHÖNWIESE, C.-D., 2000: Praktische Statistik für Meteorologen und Geowissenschaftler, Vol. 3. Gebrüder Bornträger, Berlin.

[6] HIRSCH, R. AND SLACK, J., 1984: A non-parametric trend test for seasonal data with serial dependance. *Water Resources Research, 20*, pp. 727–732.

[7] EPA (2000). Guidance for Data Quality Assessment - Practical Methods for Data Analysis. United States Environmental Protection Agency (EPA), Washington, DC 20460. EPA/600/R-96/084.

[8] TORRENCE, C. AND COMPO, G.P., 1998: A Practical Guide to Wavelet Analysis. *Bulletin of the American Meteorological Society, 79*, pp. 61-78.

[9] REPUBLIC OF LEBANON, MINISTRY OF AGRICULTURE, 2002: National report on the implementation of the UNCCD in Lebanon. A Report Prepared in Preparation for the First Session of the Committee for the Review of the Implementation of the Convention in November 2002, Second UNCCD Report, Beirut, May 2002, 28 p.

[10] GTZ-CODEL, 2001: Practitioners Guide: Identification of Desertification Prone Areas. An example from Lebanon. http://www2.gtz.de/desert/download/practitionerguide_lebanon.pdf

[11] REPUBLIC OF LEBANON, MINISTRY OF ENVIRONMENT, 2001: Lebanon State of the Environment Report, http://www.moe.gov.lb/ REPORTS/SOER2001.htm

[12] BARKOUDAH, Y., DARWISH, A.I. AND ANTOUN, M.A., 2000: Biological Diversity National Report, Biodiversity Strategy and Action Plan and Report to the Conference of the Parties, NBSAP Project SY/97/G31, Ministry of Environment, Syria, United Nation Development Program. 34 p. http://www.biodiv.org/doc/world/sy/sy-nr-01-en.pdf

[13] SARAFF, M., LARSEN, B. AND OWAYGEN, M., 2004: Cost of environmental degradation – The case of Lebanon and Tunisia. Environmental Economics Series, No. 97, The International Bank for Reconstruction and Development/THE WORLD BANK. 105 p. (http://www.moe.gov.lb/NR/rdonlyres/D5075FD1-9B98-4BA1-B5E0-8D4CBA039AE4/123/CostEnvDegLebanonTunisiaJune04EDP97.pdf)

[14] TALHOUK, S.N., DARDAS, M., DAGHER, M., CLUBBE, C., JURY, S., ZURAYK, R. AND MAUNDER, M., 2005: Patterns of floristic diversity in semi-natural coastal vegetation of Lebanon and implications for conservation. *Biodiversity and Conservation, 14(4)*, pp. 903-915

[15] WIRTH, E., 1971: Syrien – Eine geographische Landeskunde. Wissenschaftliche Buchgesellschaft, Darmstadt, 530 p.

[16] REPUBLIC OF SYRIA, MINISTRY OF AGRICULTURE AND AGRARIAN REFORM, 2003: The annual agricultural statistical abstract. Damascus, Syria.

[17] REPUBLIC OF SYRIA, MINISTRY OF DEFENCE, 1977: Climate Atlas of Syria. Damascus.

[18] ARABICNEWS, 2005: http://www.arabicnews.com/ansub/Daily/Day/981124/1998112415.html

[19] COCKS, P.S. AND EHRMAN, T.A.M., 1987: The geographic origin of frost tolerance in Syrian pasture legumes. *Journal of Applied Ecology, 24*, pp. 678-683.

[20] SHAKHATREH, Y., KAFAWIN, O., CECCARELLI, S. AND SAOUB, H., 2001: Selection of Barley Lines for Drought Tolerance in Low-Rainfall Areas. *J. Agronomy & Crop Science, 186*, pp119-127

[21] ADAMS, W.M., 1985: The downstream impacts of dam construction: Transactions *of the Institute of British Geographers N.S., 10*, pp. 292-302

[22] SCHMIDT, H. AND KARNIELI, A., 2001: Sensitivity of vegetation indices to substrate brightness in hyper-arid environment: the Makhtesh Ramon Crater (Israel) case study. *International Journal of Remote Sensing, 22(17)*, pp. 3503–3520.

[23] RAE, J, ARAB, G., NORDBLOM, T., JANI, K. AND GINTZBURGER, G., 2001: Tribes, state, and technology adoption in arid land management, Syria. Capri working paper, no. 15, International Food Policy Research Institute 2033 K Street, N.W. Washington, D.C. 20006 U.S.A., 38 p.

TimeStats: a software tool for analyzing spatial-temporal raster data archives

T. Udelhoven[a]

[a] Remote Sensing Department, Trier University, Germany, email: udelhove@uni-trier.de

ABSTRACT

TimeStats is a software tool developed for the analysis of spatial-temporal databases. From a built-in graphical user interface (GUI) tools for data cleaning, pre-processing, basic statistics and trend detection can be selected including OLS regression and non-parametric trend models. Additional tools are provided for multivariate and non-linear time-series analysis, cross spectra analysis, and continuous wavelet transform (CWT). TimeStats is programmed using the Interactive Data Language (IDL) and freely distributed with the IDL virtual machine ™. This ensures software compatibility to different hardware platforms (Microsoft Windows, Linux, Sun Solaris, and MacOS) and does not require the user to own an IDL license. The raster output files are provided with appropriate ENVI header files and are portable to most common imaging processing software interfaces.

Keywords: TimeStats, time-series analysis, AVHRR

1 INTRODUCTION

Remote sensing has been frequently recommended as the primary source for land assessment studies because it provides comprehensive spatial coverage, is intrinsically synoptic, and collects repeatedly objective data [1,2]. The increased demand of remotely gained data has generated the need for (semi-) automated tools that can assist in transferring those data into useful information and knowledge.

Table 1. Basis modules of TimeStats and key-features

Module	Features
Input/output file options	Data import (ENVI BIL-files or generic binary files)
Data cleaning	Detection and correction of outliers Correction of missing value Filtering of noisy data
Data pre-processing	Data aggregation (long-term averages, seasonal averages and variances) Anomalies from global or seasonal averages Difference images Seasonal normalization Counts of anomalies based on user defined thresholds Data normalization including z-score normalization and differencing Seasonal filtering using Fourier polynomials
Basic statistics and trends	Descriptive statistics Linear trend analysis (OLS regression) Significance tests for any trend model Non-parametric trend tests: Mann-Kendal test; seasonal Kendal test; Modified seasonal Kendall test; Kendall slope; seasonal Kendall slope; Rho rank corr and Tau rank corr. Augmented-Dickey-Fuller test for detection of "random walks"
Multiple linear and non-linear regression analysis.	Restricted and unrestricted regression (Wald statistics). Durbin-Watson test for residual analysis (OLS regression). Windowed trend analysis
Models to describe frequency components	Autocorrelation and partial autocorrelation analysis Spectral density estimation (periodogram method, Welch's method, spectral filtering and spectral leakage reduction) Amplitude and phase spectra Cross spectra analysis: cross- , phase shift-, amplitude-, and coherence spectra Continuous wavelet analysis (CWT)

Indeed many techniques for hyperspectral data analysis such as data compression and classification tools can be used for hypertemporal data evaluation, too, time-series (TS-) analysis requires a specific repertoire of methods to describe trends, cycles and stochastic components. In the spatial-temporal data bases such as compiled from NOAA/AVHRR or Spot vegetation sensors each pixel represents one time-series, usually altogether comprising several hundred thousand temporal records. Thus, hidden patterns cannot be easily found by visual inspection but must be identified using statistical tools.

The TimeStats software tool was written to analyse spatial-temporal data sets, to discover trends, semi-periodic and stochastic components and to flag anomalies at multiple granularities of time. For instance, the variability in surface reflectance of a long-term AVHRR-NDVI series may bear useful information about surface degradation and development processes. Knowledge discovery in temporal databases is currently an active interdisciplinary research field [3,4]. TimeStats consists of several modules providing tools for data import, data cleaning, pre-processing and TS-analysis tasks. Key-features are summarized in table 1. Results from time-series analysis are saved on disk using the standard ENVI format with adequate header description. TimeStats is still being improved and in the future new features will be irregularly added. A copy of TimeStats binaries and an extended user manual can be obtained from the author (udelhove@uni-trier.de). The software may be used, copied, or redistributed as long as it is intended for non-commercial purposes.

In the present study the features of TimeStats are demonstrated using 8 km Pathfinder global land cover (PAL-) data (NASA) and 1 km AVHRR-MEDOKADS data (Free University, Berlin).

2 TIME SERIES COMPONENTS

Basically, the objectives of time series analysis include description, explanation and prediction [5,6]. The accomplishment of these issues requires the assessment of different sources of data variability by statistical analysis. A temporal record is referred to be stationary if the series' mean and variance do not change over time. Depending on the considered granularity of time non-stationarity is introduced in many geo-physical time-series by different sources, including long-term trends, seasonal cycles and by the stochastic nature of the series which can be described by Autoregressive-Integrated-Moving average (ARIMA-) models [7,8]. The different sources of variability are shown in figure 1-6 by means of decomposition of a monthly NDVI record, whereat it is assumed that the different time-series components are additive.

The annual cycle in the NDVI series shown in figure 2 was modelled by a Fourier polynomial fitted to the data with a period of 12 months. To take account for the non-sinusoidal shape also the first harmonic (the six months cycle) was considered in the polynomial. The non-linear trend which is obvious from figure 3 was described by a Fourier polynomial, too, this time using a basic frequency of 192 months and by its first harmonic. By analysing the autocorrelation and partial autocorrelation function [5] the nature of the stochastic process was identified as second order auto-regressive (AR(1)-) process. The following complete model was fitted to the NDVI series by OLS regression:

$$\begin{aligned} NDVI_t = {} & a_0 + \beta_1 \cdot time + \beta_2 \cdot NDVI_{t-1} \\ & + \beta_3 \cos\cdot 2\pi \frac{1}{12} \cdot t + \beta_4 \sin\cdot 2\pi \frac{1}{12} \cdot t + \beta_5 \cos\cdot 2\pi \frac{1}{6} \cdot t + \beta_6 \sin\cdot 2\pi \frac{1}{6} \cdot t \\ & + \beta_7 \cos\cdot 2\pi \frac{1}{192} \cdot t + \beta_8 \sin\cdot 2\pi \frac{1}{192} \cdot t + \beta_9 \cos\cdot 2\pi \frac{1}{96} \cdot t + b_{10} \sin\cdot 2\pi \frac{1}{96} \cdot t \end{aligned} \quad (1)$$

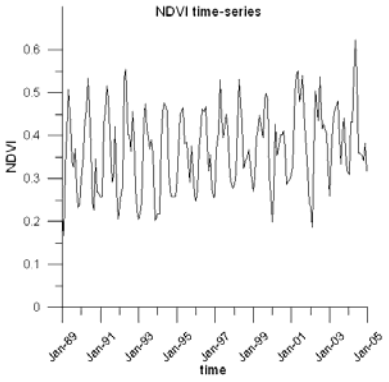

Figure 1. Monthly AVHRR/NDVI series (MEDOKADS data).

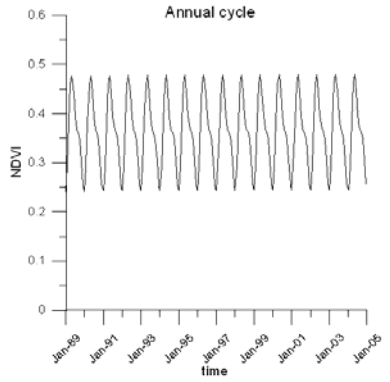

Figure 2. Modelled annual cycle.

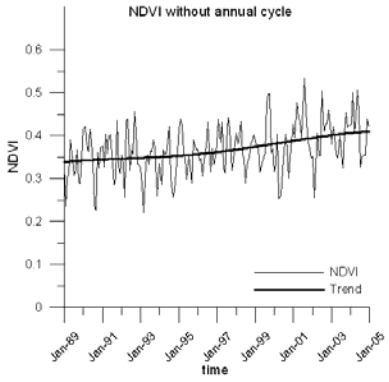

Figure 3. AVHRR/NDVI series after removal of the annual cycle.

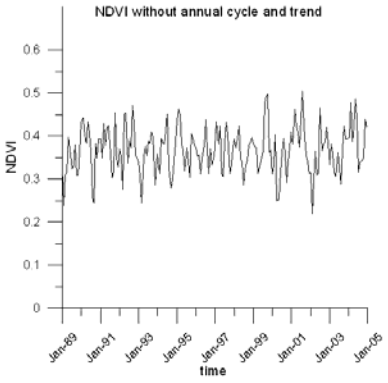

Figure 4. AVHRR/NDVI series after removal of the annual cycle and non-linear trend.

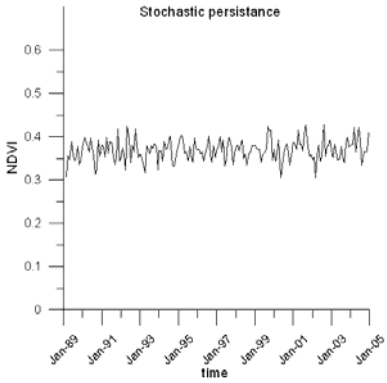

Figure 5. Stochastic persistence of AVHRR/NDVI series modelled by an AR-1 process..

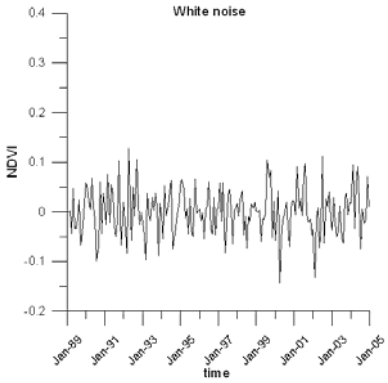

Figure 6. White-noise component after removal of the persistence component.

The white noise component shown in figure 6 was computed as residuals from fitted NDVI values according to (1) and the original NDVI record. In TimeStats all the components used in equation (1) can be individually selected from a GUI in the trend module.

2.1 Trends

TimeStats offers parametric and non-parametric methods for trend detection. Generally, the former are more powerful than nonparametric counterparts provided the measured quantities match the assumed probability distribution [10,11]. The parametric trend model in TimeStats is based on OLS regression. Non-linear structures can be modeled by normal or by Fourier polynomials. As non-parametric trend models variants from the Kendall test family were implemented including the Mann-Kendall, the Seasonal Kendall (SK), and the Modified Seasonal Kendall (MSK) test [10,12,13]. Model results and significance tests are saved into an ENVI file. Figure 7 provides an example of a generated header from the related output file. One additional feature of TimeStats is a windowed linear trend analysis, where a moving window is moved along the series and a trend model is fitted to the data for each window position depending on user defined windows lengths and numbers of overlapping points.

As an example for trend detection a subset of the AVHRR/NDVI Pathfinder data was analysed. In figure 8 the trend magnitude is described in terms of linearly modelled NDVI changes from 1982 to 1999 based on annual NDVI data. The quality of the regression model was checked using the Durbin-Watson (DW) test, which is sensitive for first order autocorrelation in the residuals [6]. Since the DW test (figure 8) points on severe positive

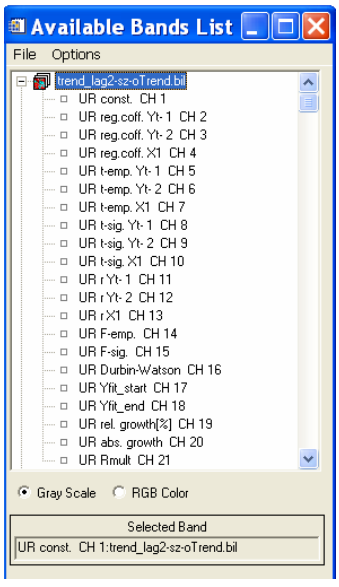

Figure 7. Structure of the generated ENVI-header using a trend model from the advanced trend module.

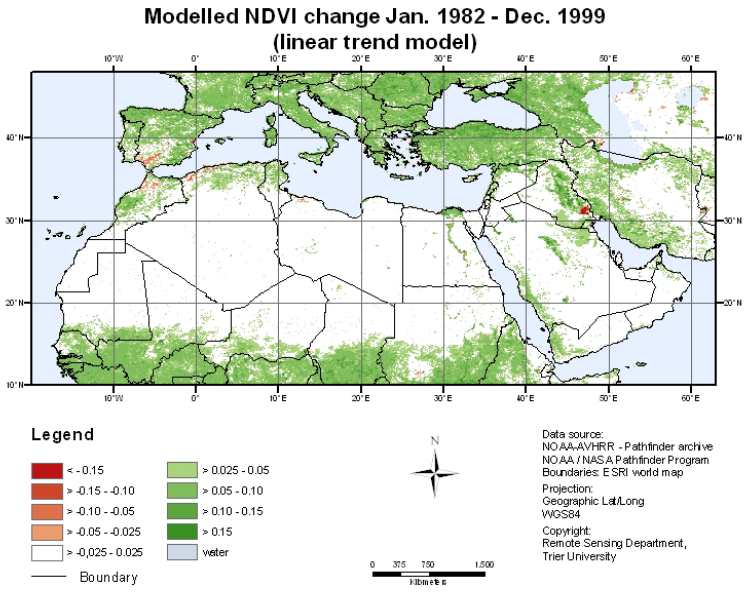

Figure 8. Modelled absolute NDVI changes (Dec. 1999 – Jan. 1982) using a linear trend model: $NDVI_t = a + \beta \cdot t$.

first order autocorrelation in large parts of the image the significance of the trend was addressed using the modified Seasonal Kendall (MSK) test instead of a standard t-test of the regression coefficient. The MSK test was applied to the monthly NDVI series because it can deal with both, seasonality and autocorrelated data [12].

The trend map reveals the abundance of an extensive greening trend for the major part of the image. Significant negative trends are only apparent in some places in Kazakhstan, Uzbekistan, Turkmenistan, the South of Iraq, Israel, the South of Egypt along the Nile, and along the Mediterranean coast of Libya, and Algiers. The modelled long-term NDVI changes indicate that NDVI differences in the observation period do only in some areas exceed 0.15 NDVI units. In spite of similar spatial trend patterns figures 8 and 10 reveal also some discrepancies between the modelled NDVI changes and the MSK test. Especially in the desert areas the latter points on locally highly positive trends, despite the estimated NDVI differences only vary between – 0.025 and 0.025. This phenomenon is referred to as "greenness of the desert". Characterized by small variances, NDVI series in the deserts have a high stochastic persistence. Even small long-term perturbations such as induced by residual orbital drift and sensor degradation effects in the PAL data, or by atmospheric attenuation such as the globally increase of aerosol content after the Mt. Pinatubo eruption in 1991 may result in small but significant artificial trends [14]. Recently, Beurs and Henebry [15] reported that especially NOAA-11 data from the PAL data set pose problems for land surface change analysis. The authors found significant upward trends during the tenure of NOAA-11 (1989-1994) leading to spurious trends in desert areas. Indeed it was found that first order autocorrelation in the residual terms of the linear trend model, as measured by the DW statistics, was greatly reduced for Sahara pixels if the time-span when NOAA-11 was flown is neglected.

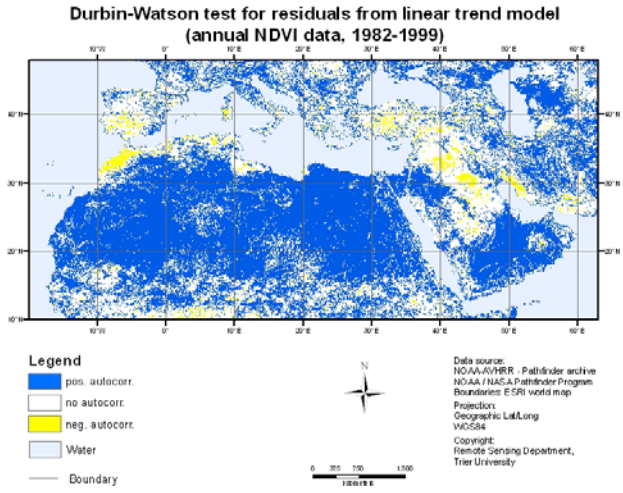

Figure 9. Durbin-Watson statistics for the trend model used in figure 7.

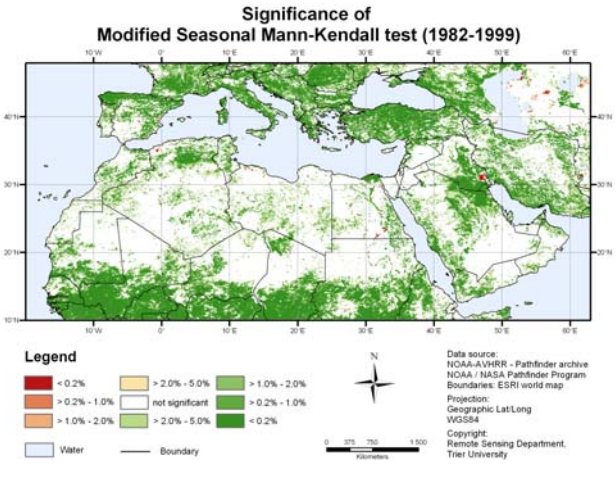

Figure 10. Significance of the Modified Seasonal-Kendall test applied to monthly PAL data (1982 – 1999).

2.2 Frequency components

One further issue in TSA is the description of cyclic components. TimeStats provides commonly used techniques for spectral analysis including autocorrelation, power spectrum and spectral density estimation. Moreover, cyclic components can be interactively analysed by the continuous wavelet transform (CWT). IDL lacks routines for advanced spectral techniques, but most methods are related to Discrete Fourier transform (DFT), which is implemented in the in IDL libraries by the Fast Fourier transform (FFT).

The power spectrum $I(\lambda)$ describes the magnitude of certain frequencies in a series. In monthly NDVI series usually the strength of the annual and semi-annual vegetation cycle is of interest. The power spectrum is derived from the Fourier transform $F(\lambda)$ of the series by the absolute value of the complex result vector [16]:

$$I(\lambda) = \sqrt{\Re\{F(\lambda))^2 + \Im(F(\lambda))^2} \tag{2}$$

where $\Re\{F(\lambda)\}$ and $\Im\{F(\lambda)\}$ denote the real and imaginary part of the series' discrete Fourier transform. The phase term is recovered from the discrete Fourier transform of the series using the following expression:

$$P(\lambda) = \tan^{-1}\left[\Im\{F(\lambda)\}/\Re\{F(\lambda)\}\right] \tag{3}$$

Amplitude and phase

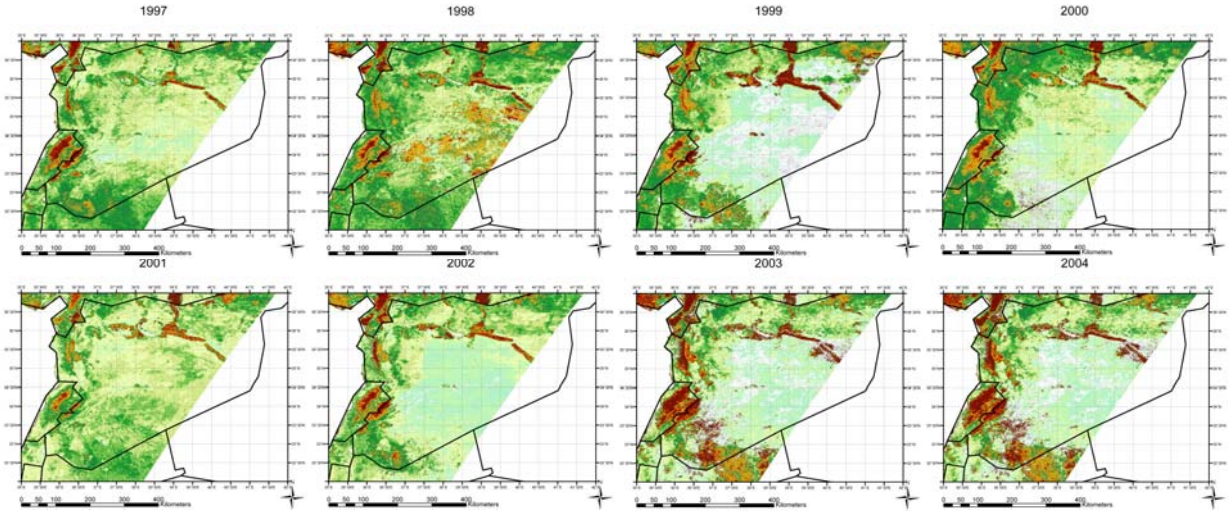

Figure 11. Annual phase of the NDVI, calculated for selected years in the observation period.

The magnitude measures the maximum variability of the record in a specific period of time, whereas the phase indicates the point in time when the maximum value occurs in the related period. The power spectrum is widely used to describe the vegetation growth cycle [17]. Vegetation phenology is largely influenced by climate, terrain characteristics and human activities. The power spectrum of the NDVI signal is particularly useful to compare the strength of the annual growth cycles of various vegetation types or to interpret inter-annual curves. The power spectrum also bears information about land-cover conditions and different vegetation classes and can be linked to physical and temporal parameters for better understanding of plant-environment interactions [18]. Amplitude and phase values at different frequencies measure the relative weights of different periodic climate processes. In monthly series, NDVI amplitude and phase values for period lengths of twelve and six months are closely related to agro-biological phenomena, such as the growth of vegetation in response to the seasonal pattern of rainfall and temperatures [18, 19]. In the example presented in figure 10 the phase term of the annual NDVI cycle was calculated separately for each year for MEDOKADS data covering Syria and Lebanon.

The strong variations visible in the individual annual NDVI phases are mainly attributed to the inner and inter-annual rainfall patterns. Thus, for reliable analysis of long-term trends in the NDVI data sufficient time-series dataset are needed in order to average out short time and climatically induced fluctuations. Plant phenology is a function of climatic conditions, edaphic properties, solar radiation, management practice, and pest/disease infestation. Inter-annual climatic changes such as temperature and precipitation profoundly influence plant phenological status such as the date of onset green-up, the rate of biomass accumulation, and the onset and rate of vegetation senescence [20]. Significant trends derived from short series lead to miss interpretations if no climatically reference data are available. This is still a problem for large parts in the world, especially in arid and semi-arid regions.

Continuous Wavelet Transform (CWT)

The continuous wavelet transform (CWT) describes a time series by sequences of wavelet coefficients, each of which representing the amplitude of the wavelet function at a particular location within the data vector and for a particular wavelet scale. The core computations of the CWT in TimeStats are accomplished using IDL routines written by Torrence and Compo [21]. The CWT produces one two dimensional scalogram as shown in figure 13 for each time-series. Applying to a total spatial-temporal database this would result in an unmanageable amount of scalograms. Thus, an interactive CWT mode was implemented in TimeStats. While the user moves the mouse pointer over the image the scalogram is computed and displayed for each actual pixel position. The parameters to determine the wavelet functions characteristics can be selected from a GUI. Available mother wavelets in TimeStats are the Morlet, Pauls and the derivative of the Gaussion (DOG). The CWT results shown in figure 13 were computed from a monthly NDVI series (PAL-data) collected from a pixel located in the newly claimed desert land in the Nile delta (Egypt). Figure 12 is divided into four parts: (a) the (normalized) original NDVI series; (b) the scalogram representing the wavelet power spectrum for different scales; (c) the global wavelet, in which the

wavelet power for each scale is integrated over time; (d) the scale-averaged series, here representing the strength and development of the annual cycle.

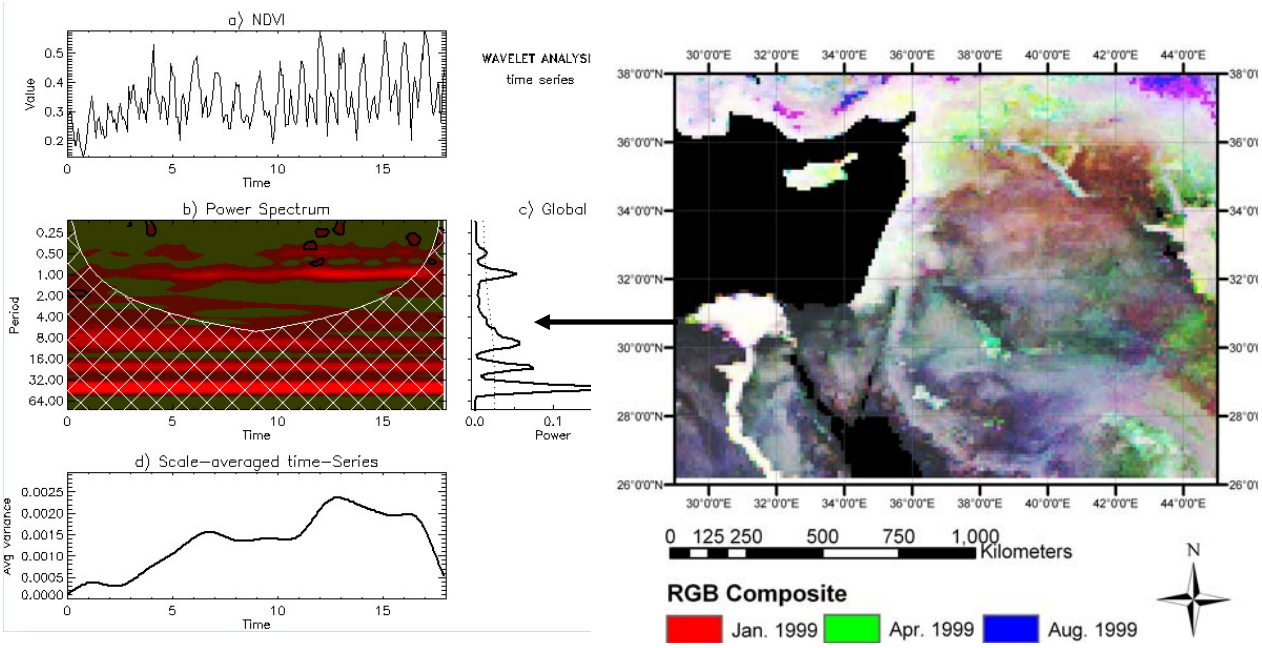

Figure 12. Scalogram calculated from a monthly Pathfinder AVHRR/NDVI time-series (1981-1999) collected from a pixel located at the West fringe of the Nile delta. The scale averaged wavelet-power (d) is related to the one year period, corresponding to the annual vegetation growth cycle.

The global wavelet shows at smaller periods two significant peaks corresponding to a semi-annual and to the annual vegetation growth cycle. The peaks at longer periods are related to a positive trend in the NDVI between 1992 and 1999. The scalogram highlights the magnitude of the wavelet power in time for each Fourier frequency. Bright red areas indicate large wavelet powers. The lower power at the beginning and at the end of the series is caused by zero padding up to the next power of two [21]. Whereas there is a strong annual cycle throughout the total range of the series, the magnitude of the six month cycle is continuously growing. The presence of the six month period is an indication that the corresponding pixel is located in a double crop area. The rotation scheme cotton, sugarcane, and peanuts mixed with winter and summer crops are common in the delta. The scale-averaged wavelet series shows the annual cycle's magnitude in more detail. The graph shows that the magnitude of the annual cycle increases over time, too. The CWT results and the positive NDVI trend clearly indicate intensification in crop production probably by enhanced irrigation during the observation period.

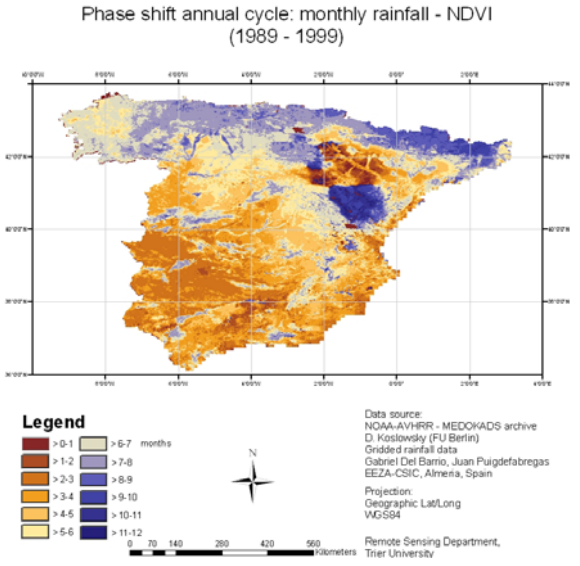

Figure 13. Cross spectra analysis: Phase spectrum.

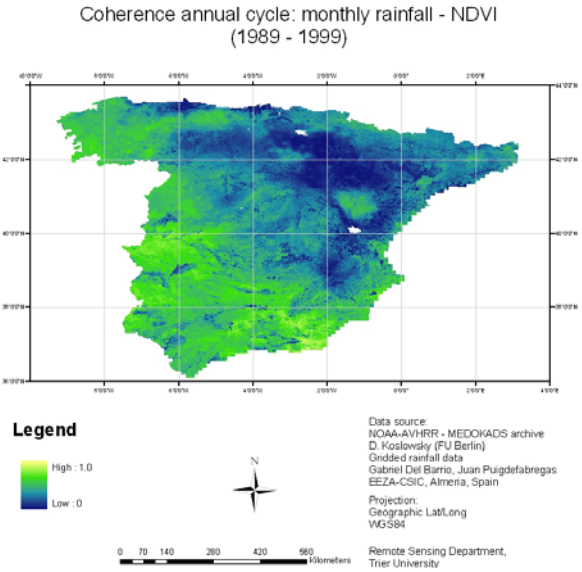

Figure 14. Cross spectra analysis: Coherence.

Cross spectra analysis

The cross-spectrum $f_{xy}(\lambda)$ is the Fourier transform of a cross-covariance function between two signals *x* and *y*:

$$f_{xy}(\lambda) = fft(x) \cdot conj(fft(y)) \tag{4}$$

The result is a complex array of coefficients. Large values will result at frequencies (1/lag) common in amplitude and phase to both signals. Different to the autocorrelation function the cross-correlation function is not symmetrical. To obtain valid results of the coherence function (see below) the cross power spectrum requires spectral filtering, otherwise it registers unity at all frequencies. To avoid such problems Welch's averaged periodogram method is implemented in TimeStats to estimate the cross spectrum [22]. Principle of Welch's method is to divide both series into overlapping sections and to multiply each section by a user defined window function (Hanning, Hamming, Tukey, boxcar). Then each section is zero-padded to the length of the input series to sustain the spectral resolution and the locations of the Fourier frequencies of the original record. Then equation (4) is applied to each section and the resulting spectra are averaged to obtain $f_{xy}(\lambda)$. The phase term P_{xy} is derived from the cross spectrum by [13]:

$$P_{xy}(\lambda) = \tan^{-1} \frac{\Im\{f_{xy}\}}{\Re\{f_{xy}\}} \tag{5}$$

The coherence spectrum is the normalized cross-spectrum. Normalization is achieved by normalizing the cross-spectrum by the product of the individual power spectra [13] (Schönwiese, 2000):

$$C_{xy}(\lambda) = \frac{|f_{xy}(\lambda)|^2}{f_x(\lambda) \cdot f_y(\lambda)} \tag{6}$$

The coherence has a range of [0,1] and can be interpreted in terms of a spectral correlation coefficient. For a given frequency a zero indicates no interference at that frequency, a coherence of one indicates a 100 percent coincidence. By the calculation of the coherence the phase information is getting lost. In figure 13 and 14 an example for a cross-spectra analysis is presented based on 1 km NDVI Medokads data and gridded monthly rainfall data from Spain (1989 – 1999).

ACKNOWLEDGMENTS

I would like to thank Dirk Koslowksy (Free University Berlin) who provided the 1 km AVHRR Medokads set and the Distributed Active Archive Center at the Goddard Space Flight Center (Greenbelt, MD, 20771) for the distribution of the Pathfinder land data. Furthermore I am very grateful to C. Torrence and G. P. Compo for their CWT software which is used in TimeStats. Their source code is available at http://paos.colorado.edu/research/wavelets.

REFERENCES

[1] GUTMAN, G. AND IGNATOV, A., 1995: Global land monitoring from AVHRR: potential and limitations. *Int. J. Remote Sensing, 16*, pp. 2301–2309.

[2] HILL, J., 2000: Semiarid Land Assessment: Monitoring Dry Ecosystems with Remote Sensing. In: Meyers, R.A. (ed.): Encyclopedia of Analytical Chemistry, pp. 8769–8794. John Wiley & Sons, Chichester.

[3] HAN, J AND KAMBER, M., 2001: Data mining: concepts and techniques. Academic Press, San Diego, 547 p.

[4] HAND, D., MANNILI, H. AND SMYTH, P., 2001: Principles of data mining. Massachusetts Institute of Technology, 546 p.

[5] PIWOWAR, J.M. AND LEDREW, E.F., 2002: ARMA time series modelling of remote sensing imagery: a new approach for climatic change studies. *Int. J. Remote Sensing*, pp. 1-24, preview article.

[6] SCHLITTGEN, R. AND STREITBERG, B., 2001: Zeitreihenanalyse. Oldenbourg, 571 p.

[7] BOX, G.E.P. AND JENKINS, G.M., 1976: Time series analysis: Forecasting and Control. revised edn., Oakland, California: Holden-Day.

[8] WEI, W., 1990: Time series analysis. Univariate and multivariate methods. Addison-Wesley, 478 p.

[9] THAS, O., VOOREN, L. V. AND OTTOY, J., 1994: Selection of Nonparametric Methods for Monotonic Trend Detection in Water Quality. URL: http://citeseer.nj.nec.com/3932.html. [5.9.2002].

[10] HIRSCH, R., SLACK, J. AND SMITH, R., 1982: Techniques of trend analysis for monthly water quality data. *Water Resources Research, 18(1)*, pp. 107–121.

[11] LOFTIS, J. C., TAYLOR, C. AND CHAPMAN, P., 1991: Multivariate tests for trend in water quality. *Water Resources Research, 27(7)*, pp.1419–1429.
[12] HIRSCH, R. AND SLACK, J., 1984: A non-parametric trend test for seasonal data with serial dependance. *Water Resources Research, 20*, pp. 727–732.
[13] SCHÖNWIESE, C.-D., 2000: Praktische Statistik für Meteorologen und Geowissenschaftler, Volume 3. Gebrüder Bornträger, Berlin.
[14] GUTMAN, G., 1999: On the use of long-term global data of land reflectances and vegetation indices derived from the advanced very high resolution radiometer. *Journal of Geophysical Research, 104 (6)*, pp. 6241-6255.
[15] BEURS, K.M. AND HENEBRY, G.M., 2004: Trend analysis of the Pathfinder AVHRR Land (PAL) NDVI data for the deserts of central Asia. *IEEE Geoscience and Remote Sensing Letters, 1(4)*, pp. 282-286.
[16] MOODY, A. AND JOHNSON, D.M., 2001: Land-surface phenologies from AVHRR using the discrete fourier transform. *Remote Sensing of Environment 75*, pp. 305-323
[17] ANDRES, L., SALAS, W.A. AND SKOLE, D., 1994: Fourier analysis of multi-temporal AVHRR data applied to a land cover classification. *Int. J. Remote Sensing, 15*, pp. 1115-1121.
[18] AZZALI, S. AND MENENTI, M., 1999: Mapping isogrowth zones on continental scale using temporal Fourier analysis of AVHRR-NDVI data. JAG, Vol. 1, pp. 9-20.
[19] AZZALI, S. AND MENENTI, M., 2000: Mapping vegetation-soil-climate complexes in southern Africa using temporal Fourier analysis of NOAA-AVHRR NDVI data. *Int. J. Remote Sensing, 21*, pp. 973-996.
[20] LEE, R., YU, F. AND PRICE, K.P., 2002: Evaluating vegetation phonological patterns in inner Mongolia using NDVI time series analysis. *Int. J. Remote Sensing, 23*, pp. 2505-2512.
[21] TORRENCE, C. AND COMPO, G.P., 1998: A Practical Guide to Wavelet Analysis. *Bulletin of the American Meteorological Society, 79*, pp. 61-78.
[22] NAIDU, P.S., 1996: Modern spectrum analysis of time-series. CRC Press, Boca Raton, 399p.